Development, Synthesis and Anticancer Evaluation of Trinuclear Platinum Group Metal Organometallic Complexes

Andrew R. Burgoyne

University of Cape Town

December 2015

Supervisor: Associate Professor Gregory S. Smith

Andrew R. Burgoyne

Development, Synthesis and Anticancer Evaluation of Trinuclear Platinum Group Metal Organometallic Complexes

by

Andrew R. Burgoyne

Thesis Presented for the Degree of

Doctor of Philosophy

Supervisor: Associate Professor Gregory S. Smith

Department of Chemistry

University of Cape Town

Republic of South Africa

December 2015

Declaration

I declare that "**Development, Synthesis and Anticancer Evaluation of Trinuclear Platinum Group Metal Organometallic Complexes**" is my own work and to the best of my knowledge has never been reported or submitted for any degree or examination in any university. All sources of information used are cited, acknowledged and completely referenced at the end of each chapter.

I grant the University of Cape Town free license to reproduce the dissertation in whole or in part for the purpose of research.

Signed by candidate

Signature Removed

Andrew R. Burgoyne

…26./…11./…2015

Acknowledgements

Firstly, I would like to express the deep appreciation I have for my supervisor, Associate Professor Gregory Smith, for the nurture and teaching he has supplied me with over this research project. I struggle to express the gratitude I have for the monumental effort you have exerted over this time. Thank you!

I would also like to acknowledge the following people for their assistance, Mr Pete Roberts for recording some of the NMR spectra. Mr Gianpiero Benincasa for microanalytical analyses and Electron Impact Mass Spectral analyses, Dr Marietjie Stander (University of Stellenbosch) for High Resolution Electro-Spray Ionisation Mass spectral analyses and Dr Hong Su for X-ray diffraction analyses. Dr Mervin Meyer (University of Western Cape) for allowing me to conduct *in vitro* ovarian and skin tissue culture experiments. Dr Catherine Kaschula and Dr Iqbal Parker for esophageal cancer screenings.

I wish to thank Dr Preshendren Govender and Dr Tameryn Stringer for their constant encouragement and support throughout my time at UCT. The quality and depth of our conversations led me to think of chemistry in a new light. To the other members of the Organometallic Research group, it has been a pleasure working alongside you and thank you all for your assistance.

I thank the K.W. Johnstone bursary programme, the UCT Doctoral Scholarship and the National Research Foundation (Innovation) for funding.

Also, thanks to Sasha who has been by my side every day, through the good and the bad. Thank you for believing in me.

Abstract

Over the past few decades metals in medicine have played to play a significant role, especially after the discovery of the anticancer properties of cisplatin. However, acquired and intrinsic resistance, toxicity and a host of side-effects have encouraged the research for new metal based anticancer agents. Organometallic complexes have proved to be successful anticancer agents and several have commenced clinical trials. The aim of this study was to prepare and characterize trinuclear platinum group organometallic complexes and investigate their *in vitro* activity.

The first series of ester containing complexes were prepared. The ligands were generated by the preparation of Schiff base ligands obtained from the condensation of 4-aminophenylmethanol and either benzaldehyde, 2-pyridinecarboxaldehyde or salicylaldehyde. Trimeric ester ligands were prepared from these monomeric ligands by reaction with trimesoyl chloride. The trimeric ligands were used to prepare a new series of trinuclear polyester organometallic complexes using the dimeric precursors, $[Ru(\eta^6\text{-}p\text{-}Pr^iC_6H_4Me)Cl_2]_2$, $[Rh(\eta^5\text{-}C_5Me_5)Cl_2]_2$ or $[Ir(\eta^5\text{-}C_5Me_5)Cl_2]_2$. The Schiff base ligands act as bidentate donors to each metal. All compounds were characterized using nuclear magnetic resonance (NMR) and Fourier transform infrared (FT-IR) spectroscopy, elemental analysis (EA) and electron impact (EI) or electrospray ionization (ESI) mass spectrometry. Model mononuclear analogues were prepared and the molecular structures of selected compounds were determined by single crystal X-ray diffraction analysis. The mono- and trimeric ligands and the metal complexes were evaluated for inhibitory effects against the human ovarian cancer cell lines A2780 (cisplatin-sensitive) and A2780*cis*R (cisplatin-resistant), and the model human skin fibroblast cell line, KMST-6. Upon coordination of the metal center an increase in the activity against the ovarian cancer cells is observed, compared to the free ligands. The trinuclear complexes displayed the greatest antiproliferative activity and exhibited selectivity over the non-tumorigenic skin cells.

The second series of new trinuclear and model mononuclear cationic monodentate Rh(III), Ir(III) and Ru(II) complexes with alkylated 1,3,5-triaza-7-phosphaadamantane (PTA) moieties were prepared. Monoalkylation of the PTA moiety was achieved by reaction with 1,3,5-tris-(bromomethyl)benzene for the trimeric ligand or benzylbromide for the monomeric ligand. The trinuclear cationic complexes were prepared from the dimeric precursors, $[Ru(\eta^6\text{-}p\text{-}Pr^iC_6H_4Me)Cl_2]_2$, $[Rh(\eta^5\text{-}C_5Me_5)Cl_2]_2$ or $[Ir(\eta^5\text{-}C_5Me_5)Cl_2]_2$, and characterized using NMR and IR spectroscopy, HR-ESI-mass spectrometry and elemental analysis. The ligands coordinate to the metals via the phosphorous of the PTA, and this was confirmed by

appropriate shifts in the ^{31}P NMR spectra. The cytotoxicities of all alkylated PTA compounds were investigated against WHCO1 esophageal cancer cell. The monomeric and trimeric ligands displayed no activity. The trinuclear Rh(III) and Ir(III) complexes were more active than the mononuclear analogues. The Ir(III) mononuclear complex proved to be the most cytotoxic and ^{1}H NMR model studies demonstrated its DNA binding ability, while UV-Vis studies demonstrated the ability of the iridium mononuclear complex to interact with the double helix structure of Red Salmon testes DNA.

The third series consists of new water soluble Rh(III) and Ir(III) sulfonated complexes. The trimeric ligand was prepared *via* a Schiff base condensation between tris-2-(aminoethyl)amine and 5-sulfonatosalicylaldehyde. Anionic trinuclear complexes were prepared from the dimeric precursors, $[Ru(\eta^6\text{-}p\text{-}Pr^iC_6H_4Me)Cl_2]_2$, $[Rh(\eta^5\text{-}C_5Me_5)Cl_2]_2$ or $[Ir(\eta^5\text{-}C_5Me_5)Cl_2]_2$. Rh(III) and Ir(III) complexes were also prepared by displacement of the labile metal-chloro ligand by reaction with pyridine, 4-methylpyridine, 4-phenylpyridine and 4-ferrocenylpyridine. The sulfonated complexes were characterized using NMR and IR spectroscopy, HR-ESI-mass spectrometry and elemental analysis. The cytotoxicities of all sulfonated compounds were investigated against WHCO1 cancer cells and the metal complexes displayed promising activity, while the ligands showed no activity. Several of the trinuclear complexes exhibited comparable activity to that of cisplatin. ^{1}H NMR model studies demonstrated the most active compound's DNA binding ability.

Publications

Journal Articles:

1. Andrew R. Burgoyne, Banothile C. E. Makhubela, Mervin Meyer, Gregory S. Smith, **Trinuclear half-sandwich Ru(II), Rh(III) and Ir(III) polyester organometallic complexes: Synthesis and *in vitro* evaluation as antitumor agents**, *European Journal of Inorganic Chemistry*, **2015**, 1433-1444.

2. Andrew R. Burgoyne, Catherine H. Kaschula, M. Iqbal Parker, Gregory S. Smith, **In vitro cytotoxicity of half-sandwich platinum group metal complexes of a cationic alkylated phosphaadamantane ligand**, *European Journal of Inorganic Chemistry*, **2016**, 1267-1273.

Conference Contributions:

1. Poster presentation: Andrew R. Burgoyne, Mervin Meyer, Gregory S. Smith, **Synthesis and Biological Evaluation of Polynuclear PGM Organometallic Complexes based on Polyester Scaffolds**, (**2014**, July) 41st International Conference on Coordination Chemistry (ICCC) Singapore, Singapore.

2. Poster presentation: Andrew R. Burgoyne, Mervin Meyer, Gregory S. Smith, **Polynuclear Rh(III), Ir(III) and Ru(II) Organometallic Complexes: Synthesis and Biological Evaluation as Anticancer Agents**, (**2014**, August) 12th European Biological Inorganic Chemistry Conference (EuroBIC) Zurich, Switzerland.

3. Poster presentation: Andrew R. Burgoyne, Catherine H. Kaschula, M. Iqbal Parker, Gregory S. Smith, **Synthesis and Cytotoxicity of Trinuclear PTA-Containing Organometallic Complexes in WHCO1 Esophageal Cancer Cells**, (**2015**, December) 1st International Symposium on Clinical and Experimental Metallodrugs in Medicine: Cancer Chemotherapy (CEMM) Hawaii, United States of America.

Abbreviations and Symbols

°	degrees
°C	degrees Celsius
Å	angstrom(s)
µM	micromolar
λ_{max}	wavelength with maximum absorbance
2D	two dimensional
A2780	cisplatin sensitive human ovarian cancer cells
A2780*cis*R	cisplatin resistant human ovarian cancer cells
ATR	attenuated total reflectance
$^{13}C\{^{1}H\}$	proton decoupled carbon-13
$CDCl_3$	deuterated chloroform
$(CD_3)_2CO$	deuterated acetone
CD_3OD	deuterated methanol
$(CD_3)_2SO$	deuterated sulfoxide
*cis*R	cisplatin-resistant
COSY	correlation spectroscopy
Cp*	1,2,3,4,5-pentamethylcyclopentadienyl
d	doublet
dd	doublet of doublets
D_2O	deuterium oxide

DCM	dichloromethane
DMSO	dimethylsulfoxide
DNA	deoxyribonucleic acid
EA	elemental analysis
EI-MS	electron impact mass spectrometry
ESI-MS	electrospray ionization mass spectrometry
HR-ESI-MS	high resolution electrospray ionization mass spectrometry
EtOH	ethanol
Et_2O	diethyl ether
Fc	ferrocenyl
FDA	food and drug administration
FT-IR	fourier transform infrared spectroscopy
g	gram(s)
5'-GMP	guanosine 5′-monophosphate
HEK	human embryonic kidney cells
HEPES	4-(2-hydroxyethyl)-1-piperazineethanesulfonic acid
HR	high-resolution
HSQC	heteronuclear single quantum correlation
Hz	hertz
IC_{50}	50% inhibitory concentration
*i*PrOH	isopropyl alcohol

IR	infrared
J	coupling constant
KMST-6	normal human fibroblast skin cells
m	multiplet
MeOH	methanol
MHz	megahertz
mol	mole(s)
mmol	millimole(s)
MP	melting point
MTT	3-(4,5-Dimethylthiazol-2-yl)-2,5-diphenyltetrazolium bromide
m/z	mass to charge ratio
$NaBPh_4$	sodium tetraphenylborate
NMR	nuclear magnetic resonance
p-cy	*para*-cymene
PGM	platinum group metal(s)
$^{31}P\{^{1}H\}$	proton decoupled phosphorous-31
ppm	parts per million
PTA	1,3,5-triaza-7-phosphatricyclo[3.3.1.1]decane
pyr	pyridine
RAPTA	ruthenium-arene PTA

RI	resistance index
RNA pol II	ribonucleic acid polymerase II
s	singlet
sep	septet
SI	selectivity index
t	triplet
THF	tetrahydrofuran
UV/Vis	ultraviolet-visible
WHCO1	human esophageal cancer cells
XRD	X-ray diffraction

Contents

Chapter 1: Introduction and Literature Review

1. Overview of Cancer

One of the leading global causes of death is cancer (Figure 1.1). The World Health Organization defines cancer as “the uncontrolled growth and spread of cells”. In 2012 there were 32.6 million people living worldwide with cancer, while there were 8.2 million deaths due to cancer and 14.1 million new cases of cancer.[1] Furthermore, these numbers are expected to grow in the coming decades. The four most common types include: lung, female breast, bowel and prostate cancer.

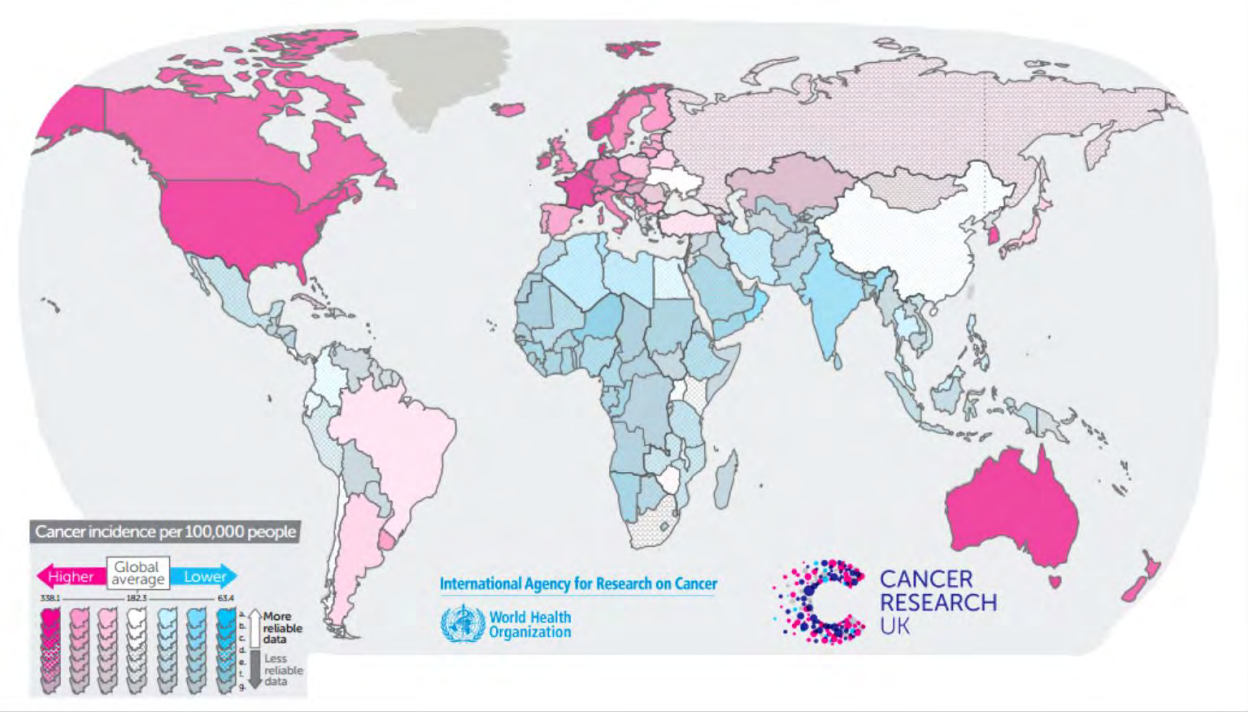

***Figure 1.1**: Map showing cancer incidences per 100 000 people compared to global averages by country.*[1]

Surgery and radiotherapy dominated cancer treatment up until 1950. In the 1940s chemotherapy began as an alternative, when nitrogen mustards (HN2, Figure 1.2) were used

to treat lymphomas. In the ensuing decades, much research has moved toward new drugs which inhibit growth and spread of malignant tissue. Cancer patients have seen an improvement in life expectancy or cures as new research has progressed.

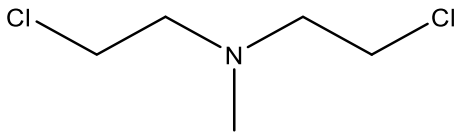

***Figure 1.2**: HN2 or mustine, a nitrogen mustard, is a non-specific DNA alkylating agent.*

One of the struggles with chemotherapy is the lack of selectivity and the undesired side-effects with this treatment. The side effects include nausea, vomiting and may even include renal failure. Currently, the drugs which are in clinical use obtain their selectivity by relying on the high metabolic rates of tumors.[2] However, this leads to the unintentional toxicity to bone marrow and the gastrointestinal tract, as these tissues and organs undergo constant cellular replacement.

In addition, the occurrence of resistance to chemotherapies represents a major issue. This can be intrinsic or acquired resistance. Intrinsic resistance is based on mutations that can spontaneously occur in cell proliferation due to genetic instability.[3] Contrastingly, acquired resistance only develops post-exposure to the chemotherapeutics.

Since the introduction of chemotherapy to treat cancer, a plethora of compounds has been investigated to overcome these hurdles.

1.1. Metals in Cancer Treatment

Metal-based drugs offer novel mechanisms of action and aim to achieve a more targeted approach,[4] which will likely result in greater selectivity and fewer side effects. Metal-based drugs are able to coordinate multiple different ligands in a three dimensional manner and thus offer many tailored advantages over organic and carbon based drugs.[5] Carbon based compounds are unable to contain the wide variety of geometries, kinetic properties and coordination numbers that are attained by metal complexes.[6]

1.1.1. Platinum-based Complexes

Michele Peyrone, in 1844, first described *cis*-diamminedichloroplatinum(II) (cisplatin, Figure 1.3), originally known as Peyrone's chloride.[7] More than a century passed before Barnett Rosenberg, in 1965, serendipitously discovered its anticancer activity.[8] Cisplatin is most active against solid tumors found in testes and ovaries,[9] and is the world's most widely used anticancer drug.[10-12] Stumbling upon this was a significant milestone in medicinal inorganic chemistry.

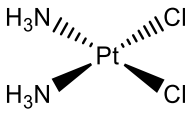

***Figure 1.3**: Cisplatin, a platinum based anticancer complex, or Peyrone's Chloride.*

The target of cisplatin is DNA,[9] particularly the DNA base guanine, where stable DNA-Pt complexes with intra-strand cross-links are formed[13-15] and DNA alteration prevents further replication. This was shown by the laboratory of Lippard, where transcription of RNA pol II was inhibited[16] and cell apoptosis was induced.

Drug resistant tumors severely limit the clinical applications of cisplatin.[17] There are 4 main reasons for resistance to cisplatin. These can be classed as:

(a) Increase in tolerance to cisplatin-DNA adducts and failure of cell death pathways,
(b) Activation of repairing mechanisms of platinum-DNA adducts,
(c) Inactivation by thiol-containing species, and
(d) Insufficient drug accumulation

To overcome the issues of resistance, analogues of cisplatin were investigated.[18] This was achieved by replacing the readily exchangeable chloride ligands with others which reduced the rate of aquation.[19] These second generation FDA approved platinum drugs (Figure 1.4) are in current use and include oxaliplatin which is used for advanced colorectal cancer treatment, and carboplatin which is mainly used for ovarian, lung, head and neck cancers.

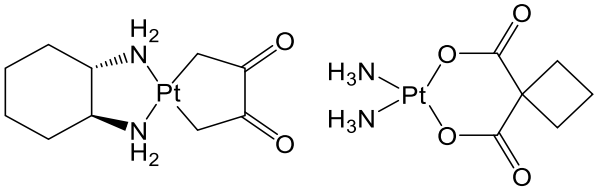

***Figure 1.4**: Second generation Pt drug complexes, oxaliplatin (left) and carboplatin (right).*

1.1.2. Alternative Metals as Therapeutic Agents

Apart from Pt anticancer agents, other metal-based anticancer drugs have been investigated.[20] These have been further studied as they result in fewer side effects. New metal-based anticancer drugs have the potential to overcome platinum resistance, reduce toxic side effects and widen the spectrum of cancer types which can be treated.

In particular, other platinum group metals, such as rhodium, iridium and ruthenium have been an exciting point of interest, despite their cost, within the field of antitumor drug design.[21] The inclusion of a ferrocenyl moiety has in some cases shown a marked increase in activity.[22]

1.1.2.1. Rhodium(III)

Little research has gone into rhodium-based drugs, which makes them ideal candidates for further development of anticancer drugs. Rhodium and iridium lend themselves to easy coordination to *N,N'*-, *N,P*-, *N,O*- or *C,N*-donor ligands. A few studies have been reported on Rh(III) compounds with antitumor activity.[23-25] The simple complex *mer*-[$RhCl_3(NH_3)_3$] reported decades ago exhibited anticancer properties.[26-27] Sheldrick and co-workers prepared half-sandwich Rh(III) complexes from pyridyl ligands which displayed antiproliferative activity.[28-30]

In the case of cyclometalated Rh(III) arene systems, in which a metal-carbon bond is formed to an anionic aromatic ring, good antitumor activity is observed. Smith and co-workers reported on some mononuclear cyclometalated Rh(III) half-sandwich complexes (Figure 1.5, left) cytotoxic against cisplatin-sensitive human ovarian cancer cells, A2780, and cisplatin-resistant cells, A2780*cis*R.[31] The complexes showed good selectivity when tested against normal human embryonic kidney cells, HEK. In another study by Smith and co-workers neutral (Figure 1.5, left and right) and cationic complexes (Figure 1.5, center) with pentamethylcyclopentadienyl (η^5-C_5Me_5) Rh(III) were prepared, based on 2-iminopyridyl and salicylaldimines ligands.[32]

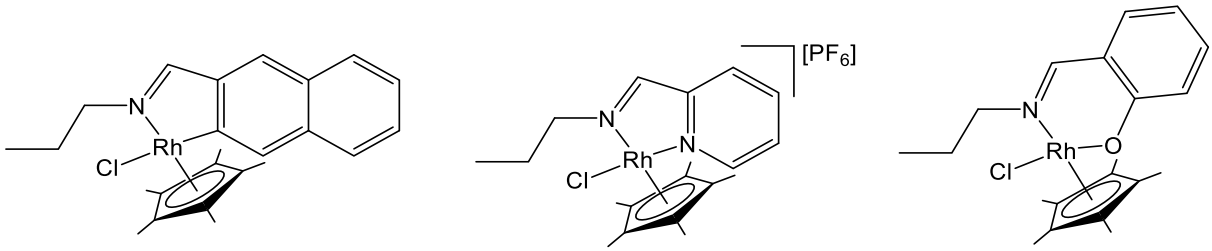

Figure 1.5*: Cyclometalated naphthaldimine (left), 2-Iminopyridyl (center) and salicylaldimine (right) Rh(III) metal complexes for anticancer study.*

It was reported that these complexes display moderate antitumor activity against A2780 and A2780*cis*R cell lines.

Keppler and co-workers prepared aqueous stable rhodium(III) complexes of a general formula [Rh(η^5-C_5Me_5)(L)Cl] (where L = 1,2-dimethyl-3-hydroxy-pyridin-4(1H)-one or 2-pyridine carboxylic acid; Figure 1.6).[33]

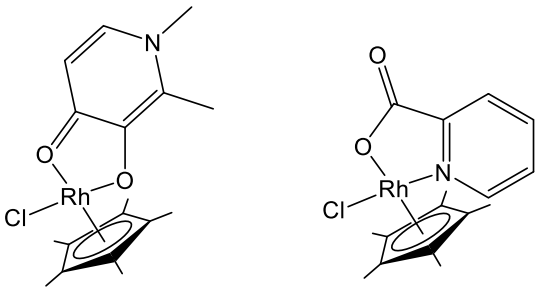

Figure 1.6*: Rh(III) complexes prepared from 1,2-dimethyl-3-hydroxy-pyridin-4(1H)-one (left) 2-pyridine carboxylic acid (right) for anticancer study.*

These complexes displayed moderate *in vitro* cytotoxicities against human ovarian carcinomas (CH1), colon carcinomas (SW480) and non-small cell lung carcinomas (A549). The moderate activity is attributed to the complexes high stability and the consequent incapability to form aqua species by displacement of the chloro-ligand.

1.1.2.2. Iridium(III)

The low spin $5d^6$ iridium(III) complexes have often been thought to be inert[34-35] and yet the number of organometallic iridium complexes are quite extensive.[36-53] π-Bonded carbon-bound arenes impart a balance between hydrophobicity and hydrophilicity that is required for targeting biomolecules and cellular uptake.[54-56] The Cp* ligand is negatively charged and stabilizes Ir(III) complexes.

Sadler and co-workers prepared a series of Ir(III) half-sandwich complexes, with various functionalized arene systems, of the general formula $[Ir(\eta^5\text{-}Cp^x)(XY)Cl]^{0/+}$ where Cp^x = Cp*, tetramethyl(phenyl)cyclopentadienyl (Cp^{Ph}) or tetramethyl(biphenyl)cyclopentadienyl (Cp^{Biph}), and XY = 1,10-phenanthroline, 2,2'-bipyridine, ethylenediamine or picolinate, (Figure 1.7).[36]

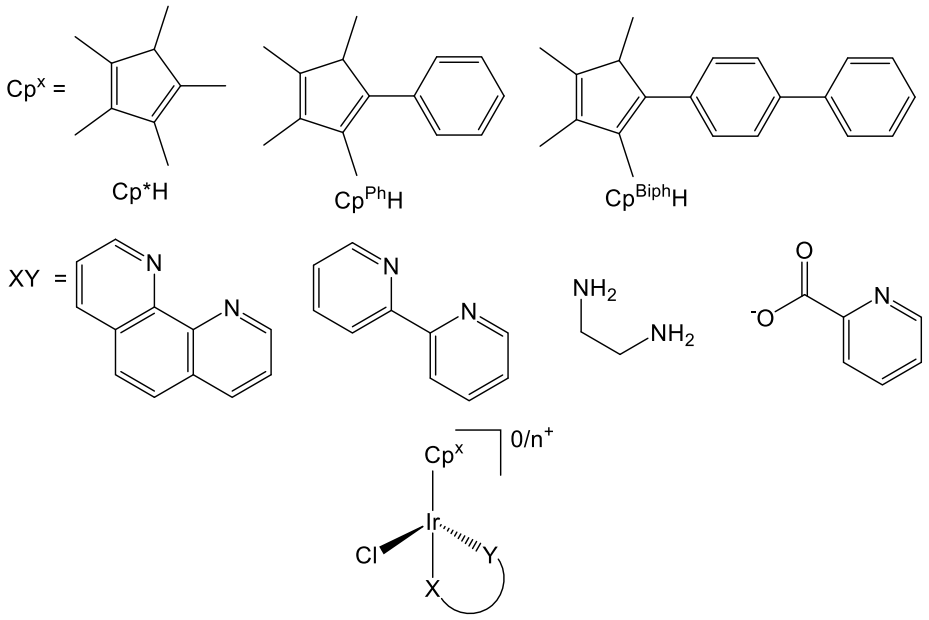

***Figure 1.7**: Some Ir(III) arene complexes studied as anticancer complexes.*

It was found that the activity of the complexes increased as the arene was exchanged from Cp* to Cp^{Ph} and then to Cp^{Biph}, which was the most active in the nanomolar range.

Sadler and co-workers, for comparison, then extended the series to cyclometalated Ir(III) complexes (Figure 1.8) of the general formula $[Ir(\eta^5\text{-}Cp^x)(C\text{^}N)Cl]$ where Cp^x = Cp*, Cp^{Ph} or Cp^{Biph}, C^N = 2-(*p*-tolyl)pyridine, 2-phenylquinoline, 2-(2,4-difluorophenyl)pyridine or 2-phenylpyridine.[48]

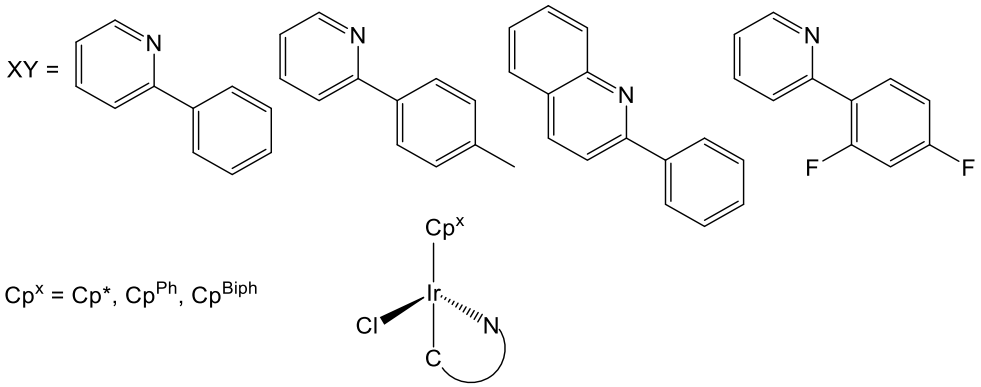

***Figure 1.8**: A series of cyclometalated Ir(III) complexes that show promising cytotoxicity.[48]*

All complexes showed potent cytotoxicity towards human ovarian cancer cells A2780. A similar trend was observed for that of the cyclometalated complexes, in comparison to that of the XY donor complexes previously made, with the activity of the arenes found to be Cp* < Cp^{Ph} < Cp^{Biph}, which was the most active in the sub-micromolar range. The high potency of the Cp^{Biph} was attributed to the extended phenyl rings and its ability to intercalate with DNA.[23, 48]

Work done by Kollipara and co-workers shows that half-sandwich PGM complexes with bithiazole ligands (Figure 1.9) with the general formula [M(arene)(L)Cl], where M = Ru, Rh or Ir; arene = *p*-cymene or Cp*; L = 2,2'-dimethyl-4,4'-bithiazole, 2,2'-diamino-4,4'-bithiazole or 2,2'-diphenyl-4,4'-bithiazole, are active against two human breast carcinoma cell lines, MDA-MB-231 and T47D.[47] Interestingly, the Ir(III)-based complexes were found to be more active than the Ru(II) and Rh(III) complexes under both aerobic and hypoxic conditions. This may be attributed towards a large number of reasons, including the hydrophobicity, cell uptake or possible DNA binding.[36]

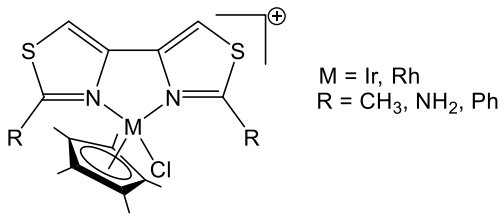

***Figure 1.9**: A series of bithiazole-containing metal complexes, where the Ir(III) complexes were the most active against human breast carcinoma cells.*

1.1.2.3. Ferrocene

Ferrocene, $[Fe(\eta^5\text{-}C_5H_5)_2]$, a sandwich compound discovered[57-58] and characterized[59-60] in the 1950s led to the reporting of many publications in just two decades.[61] It has been said that this may have been the start of a new Iron Age.[62]

It has been shown that many compounds containing a ferrocenyl moiety exhibit good antitumor activity.[63] Work by Costa-Lotufo, Jaouen and co-workers reported that the introduction of a ferrocenyl moiety to 1,1,2-triphenylbut-1-ene, which had been previously regarded as inactive, induced a concentration decrease in cancer cell viability.[64] 2-Ferrocenyl-1,1-diphenylbut-1-ene (Figure 1.10) caused cell death by apoptosis, due to interference with the cell cycle in the G_1G_0 phase, while necrosis was only observed at the highest concentration tested.

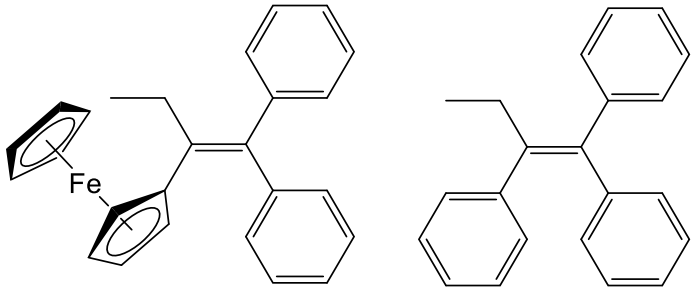

***Figure 1.10**: 2-Ferrocenyl-1,1-diphenylbut-1-ene (left) showed superior antitumor activity compared to the organic analogue, 1,1,2-triphenylbut-1-ene (right).*

Jaouen and co-workers also prepared a large series of ferrocenophane tetrasubstituted olefin derivatives (Figure 1.11) which exhibited high cytotoxicity against human independent breast MDA-MB-231 and prostate PC3 cancer cells.[65]

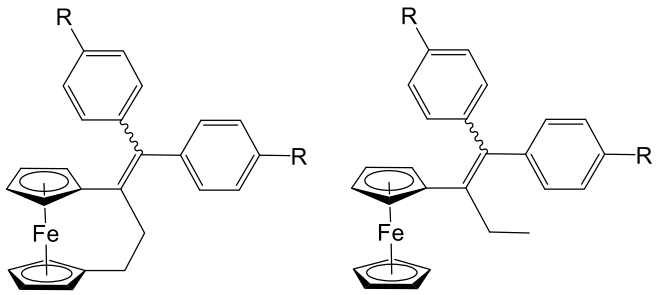

R = H, OH, OAc, NH_2, NHAc, Br, CN

***Figure 1.11**: Ferrocenophane derivatives that exhibit high antitumor activity.*

The activity of these ferrocenyl-derived compounds is well into the nanomolar range. This potent antitumor activity is attributed to the ferrocene moiety. Lead compounds were selected for screening against the NCI-DTP 60-cell line panel and the mean cytotoxicity over the cell lines tested was better than cisplatin.

Nieto and co-workers prepared heterobimetallic dinuclear Pt(II)-ferrocenyl complexes (Figure 1.12) which showed antitumor activity in the low micromolar range in several cancer cell lines.[66]

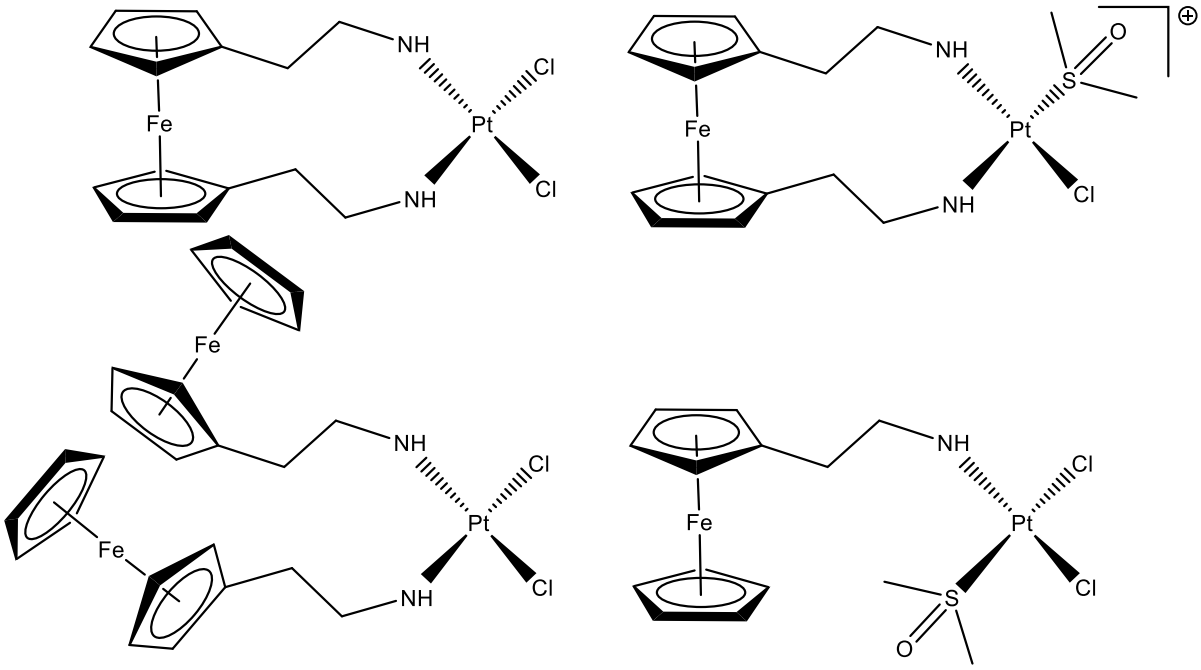

***Figure 1.12**: Heterobimetallic Pt(II) complexes with β-aminoethylferrocenes.*

Smith and co-workers prepared polynuclear RAPTA complexes coordinated to bidentate *N,O*- or *N,N*-donor amine ligands (Figure 1.13). Nine of the twelve compounds slowed the proliferation of ovarian cancer cells by more than half at a 5 μM Fe concentration.[67]

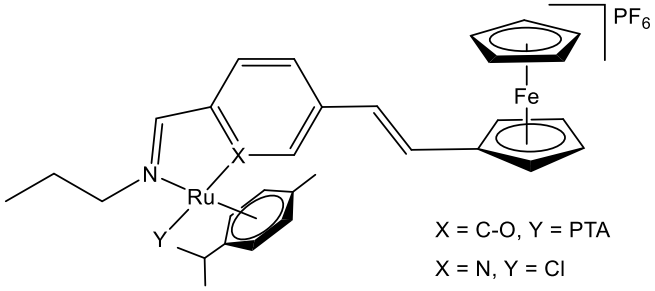

***Figure 1.13**: Ferrocenyl-derived polynuclear N,O- and N,N-RAPTA complexes.*

1.1.2.4. Ruthenium(II)

Currently, ruthenium-containing metal complexes appear to be the best alternatives to Pt drugs as they accumulate in cells which undergo rapid division like tumors. Ru metal centers mimic iron and bind to the protein transferrin,[68] which transports Fe into cells. Within tumorigenic cells transferrin protein receptors are overly expressed.[69] However, Ru has higher affinity for 'soft' ligands than Fe and exhibits slower binding kinetics with high stability constants.

Recently it has become apparent that DNA is not the primary target molecule of ruthenium-arene complexes, as findings have shown that these systems bind to enzymes and target biologically important proteins instead.[70-72] This new insight assists with the understanding of the activity of these complexes.

Different ruthenium complexes display various mechanisms which lead to their anticancer activity. One accepted mode of action is the formation of Ru-aqua complexes by the aquation of the labile Ru-Cl bond. These complexes often then interact with DNA to form adducts, or intercalate between DNA base pairs through available arene systems or interact with proteins and other important biological molecules.

An attractive feature of Ru is that it has access to a range of oxidation states (II, III and IV) under physiological conditions and interchanging between these different oxidation states within the cell is easily attainable because of the low energy barriers between them.

The first Ru(III) complexes to enter clinical trials were *trans*-[$Ru^{III}Cl_4$(dimethylsulfoxide)imidazole], NAMI-A (Figure 1.14, left) and indazolium *trans*-[$Ru^{III}Cl_4$(indazole)], KP1019 (Figure 1.14, right).[73-76] The activity of these imidazolium and indazolium stabilized anionic Ru(III) complexes can be explained by their activation by cellular reduction to Ru(II), which is able to coordinate to biomolecules and further explains their increased reactivity.[20, 77-79] However in the case of KP1019 only mild treatment-related toxicities were displayed, which encouraged further development. The latest lead drug to come out of this class of compounds is the more water-soluble sodium salt analogue, NKP1339 (Figure 1.14, right) which has successfully completed a clinical phase I trial and is on the edge of clinical application.[80] NKP1339 targets GRP78, which regulates the endoplasmic reticulum stress and is up-regulated in cancer cells, and NKP1339 results in down-regulation which leads to tumor cell death.[81]

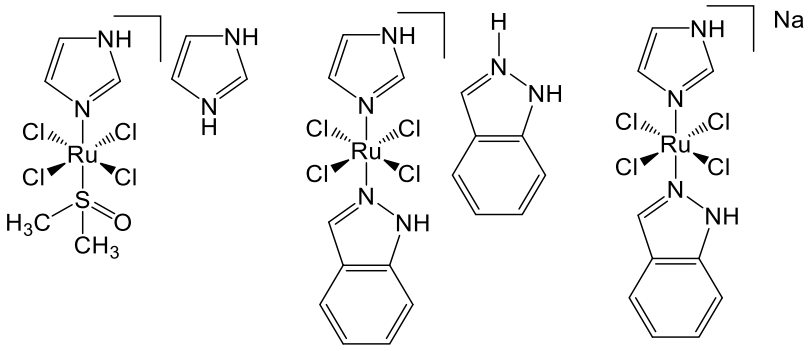

***Figure 1.14**: NAMI-A (left), KP1019 (center) and NKP1339 (right).*

Reports show that NKP1339 interacts with serum proteins and has a high affinity towards proteins in the bloodstream, namely transferrin and albumin.[82-83] These two proteins behave as transport and delivery agents for ruthenium complexes.[84] NKP1339 displayed near 4-fold enhanced mean survival of the hepatoma xenograft Hep3B when used in combination with Sorafenib, a tyrosine kinase inhibitor and approved drug for advanced renal cancer.[80, 85]

Ru(III) complexes are more inert than complexes formed with Ru(II) and often drugs are administered as Ru(III). This causes less damage to healthy cells, increasing selectivity, and the metal is reduced to Ru(II) in cancer cells,[69] which tend to contain a more chemically reducing environment. This environment is due to the increased metabolic rate of the rapidly dividing cell and its remoteness from the blood supply, both of which cause a lower concentration of molecular oxygen. This theory has undergone intense scrutiny and criticism.

Of interest amongst the organometallic Ru complexes are the half-sandwich Ru complexes, which have been extensively explored as they have shown potential as anticancer agents.[86-87] Pioneering in this field are the works by Dyson and Sadler.[86, 88-108]

The arene moiety promotes diffusion of the complex into the cell through the membrane by its hydrophobic nature. The biological properties of the complex can be modulated by occupying a variety of mono-, bi- and tridentate ligands in the remaining three coordination sites.

Sadler and co-workers prepared a Ru(II) arene complex, $[Ru(\eta^6\text{-biphenyl})(en)Cl][PF_6]$ (RM175, Figure 1.15, en = ethylenediamine).[109] RM175 displays good activity against A2780 human ovarian cancer cells and is comparable to cisplatin. In addition, RM175 shows moderate activity against the cisplatin resistant cell line.[94]

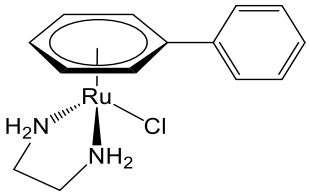

***Figure 1.15**: The structure of RM175.*

Dyson and co-workers prepared complexes of the general formula [Ru(η^6-arene)(PTA)Cl_2] (RAPTA, where PTA = 1,3,5-triaza-7-phosphatricyclo[3.3.1.1]decane).[96, 103, 110-114] RAPTA-C, [Ru(η^6-*p*-cymene)(PTA)Cl_2] was found to be relatively inactive *in vitro* yet it was active against lung metastasis in CBA mice.[112] The Rh(III) and Ir(III) analogues containing 1,2,3,4,5-pentamethylcyclopentadiene, Cp*, were prepared for investigation for inhibition of enzymes.[44] The Rh(III) and Ir(III) analogues (Figure 1.16) were found to be inactive compared to RAPTA-C. The greater activity of RAPTA-C was attributed to its ability to form stronger metal-sulfur bonds at the active site of cathepsin B, a lysosomal cysteine protease involved in protein degradation and antigen processing.

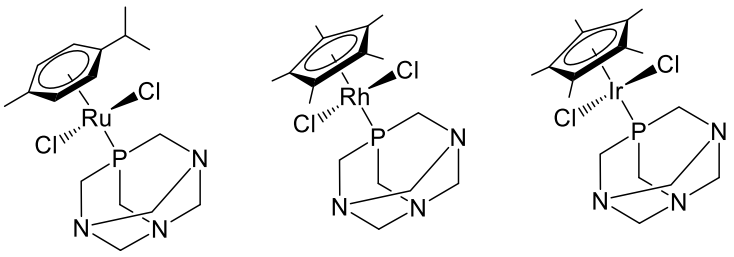

***Figure 1.16**: RAPTA-C (left) and η^5-C_5Me_5 derivatives Rh(III) (center) and Ir(III) (right).*

1.2. Multinuclearity

Initially platinum-based anticancer drugs remained the focus of the development of new drugs to replace cisplatin. By increasing the DNA inter-strand cross-links and thus increasing the number of moieties which have DNA affinity, scientists aim to increase the activity of Pt complexes. Farrell's trinuclear cationic complex (BBR3464, Figure 1.17) [μ-*trans*-$Pt(NH_3)_2${*trans*-$PtCl(NH_3)_2\{NH_2(CH_2)_6NH_2\}$}$_2$][$NO_3$]$_4$ demonstrated the ability to overcome cisplatin resistance,[115] yet was not approved.

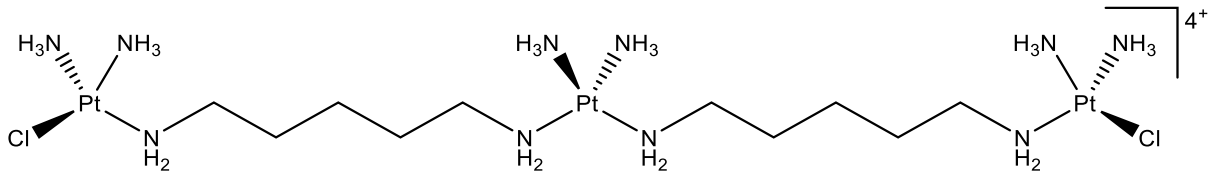

***Figure 1.17**: BBR3464, a cationic trinuclear Pt complex.*

Jansen and co-workers prepared a tetranuclear analogue of BBR3464 based on a 1,4-diaminobutanepoly(propyleneimine) scaffold (Figure 1.18). This tetraplatinum based complex, DAB(PA-tPt-Cl)$_4$, showed an ability to bind to the model nucleoside guanine- 5′-monophosphate (5'-GMP), at each Pt metal, through N7 on the model base pair.[116] This Pt complex showed only moderate anticancer activity against two separate mouse leukemia cell lines, L1210/0 and L1210/2, and was less cytotoxic against several human tumor cell lines.

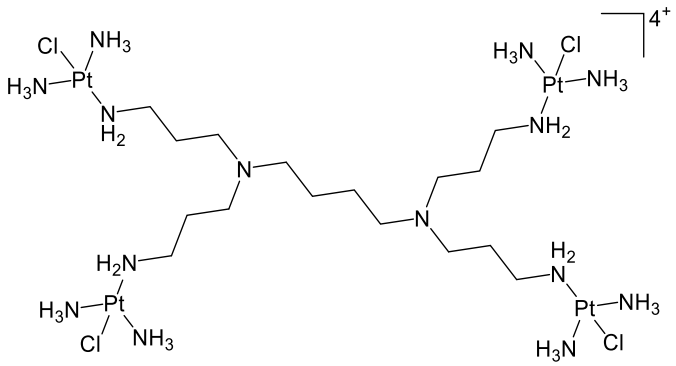

Figure 1.18: DAB(PA-tPt-Cl)$_4$, a cationic tetranuclear Pt complex.

Since then some focus has remained on multinuclearity,[117-120] while a shift in interest of the metal used has swung to others. Sadler and co-workers prepared a dinuclear complex, [{Ru(η^6-biphenyl)Cl(en)}$_2$-(CH$_2$)$_6$]$^{2+}$ (Figure 1.19, left), which is capable of double DNA intercalation through induced-fit recognition by epimerization at the stereogenic centers.[121] The intercalation properties of the mononuclear analogue are significantly lower than those of the dinuclear complex, and this was attributed to the ability of both the free phenyl rings being able to intercalate and cause cross-linking and interstrand cross-links within the DNA.

Keppler and co-workers have shown that the activity of pyridine linker-derived ruthenium-arene dinuclear complexes is related to the length and lipophilicity of the linkers. The most cytotoxic complex contains a 32-carbon-long linker chain (Figure 1.19, right).

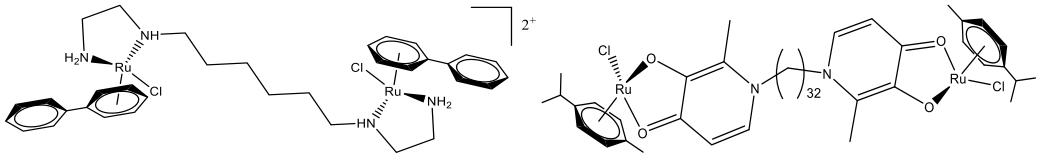

***Figure 1.19**: Dinuclear ruthenium-arene complexes which exhibit high cytotoxicity.*

The increasingly high activity of these complexes is due to the enabling ability of the complexes to cross-link biological molecules with longer chains.[54, 122]

1.3. Concluding Remarks

The exponentially increasing number of diagnosed cases of cancer threatens all. Complications arising from the acquired or intrinsic resistance to currently used chemotherapies, along with the general toxicity and poor selectivity to differentiate from normal healthy tissues or organs, demands the development of new compounds to overcome these and other hurdles.

Polynuclear PGM complexes have become of interest in bioorganometallic chemistry with specific design for use as anticancer chemotherapeutics. The evidence of their anticancer activity provides encouragement for further research and development of this class of complexes.

1.4. Aim and Specific Objectives of this Thesis

1.4.1. Aims

There have been many monometallic arene complexes synthesized for antitumor activity investigation. There is still much room for research to improve on multinuclearity, activity and selectivity. In general, this research project aimed to:

- Prepare and characterize new trimeric ligands.
- Coordinate the PGMs Rh(III), Ir(III) or Ru(II) to form polynuclear complexes.
- Evaluate these complexes for their biological activity as anticancer agents.

1.4.2. Objectives

1.4.2.1. Synthetic Objectives

This project focused on the synthesis of mono- and polynuclear Rh(III), Ir(III) and Ru(II) complexes, which were characterized using a range of analytical and spectroscopic techniques. These complexes are divided into three classes of compounds, based on the different ligand types to which the metals are coordinated.

1. The preparation of new different polyester ligands and their coordination to PGMs (Figure 1.20). The different polyester ligands coordinated to the metal arenes in a bidentate manner (*C,N*-, *N,N*- or *N,O*-chelating). Benzyl alcohol mononuclear complexes were also prepared for comparative purposes.

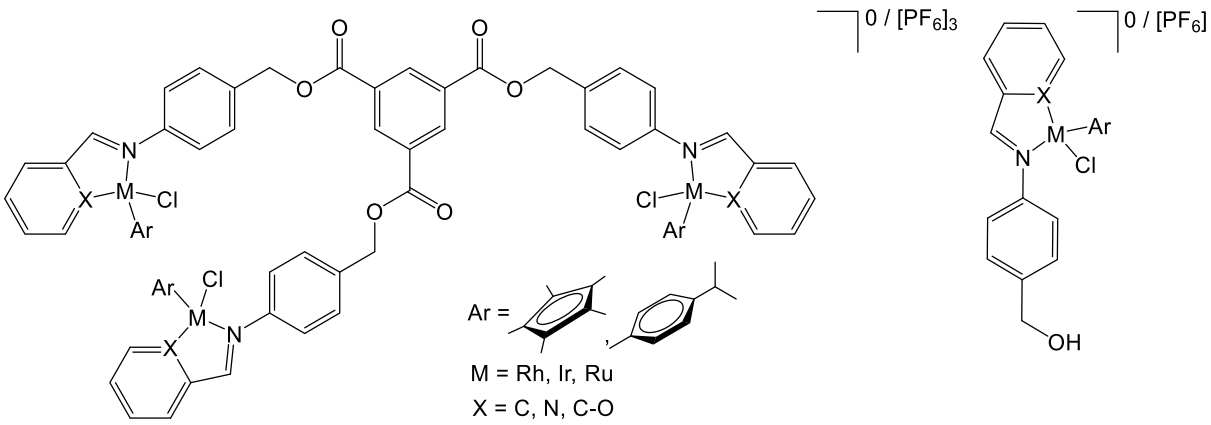

***Figure 1.20**: The general structure of polyester rhodium(III), iridium(III) and ruthenium(II)-arene complexes.*

2. The synthesis of a new trimeric cationic ligand based on alkylated PTA, by quaternization of a nitrogen, for coordination to PGMs (Figure 1.21). Mononuclear analogues were also prepared.

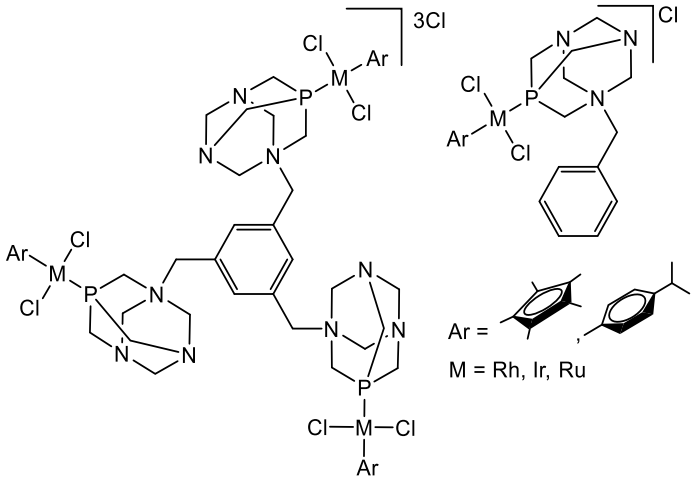

***Figure 1.21**: Tri- (left) and mononuclear (right) rhodium(III), iridium(III) and ruthenium(II)-arene complexes based on alkylated PTA ligands with a benzyl central core.*

3. The bidentate (*N,O*-) coordination of Rh(III) and Ir(III) Cp* fragments to mono- and trimeric anionic sulfonated ligands to form water-soluble complexes. The chlorides were displaced by a series of *N*-donor ligands to form sulfonated cationic complexes (Figure 1.22).

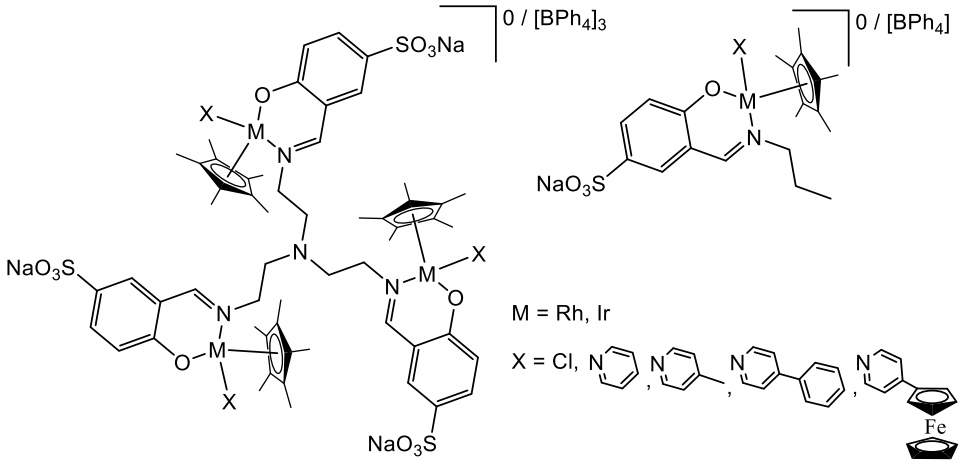

***Figure 1.22**: Sulfonated tri- (left) and mononuclear (right) rhodium(III) and iridium(III)-Cp* complexes.*

All compounds have been characterized using analytical and spectroscopic techniques. These include NMR and FT-IR spectroscopy, elemental analysis and mass spectrometry.

1.4.2.2. Biological Evaluation

After characterization of the complexes, ensuring purity, all the trinuclear metal-arene complexes were evaluated for *in vitro* antitumor activity in either human ovarian cancer cells (A2780 and A2780*cis*R) or human esophageal cancer cells (WHCO1). Ovarian cancer was selected due to its prevalence in women is one of the leading causes of cancer related deaths.[123] Selectivity was investigated, for selected complexes, by analyzing cytotoxicity against normal human fibroblasts (KMST-6).

NMR experiments were performed to study the stability and interactions of the most active complexes with model DNA 5'-GMP and small biological molecules.

The ability of the alkylated PTA complexes to interact with Red Salmon testes DNA was studied by UV-Vis spectroscopy, to complement the NMR studies.

1.5. References

[1] J. Ferlay, I. Soerjomataram, R. Dikshit, S. Eser, C. Mathers, M. Rebelo, D. M. Parkin, D. Forman and F. Bray, *Int. J. Cancer* **2014**, *136*, E359-E386.

[2] D. Tennant, R.V. Duran and E. Gottlieb, *Nat. Rev. Cancer* **2010**, *10*, 267-277.

[3] G.K. Dy and A. Adjei, *Cancer* **2008**, *113*, 1857-1887.

[4] M. Frezza, S. Hindo, D. Chen, A. Davenport, S. Schmitt, D. Tomco and Q. P. Dou, *Curr. Pharm. Des.* **2010**, *16*, 1813-1825.

[5] S. P. Fricker, *Dalton Trans.* **2007**, 4903-4917.

[6] I. Ott and R. Gust, *Arch. Pharm.* **2007**, *340*, 117-126.

[7] M. Peyrone, *Ann. Chem. Pharm.* **1844**, *51*, 1, translated into English by Dr Sheridan Muspratt as: 'Action of Ammonia upon the Protochloride of Platinum', *Med. Times*, **1844**, *10*, 381.

[8] B. Rosenberg, L. Vancamp, J. E. Trosko and V. H. Mansour, *Nature* **1969**, *222*, 385-386.

[9] Y. Jung and S Lippard, *J. Chem. Rev.* **2007**, *107*, 1387-1407.

[10] Y. He, Y. Ding, D. Wang, W. Zhang, W. Chen, X. Liu, W. Qin, X. Qian, H. Chen and Z. Guo, *Chem. Sci.* **2015**, *6*, 2074-2078.

[11] T. Boulikas and M. Vougiouka, *Oncol. Rep.* **2003**, *10*, 1663-1682.

[12] N. J. Wheate, S. Walker, G. E. Craig and R. Oun, *Dalton Trans.* **2010**, *39*, 8113-8127.

[13] R.A. Alderden, H. R. Mellor, S. Modok, T.W. Hambley and R. Callaghan, *Biochem. Pharmacol.* **2006**, *71*, 1136-1145.

[14] J. Reedijk, *Proc. Natl. Acad. Sci. U.S.A.* **2003**, *100*, 3611-3616.

[15] B. Rosenberg, E. Renshaw, L. Vancamp, J. Hartwick and J. Drobnik, *J. Bacteriol.* **1967**, *93*, 716-721.

[16] W.H. Ang, M. Myint and S.J. Lippard, *J. Am. Chem. Soc.* **2010**, *132*, 7429-7435.

[17] J. Graham, M. Mushin and P. Kirkpatrick, *Nat. Rev. Drug Discovery* **2004**, *3*, 11-12.

[18] O. Rixe, W. Ortuzar, M. Alvarez, R. Parker, E. Reed, K. Paull and T. Fojo, *Biochem. Pharmacol.* **1996**, *52*, 1855-1865.

[19] H. S. Oberoia, N. V. Nukolovab, A. V. Kabanovb and T. K. Bronich, *Adv. Drug Deliv. Rev.* **2013**, *65*, 1667-1685.

[20] M.J. Clarke, F. Zhu and D.R. Frasca, *Chem. Rev.* **1999**, *99*, 2511-2533.

[21] Z. Almodares, S.J. Lucas, B.D. Crossley, A.M. Basri, C.M. Pask, A.J. Hebden, R.M. Phillips and P.C. McGowan, *Inorg. Chem.* **2014**, *53*, 727-736.

[22] C. Mu, S. W. Chang, K. E. Prosser, A. W. Y. Leung, S. Santacruz, T. Jang, J. R. Thompson, D. T. T. Yapp, J. J. Warren, M. B. Bally, T. V. Beischlag and C. J. Walsby, *Inorg. Chem.* **2016**, *55*, 177-190.

[23] Y. Geldmacher, M. Oleszak and W.S. Sheldrick, *Inorg. Chim. Acta* **2012**, *393*, 84-102.

[24] S. Top, I. Efremenko and M.N. Rager, *J. Inorg. Chem.* **2011**, *50*, 271-284.

[25] C-H. Leunga, H-J. Zhong, D.S-H. Chan and D-L. Ma, *Coord. Chem. Rev.* **2013**, 1764-1776.

[26] A. Taylor and N. Carmichael, *Cancer Studies* **1953**, *2*, 36-79.

[27] M.J. Cleare and P.C. Hydes, *Met. Ions Biol. Syst.* **1980**, *11*, 1-62.

[28] S. Schäfer, I. Ott, R. Gust and W.S. Sheldrick, *Eur. J. Inorg. Chem.* **2007**, *19*, 3034-3046.

[29] M.A. Nazif, R. Rubbiani, H. Alborzinia, I. Kitanovic, S. Wölfl, I. Ott and W.S. Sheldrick, *Dalton Trans.* **2012**, *41*, 5587-5598.

[30] Y. Geldmacher, K. Splith, I. Kitanovic, H. Alborzinia, S. Can, R. Rubbiani, M.A. Nazif, P. Wefelmeier, A. Prokop, I. Ott, S. Wölfl, I. Neundorf and W.S. Sheldrick, *J. Biol. Inorg. Chem.* **2012**, *17*, 631-646.

[31] L.C. Sudding, R. Payne, P. Govender, F. Edafe, C.M. Clavel, P.J. Dyson, B. Therrien and G.S. Smith, *J. Organomet. Chem.* **2014**, *774*, 79-85.

[32] R. Payne, P. Govender, B. Therrien, C.M. Clavel, P. J. Dyson and G. S. Smith, *J. Organomet. Chem.* **2013**, *729*, 20-27.

[33] É.A. Enyedy, O. Dömötör, C.M. Hackl, A.Roller, M.S. Novak, M.A. Jakupec, B.K. Keppler and W. Kandioller, *J. Coord. Chem.* **2015**, *68*, 1583-1601.

[34] L. Helm and A.E. Merbach, *Coord. Chem. Rev.* **1999**, *187*, 151-181.

[35] A. Wilbuer, D.H. Vlecken, D.J. Schmitz, K. Kraling, K. Harms, C.P. Bagowski and E. Meggers, *Angew. Chem. Int. Ed.* **2010**, *49*, 3839-3842.

[36] Z. Liu, A. Habtemariam, A.M. Pizarro, S.A. Fletcher, A. Kisova, O. Vrana, L. Salassa, P.C.A. Bruijnincx, G.J. Clarkson, V. Brabec and P.J. Sadler, *J. Med. Chem.* **2011**, *54*, 3011-3026.

[37] Z. Liu, L. Salassa, A. Habtemariam, A.M. Pizarro, G.J. Clarkson and P.J. Sadler, *Inorg. Chem.* **2011**, *50*, 5777-5783.

[38] S. Schäfer and W.S. Sheldrick, *J. Organomet. Chem.* **2007**, *682*, 1300-1309.

[39] U. Sliwinska, F.P. Pruchnik, S. Ulaszewski, M. Latocha and D. Nawrocka-Musial, *Polyhedron* **2010**, *29*, 1653-1659.

[40] S.K. Leung, K.Y. Kwok, K.Y. Zhang and K.K.W. Lo, *Inorg. Chem.* **2010**, *49*, 4984-4995.

[41] M. Ali Nazif, J.A. Bangert, I. Ott, R. Gust, R. Stoll and W.S. Sheldrick, *J. Inorg. Biochem.* **2009**, *103*, 1405-1414.

[42] H. Amouri, J. Moussa, A.K. Renfrew, P.J. Dyson, M.N. Rager and L.M. Chamoreau, *Angew. Chem. Int. Ed.* **2010**, *49*, 7530-7533.

[43] S. Wirth, C. Rohbogner, M. Cieslak, J. KazmierczakBaranska, S. Donevski, B. Nawrot and I.P. Lorenz, *J. Biol. Inorg. Chem.* **2010**, *15*, 429-440.

[44] A. Casini, F. Edafe, M. Erlandsson, L. Gonsalvi, A. Ciancetta, N. Re, A. Ienco, L. Messori, M. Peruzzini and P.J. Dyson, *Dalton Trans.* **2010**, *39*, 5556-5563.

[45] M. Gras, B. Therrien, G. Süss-Fink, A. Casini, F. Edafe and P.J. Dyson, *J. Organomet. Chem.* **2010**, *695*, 1119-1125.

[46] C.G. Hartinger, *Angew. Chem. Int. Ed.* **2010**, *49*, 8304-8305.

[47] M. Kalidasan, S. Forbes, Y. Mozharivskyj, M. Ahmadi, Z. Ahmadihosseini, R.M. Phillips and M.R. Kollipara, *Inorg. Chim. Acta* **2014**, *421*, 349-358.

[48] Z. Liu, A. Habtemariam, A.M. Pizarro, G.J. Clarkson and P.J. Sadler, *Organometallics* **2011**, *30*, 4702-4710.

[49] N.R. Palepu, S.L. Nongbri, J.R. Premkumar, A.K. Verma, K. Bhattacharjee, S.R. Joshi, S. Forbes, Y. Mozharivskyj, R. Thounaojam, K. Aguan and M.R. Kollipara, *J. Biol. Inorg. Chem.* **2015**, *20*, 619-638.

[50] M.U. Raja, J. Tauchman, B. Therrien, G. Süss-Fink, T. Riedel and P.J. Dyson, *Inorg. Chim. Acta* **2014**, *409*, 479-483.

[51] R.K. Gupta, R. Pandey, G. Sharma, R. Prasad, B. Koch, S. Srikrishna, P.Z. Li, Q. Xu and D.S. Pandey, *Inorg. Chem.* **2013**, *52*, 3687-3698.

[52] S.J. Lucas, R.M. Lord, R.L. Wilson, R.M. Phillips, V. Sridharana and P.C. McGowan, *Dalton Trans.* **2012**, *41*, 13800-13802.

[53] S. Betanzos-Lara, Z. Liu, A. Habtemariam, A.M. Pizarro, B. Qamar and P.J. Sadler, *Angew. Chem. Int. Ed.* **2012**, *51*, 3897-3900.

[54] M.G. Mendoza-Ferri, C.G. Hartinger, M.A. Mendoza, M. Groessl, A.E. Egger, R.E. Eichinger, J.B. Mangrum, N. P. Farrell, M. Maruszak, P.J. Bednarski, F. Klein, M.A. Jakupec, A.A. Nazarov, K. Severin and B.K. Keppler, *J. Med. Chem.* **2009**, *52*, 916-925.

[55] B.T. Loughrey, P.C. Healy, P.G. Parsons and M.L. Williams, *Inorg. Chem.* **2008**, *47*, 8589-8591.

[56] R.E. Aird, J. Cummings, A.A. Ritchie, M. Muir, R.E. Morris, H. Chen, P.J. Sadler and D.I. Jodrell, *Br. J. Cancer* **2002**, *86*, 1652-1657.

[57] T.J. Kealy and P.L. Pauson, *Nature* **1951**, *168*, 1039-1040.

[58] S.A. Miller, J.A. Tebboth and J.F. Tremaine, *J. Chem. Soc.* **1952**, 632-635.

[59] G. Wilkinson, M. Rosenblum, M.C. Whiting and R.B. Woodward, *J. Am. Chem. Soc.* **1952**, *74*, 2125-2126.

[60] E.O. Fischer and W. Pfab, *Z. Naturforsch.* **1952**, *7*, 377-379.

[61] L. Gmelin, *Eisen-Organische Verbindungen: Ferrocen 1: Ferrocen und einkernige monosubstituierte Derivate mit Substituenten aus C, H und/oder Halogen*, Springer-Verlag, Berlin, Germany, **1974**,

[62] S.S. Braga and A.M.S. Silva, *Organometallics* **2013**, *32*, 5626-5639.

[63] C. Ornelas, *New J. Chem.* **2011**, *35*, 1973-1985.

[64] A.C. de Oliveira, E.G. da Silva, D.D. Rocha, E.A. Hillard, P. Pigeon, G. Jaouen, F.A.R. Rodrigues, F.C. de Abreu, F. da Rocha Ferreira, M.O.F. Goulart and L.V. Costa-Lotufo, *ChemMedChem* **2014**, *9*, 2580-2586.

[65] M. Görmen, P. Pigeon, S. Top, E.A. Hillard, M. Huch, C.G. Hartinger, F. de Montigny, M.A. Plamont, A. Vessires and G. Jaouen, *ChemMedChem* **2010**, *5*, 2039-2050.

[66] D. Nieto, A.M. Gonzalez-Vadillo, S. Brauna, C J. Pastor, C. Rios-Luci, L.G. Leon, J.M. Padron, C. Navarro-Ranninger and I. Cuadrado, *Dalton Trans.* **2012**, *41*, 432-441.

[67] P. Govender, H. Lemmerhirt, A.T. Hutton, B. Therrien, P.J. Bednarski and G.S. Smith, *Organometallics* **2014**, *33*, 5535-5545.

[68] M. Pongratz, P. Schluga, M.A. Jakupec, V.B. Arion, C.G. Hartinger, G. Allmaier and B.K.J. Keppler, *Anal. At. Spectrom.* **2004**, *19*, 46-51.

[69] P. Schluga, C.G. Hartinger, A. Egger, E. Reisner, M. Galanski, M.A. Jakupec and B.K. Keppler, *Dalton Trans.* **2006**, *14*, 1796-1802.

[70] K.J. Kilpin and P.J. Dyson, *Chem. Sci.* **2013**, *4*, 1410-1419.

[71] E. Meggers, *Angew. Chem. Int. Ed.* **2011**, *50*, 2442-2448.

[72] U. Schatzschneider and N. Metzler-Nolte, *Angew. Chem. Int. Ed.* **2006**, *45*, 1504-1507.

[73] G. Sava, E. Alessio, A. Bergamo and G. Mestroni, *Topics in Biological Inorganic Chemistry, ed. M.J. Clarke and P.J. Sadler, Springer-Verlag, Berlin* **1999**, *vol. 1*, p. 143.

[74] A. Bergamo, S. Zorzet, B. Gava, A. Sorc, E. Alessio, E. Iengo and G. Sava, *Anti-Cancer Drugs* **2000**, *11*, 665-672.

[75] J.M. Rademaker-Lakhai, D. Van Den Bongard, D. Pluim, J.H. Beijnen and J.H.M. Schellens, *Clin. Cancer Res.* **2004**, *10*, 3717-3727.

[76] M. Groessl, C.G. Hartinger, K. Polec-Pawlak, M. Jarosz, P.J. Dyson and B.K. Keppler, *Chem. Biodiversity* **2008**, *5*, 1609-1614.

[77] M.J. Clarke, *Coord. Chem. Rev.* **2003**, *236*, 209-233.

[78] M.J. Clarke, *Coord. Chem. Rev.* **2002**, *232*, 69-93.

[79] A.D. Kelman, M.J. Clake, S.D. Edmonds and H.J. Peresie, *J. Clin. Hematol. Oncol.* **1977**, *7*, 274-288.

[80] R. Trondl, P. Heffeter, C.R. Kowol, M.A. Jakupec, W.Berger and B.K. Keppler, *Chem. Sci.* **2015**, *5*, 2925-2932.

[81] N.R. Dickson, S.F. Jones, H.A. Burris, R.K. Ramanathan, G.J. Weiss, J.R. Infante, J.C. Bendell, W.McCulloch and D.D. Von Hoff, *J. Clin. Oncol.* **2011**, *29*, Suppl. Abstr 2607.

[82] F. Kratz, B.K. Keppler, M. Hartmann, L. Messori and M.R. Berger, *Met.-Based Drugs* **1996**, *3*, 15-23.

[83] M. Sulyok, S. Hann, C.G. Hartinger, B.K. Keppler, G. Stingeder and G. Koellensperger, *J. Anal. At. Spectrom.* **2005**, *20*, 856-863.

[84] F. Kratz and B. Elsadek, *J. Control. Release* **2011**, *161*, 1-16.

[85] P. Heffeter, B. Atil, K. Kryeziu, D. Groza, G. Koellensperger, W. Körner, U. Jungwirth, T. Mohr, B.K. Keppler and W. Berger, *Eur. J. Cancer* **2013**, *49*, 3366-3375.

[86] C.G. Hartinger, M. Groessl, S.M. Meier, A. Casini and P.J. Dyson, *Chem. Soc. Rev.* **2013**, *42*, 6186-6199.

[87] G.S. Smith and B. Therrien, *Dalton Trans.* **2011**, *40*, 10793-10800.

[88] W.H. Ang and P. J. Dyson, *Eur. J. Inorg. Chem.* **2006**, 4003-4018.

[89] N.P.E. Barry and P.J. Sadler, *Chem. Commun.* **2013**, *49*, 5106-5131.

[90] C.G. Hartinger, N. Metzler-Nolte and P.J. Dyson, *Organometallics* **2012**, *31*, 5677-5685.

[91] A.F.A. Peacock and P.J. Sadler, *Chem. Asian J.* **2008**, *3*, 1890-1899.

[92] A.L. Noffke, A. Habtemariam, A.M. Pizarro and P.J. Sadler, *Chem. Commun.* **2012**, *48*, 5219-5246.

[93] G. Sava, A. Bergamo and P. J. Dyson, *Dalton Trans.* **2011**, *40*, 9069-9075.

[94] Y.K. Yan, M. Melchart, A. Habtemariam and P.J. Sadler, *Chem. Commun.* **2005**, *38*, 4764-4776.

[95] C.S. Allardyce, A. Dorcier, C. Scolaro and P.J. Dyson, *Appl. Organomet. Chem.* **2005**, *19*, 1-10.

[96] C.G. Hartinger and P.J. Dyson, *Chem. Soc. Rev.* **2009**, *38*, 391-401.

[97] F. Wang, H. Chen, J.A. Parkinson, P. del S. Murdoch and P.J. Sadler, *Inorg. Chem.* **2002**, *41*, 4509-4523.

[98] H. Chen, J.A. Parkinson, R.E. Morris and P.J. Sadler, *J. Am. Chem. Soc.* **2003**, *125*, 173-186.

[99] A.F.A. Peacock, A. Habtemariam, R. Fernandez, V. Walland, F.P.A. Fabbiani, S. Parsons, R.E. Aird, D.I. Jodrell and P.J. Sadler, *J. Am. Chem. Soc.* **2006**, *128*, 1739-1748.

[100] T. Bugarcic, O. Nováková, A. Halámiková, L. Zerzánková, O. Vrána, J. Kašpárková, A. Habtemariam, S. Parsons, P.J. Sadler and V. Brabec, *J. Med. Chem.* **2008**, *51*, 5310-5319.

[101] T. Bugarcic, A. Habtemariam, J. Stepankova, P. Heringova, J. Kasparkova, R.J. Deeth, R.D.L. Johnstone, A. Prescimone, A. Parkin, S. Parsons, V. Brabec and P.J. Sadler, *Inorg. Chem.* **2008**, *47*, 11470-11486.

[102] P. J. Dyson and G. Sava, *Dalton Trans.* **2006**, 1929–1933.

[103] W.H. Ang, E. Daldini, C. Scolaro, R. Scopelliti, L. Juillerat-Jeannerat and P.J. Dyson, *Inorg. Chem.* **2006**, *45*, 9006-9013.

[104] D.V. Deubel and J.K.C. Lau, *Chem. Commun.* **2006**, 2451-2453.

[105] C. Gossens, A. Dorcier, P.J. Dyson and U. Rothlisberger, *Organometallics* **2007**, *26*, 3969-3975.

[106] A.K. Renfrew, R. Scopelliti and P.J. Dyson, *Inorg. Chem.* **2010**, *49*, 2239-2246.

[107] A.K. Renfrew, L. Juillerat-Jeanneret and P. J. Dyson, *J. Organomet. Chem.* **2011**, *696*, 772-779.

[108] W.H. Ang, A. Casini, G. Sava and P.J. Dyson, *J. Organomet. Chem.* **2011**, *696*, 989-998.

[109] R.E. Morris, R.E. Aird, P.d.S. Murdoch, H. Chen, J. Cummings, N.D. Hughes, S. Pearsons, A. Parkin, G. Boyd, D.I. Jodrell and P.J. Sadler, *J. Med. Chem.* **2001**, *44*, 3616-3621.

[110] C. Scolaro, A. Bergamo, L. Brescacin, R. Delfino, M. Cocchietto, G. Laureneczy, T.J. Geldbach, G. Sava and P.J. Dyson, *J. Med. Chem.* **2005**, *48*, 4161-4171.

[111] C. Scolaro, T.J. Geldbach, S. Rochat, A. Dorcier, C. Gossens, A. Bergamo, M. Cocchietto, I. Tavernelli, G. Sava, U. Rothlisberger and P.J. Dyson, *Organometallics* **2006**, *25*, 756-765.

[112] P.J. Dyson, *Chimia* **2007**, *61*, 698-703.

[113] A.K. Renfrew, A.D. Phillips, E. Tapavicza, R. Scopelliti, U. Rothlisberger and P.J. Dyson, *Organometallics* **2009**, *28*, 5061-5071.

[114] M. Hanif, A.A. Nazarov, A. Legin, M. Groessl, V.B. Ario, M.A. Jakupec, Y.O. Tsybin, P.J. Dyson, B.K. Keppler and C.G. Hartinger, *Chem. Commun.* **2012**, *48*, 1475-1477.

[115] C. Billecke, S. Finniss, L. Tahash, C. Miller, T. Mikkelsen, N. P. Farrell and O. Bogler, *Neuro-Oncol.* **2006**, *8*, 215-226.

[116] B.A. Jansen, J. van de Zwan, J. Reedijk, H. de Dulk and J. Brouwer, *Eur. J. Inorg. Chem.* **1999**, *9*, 1429-1433.

[117] F. Giannini, J. Furrer, A-F. Ibao, G. Süss-Fink, B. Therrien, O. Zava, M. Baquie, P. Dyson and P. Stepnicka, *J. Biol. Inorg. Chem.* **2012**, *17*, 951-960.

[118] F. Giannini, L. E. H. Paul, J. Furrer, B. Therrien and G. Süss-Fink, *New J. Chem.* **2013**, *37*, 3503-3511.

[119] J. Furrer and G. Süss-Fink, *Coord. Chem. Rev.* **2016**, *309*, 36-50.

[120] P. Tomsik, D. Muthna, M. Rezacova, S. Micuda, J. Cmielova, M. Hroch, R. Endlicher, Z. Cervinkova, E. Rudolf, S. Hann, D. Stibal, B. Therrien and G. Suss-Fink, *J. Organomet. Chem.* **2015**, *782*, 42-51.

[121] H. Chen, J.A. Parkinson, O. Novakova, J. Bella, F. Y. Wang, A. Dawson, R. Gould, S. Parsons, V. Brabec and P.J. Sadler, *Proc. Natl. Acad. Sci. U. S. A.* **2003**, *100*, 14623-14628.

[122] M.G. Mendoza-Ferri, C.G. Hartinger, R.E. Eichinger, N. Stolyarova, K. Severin, M.A. Jakupec, A.A. Nazarov and B.K. Keppler, *Organometallics* **2008**, *27*, 2405-2407.

[123] SEER Cancer Statistics Factsheets: Ovary Cancer. National Cancer Institute, Retrieved 4/7/2016, from http://www.ovariancancer.org/about/statistics/

Chapter 2: Synthesis, Characterization and Antitumor Activity of Trinuclear Rh(III), Ir(III) and Ru(II) Functionalized Aromatic Esters

2. Introduction

Ester functional groups increase the lipophilic nature of compounds and can promote the transport of the molecule through membranes.[1-2] Because of this, esters are important within the field of medicinal chemistry.

There are several examples of bioactive compounds which contain ester functionality. These include bezafibrate (Figure 2.1a), an oral hypolipidemic agent,[3] derivatives of cinnamic acid (Figure 2.1b), which exhibit *in vitro* antiinflammatory effects[4] and esters prepared from 4-acetyl-2-(2-hydroxyethyl)-5,6-bis(4-chlorophenyl)-2H-pyridazin-3-one (Figure 2.1c) used as antihypertensive agents.[5] Reports show that trivanillic ester polyphenols (Figure 2.1d) exhibit cytostatic biological properties and have the ability to inhibit kinase enzymes in tumors resistant to pro-apoptotic stimuli.[6]

Large macromolecular molecules containing ester moieties have been reported to act as micelles or in conjuction with coordinated known drugs to show cytotoxicity.[7-11] These systems result in enhanced targeting of tumors and improved efficiency of the treatment.[12-14] Polyester dendrimers display excellent advantages as drug delivery vehicles due to their low toxicity and demonstrate biodegradability.[15]

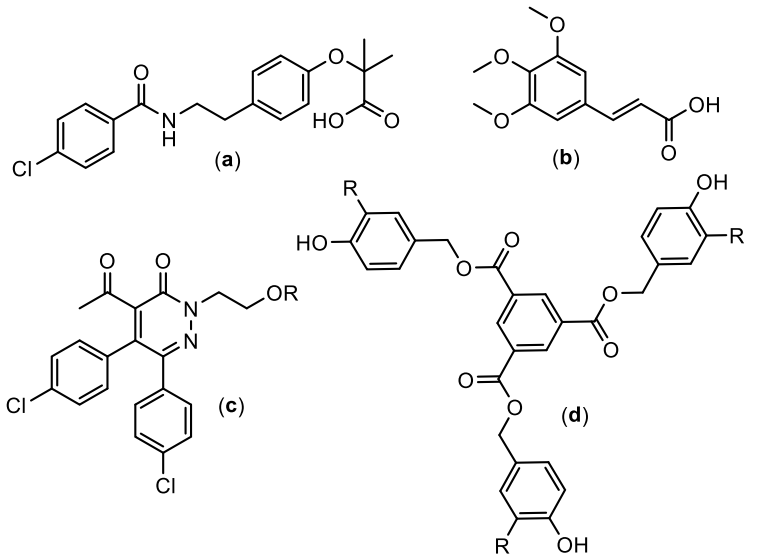

Figure 2.1*: Aromatic ester precursors bezafibrate (**a**) and cinnamic acid (**b**), ester pyridazin derivatives (**c**) and cytostatic trivanillates (**d**) studied for different bioactivities.*

Reports showing the incorporation of ruthenium-arene to mononuclear or dinuclear esters provide evidence of their anticancer activity. A RAPTA complex (Figure 2.2 left) with an ethacrynoate ester as part of the arene was found to have superior activity in inhibition of glutathione-S-transferases than the Ru complex and the ethacrynic acid.[16-18] Hu and co-workers prepared ruthenium-arene complexes with 5-fluorouracil-1-methyl isonicotinate (Figure 2.2 right) which was moderatively more active against the human hepatocellular carcinoma cells, BEL-7402, than 5-fluorouracil.[19]

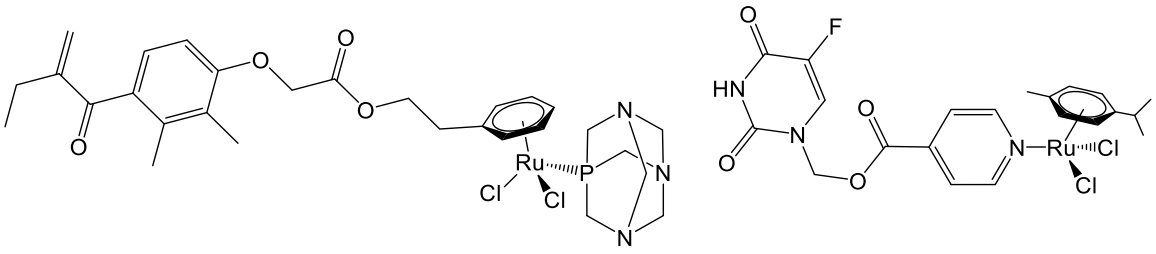

Figure 2.2*: RAPTA complex with ethacrynate derivatized arene (left) and 5-fluorouracil-1-methyl isonicotinate ruthenium-arene complex (right).*

Dyson and co-workers prepared mono- and dinuclear ferrocenyl pyridine based linker dinuclear complexes $[Ru(\eta^6\text{-arene})Cl_2]_2(NC_5H_4OOC\text{-}C_5H_4FeC_5H_4\text{-}COOC_5H_4N)$, where arene

= hexamethylbenzene or *p*-cymene (Figure 2.3), which were twice as active as their mononuclear analogues.[20]

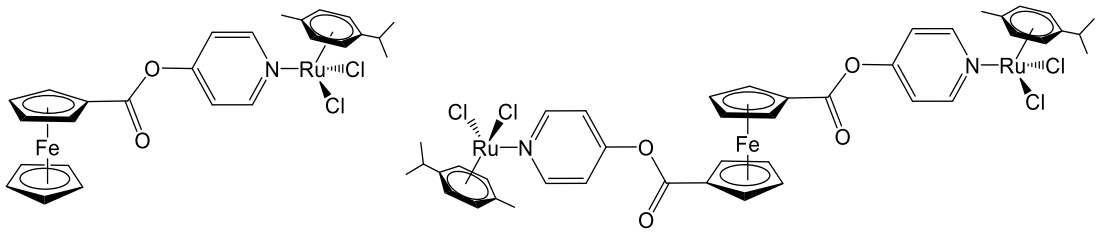

***Figure 2.3**: Mono- (left) and dinuclear (right) pyridyl ester ruthenium-arene complexes.*

Smith and co-workers prepared a series of di- and tripyridyl ester rhodium(III), iridium(III) and ruthenium(II)-arene complexes (Figure 2.4). The free ligands and the dinuclear systems were inactive against human ovarian cisplatin sensitive (A2780) and cisplatin resistant cancer cells (A2780*cis*R), while the trinuclear complexes showed moderate activity and selectivity, by evaluation against human embryonic kidney (HEK) cells.[21]

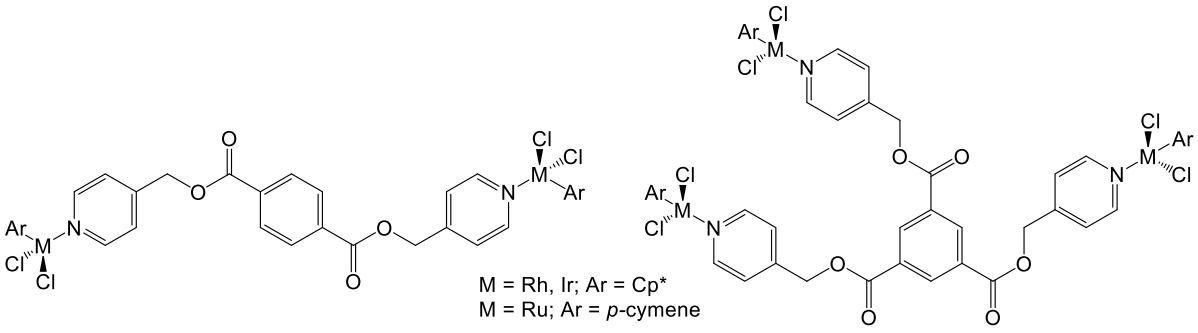

***Figure 2.4**: Di- (left) and trinuclear (right) pyridyl ester rhodium(III), iridium(III) and ruthenium(II)-arene complexes.*

In this chapter, the synthesis, characterization and biological evaluation of new trinuclear ester-containing rhodium(III), iridium(III) and ruthenium(II)-arene complexes is described. Mononuclear analogues were also prepared for comparison. Spectroscopic and analytical techniques were used to support and confirm the suggested structures, and these are discussed herein, along with the biological activity of these complexes.

2.1. Synthesis and Characterization of *C,N*-Benzaldimine, *N,N*-Pyridylimine and *N,O*-Salicylaldimine Ligands

The Schiff base products 4-(benzylideneamino)benzyl alcohol, **2.1**,[22] and 4-(salicylideneamino)benzyl alcohol, **2.3**,[23] were synthesized using known methods. 4-(Pyridylideneamino)benzyl alcohol, **2.2**, was prepared by reacting 4-aminophenylmethanol with 2-pyridinecarboxaldehyde (Scheme 2.1).

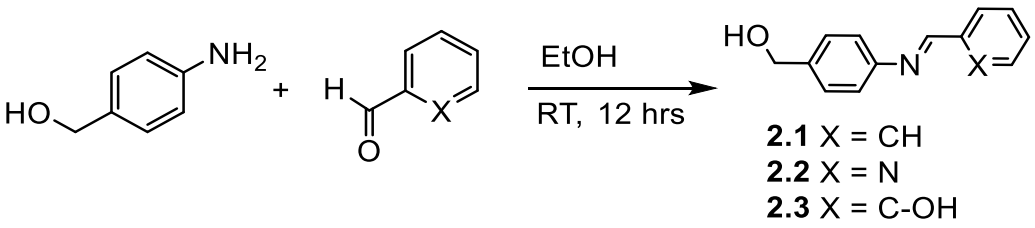

Scheme 2.1 *Synthesis of C,N-benzaldimine, N,N-pyridylimine and N,O-salicylaldimine ligands* ***2.1-2.3****.*

The reactants were stirred at room temperature for 12 hours in ethanol. Ligand **2.2** was precipitated using hexane and isolated as a pale brown solid in 86% yield. **2.2** is soluble in most organic solvents such as dichloromethane, chloroform, methanol, ethanol and dimethylsulfoxide. Spectroscopic (^{1}H NMR, ^{13}C{^{1}H} NMR and FT-IR spectroscopy) and analytical data (elemental analysis and mass spectrometry) confirmed the structural integrity of **2.2**.

The ^{1}H NMR and ^{13}C{^{1}H} NMR spectra of **2.2** were recorded in deuterated chloroform ($CDCl_3$) and were comparable with the benzaldimine[22] and salicylaldimine[23] analogues.

The ^{1}H NMR spectrum of **2.2** (Figure 2.5) shows a downfield shift in the signals assigned for the aromatic phenyl C-H protons from δ 6.60 ppm and δ 7.09 ppm to δ 7.21 ppm and δ 7.35 ppm respectively, and resonate in a similar range to **2.1**[22] and **2.3**,[23] as reported in literature. This downfield shift may be as a result of the electron withdrawing effects of the newly formed imine moiety. The pyridyl protons resonate in the aromatic region, δ 7.40 ppm to δ 8.72 ppm. The signal assigned to the imine proton appears as a singlet at δ 8.60 ppm (Table 2.1), while the doublet at δ 8.72 ppm is assigned for the proton *para* to the pyridyl nitrogen. The signal for the two aliphatic protons appears at δ 4.74 ppm.

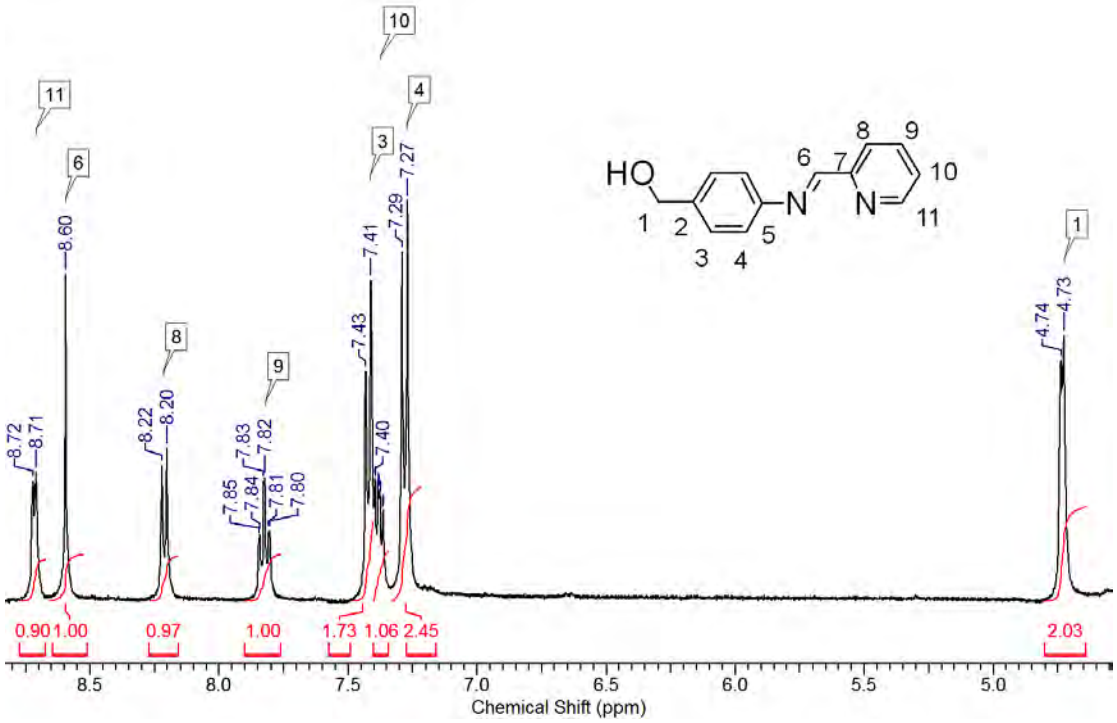

Figure 2.5 *^{1}H NMR spectrum of N,N-pyridylimine ligand **2.2** in $CDCl_3$.*

The $^{13}C\{^{1}H\}$ NMR spectrum of **2.2** displayed the expected carbon signals. Signals for the aromatic carbons appear in the region δ 154 – 121 ppm and a signal at δ 160.42 ppm is assigned as the imine carbon. The aliphatic carbon results in a signal at δ 64.83 ppm (Table 2.1).

The use of infrared (FT-IR) spectroscopy confirmed that the Schiff base product **2.2** did form and this was identified by the presence of an stretching vibration at 1630 cm^{-1}, which is assigned to the newly formed $C{=}N_{imine}$ bond (Table 2.1). Band are observed at 1583 cm^{-1} due to the $C{=}N_{pyridyl}$ stretching and at 1021 cm^{-1} for the C-O bond vibration.

Table 2.1 *Selected spectroscopic and analytical data for N,N-pyridylimine ligand **2.2**.*

Compound	^{1}H NMR (Imine, -CH_2) [ppm][a]	$^{13}C\{^{1}H\}$ NMR (Imine, -CH_2) [ppm][a]	IR (Imine) [cm^{-1}][b]	MS [*m/z*][c]
2.2	8.60, 4.73	160.42, 64.83	1630	$[M]^+$ = 212.07

[a]Recorded in $CDCl_3$; [b]Recorded as KBr pellet; [c]EI-MS.

Electron impact mass spectrometry (EI-MS) analysis of **2.2** reveals a base peak for the product formed at *m/z* 212.07 $[M]^+$ (Table 2.1). After extensive drying under vacuum elemental analysis (EA) data for **2.2** found calculated experimental data within acceptable limits.

Next, the trimeric ester-containing ligands **2.4-2.6** were prepared by reaction of **2.1-2.3** with trimesoyl chloride in the presence of the base trimethylamine, to mop up hydrochloric acid formed, in dichloromethane (Scheme 2.2). All three ligands were isolated in high yields as air and moisture stable solids, which are soluble in most organic solvents.

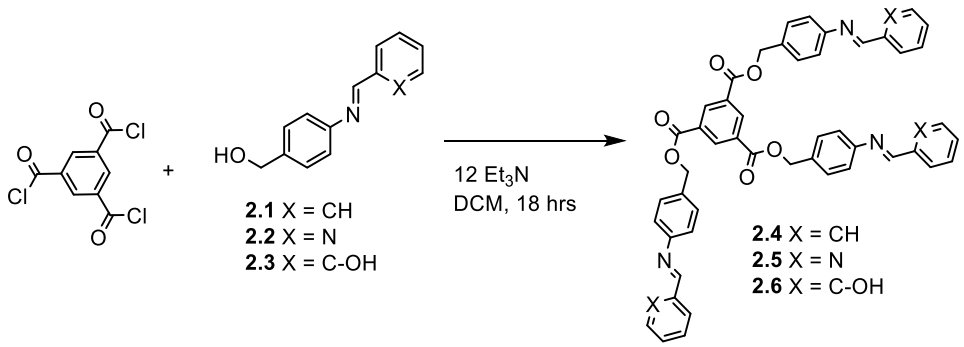

Scheme 2.2 *Synthesis of trinuclear C,N-benzaldimine, N,N-pyridylimine and N,O-salicylaldimine ester ligands* ***2.4-2.6****.*

The ^{1}H NMR and $^{13}C\{^1H\}$ NMR spectra of **2.4-2.6** were recorded in $CDCl_3$ and notable shifts are evident of the formation of the ester moiety. Upon formation of the ester functional group the signals observed in the ^{1}H NMR spectrum for the aliphatic protons shift downfield to δ 5.37 – 5.42 ppm from δ 4.65 – 4.83 ppm. The presence of the benzene core is confirmed by the presence of a sharp singlet in the region δ 8.85 – 8.95 ppm (Table 2.1), due to the strong electron withdrawing effect of the ester moieties. The signals for the phenyl and benzyl or pyridyl or salicyl protons remain relatively unchanged.

A deshielding effect is also observed in the $^{13}C\{^1H\}$ NMR spectra of **2.4-2.6** where signals for the aliphatic carbons shift to δ 66.94 – 67.91 ppm from ca. δ 65 ppm for **2.1-2.3**. The most deshielded signals at δ 164.58 – 165.25 ppm are attributed to the carbonyl carbon of the newly formed ester moiety. The presence of the benzene core result in resonance signals at δ 130.25 – 131.46 ppm and δ 133.10 – 134.80 ppm (Table 2.2). The signals for the phenyl, imine and benzyl or pyridyl or salicyl carbons remain relatively unchanged.

Table 2.2 *Selected spectroscopic and analytical data for trinuclear esters* ***2.4-2.6****.*

Compound Number	^{1}H NMR (-CH_2, core) [ppm][a]	^{13}C{^{1}H} NMR (core) [ppm][a]	FT-IR [C-C(O)-O, C=O] [cm^{-1}][b]	EI-MS [M+3H]$^{3+}$ [*m/z*][c]
2.4	5.41, 8.92	130.25, 133.10	1231, 1724	266.15
2.5	5.45, 8.95	130.43, 134.12	1324, 1719	265.28
2.6	5.37, 8.85	131.46, 134.80	1232, 1728	280.10

[a]Recorded in $CDCl_3$; [b]Recorded as KBr pellet; [c]ESI-MS.

FT-IR spectroscopy reveals that the $\nu_{C=O}$ bond vibration, of the esters of **2.4-2.6**, is in the region 1719 – 1728 cm^{-1}. The C-C(O)-O bond within the ester results in a vibration which is assigned to strong absorption bands which are observed around 1231 – 1234 cm^{-1}. No shift is observed in the absorption band associated with the $C=N_{imine}$ or $C=N_{pyr}$ bond vibration upon esterification.

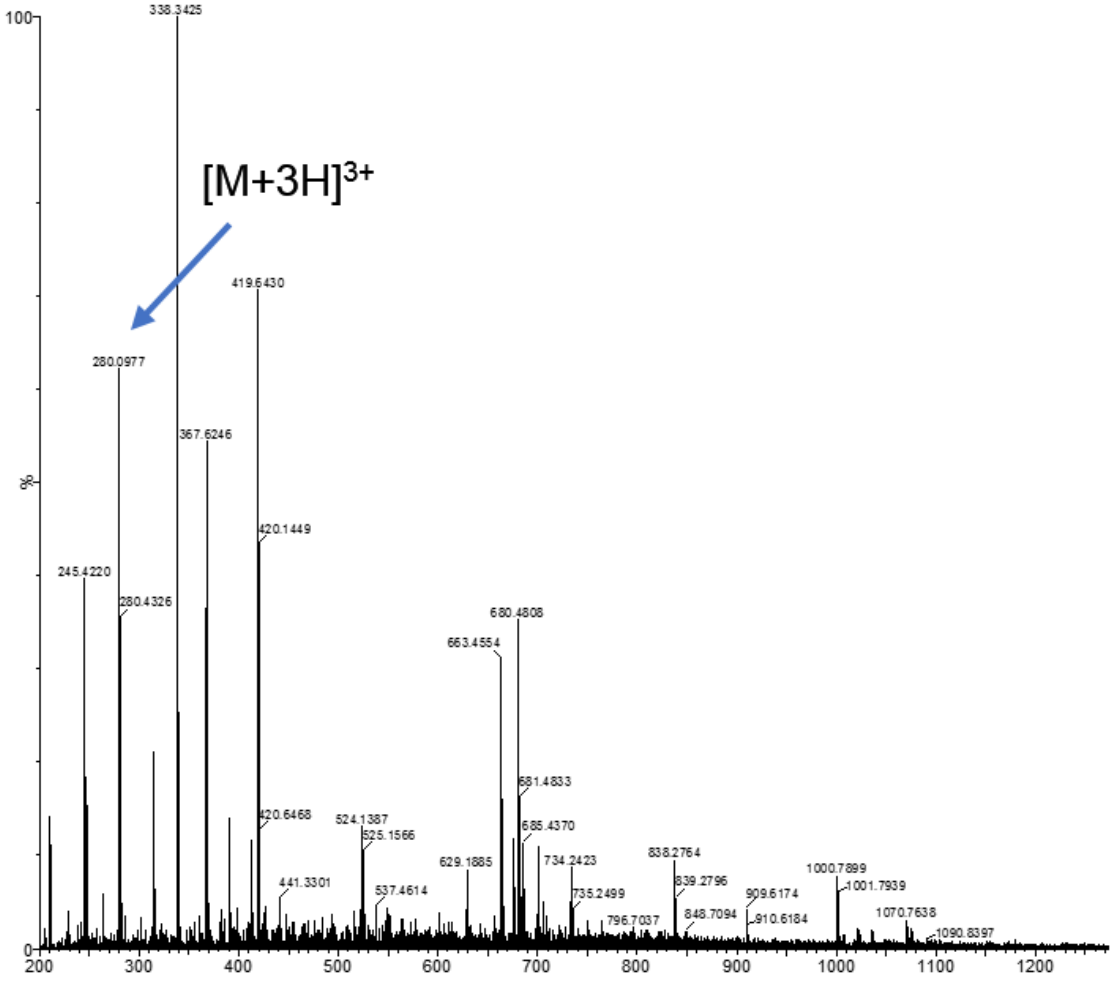

Figure 2.6 *ESI mass spectrum of trinuclear N,O-salicylaldimine ligand* ***2.6****.*

Further evidence for the formation of the ester and trimeric nature of **2.4-2.6** is supported by electrospray ionization mass spectrometry (ESI-MS), which shows peaks assigned as the adduct $[M+3H]^{3+}$ for each ligand. For **2.4** *m/z* = 266.15, **2.5** *m/z* = 265.28 and **2.6** *m/z* = 280.10 (Figure 2.6). After extensive drying under vacuum, EA data for **2.4-2.6** showed calculated experimental data within acceptable limits.

2.2. Synthesis and Characterization of *C,N*-Benzaldiminato, *N,N*-Pyridylimine and *N,O*-Salicylaldiminato PGM Complexes

Ligands **2.1-2.6** were reacted with the metal-containing precursors, dichloro(pentamethylcyclopentadienyl)rhodium(III) dimer, dichloro(pentamethylcyclopentadienyl)iridium(III) dimer or dichloro(*p*-cymene)ruthenium(II) dimer to yield the corresponding mononuclear complexes **2.7-2.14** (Scheme 2.3) or trinuclear complexes **2.15-2.22** (Scheme 2.4).

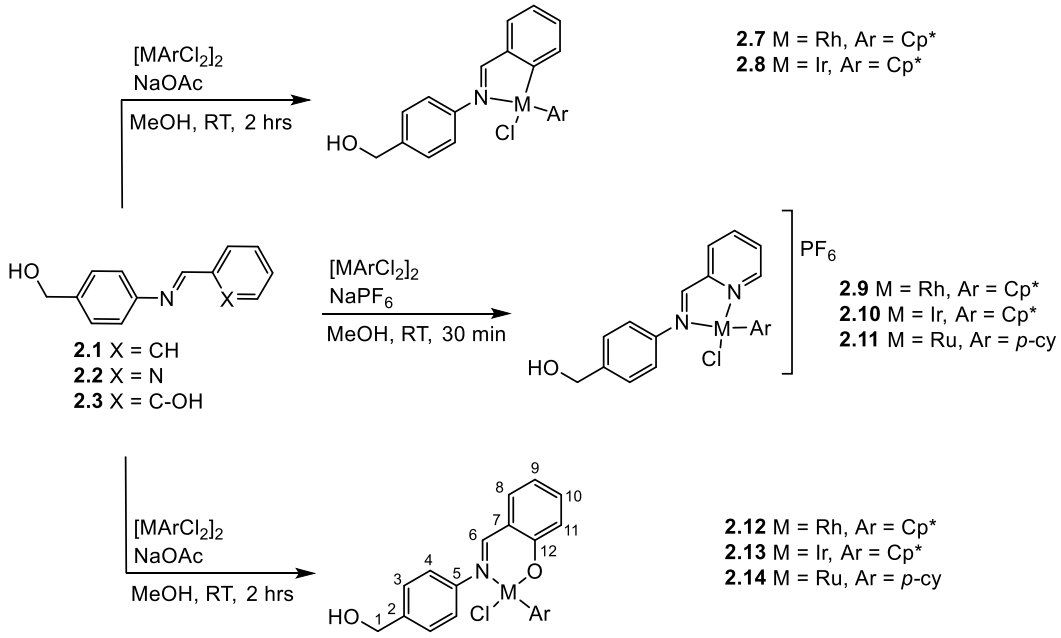

Scheme 2.3 *Synthesis of mononuclear C,N-benzaldiminato, N,N-pyridylimine and N,O-salicylaldiminato complexes* ***2.7-2.14****.*

The complexes **2.7-2.14** were prepared using similar methods. For the *N,N*-bidentate complexes the appropriate ligand and dimer were stirred in methanol or a mixture of ethanol and dichloromethane followed by addition of sodium hexafluorophosphate to precipitate the

cationic products **2.9-2.11** and **2.17-2.19**. For the *C,N*- and *N,O*-bidentate complexes, the appropriate ligand and sodium acetate were stirred in methanol or a mixture of ethanol and dichloromethane followed by addition of the appropriate dimer. The resulting products **2.7, 2.8, 2.12-2.16** and **2.20-2.22** were precipitated from the reaction using diethyl ether. Complexes **2.7-2.22** were isolated as air and moisture stable yellow, orange or red solids in moderate to high yields and are soluble in most organic solvents.

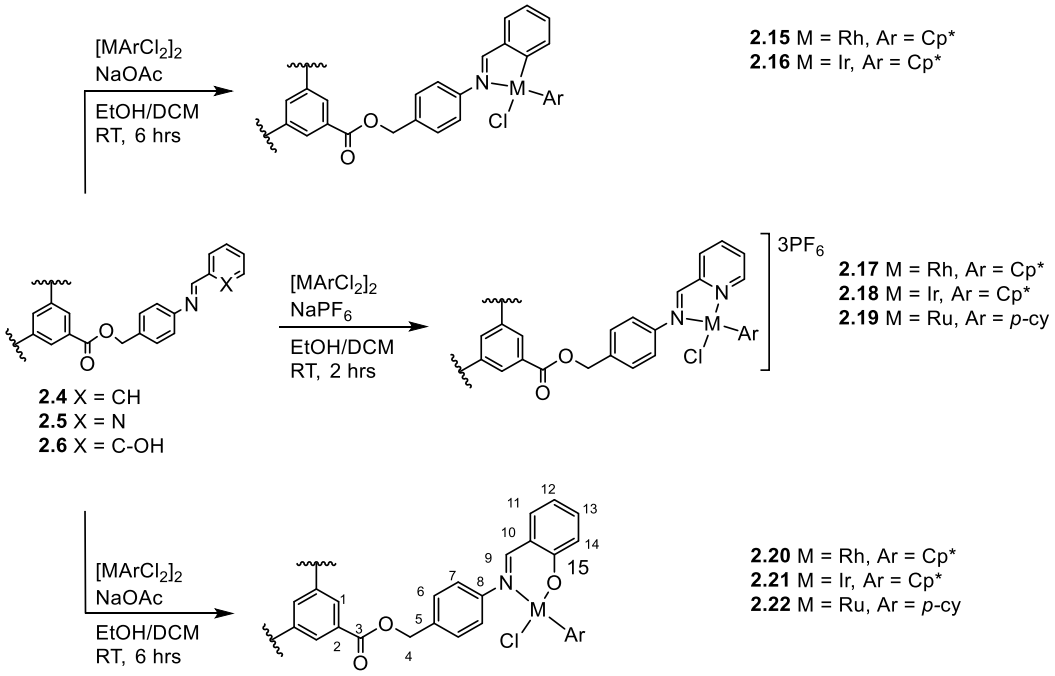

Scheme 2.4 *Synthesis of trinuclear C,N-benzaldiminato, N,N-pyridylimine and N,O-salicylaldiminato complexes* ***2.15-2.22****.*

The mono- and trinuclear *C,N*-cyclometalated ruthenium(II) complexes were unable to be isolated. Various solvents including methanol, ethanol and dichloromethane were used with a number of bases, such as sodium and potassium acetate. However, the red solid obtained revealed mixtures of unreacted ligand **2.1** or **2.4** and dichloro(*p*-cymene)ruthenium(II) dimer. Difficulty in obtaining *C,N*-cyclometalated ruthenium(II) complexes has been reported.[24-25]

Complexes **2.7-2.22** are new compounds and were fully characterized with several spectroscopic and analytical techniques, including X-ray crystallography. Evidence for bidentate coordination occurring via the imine nitrogen and the cyclometalated benzyl carbon or the pyridyl nitrogen or the phenolic oxygen to the metal arene were obtained from the NMR and FT-IR analyses.

The ^{1}H NMR spectra of complexes **2.7-2.22** were recorded in $CDCl_3$, with the exception of the *N,N*-pyridylimine complexes, **2.9-2.11** and **2.17-2.19**, which were recorded in deuterated acetone, $(CD_3)_2CO$, and show relevant peaks for the proposed structures.

The ^{1}H NMR spectra for the *C,N*-benzaldiminato complexes **2.7**, **2.8**, **2.15** and **2.16** all show an upfield shift of the imine proton from ca. δ 8.92 ppm to ca. δ 8.16 ppm for the rhodium(III) or δ 8.33 ppm for the iridium(III) complexes (Table 2.3). Metal coordination *via* the imine nitrogen leads to less electron density in the hydrogen of the adjacent carbon because of back bonding between the empty π* orbital of the imine nitrogen and a full d-orbital of the bonded metal. The $^{13}C\{^{1}H\}$ NMR spectra of the *C,N*-benzaldiminato complexes gave the expected number of carbon signals for the given structures. An upfield shift was observed for the resonance of the imine carbon from ca. δ 160.54 ppm to ca. δ 170.96 ppm.

Table 2.3 *Selected spectroscopic and analytical data for C,N-benzaldiminato complexes* ***2.7, 2.8, 2.15*** *and* ***2.16****.*

Compound Number	**^{1}H NMR** (imine) [ppm][a]	**$^{13}C\{^{1}H\}$ NMR** (imine) [ppm][a]	**FT-IR** Imine (complex, ligand) [cm^{-1}][b]	**ESI-MS** $[M\text{-}nCl]^{n+}$ [*m/z*][c]
2.7	8.17	172.29	1588, 1626	448.11[d]
2.8	8.30	175.46	1583, 1626	538.17[d]
2.15	8.15	173.79	1614, 1628	500.11[e]
2.16	8.35	176.07	1613, 1628	590.16[e]

[a]Recorded in $CDCl_3$; [b]Recorded as KBr pellet; [c]ESI-MS; [d]n = 1; [e]n = 3.

Further evidence to support coordination of the metal to the imine nitrogen is seen in the infrared spectra. A shift in the $\nu_{C=Nimine}$ absorption band to lower wavenumbers, ca. 1586 cm^{-1} for the mononuclear or ca. 1614 cm^{-1} for the trinuclear complexes, in comparison to the uncoordinated ligand, ca. 1627 cm^{-1}, confirms coordination of the metal. These shifts are due to the electron withdrawing nature of the coordinated metal which causes a weakening of the $\nu_{C=Nimine}$ bond and results in the shift of the stretching vibration to lower wavenumbers. ESI-MS, in the positive mode, was used to assist in characterizing the proposed structures of the *C,N*-cyclometalated complexes. The mononuclear complexes **2.7** and **2.8** exhibited a cationic base peak corresponding to the loss of the chloro-ligand of the metal, while the trinuclear complexes **2.15** and **2.16** showed triply charged base peaks corresponding to the loss of three chloro-ligands.

The ^{1}H NMR spectra for the *N,N*-pyridylimine complexes **2.9-2.11** and **2.17-2.19** all show a downfield shift of the imine proton from ca. δ 8.57 ppm to ca. δ 8.95 ppm for the rhodium(III) or δ 9.77 ppm for the iridium(III) or δ 8.94 ppm for the ruthenium(II) complexes (Table 2.4). The ^{13}C{^{1}H} NMR spectra of the *N,N*-pyridylimine complexes gave the expected number of carbon signals for the proposed structures. A downfield shift was observed for the resonance of the imine carbon from ca. δ 160.46 ppm to ca. δ 167.80 ppm. ESI-MS results show molecular ion peaks with a loss of the PF_6^- counter-ion for the *N,N*-pyridylimine complexes **2.9-2.11** and **2.17-2.19**.

Table 2.4 *Selected spectroscopic and analytical data for N,N-pyridylimine complexes* ***2.9-2.11*** *and* ***2.17-2.19****.*

Compound Number	**^{1}H NMR** (imine) [ppm][a]	**^{13}C{^{1}H} NMR** (imine) [ppm][a]	**FT-IR** Imine (complex, ligand) [cm^{-1}][b]	**ESI-MS** $[M\text{-}nPF_6]^{n+}$ [*m/z*][c]
2.9	8.95	166.62	1598, 1630	485.09[d]
2.10	9.35	168.09	1622, 1630	575.14[d]
2.11	8.91	167.65	1628, 1630	483.08[d]
2.17	8.95	168.49	1617, 1597	537.75[e]
2.18	9.42	168.49	1617, 1597	627.14[e]
2.19	8.97	167.44	1611, 1597	536.17[e]

[a]Recorded in $(CD_3)_2CO$; [b]Recorded as KBr pellet; [c]ESI-MS; [d]n = 1; [e]n = 3.

The ^{1}H NMR spectra for the *N,O*-salicylaldiminato complexes **2.12-2.14** and **2.20-2.22** all showed an upfield shift of the imine proton from ca. δ 8.56 ppm to ca. δ 7.93 ppm for the rhodium(III), ca. δ 8.00 ppm for the iridium(III) or ca. δ 7.84 ppm for the ruthenium(II) complexes (Table 2.5). The ^{13}C{^{1}H} NMR spectra of the *N,O*-salicylaldiminato complexes gave the expected number of carbon signals for the given structures. An upfield shift is observed for the resonance of the imine carbon from ca. δ 162.83 ppm to ca. δ 164.46 ppm for the rhodium(III) and ruthenium(II) complexes, while a downfield shift to ca. δ 160.96 ppm is observed for the iridium(III) complexes. The *N,O*-salicylaldiminato complexes display a shift of the $C{=}N_{imine}$ stretching vibration to lower wavenumbers from ca. 1621 cm^{-1} to ca. 1613 cm^{-1}. Similarly to the *C,N*-cyclometalated complexes, the *N,O*-salicylaldiminato complexes displayed molecular ion base peaks which correspond to the loss of the chloro-ligand.

Table 2.5 *Selected spectroscopic and analytical data for N,O-salicylaldiminato complexes* ***2.12-2.14*** *and* ***2.20-2.22****.*

Compound Number	^{1}H NMR (imine) [ppm][a]	^{13}C{^{1}H} NMR (imine) [ppm][a]	FT-IR Imine (complex, ligand) [cm^{-1}][b]	ESI-MS [M-nCl]$^{n+}$ [*m/z*][c]
2.12	7.90	164.39	1617, 1620	464.11[d]
2.13	7.99	160.94	1610, 1620	554.17[d]
2.14	7.94	164.40	1612, 1620	462.10[d]
2.20	7.96	164.58	1612, 1622	516.10[e]
2.21	8.01	161.03	1613, 1622	605.50[e]
2.22	7.73	164.46	1614, 1622	514.10[e]

[a]Recorded in $CDCl_3$; [b]Recorded as KBr pellet; [c]ESI-MS; [d]n = 1; [e]n = 3.

In the ^{1}H NMR spectra of the pentamethylcyclopentadienyl derivatives the methyl protons of the pentamethylcyclopentadienyl ligand are observed at ca. δ 1.31 – 1.60 ppm (Figure 2.7).

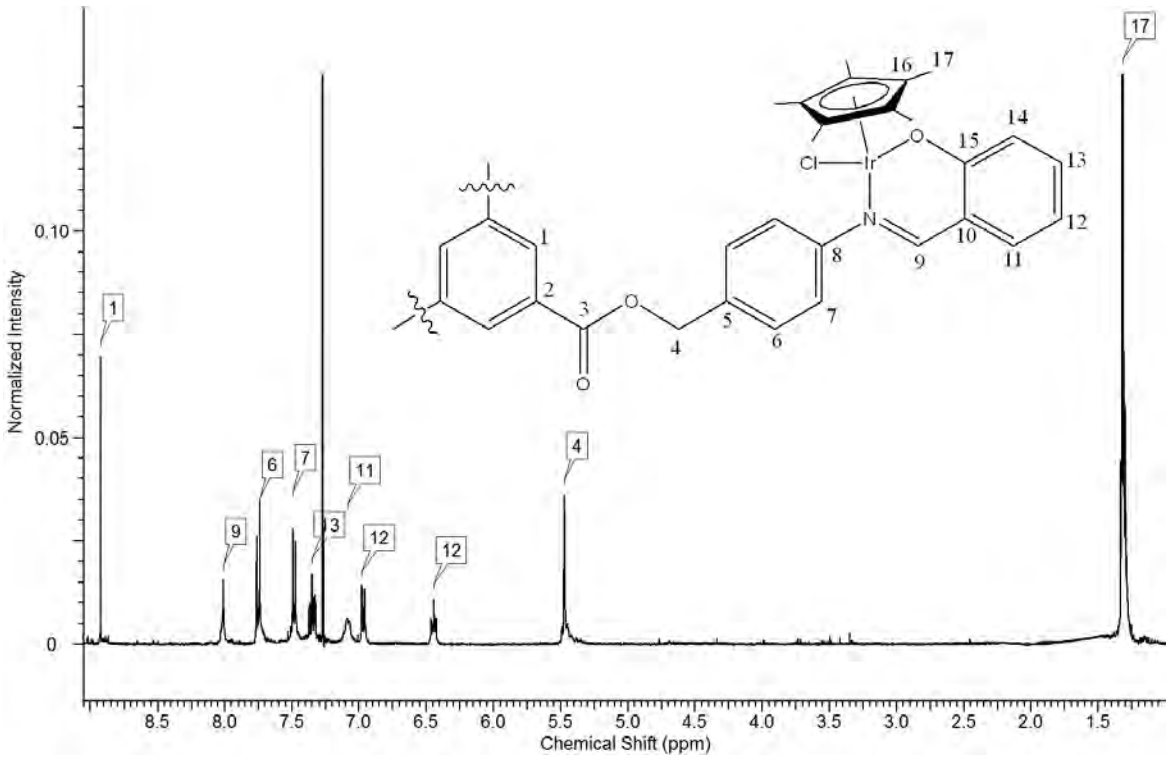

Figure 2.7 *^{1}H NMR spectrum of the trinuclear N,O-salicylaldiminato complex* ***2.21****.*

The aromatic carbon atoms of the ring are observed in the $^{13}C\{^{1}H\}$ NMR spectra at ca. δ 97.61 – 93.64 ppm for the rhodium(III) and ca. δ 85.75 - 90.35 ppm for the iridium(III) complexes, while the carbon resonances for the methyl substituents are observed at ca. δ 7.96 – 8.93 ppm for the rhodium(III) (Figure 2.8) and ca. δ 7.66 – 8.76 ppm for the iridium(III) complexes.

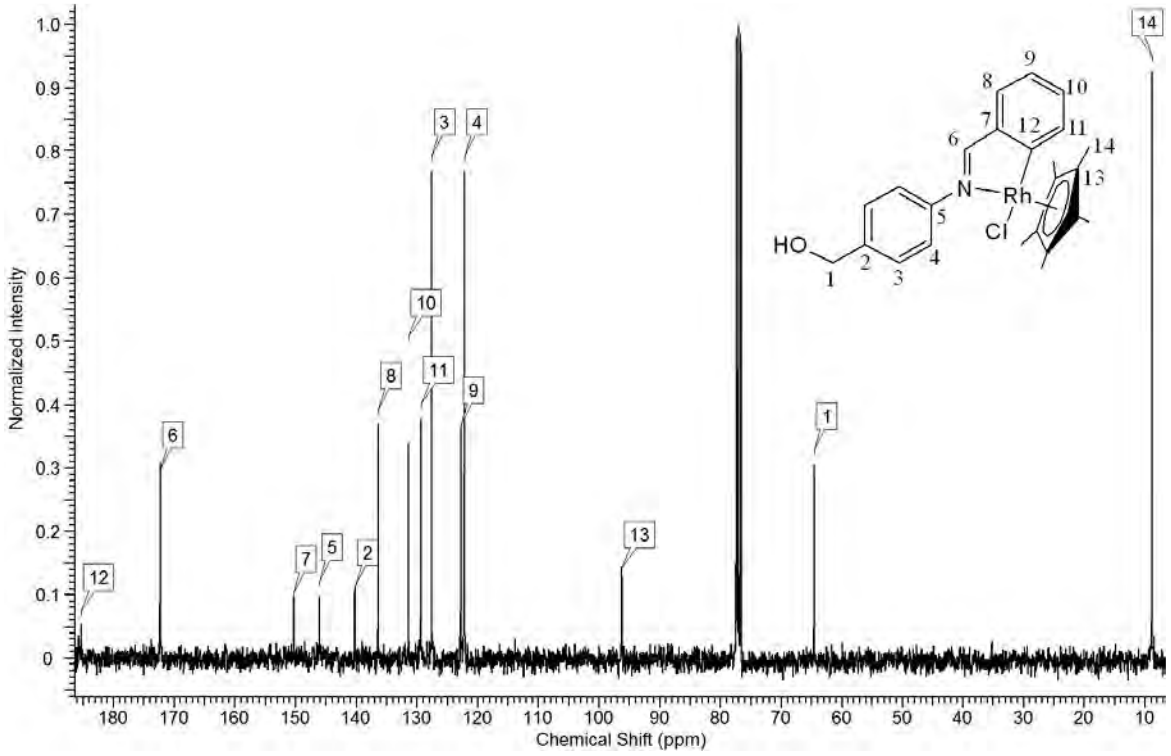

Figure 2.8 *$^{13}C\{^{1}H\}$ NMR spectrum of the mononuclear C,N-benzaldiminato complex* ***2.7****.*

In the ^{1}H NMR spectra of the *p*-cymene derivatives, **2.12-2.14** and **2.20-2.22**, the aromatic protons of the *p*-cymene ring display four distinct doublets in the region δ 6.11 – 4.28 ppm (Figure 2.9). The splitting of these signals into individual signals is attributed to the formation of a chiral center at the metal atom. A multiplet is observed between δ 2.82 – 2.52 ppm is assigned to the single proton of the isopropyl group, while the methyl protons on the isopropyl group exhibit one doublet per methyl group in the range δ 1.13 – 1.11 ppm. A singlet is observed at δ 2.30 – 2.01 ppm and is assigned as the methyl group *para* to the isopropyl moiety on the *p*-cymene ring.

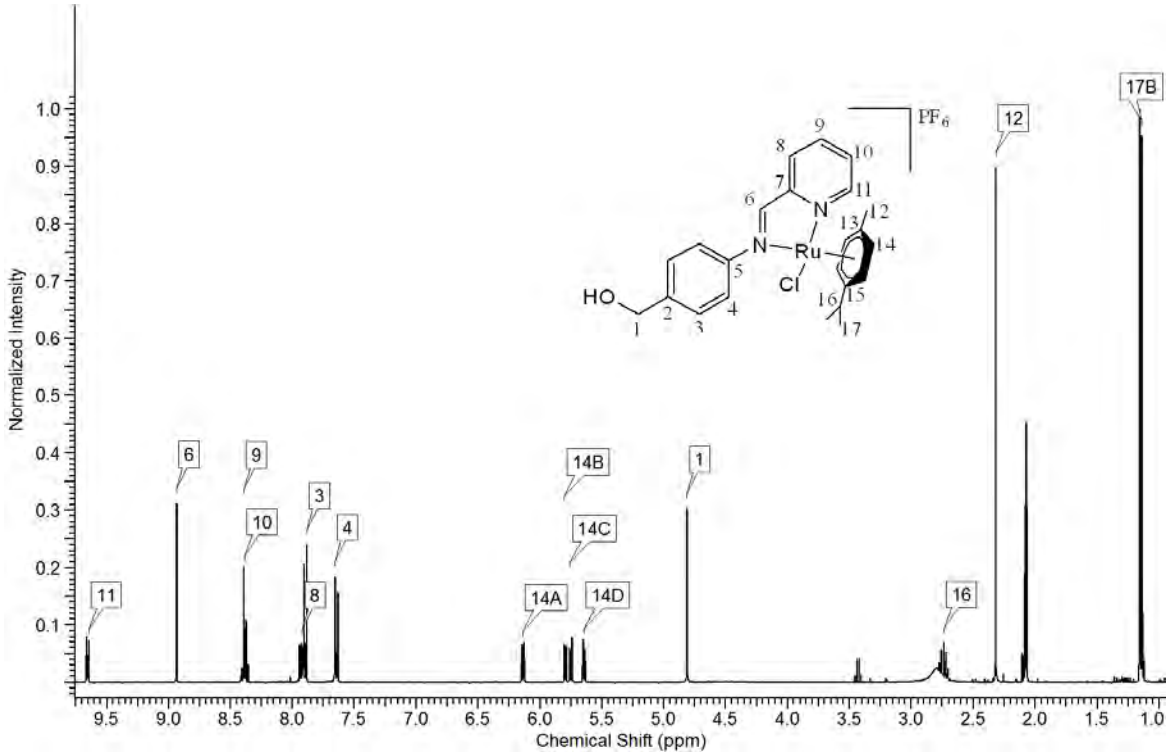

Figure 2.9 *^{1}H NMR spectrum of the mononuclear N,N-pyridylimine complex* ***2.11****.*

In the $^{13}C\{^{1}H\}$ NMR spectra the methyl carbons of the isopropyl moiety are observed as two signals at ca. δ 22.32 ppm and ca. δ 21.81 ppm, due to their existence in different environments. Similarly, the four aromatic carbons exhibit four separate signals in the range ca. δ 87.80 – 78.08 ppm (Figure 2.10). Signals at δ 103.12 ppm and δ 100.00 ppm were assigned for the quaternary carbons of the aromatic ring, while a signal at δ 30.98 was attributed to the tertiary carbon of the isopropyl group and the most upfield observed signal at ca. δ 18.50 ppm was assigned to the methyl carbon *para* to the isopropyl moiety.

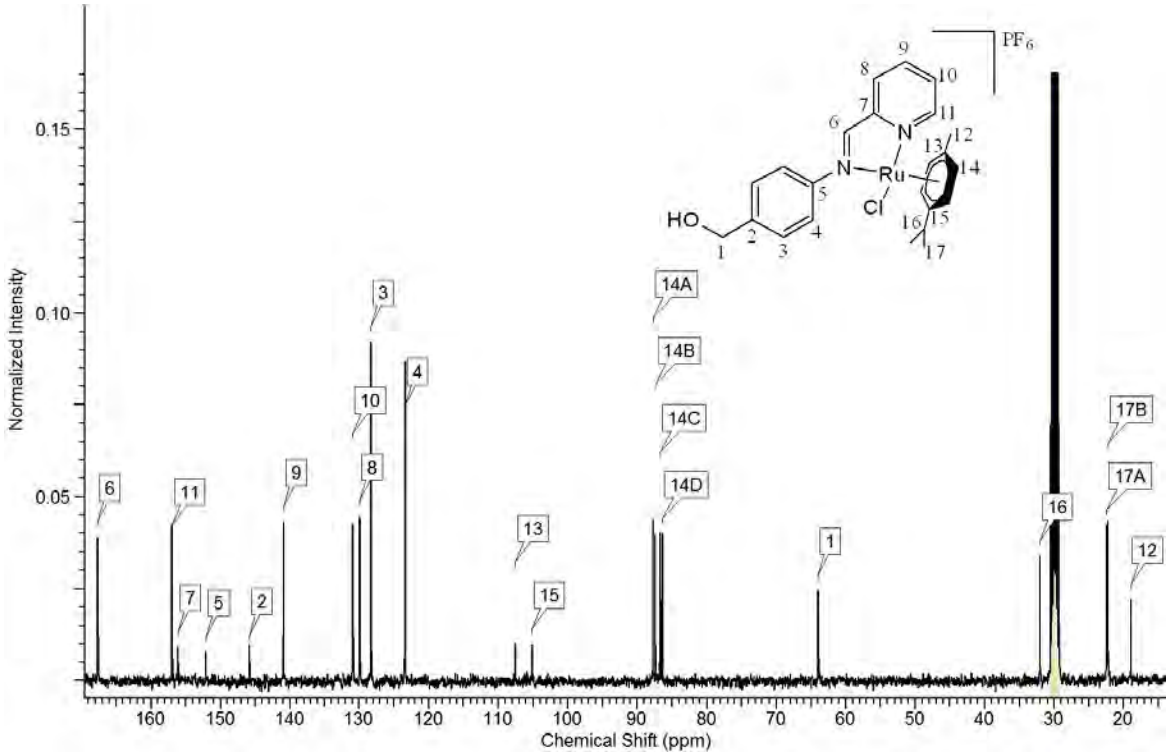

Figure 2.10 *$^{13}C\{^{1}H\}$ spectrum of the mononuclear N,N-pyridylimine complex* ***2.11****.*

Elemental analysis results for the rhodium(III), iridium(III) and ruthenium(II) complexes are consistent with the calculated values for the proposed structures of **2.7-2.22**.

2.3. X-ray Crystallography

The molecular structures of the mononuclear complexes **2.7-2.14** were confirmed by single crystal XRD. Crystals of the *C,N*-benzaldiminato and *N,O*-salicylaldiminato complexes were grown by slow diffusion of hexane into a solution of chloroform, while hexane and acetone were used for the *N,N*-pyridylimine complexes. No suitable crystals were obtained for the trinuclear complexes. Tables 1-3 (Chapter 5 - Experimental) summarizes the crystal data and refinement parameters for **2.7-2.14**.

The complexes adopt the expected pseudo-tetrahedral or “piano-stool” geometry around the metal center. The metal coordinates to the pentamethylcyclopentadienyl or *p*-cymene ligand, one chloride ligand and either the *C,N*-, *N,N*- or *N,O*-ligand in a bidentate-chelating mode through its imine nitrogen and its cyclometalated carbon (Figure 2.11), pyridyl nitrogen or phenolic oxygen (Figure 2.12), respectively.

Complexes **2.7-2.11** all crystallize in the triclinic space group *P*-1, while **2.12** crystallizes in the orthorhombic *Pna*2_1 space group, **2.13** crystallizes in the monoclinic *P*2_1 and **2.14** crystallizes in the monoclinic *Cc* space group. The M-N_{imine} bond distance ranges between 2.089 – 2.121 Å, while the M-Cl bond length is significantly longer and ranges between 2.393 – 2.443 Å.

A comparison can be drawn from the second non-imine donor bond involved in the bidentate chelation of the metal to the ligand. The *C,N*-benzaldiminato complexes **2.7** and **2.8** exhibit a M-C bond distance in the range 2.038 – 2.046 Å, while the *N,N*-pyridylimine complexes have a M-N_{pyr} bond distance of 2.097 – 2.105 Å and the *N,O*-salicylaldiminato complexes have a M-O bond length of 2.073 – 2.080 Å. Thus, for the complexes **2.7-2.14** it can be said that the following bond lengths have the following relationship: M-C < M-O < M-N_{pyr}.

The bond angles formed by the metal center are near orthogonal. However the C-M-N_{imine} bond angles of **2.7** and **2.8** are as small as ca. 78° and the N_{pyr}-M-N_{imine} bond angles of **2.9-2.11** are the smallest at ca. 76°. Complexes **2.7-2.14** exhibit similar geometric parameters and these are in agreement with other analogous rhodium(III), iridium(III) and ruthenium(II) mononuclear complexes reported in literature.[26-34]

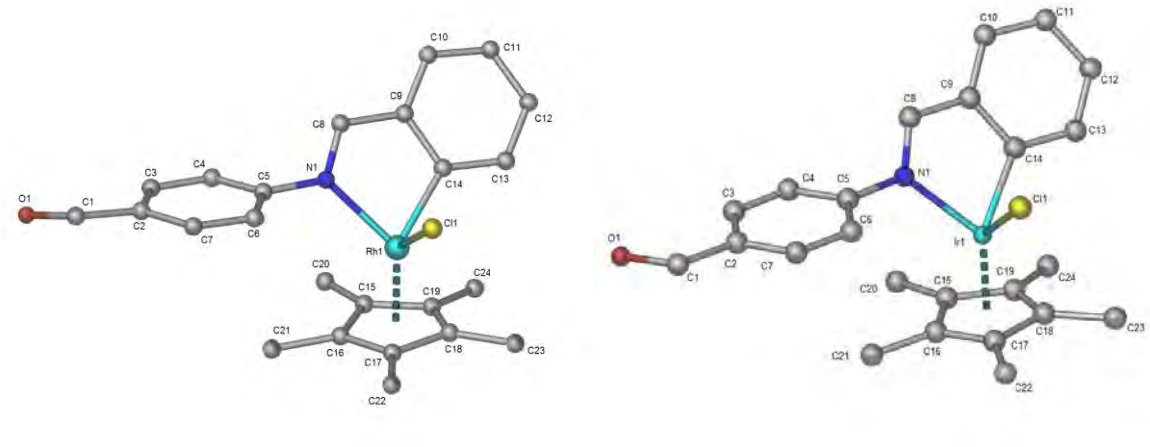

Figure 2.11 *Molecular structures of* ***2.7*** *(left) and* ***2.8*** *(right) with hydrogen atoms omitted for clarity.*

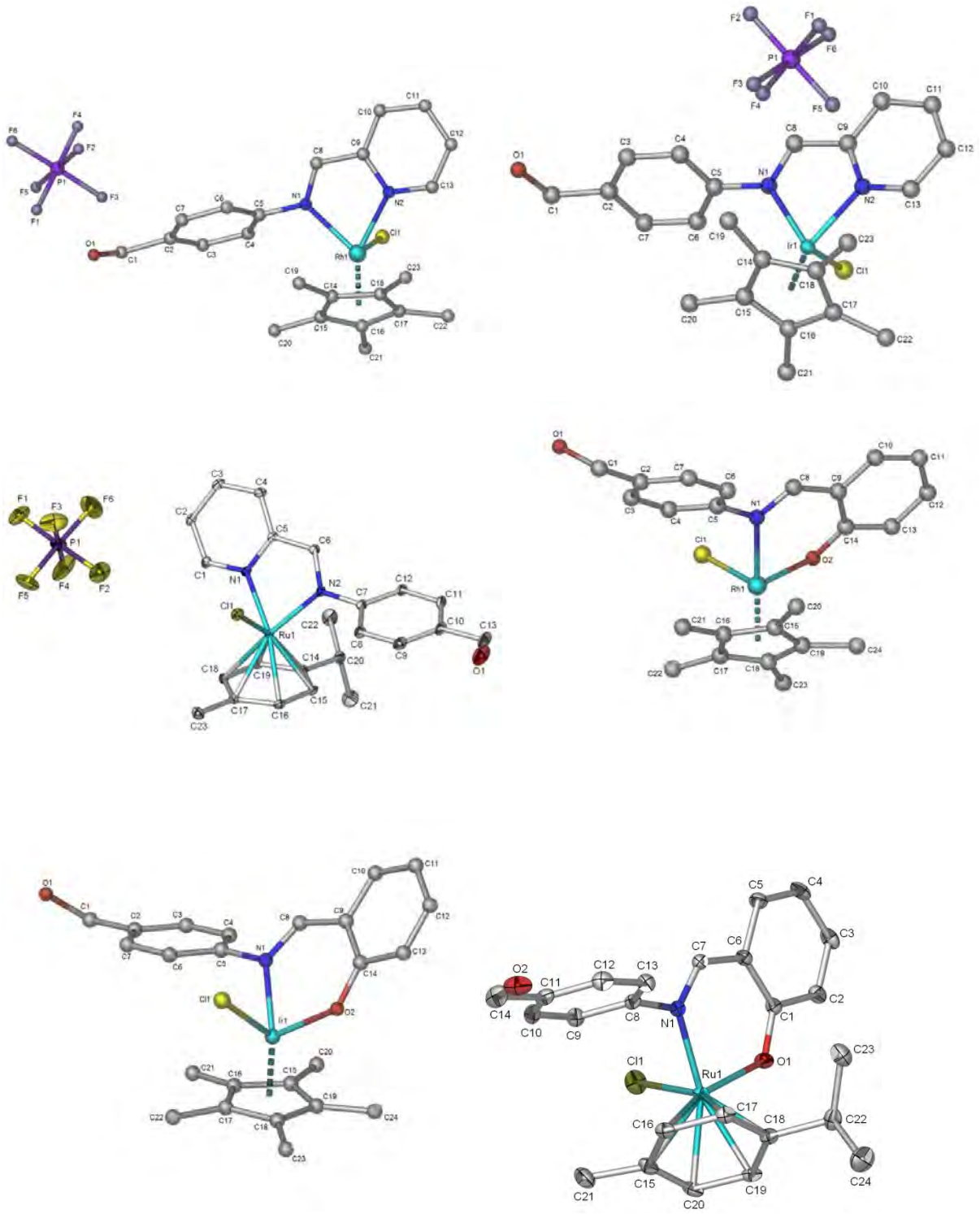

Figure 2.12 *Molecular structures of* ***2.9*** *(top left),* ***2.10*** *(top right),* ***2.11*** *(center left),* ***2.12*** *(center right),* ***2.13*** *(bottom left) and* ***2.14*** *(bottom right) with hydrogen atoms omitted for clarity.*

Table 2.6. *Selected bond lengths and angles for complexes* ***7-14****.*

Inter-atomic distances (Å)	**2.7**	**2.8**	**2.9**	**2.10**	**2.11**	**2.12**	**2.13**	**2.14**
M-N_{imine}	2.090(16)	2.089(4)	2.121(3)	2.098(2)	2.089(2)	2.118(4)	2.100(3)	2.083(2)
M-C	2.038(2)	2.046(5)	-	-	-	-	-	-
M-N_{pyr}	-	-	2.105(3)	2.097(2)	2.100(2)	-	-	-
M-O	-	-	-	-	-	2.073(3)	2.080(3)	2.076(2)
M-Cl	2.398(6)	2.398(13)	2.393(14)	2.395(8)	2.402(6)	2.434(14)	2.443(9)	2.416(7)
Angles (°)								
Cl-M-N_{imine}	91.85(5)	87.20(11)	89.48(10)	87.84(7)	85.37(7)	91.39(11)	85.56(10)	84.71(5)
Cl-M-C	89.24(6)	86.80(13)	-	-	-	-	-	-
C-M-N_{imine}	78.38(8)	77.68(17)	-	-	-	-	-	-
Cl-M-N_{pyr}			86.21(11)	85.01(7)	84.31(7)	-	-	-
N_{pyr}-M-N_{imine}	-	-	76.35(14)	76.06(9)	76.76(2)	-	-	-
Cl-M-O	-	-	-	-	-	85.83(14)	82.94(10)	84.87(5)
O-M-N_{imine}						87.43(15)	88.29(11)	88.31(6)

2.4. *In vitro* Biological Activity

The *in vitro* antitumor activity of the ligands **2.1-2.6**, the mono- **2.7-2.14** and trinuclear complexes **2.15-2.22** was established against cisplatin-sensitive A2780 and cisplatin-resistant A2780*cis*R human ovarian cancer cell lines. The toxicity of these compounds was also explored by using the normal human fibroblast skin cell line KMST-6 (Table 2.7). Cisplatin was tested against all three cell lines as a comparison.

The ligands **2.1-2.6** (Table 2.7) and mononuclear complexes **2.7-2.14** exhibit poor or no activity in either the A2780 or A2780*cis*R cell lines. It is evident that upon coordination of a half-sandwich organometallic moiety to a ligand there is an increase in cytotoxicity (Figure 2.13).

Table 2.7. *IC_{50} values determined against A2780 and A2780cisR human ovarian cancer cells, and KMST-6 normal skin tissue cells for ligands **2.1-2.6**.*

Compound Number	Ligand	Metal	IC_{50} (μM)					
			A2780	SI[a]	A2780*cis*R	SI[b]	RI[c]	KMST-6
2.1	*C,N*-		>200	-	132.51 ± 5.98	1.35	-	179.33 ± 4.24
2.2	*N,N*-		>200	-	156.41 ± 2.37	1.20	-	188.38 ± 6.33
2.3	*N,O*-		>200	-	>200	-	-	157.05 ± 2.82
2.4	*C,N*-		42.42 ± 1.71	2.53	172.88 ± 6.23	0.62	4.08	107.48 ± 2.77
2.5	*N,N*-		87.63 ± 3.49	1.30	68.25 ± 1.48	1.67	0.78	114.10 ± 3.72
2.6	*N,O*-		169.96 ± 3.16	0.75	55.98 ± 3.28	2.27	0.33	127.02 ± 0.65

[a]KMST-6/A2780; [b]KMST-6/A2780*cis*R; [c]A2780*cis*R/A2780.

The trinuclear complexes **2.15-2.22** display the greatest cytotoxicity in the A2780 or A2780*cis*R cell lines. This increase in activity can be attributed to the increased number of metal centers present. The relationship between the number of metal atoms coordinated and the activity has been established previously for PGM complexes.[3, 32-36] The two most active compounds are the cationic *N,N*-pyridylimine complexes. The trinuclear iridium(III) complex **2.18** displays the greatest activity in the cisplatin sensitive A2780 cell line with an IC_{50} value = 11.58 μM, while the trinuclear rhodium(III) complex **2.17** displays similar activity in the cisplatin resistant cell line A2780*cis*R with an IC_{50} value = 10.61 μM. The activity of **2.18** is still, however, one order of magnitude lower than that of the IC_{50} value of cisplatin in A2780 cells, while the

activity of **2.17** is comparable to that of cisplatin. The increased activity of cationic complexes have been previously reported.[32, 34] This might be attributed to the electrostatic interactions between the cationic complexes and the anionic sugar-phosphate backbone of DNA.[37]

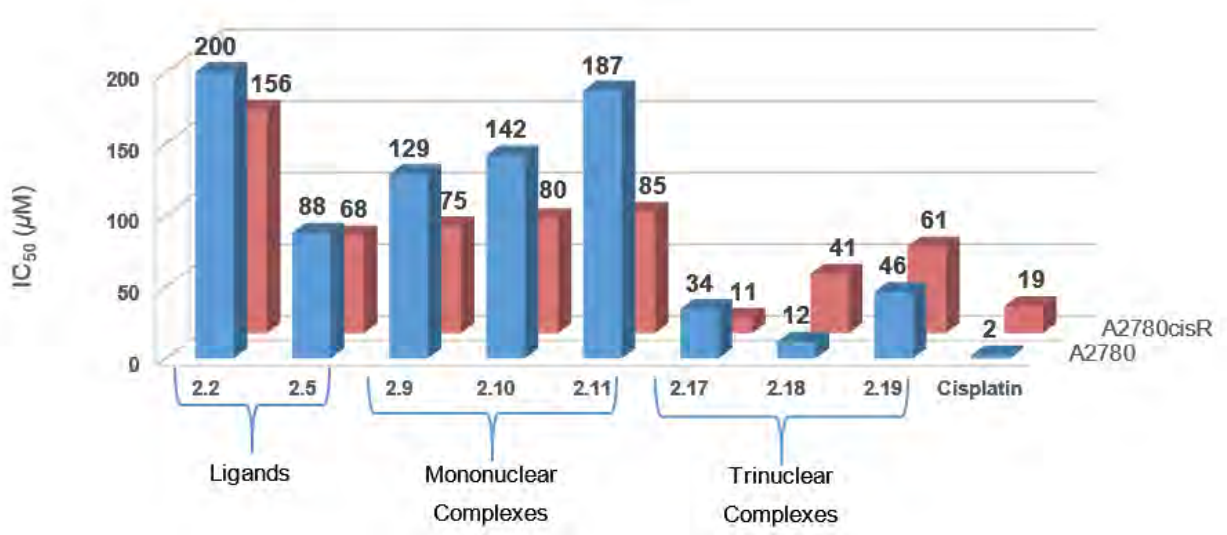

Figure 2.13 *Effect of coordination of a metal on the cytotoxicity against A2780 and A2780cisR cells, shown for ligands* ***2.2*** *and* ***2.5*** *and mono-* ***2.9-2.11****, trinuclear complexes* ***2.17-2.19*** *and cisplatin.*

Table 2.8. *IC_{50} values determined against A2780 and A2780cisR human ovarian cancer cells, and KMST-6 normal skin tissue cells for CN-complexes* ***2.7, 2.8, 2.15*** *and* ***2.16****.*

Complex Number	Ligand	Metal	IC_{50} (μM)					
			A2780	SI[a]	A2780*cis*R	SI[b]	RI[c]	KMST-6
2.7	*C,N*-	Rh	89.32 ± 2.79	1.00	125.63 ± 2.80	0.71	1.41	89.24 ± 4.24
2.8		Ir	174.81 ± 7.14	1.07	117.66 ± 3.11	1.61	0.67	189.99 ± 5.87
2.15		3 Rh	37.71 ± 1.58	0.71	35.78 ± 2.24	0.74	0.95	26.59 ± 5.92
2.16		3 Ir	19.20 ± 1.91	0.55	20.03 ± 0.73	0.53	1.04	10.56 ± 0.25

[a]KMST-6/A2780; [b]KMST-6/A2780*cis*R; [c]A2780*cis*R/A2780.

Table 2.9. *IC_{50} values determined against A2780 and A2780cisR human ovarian cancer cells, and KMST-6 normal skin tissue cells for NN-complexes* ***2.9-2.11*** *and* ***2.17-2.19****.*

Complex Number	Ligand	Metal	IC_{50} (μM)					
			A2780	SI[a]	A2780*cis*R	SI[b]	RI[c]	KMST-6
2.9	*N,N*-	Rh	128.64 ± 3.64	0.88	74.71 ± 6.16	1.52	0.58	113.78 ± 2.37
2.10		Ir	141.88 ± 1.19	0.71	80.20 ± 1.71	1.25	0.57	100.54 ± 5.01
2.11		Ru	187.08 ± 8.25	0.71	84.72 ± 3.16	1.57	0.45	133.16 ± 3.16
2.17		3 Rh	34.34 ± 1.94	1.26	10.61 ± 0.40	4.09	0.31	43.39 ± 3.72
2.18		3 Ir	11.58 ± 4.35	7.29	41.45 ± 3.28	2.04	3.58	84.40 ± 1.16
2.19		3 Ru	46.29 ± 0.85	1.56	60.50 ± 0.56	1.19	1.31	72.13 ± 1.48

[a]KMST-6/A2780; [b]KMST-6/A2780*cis*R; [c]A2780*cis*R/A2780.

Table 2.10. *IC_{50} values determined against A2780 and A2780cisR human ovarian cancer cells, and KMST-6 normal skin tissue cells for NO-complexes* ***2.12-2.14*** *and* ***2.20-2.22****.*

Complex Number	Ligand	Metal	IC_{50} (μM)					
			A2780	SI[a]	A2780*cis*R	SI[b]	RI[c]	KMST-6
2.12	*N,O*-	Rh	63.08 ± 5.32	1.77	133.64 ± 3.56	0.84	2.12	111.84 ± 3.67
2.13		Ir	107.00 ± 3.95	1.09	109.91 ± 5.92	1.06	1.03	116.20 ± 4.35
2.14		Ru	69.86 ± 6.99	1.54	100.22 ± 3.95	1.07	1.43	107.48 ± 1.19
2.20		3 Rh	30.47 ± 1.12	2.63	36.93 ± 0.65	1.91	1.21	80.20 ± 1.96
2.21		3 Ir	30.79 ± 1.16	2.76	50.49 ± 3.08	1.66	1.64	85.04 ± 3.64
2.22		3 Ru	33.38 ± 2.44	2.94	36.93 ± 1.12	2.66	1.11	98.28 ± 3.11
Cisplatin		Pt	1.97 ± 3.41	22.36	18.90 ± 0.81	2.33	9.59	44.04 ± 1.97

[a]KMST-6/A2780; [b]KMST-6/A2780*cis*R; [c]A2780*cis*R/A2780.

The establishment of the selectivity of antitumor agents for cancerous cells over non-tumorigenic cells is important. The *in vitro* activity of **2.1-2.22** was investigated against normal KMST-6 cells. To measure the potency of the tested compounds towards only tumorigenic cells, the selectivity index (SI) was calculated as the ratio of the IC_{50} of KMST-6 to the IC_{50} of A2780 or A2780*cis*R cells.[38] Optimal SI values are in excess of SI > 1. The trinuclear *N,N*-pyridylimine and *N,O*-salicylaldiminato complexes **2.17-2.22** show moderate selectivity towards the tumorigenic ovarian cells (Figure 2.14). The SI ranges from as low as 1.19 for

2.19 in A2780*cis*R up to 7.29 for **2.18** in A2780. The trinuclear *C,N*-benzaldiminato complexes **2.15** and **2.16** display poor selectivity and general toxicity against the cells tested, as the calculated SI values were < 1.

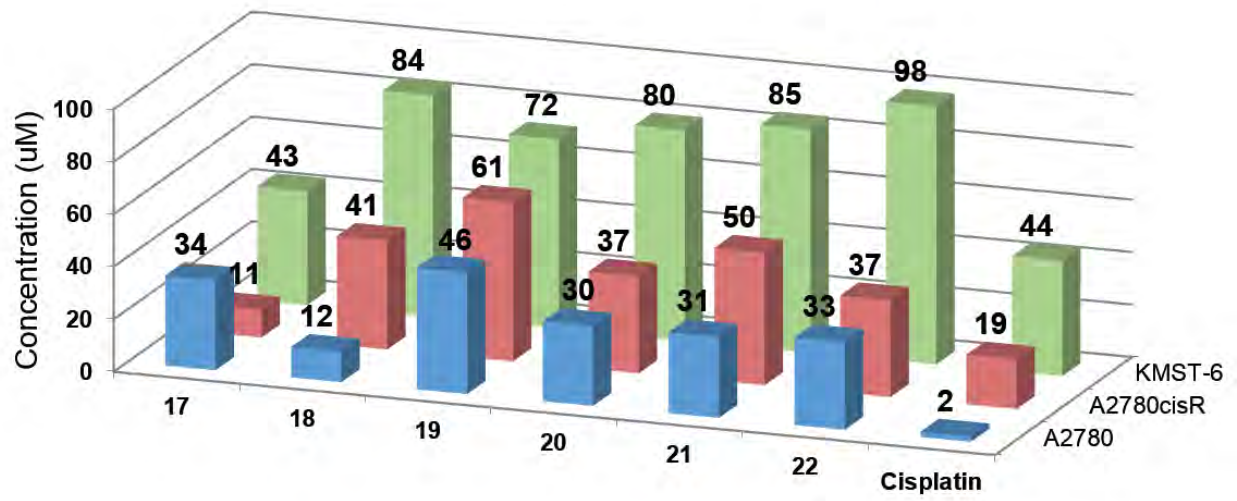

Figure 2.14 *Cytotoxicity of trinuclear complexes* ***2.17-2.19*** *and cisplatin against A2780, A2780cisR and non-tumorigenic KMST-6 cells for selectivity comparison.*

The resistance index (RI) can be calculated as a ratio of the IC_{50} of A2780*cis*R to the IC_{50} of A2780 cells.[39] This index determines the resistance of the complexes in the A2780 cisplatin-sensitive cell line as opposed to the A2780*cis*R cisplatin-resistant cell line, this comparison between activities in the two cell lines allows for inferences to be made into if mechanisms of action are similar to that of cisplatin. All the mononuclear *N,N*-pyridylimine complexes **2.9-2.11** display RI values lower than 1, as they are more active in the A2780*cis*R cisplatin-resistance cells, with no cross-resistance observed (Figure 2.15). Most of the trinuclear complexes display similar activity in both the A2780 and A2780*cis*R cell lines, and thus the RI values are approximately ≈ 1, and display no cross-resistance to cisplatin. Exceptions are the trinuclear rhodium(III) *N,N*-pyridylimine complex **2.17** and the trinuclear iridium(III) *N,N*-pyridylimine complex **2.18**, which display RI values of 0.31 and 3.58 due to their high activities in the A2780*cis*R and A2780 cell lines, respectively (Figure 2.16). Cisplatin shows a significant decrease in activity from the A2780 to the A2780*cis*R cell lines with a RI ≈ 10.

Overall, all the complexes show no cross resistance to cisplatin as the RI values ≈ 1 and in most cases the cytotoxicities are roughly comparable in both tumorigenic cell lines tested. This suggests a different mode of action to that of cisplatin.

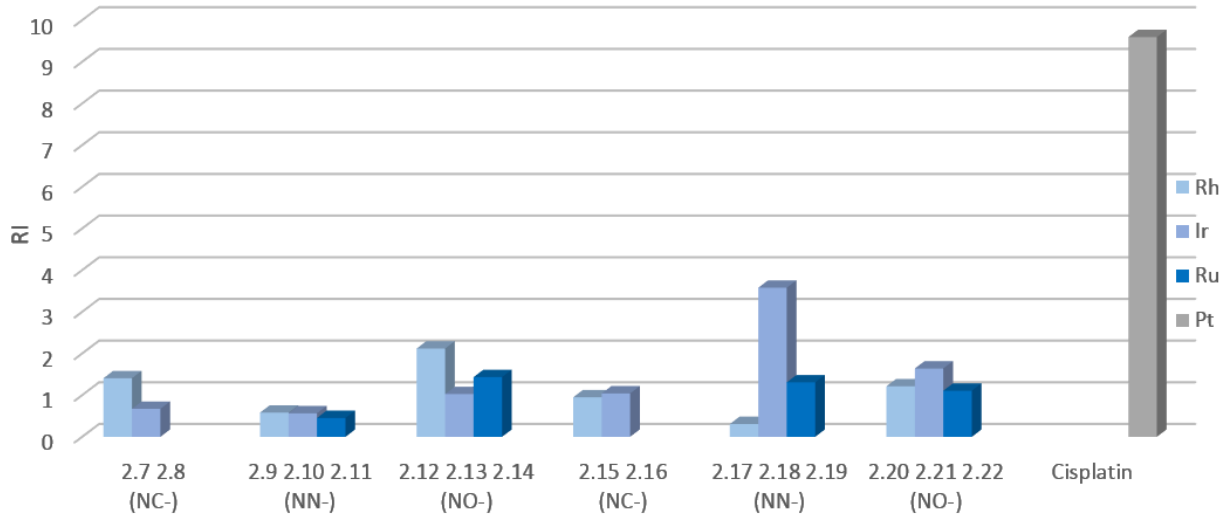

Figure 2.15 *Effect of varying the bidentate donor atoms and the metal arene on the cytotoxicity against A2780 and A2780cisR, plotted as the resistance index (RI), where RI = IC_{50} of A2780cisR / IC_{50} of A2780.*

It is important to note that all these bidentate complexes evaluated in this study against the A2780 and A2780*cis*R cell lines displayed increased cytotoxicity in comparison to the monodentate metal complexes previously reported.[21] This displays the greater activity of the chelate effect, which has been exhibited by other bidentate[35, 40] complexes.

2.5. Stability in Aqueous Media and DMSO

Prior to further testing, the stability of drugs in solution needs to be established. It has been reported that mononuclear metal complexes that contain a chloride ligand after uptake into the cell are activated by substitution of the labile M-Cl bond to an intermediate M-aqua species. The formation of this activated aqua species can be observed by NMR spectroscopy.[41-42]

Therefore, to further understand the cytotoxicity of the complexes, a stability investigation was performed on selected complexes. The stability of the complexes in a 50:50 mixture of deuterated-dimethylsulfoxide, $(CD_3)_2SO$, and water was studied. This solution was chosen as

it represents the method in which the stock solutions are prepared for cytotoxic studies. The stability was monitored using ^{1}H NMR spectroscopy over time at the physiological temperature of 37 ^{o}C.

The trinuclear *N,N*-pyridylimine complexes **2.17-2.19** display the greatest activities; thus the trinuclear iridium(III) complex **2.18**, which displays the greatest activity, and its mononuclear analogue **2.10** were chosen, for testing, along with **2.13**, the mononuclear *N,O*-salicylaldiminato iridium(III) equivalent. The trinuclear iridium(III) complex **2.18** and the two mononuclear complexes **2.10** and **2.13** all show stability in a mixture of $(CD_3)_2SO$ and water, as monitored by ^{1}H NMR spectroscopy. After 24 hours in solution none of the aforementioned complexes showed signs of degradation, as the spectra remained unchanged over the tested time (Figure 2.16).

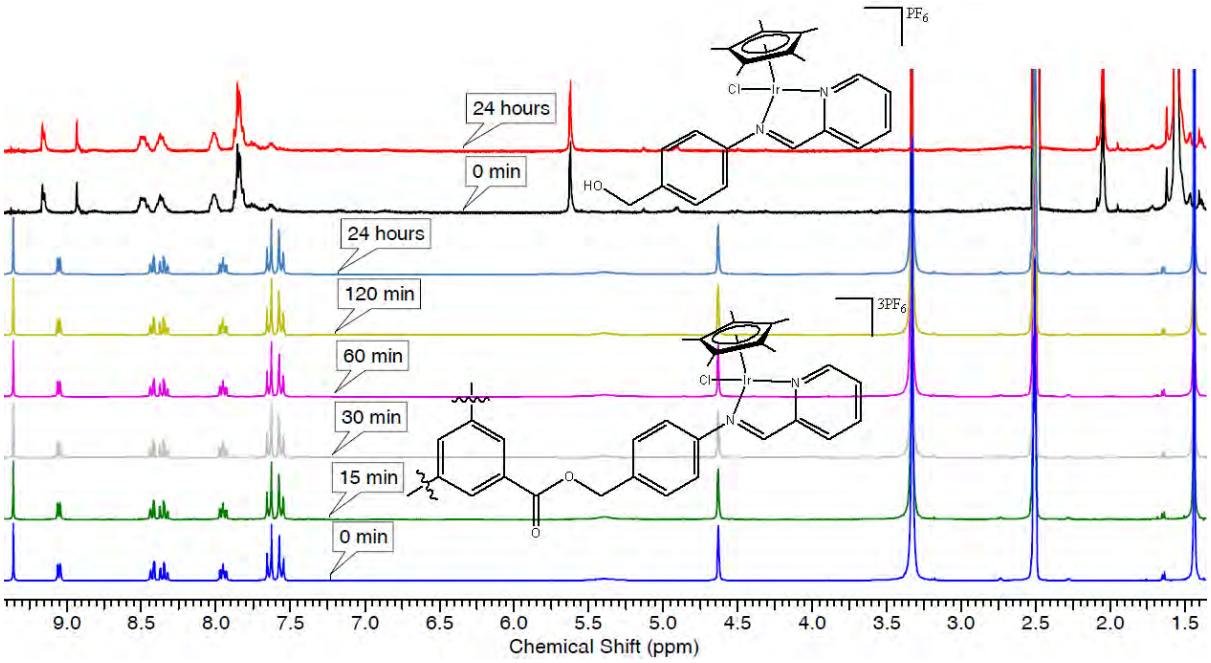

Figure 2.16 *^{1}H NMR spectra of mononuclear **2.10** (top two spectra) and trinuclear complex **2.18** in $(CD_3)_2SO$ and H_2O (50:50) as recorded over 24 hours.*

The stability towards aqueous media of these complexes might be a possible cause of the low cytotoxicity of this series of complexes as the active aqua species is not observed to form. This might suggests that these complexes operate *via* some other mode of action to those which undergo hydrolysis and form the aqua species.

2.6. Interactions with Model DNA 5'-GMP

Administered drugs encounter many important biological molecules and often interact with these, which affects the activity of the compounds. Ruthenium-arene complexes have a strong affinity towards DNA[43-44] and mechanistic studies report that these complexes bind selectively to the nucleotide base-pair guanine.[45-46] Thus, interactions between the mononuclear *N,N*-pyridylimine **2.10** or *N,O*-salicylaldiminato **2.13** iridium(III) complexes and the nucleotide 5'-GMP in $(CD_3)_2SO$ and water 50:50 at 37 °C was monitored by ^1H NMR spectroscopy for 24 hours.

The cationic *N,N*-pyridylimine complex **2.10** showed no signs of interactions with 5'-GMP and the nucleotide was unable to displace the chloride ligand (Figure 2.17c). However, the neutral *N,O*-salicylaldiminato complex **2.13** did interact with the nucleotide and shifts in the resonances of the signals in the ^1H NMR spectrum were observed after 24 hours (Figure 2.17e).

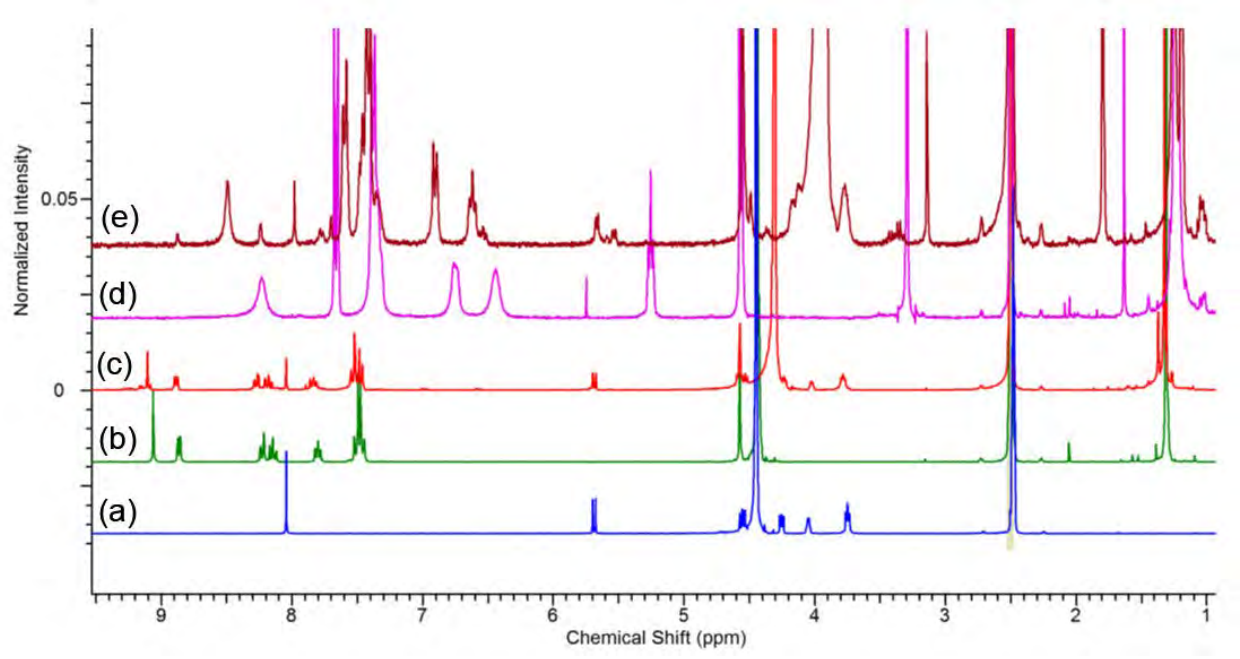

Figure 2.17 *^1H NMR spectra of (a) 5'-GMP, (b)* ***2.10****, (c) reaction mixture of* ***2.10*** *with 5'-GMP, (d)* ***2.13****, (e) reaction mixture of* ***2.13*** *with 5'-GMP.*

The signal for the proton at C8 on 5'-GMP was observed to shift downfield from δ 8.04 ppm to δ 8.88 ppm. Similar shifts in signals in the ^1H NMR spectra of ruthenium(II) complexes have been reported.[45] This suggests that **2.13** interacts with 5'-GMP by coordination to N7 by

displacing the chloride ligand and resulting in a cationic species stabilized by the chloride ion (Figure 2.18). This evidence supports the suggestion that the neutral complexes target DNA, while the cationic complexes have other important targets, possibly proteins, or have a different mode of action.

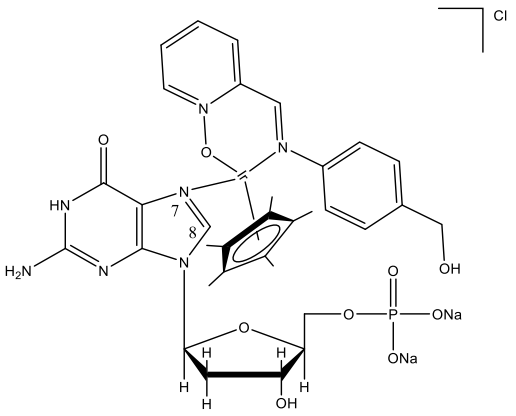

Figure 2.18 *Proposed structure of the product of the reaction between* ***2.13*** *with 5'-GMP.*

2.7. Calculated Lipophilicity Determination: log *P*

In addition to the size and multinuclearity of the trinuclear complexes, this series of compounds contains ester functionalities. Log *P* is a quantification of a compounds hydrophilicity and is used in determining if a compound can diffuse into cells. The lipophilicity of the monomeric ligands **2.1-2.3** and the trimeric ester containing ligands **2.4-2.6** was calculated using MarvinSketch[47] (Table 2.11). It is evident that upon formation of the ester moiety in **2.4-2.6** the ligands become more lipophilic, as shown by the calculated log *P* values (Table 2.11).

Table 2.11. *The log P Values determined by Marvin Sketch of monomeric and trimeric ligands* ***2.1-2.6*** *and cytotoxicities in A2780, A2780cisR and KMST-6.*

Compound Number	log *P*[a]	A2780	A2780*cis*R	KMST-6
2.1	3.08	>200	132.51 ± 5.98	179.33 ± 4.24
2.2	2.54	>200	156.41 ± 2.37	188.38 ± 6.33
2.3	2.78	>200	>200	157.05 ± 2.82
2.4	12.78	42.42 ± 1.71	172.88 ± 6.23	107.48 ± 2.77
2.5	11.15	87.63 ± 3.49	68.25 ± 1.48	114.10 ± 3.72
2.6	11.87	169.96 ± 3.16	55.98 ± 3.28	127.02 ± 0.65

[a]Log *P* values calculated using MarvinSketch V. #5.9.4

A correlation is seen between the log *P* and the cytotoxicity. The increased activity of the ester containing trimeric ligands **2.4-2.6** as compared to that of the monomeric ligands **2.1-2.3** might be the result of increased cellular uptake, as the more lipophilic ligands are able to cross cellular membranes.

Calculated electrostatic potential surfaces[47] of the trimeric *C,N*-benzaldimine ligand **2.4** are shown (Figure 2.19) on a space filling model of the ligand, at different orientations. Red indicates an area of electron-deficiency, which is localized around the core due to the three ester functionalities, while blue is representative of electron-rich areas, which coincide with the aromatic rings.

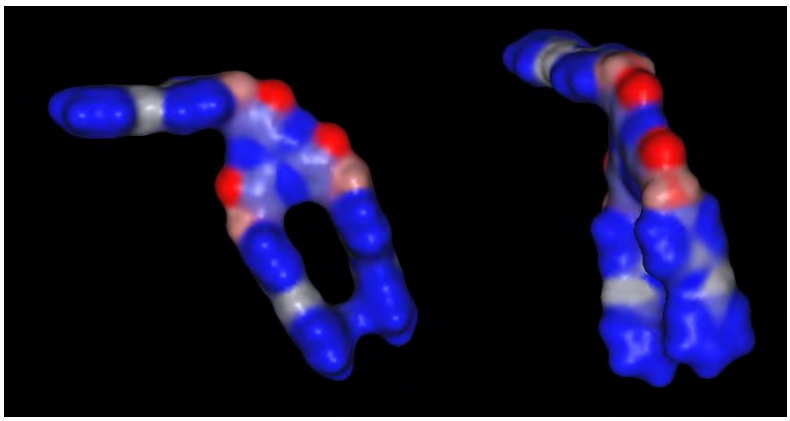

Figure 2.19 *Calculated electrostatic potential maps[47] depicting the difference in polarity of the trimeric C,N-benzaldiminato ligand* ***2.4*** *at different orientations.*

2.8. Overall Summary

A series of new mononuclear **2.7-2.14** and trinuclear **2.15-2.22** rhodium(III), iridium(III) and ruthenium(II) complexes based on *C,N*-benzaldimine, *N,N*-pyridylimine, *N,O*-salicylaldimine ligands were synthesized. The compounds were all characterized by various spectroscopic and analytical techniques, namely ^{1}H, $^{13}C\{^{1}H\}$ NMR and infrared spectroscopy, mass spectrometry and elemental analysis. Single crystal XRD was utilized to obtain the molecular structures of the mononuclear complexes **2.15-2.22** and confirm the proposed structures. Coordination of the metal occurs in a bidentate fashion through the imine nitrogen and the benzyl-carbon, pyridyl-nitrogen or phenolic-oxygen atoms.

The *in vitro* antitumor activity of all the compounds was evaluated against the A2780 and A2780*cis*R ovarian cancer cell lines. It should be noted that bidentate chelation results in improved activity. The trinuclear complexes **2.15-2.22** exhibit the highest activity and display

no cross-resistance to cisplatin. In particular the trinuclear *N,N*-pyridylimine complexes **2.17** and **2.18** are the most active and the *C,N*-benzaldiminato complexes display poor selectivity towards normal KMST-6 cells. The *N,O*-salicylaldiminato complexes display evidence of interactions with 5'-GMP *via* the N7 atom, yet the cationic *N,N*-pyridylimine complexes do not. This suggests that DNA may be a possible target for the neutral complexes, while other targets may be important for the cationic complexes.

2.9. References

[1] S. Pandey, P. Garg, K.T. Lim, J. Kim, Y-H. Choung, Y-J. Choi, P-H. Choung, C-S. Cho and J.H. Chung, *Biomaterials* **2013**, *34*, 3716-3728.

[2] R.V. Tak, D. Pal, H. Gao, S. Dey and A.K. Mitra, *J. Pharm. Sci.* **2001**, *90*, 1505-1515.

[3] B.P. Bandgar, R.J. Sarangdhar, K. Fruthous, J. Mookkan, S. Chaudhary, H.V. Chavan, S.B. Bandgar and V.Y. Kshirsagar, *Eur. J. Med. Chem.* **2012**, *57*, 217-224.

[4] S. Kumar, P. Arya, C. Mukherjee, B.K. Singh, N. Singh, V.S. Parmar, A.K. Prasad and B. Ghosh, *Biochemistry* **2005**, *44*, 15944-15952.

[5] S.W. Fogt, J.A. Scozzie, R.D. Heilman and L.J. Powers, *J. Med. Chem.* **1980**, *23*, 1445-1448.

[6] D. Lamoral-Theys, L. Pottier, F. Kerff, F. Dufrasne, F. Proutière, N. Wauthoz, P. Neven, L. Ingrassia, P. Van Antwerpen, F. Lefranc, M. Gelbcke, B. Pirotte, J. Kraus, J. Nève, A. Kornienko, R. Kiss and J. Duboisa, *Tetrahedron* **2010**, *18*, 3823-3833.

[7] O.L.P. De Jesús, H.R. Ihre, L. Gagne, J.M.J. Fréchet and Jr. Szoka, F.C., *Bioconjugate Chem.* **2002**, *13*, 453-461.

[8] A.L. Acton, C. Fante, B. Flatley, S. Burattini, I.W. Hamley, Z. Wang, F. Greco and W. Hayes, *Biomacromolecules 14*, 564-574.

[9] X. Ma, Z. Zhou, E. Jin, Q. Sun, B. Zhang, J. Tang and Y. Shen, *Macromolecules* **2013**, *46*, 37-42.

[10] C. Gong, S. Deng, Q. Wu, M. Xiang, X. Wei, L. Li, X. Gao, B. Wang, L. Sun, Y. Chen, Y. Li, L. Liu, Z. Qian and Y. Wei, *Biomaterials* **2013**, *34*, 1413-1432.

[11] Y. Xiao, H. Hong, A. Javadi, J.W. Engle, W. Xu, Y. Yang, Y. Zhang, T.E. Barnhart, W. Cai and S. Gong, *Biomaterials* **2012**, *33*, 3071-3082.

[12] R. Duncan, *Cancer Res.* **1992**, *46*, 175-210.

[13] H. Maeda, L.W. Seymour and Y. Miyamoto, *Bioconjugate Chem.* **1992**, *3*, 351-362.

[14] L.W. Seymour, Y. Miyamoto, H. Maeda, M. Brereton, J. Strohalm, K. Ulbrich and R. Duncan, *Eur. J. Cancer* **1995**, *31A*, 766-770.

[15] J.K. Twibanire and T.B. Grindley, *Polymers* **2014**, *6*, 179-213.

[16] W.H. Ang, E. Daldini, L. Juillerat-Jeanneret and P.J. Dyson, *Inorg. Chem.* **2007**, *46*, 9048-9050.

[17] W.H. Ang, A. De Luca, C. Chapuis-Bernasconi, L. Juillerat-Jeanneret, M. Lo Bello and P.J. Dyson, *ChemMedChem* **2007**, *2*, 1799-1806.

[18] W.H. Ang, L.J. Parker, A. De Luca, L. Juillerat-Jeanneret, C.J. Morton, M. Lo Bello, M.W. Parker and P.J. Dyson, *Angew. Chem. Int. Ed.* **2009**, *48*, 3854-3857.

[19] K.-G. Liu, X.-Q. Cai, X.-C. Li, D.-A. Qin and M.-L. Hu, *Inorg. Chim. Acta* **2012**, *388*, 78-83.

[20] M. Auzias, B. Therrien, G. Süss-Fink, P. Štěpnička, W.H. Ang and P. J. Dyson, *Inorg. Chem.* **2008**, *47*, 578-583.

[21] P. Chellan, K.M. Land, A. Shokar, A. Au, S.H. An, D. Taylor, P.J. Smith, T. Riedel, P. J. Dyson, K. Chibale and G.S. Smith, *Dalton Trans.* **2014**, *43*, 513-526.

[22] Ivonne A. Müller, Felix Kratz, Manfred Jung and André Warnecke, *Tetrahedron Lett.* **2010**, *51*, 4371-4374.

[23] M. Sánchez, H. Höpfl, M.E. Ochoa, N. Farfán, R. Santillan and S. Rojas-Lima, *Chem. Eur. J.* **2002**, *8*, 612-621.

[24] B. Li, T. Roisnel, C. Darcel and P.H. Dixneuf, *Dalton Trans.* **2012**, *41*, 10934-10937.

[25] Y. Boutadla, D.L. Davies, R.C. Jones and K. Singh, *Chem. Eur. J.* **2011**, *17*, 3438-3448.

[26] L.C. Sudding, P. Chellan, P. Govender and G.S. Smith, *J. Inorg. Organomet. Polym.* **2015**, *25*, 457-465.

[27] P. Govindaswamy, B. Therrien, G. Süss-Fink, P. Stepnicka and J. Ludvik, *J. Organomet. Chem.* **2007**, *692*, 1661-1671.

[28] G. Gupta, S. Gloria, S.L. Nongbri, B. Therrien and K.M. Rao, *J. Organomet. Chem.* **2001**, *696*, 2014-2022.

[29] T.-T. Thai, B. Therrien and G. Süss-Fink, *Inorg. Chem. Commun.* **2009**, 806-807.

[30] L.C. Sudding, R. Payne, P. Govender, F. Edafe, C.M. Clavel, P.J. Dyson, B. Therrien and G.S. Smith, *J. Organomet. Chem.* **2014**, *774*, 79-85.

[31] P. Govender, H. Lemmerhirt, A.T. Hutton, B. Therrien, P.J. Bednarski and G.S. Smith, *Organometallics* **2014**, *33*, 5535-5545.

[32] P. Govender, A.K. Renfrew, C.M. Clavel, P. J. Dyson, B. Therrien and Gregory S. Smith, *Dalton Trans.* **2011**, *40*, 1158-1167.

[33] P. Govender, L.C. Sudding, C.M. Clavel, P. J. Dyson, B. Therrien and G. S. Smith, *Dalton Trans.* **2013**, *42*, 1267-1277.

[34] R. Payne, P. Govender, B. Therrien, C.M. Clavel, P. J. Dyson and G. S. Smith, *J. Organomet. Chem.* **2013**, *729*, 20-27.

[35] M.G. Mendoza-Ferri, C.G. Hartinger, R.E. Eichinger, N. Stolyarova, K. Severin, M.A. Jakupec, A.A. Nazarov and B.K. Keppler, *Organometallics* **2008**, *27*, 2405-2407.

[36] M.G. Mendoza-Ferri, C.G. Hartinger, M.A. Mendoza, M. Groessl, A.E. Egger, R.E. Eichinger, J.B. Mangrum, N. P. Farrell, M. Maruszak, P.J. Bednarski, F. Klein, M.A. Jakupec, A.A. Nazarov, K. Severin and B.K. Keppler, *J. Med. Chem.* **2009**, *52*, 916-925.

[37] A.M. Pyle and J.K. Barton, *Prog. Inorg. Chem.* **1990**, *38*, 413-476.

[38] S. Machana, N. Weerapreeyakul and S. Barusrux, *Asian Pac. J. Trop. Biomed.* **2012**, *2*, 368-374.

[39] W. Xu, S. Wang, Q. Chen, Y. Zhang, P. Ni, X. Wu, J. Zhang, F. Qiang, A. Li, O. D. Røe, S. Xu, M. Wang, R. Zhang and J. Zhou, *Cell Death Dis.* **2014**, *5*, 1055-1066.

[40] M.G. Mendoza-Ferri, C.G. Hartinger, A.A. Nazarov, R.E. Eichinger, M.A. Jakupec, K. Severin and B.K. Keppler, *Organometallics* **2009**, *28*, 6260-6265.

[41] C. Gossens, A. Dorcier, P.J. Dyson and U. Rothlisberger, *Organometallics* **2007**, *26*, 3969-3975.

[42] C. Scolaro, C.G. Hartinger, C.S. Allardyce, B.K. Keppler and P.J. Dyson, *J. Inorg. Biochem.* **2008**, *102*, 1743-1748.

[43] M. Groessl, Y.O. Tsybin, C.G. Hartinger, B.K. Keppler and P.J. Dyson, *J. Biol. Inorg. Chem.* **2010**, *15*, 677-688.

[44] A.E. Egger, C.G. Hartinger, A.K. Renfrew and P.J. Dyson, *J. Biol. Inorg. Chem.* **2010**, *15*, 919-927.

[45] A. Dorcier, P. J. Dyson, C. Gossens, U. Rothlisberger, R. Scopelliti and I. Tavernelli, *Organometallics* **2005**, *24*, 2114-2123.

[46] A. Dorcier, C.G. Hartinger, R. Scopelliti, R.H. Fish, B.K. Keppler and P. J. Dyson, *J. Inorg. Biochem.* **2008**, *102*, 1066-1076.

[47] MarvinSketch, ChemAxon, (2013) V. #5.9.4

Chapter 3: Synthesis, Characterization and Antitumor Activity of New Trinuclear Alkylated PTA containing Rh(III), Ir(III) and Ru(II) complexes

3. Introduction

Due to its' water solubility, PTA has been used to assist in solubilizing some organometallic complexes.[1-2] RAPTA complexes have shown to exhibit selective and potent antitumor activity[3-4] particularly *in vivo* against metastatic[5] and primary tumors.[6] PTA-derived compounds seem to impart a pH-dependent activity which provides an opportunity to be biologically active.

PTA and its derivatives easily undergo alkylation at one of the equivalent nitrogen atoms introducing a positive charge. It was established soon after the first preparation of PTA that it can be methylated at an N-atom by methyl iodide.[7-8] Alkylation has shown to increase hydrophilicity of the PTA moiety to afford water-soluble complexes.[9-13]

Alkylated RAPTA analogues have been found to interact with model DNA bases, which is a commonly acknowledged mechanism of action, for this class of compounds, explaining their antitumor activity.[13] Alkylated Rh- and Ir-PTA half-sandwich analogues have not been explored extensively, although displaying promising antitumor activity.[14]

Kathó and co-workers prepared a water-soluble monodentate dinuclear Ru(II) complex $[Ru_2(\eta^6\text{-}p\text{-cymene})_2Cl_2\{(PTA)CH_2C_6H_4CH_2(PTA)\}][Cl]_2$ (Figure 3.1) but no biological application of this compound was studied.[15]

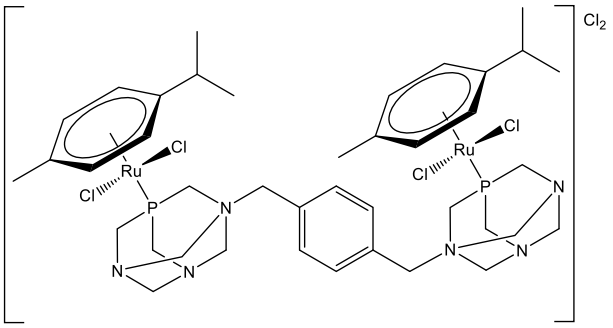

Figure 3.1 *Dinuclear $[Ru_2(\eta^6\text{-p-cymene})_2Cl_2\{(PTA)CH_2C_6H_4CH_2(PTA)\}][Cl]_2$.*

In this chapter, the preparation and characterization of a new trimeric tricationic alkylated PTA-based ligand is described. This trimeric ligand was used to prepare trinuclear rhodium-Cp*, iridium-Cp* and ruthenium-arene complexes. Mononuclear analogues were also prepared for comparison. The proposed structures were confirmed using spectroscopic and analytical techniques. The discussion of the biological activity of these complexes is included.

3.1. Synthesis and Characterization of Cationic Alkylated Ligands

The monomeric cationic alkylated PTA ligand **3.1**[12] was synthesized using known methods. The bromide analogue was used to prepare 1,3,5-tris(chloromethyl)benzene by simple halogen metathesis[16] and was reacted with PTA to afford **3.2**.

The reactants were refluxed in acetone to afford the cationic alkylated PTA salt **3.2**, which was filtered on a Hirsch funnel and washed with tetrahydrofuran and copious amounts of dichloromethane. **3.2** was isolated as a hygroscopic beige salt with a near stoichiometric yield of 97% and is soluble in water, dimethylsulfoxide and methanol yet insoluble in dichloromethane, tetrahydrofuran and diethylether. Spectroscopic (^{1}H NMR, ^{13}C{^{1}H} ^{31}P{^{1}H} NMR and FT-IR spectroscopy) and analytical data (elemental analysis and mass spectrometry) confirmed the proposed structure of the trimeric ligand **3.2**.

The ^{1}H, ^{13}C{^{1}H} and ^{31}P{^{1}H} NMR spectra of **3.2** were recorded in deuterium oxide (D_2O) and were comparable with the monomeric analogue.[12] A single nitrogen of the PTA moiety was alkylated once and only mono-alkylation was observed. Evidence for this is shown in the ^{1}H and ^{13}C{^{1}H} NMR spectra.

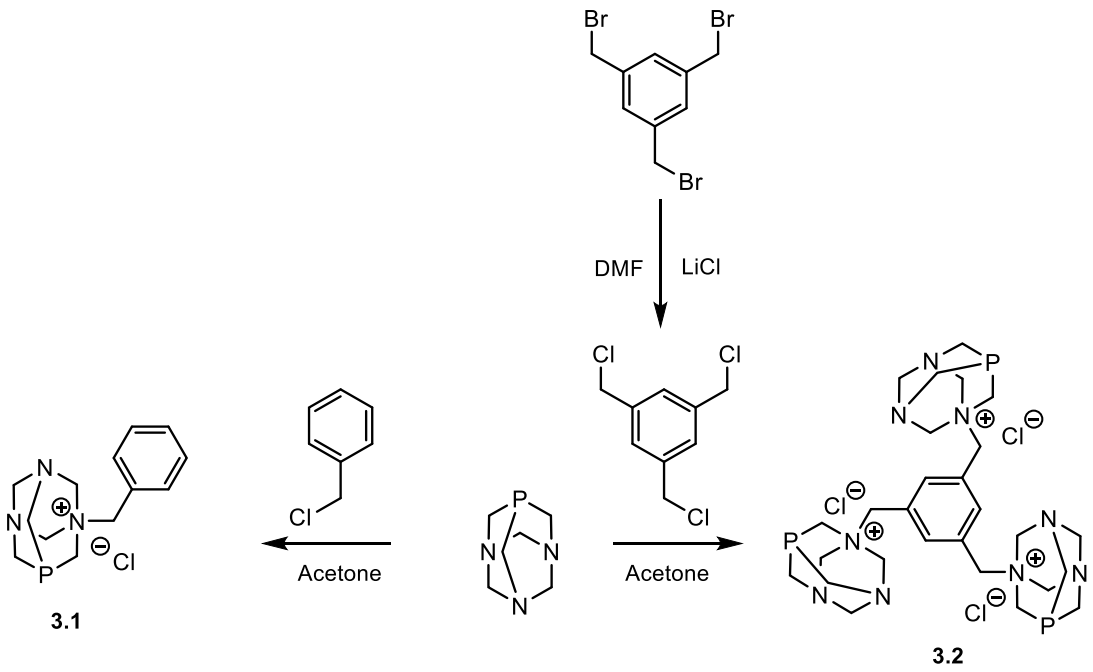

Scheme 3.1 *Synthesis of cationic alkylated PTA ligands* ***3.1*** *and* ***3.2****.*

In the ^{1}H NMR spectrum of **3.2**, the proton resonance of the benzyl core is observed as a sharp singlet at δ 7.95 ppm. Evidence for alkylation of the PTA is observed in the splitting pattern of the $–CH_2$ protons of the PTA. Upon quaternization of the nitrogen atom the protons exist in an AB spin system and are assigned as either axial or equatorial. Other alkylated PTA compounds with $–CH_{Ax}H_{Eq}$ protons have been reported previously.[10, 17-19]

Upon alkylation of the PTA cage the six sets of $–CH_2$ protons exist in four environments (Figure 3.2). As a result of alkylation three quartets and one doublet are observed in the ^{1}H NMR spectrum. In the case of **3.2**, the most downfield quartet for the four protons of $N\text{-}CH_2\text{-}N^+$ (Figure 3.2 at blue position 1) is observed at δ 5.14 ppm ($J_{H\text{-}H}$ = 12 Hz), a less intense quartet for two protons is observed at δ 4.63 ppm ($J_{H\text{-}H}$ = 9 Hz) of $N\text{-}CH_2\text{-}N$ (Figure 3.2 at orange position 2) and the third quartet for four protons of $P\text{-}CH_2\text{-}N$ (Figure 3.2 at green position 3) appears upfield at δ 4.02 ppm ($J_{H\text{-}H}$ = 9 Hz). A doublet at δ 4.47 ppm ($J_{H\text{-}H}$ = 6 Hz) was assigned as the two protons of $P\text{-}CH_2\text{-}N^+$.

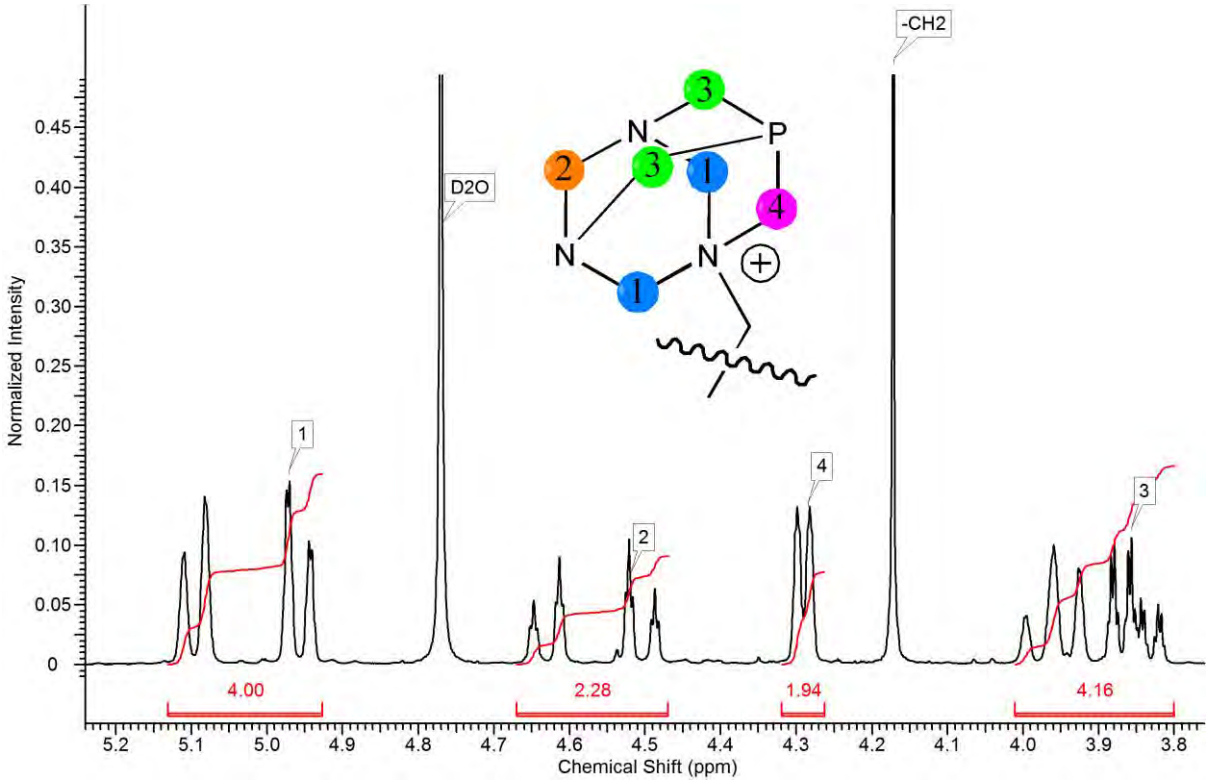

Figure 3.2 *A representative example of a ^{1}H NMR spectrum displaying the four different alkyl environments of an alkylated PTA ligand.*

Signals in the $^{13}C\{^{1}H\}$ NMR spectrum at δ 139.38 ppm and δ 127.67 ppm were assigned as the secondary and tertiary carbons of the aromatic benzyl core, respectively. The $–CH_2$ carbons between the aromatic core and the PTA cages exhibited signals at δ 65.23 ppm.

Heteronuclear Spin-Quantum Coupling Spectroscopy (HSQC) allows identification of which protons are coupling with other nuclei, such as ^{13}C, and allow for the correlation of which protons are situated on their respective carbons. Use of $[^{1}H\text{-}^{13}C]$ HSQC NMR spectroscopy aided with the assignment of the signals for the $–CH_2$ carbons of the PTA moiety (Figure 3.3).

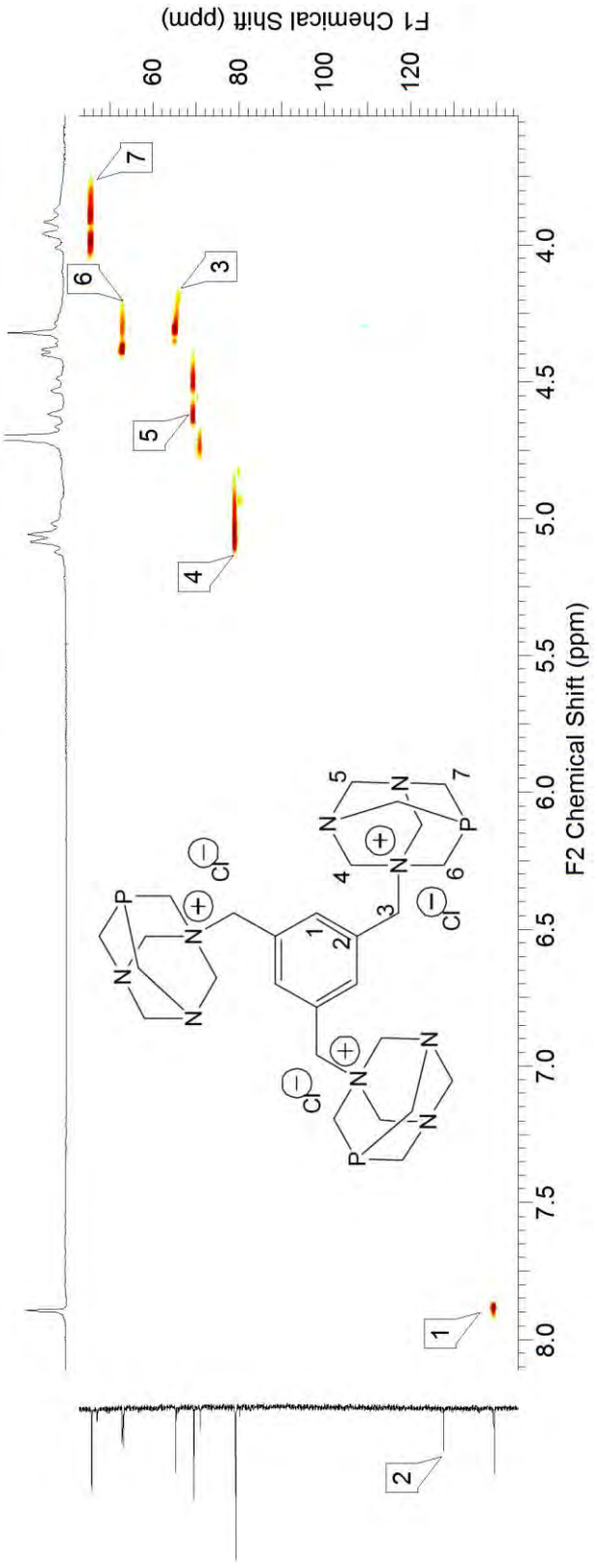

Figure 3.3 *[^{1}H- ^{13}C] HSQC NMR spectrum of trimeric alkylated PTA ligand* ***3.2*** *in D_2O.*

The alkylation of the PTA moiety was further confirmed by the presence of four signals in the $^{13}C\{^{1}H\}$ NMR spectrum. The signals at δ 79.18 ppm and δ 69.46 ppm were assigned as N-CH_2-N^+ and N-CH_2-N, respectively. Two doublets, due to the carbons coupling with the NMR spin-active phosphorous, at δ 52.93 ppm (J_{P-C} = 24 Hz,) and δ 45.61 ppm (J_{P-C} = 14 Hz) were assigned as P-CH_2-N^+ and P-CH_2-N, respectively.

The presence of a singlet in the $^{31}P\{^{1}H\}$ NMR spectrum at δ -81.95 ppm (Table 3.1) attested to the presence of only one phosphorous species and the purity of **3.2**. Furthermore, high resolution electrospray ionization mass spectrometry (HR-ESI-MS) which shows *m/z* = 196.0998 for the trimeric ligand, after the loss of the three stabilizing chloride anions, as $[M-3Cl]^{3+}$. This mass spectrometry data confirms the triple charge of the ligand. These spectral data assignments are comparable with the alkylated PTA dimer ligand prepared by Kathó and co-workers.[20]

Table 3.1 *$^{31}P\{^{1}H\}$ NMR resonance signals and mass spectral data for compounds **3.1** and **3.2**.*

Compound	$^{31}P\{^{1}H\}$ NMR [ppm][a]	HR-ESI-MS $[M-nCl]^{n+}$ [*m/z*]
3.1	-82.61	248.1307[b]
3.2	-81.95	196.0998[c]

[a]Recorded in D_2O; [b]n = 1; [c]n = 3.

The tricationic salt **3.2** displayed elemental analysis percentages outside of acceptable limits, despite extensive drying, and these were due to the hygroscopic nature of the ligand. Recalculation of the percentages with the inclusion of water gave percentages within acceptable limits. In the ^{1}H NMR spectrum a peak assigned as water was observed, which supports the inclusion of water in the sample.

3.2. Synthesis and Characterization of Trinuclear Rhodium(III), Iridium(III) and Ruthenium(II) PGM Complexes

Reaction of the alkylated PTA ligands **3.1** or **3.2** with the precursors dichloro(pentamethylcyclopentadienyl)rhodium(III) dimer, dichloro(pentamethylcyclopentadienyl)iridium(III) dimer or dichloro(*p*-cymene)ruthenium(II) dimer yielded the

mononuclear complexes **3.3-3.5** (Scheme 3.2) or the trinuclear complexes **3.6-3.8** (Scheme 3.3).

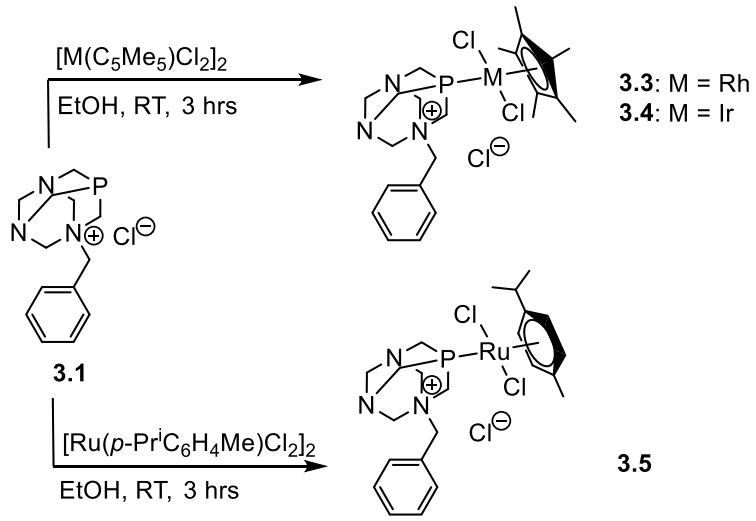

Scheme 3.2 *Synthesis of mononuclear cationic alkylated PTA complexes **3.3-3.5**.*

The complexes **3.3-3.5** were prepared by stirring the appropriate ligand and dimer together as a solution at room temperature. For the preparation of the trinuclear complexes, the reactants were stirred in a mixture of methanol and dichloromethane, while ethanol was used in preparing the mononuclear complexes. The resulting complexes **3.3-3.8** were precipitated from the reaction using diethyl ether as red, orange or yellow hygroscopic solids in moderate yields. The complexes are water-soluble and are soluble in most organic solvents. The mononuclear complexes **3.3-3.5** exhibited greater water solubility, in the range 14-21 mg/ml, than the trinuclear complexes **3.6-3.8** which displayed aqueous solubility in the range 3-12 mg/ml.

Complexes **3.3-3.8** are new and characterization with analytical and spectroscopic techniques was performed. Confirmation of the monodentate coordination occurring through the PTA phosphorous was obtained from the NMR analyses. The NMR spectra of **3.3-3.8** were recorded in deuterium oxide, D_2O, and show relevant peaks which confirm the proposed structures.

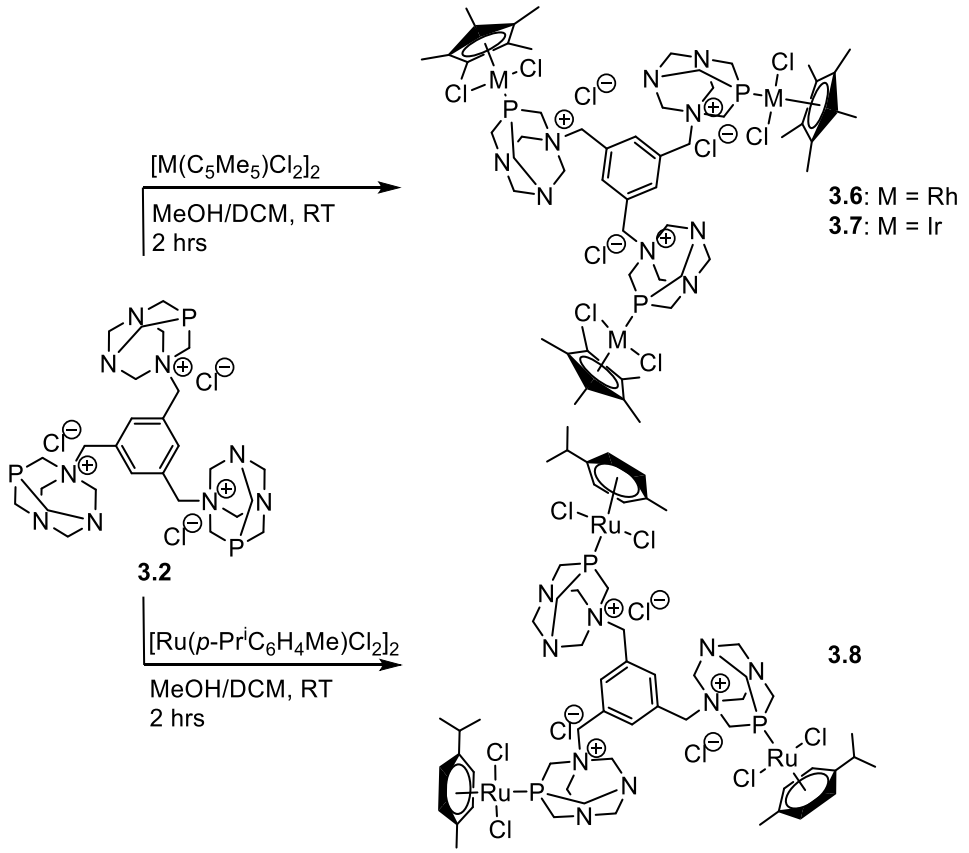

Scheme 3.3 *Synthesis of trinuclear cationic alkylated PTA complexes **3.6-3.8**.*

In both the ^{1}H and $^{13}C\{^{1}H\}$ NMR spectra the signals for the protons and carbons of the aromatic core and the -CH_2 bridge linking the core to the PTA remained largely unchanged.

For the mononuclear complexes **3.3-3.5** a multiplet is observed in the ^{1}H NMR spectra for the four aromatic benzyl protons at ca. δ 7.57 ppm and a sharp singlet is observed at ca. δ 4.36 ppm for the –CH_2 protons linking the benzyl ring to the PTA. For the trinuclear complexes **3.6-3.8**, a singlet is observed for the benzyl core at ca. δ 7.86 ppm and another singlet at ca. δ 4.37 ppm for the -CH_2 protons.

In the $^{13}C\{^{1}H\}$ NMR spectra of the mononuclear complexes **3.3-3.5** four signals are observed in the range δ 124.20 – 134.21 ppm for the benzyl carbons. Two signals, which are assigned to the aromatic core, are observed for the trinuclear complexes **3.6-3.8** at ca. δ 126.91 ppm and ca. δ 142.42 ppm. The upfield signal at δ 126.91 ppm was assigned as the tertiary carbon of the aromatic core and the downfield signal at δ 142.42 ppm was assigned as the secondary carbon, due to ^{1}H, ^{13}C HSQC coupling.

The most significant shifts in the ^{1}H and $^{13}C\{^{1}H\}$ NMR spectra were for the signals assigned to that of the PTA cage. These shifts are attributed due to coordination of the metal-arene to

the phosphorous of the PTA. The resonances assigned to the PTA cage for the complexes **3.3-3.8** are recorded in Table 3.2, and ligands **3.1** and **3.2** have been included for comparison.

The largest shifts in the ^{1}H NMR spectra upon coordination were observed in the signals assigned to as P-CH_2-N^+ and P-CH_2-N (Table 3.2). The signals assigned to the protons of P-CH_2-N^+ shifted downfield upon coordination of the metal-arene from δ 4.29 ppm to ca. δ 4.46 ppm for the mononuclear complexes **3.3-3.5** and from δ 4.47 ppm to ca. δ 4.56 ppm in the trinuclear complexes **3.6-3.8**. Similarly, the signals assigned to the protons of P-CH_2-N displayed a larger downfield shift from δ 3.94 ppm to ca. δ 4.30 ppm for the mononuclear complexes **3.3-3.5** and from δ 4.00 ppm to ca. δ 4.28 ppm in the trinuclear complexes **3.6-3.8**.

Table 3.2 *^{1}H and ^{13}C{^{1}H} NMR resonance signals for the PTA cages of compounds* **3.1-3.8***.*

Compound	**^{1}H NMR** [ppm]				**^{13}C{^{1}H} NMR** [ppm]			
	N-CH_2-N^+	N-CH_2-N	P-CH_2-N^+	P-CH_2-N	N-CH_2-N^+	N-CH_2-N	P-CH_2-N^+	P-CH_2-N
3.1[a]	5.03	4.57	4.29	3.94	79.61	69.97	52.74	46.10
3.2[b]	5.12	4.78	4.47	4.00	79.18	69.46	52.93	45.61
3.3[a]	5.08	4.70	4.47	4.38	79.28	69.38	51.48	46.08
3.4[a]	5.10	4.60	4.48	4.24	81.19	71.06	51.85	46.82
3.5[a]	5.09	4.69	4.43	4.27	79.28	69.33	52.23	48.17
3.6[b]	5.16	4.96	4.53	4.27	80.62	69.27	49.45	45.82
3.7[b]	5.18	4.64	4.52	4.24	80.70	69.48	49.31	45.12
3.8[b]	5.89	5.13	4.63	4.34	80.57	69.11	55.64	48.01

[a]Recorded in CD_3OD; [b]Recorded in D_2O.

In the ^{1}H NMR spectra of the rhodium pentamethylcyclopentadienyl derivatives, **3.3** and **3.6**, the methyl protons of the pentamethylcyclopentadienyl ligand exhibit a doublet at ca. δ 1.71 ppm (J_{H-P} = 4 Hz). Sharp and co-workers previously reported a Rh(II)-Cp* complex which exhibited a similar proton-phosphorous coupling, which resulted in the signals for the protons of the pentamethylcyclopentadienyl ring in the ^{1}H NMR spectrum appearing as a doublet which integrates for 15 protons.[21] In the iridium(III) pentamethylcyclopentadienyl derivatives, **3.4** and **3.7**, a doublet is observed upfield at ca. δ 1.76 ppm (J_{H-P} = 4 Hz) and this is assigned to

the methyl protons. In the $^{13}C\{^1H\}$ NMR spectra the aromatic carbons of the pentamethylcyclopentadienyl ring are observed at ca. δ 101.99 ppm for the rhodium(III) and at ca. δ 95.49 ppm for the iridium(III) complexes. The methyl substituents on the pentamethylcyclopentadienyl ring display signals further upfield at ca. δ 9.03 ppm for the rhodium(III) (Figure 3.4) and at ca. δ 9.12 ppm for the iridium(III) complexes.

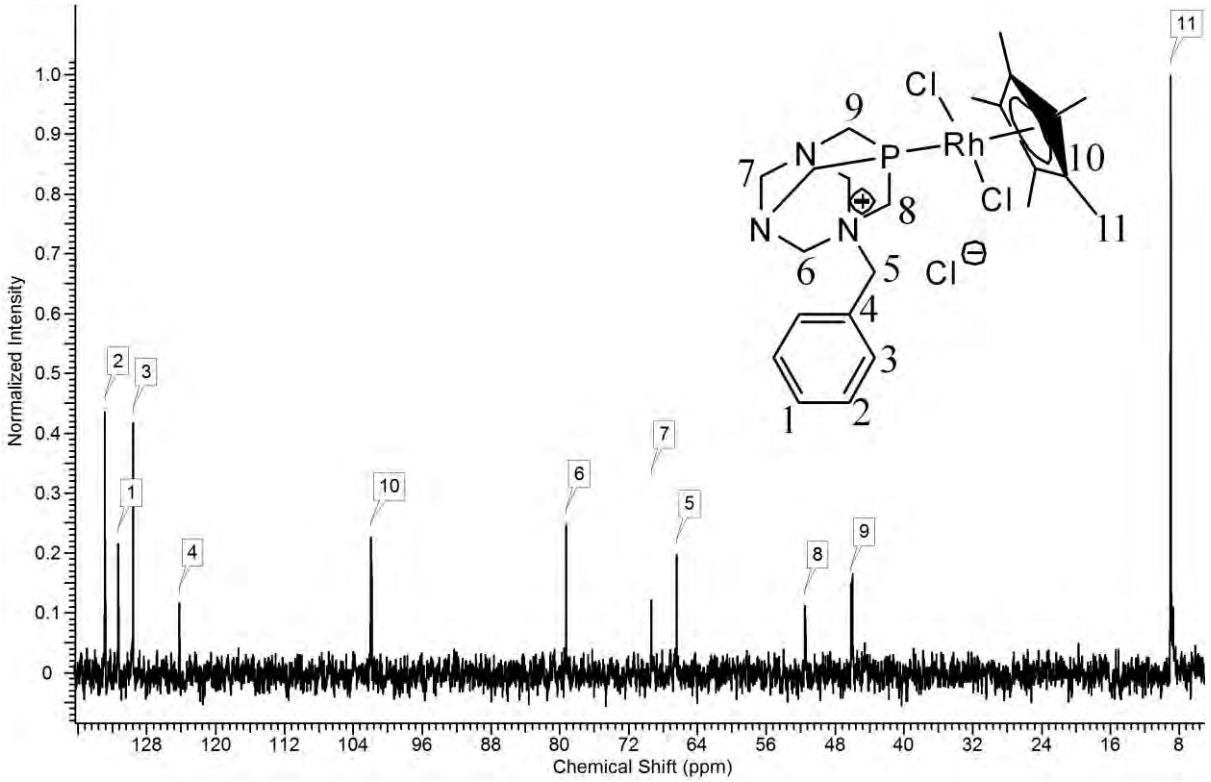

Figure 3.4 *$^{13}C\{^1H\}$ NMR spectrum of complex **3.3**.*

The signals for the aromatic protons of the *p*-cymene ring in the ^1H NMR spectrum of the trinuclear ruthenium(II) complex **3.8** are observed as a multiplet in the range δ 5.86 – 5.92 ppm. The methyl protons of the *p*-cymene moiety appear as a singlet at δ 2.04 ppm and as a doublet upfield at δ 1.20 ppm (J = 7 Hz). In the $^{13}C\{^1H\}$ NMR spectrum of **3.8** the signals at δ 108.32 ppm, δ 99.23 ppm, δ 89.04 ppm, δ 86.57 ppm provide confirmation of the aromatic carbons of the *p*-cymene ring. Further upfield, resonances at δ 21.33 ppm and δ 30.78 ppm were assigned to the *iso*propyl moiety and the methyl carbon of the *p*-cymene ring exhibited a signal at δ 17.93 ppm.

The downfield shift in the singlet, for the iridium(III) or ruthenium(II) complexes, or doublet, for the rhodium(III) complexes, observed in the $^{31}P\{^1H\}$ NMR spectra of complexes **3.3-3.8** provide

evidence that coordination to the metal arene occurs *via* the phosphorous in the PTA cage (Figure 3.5).

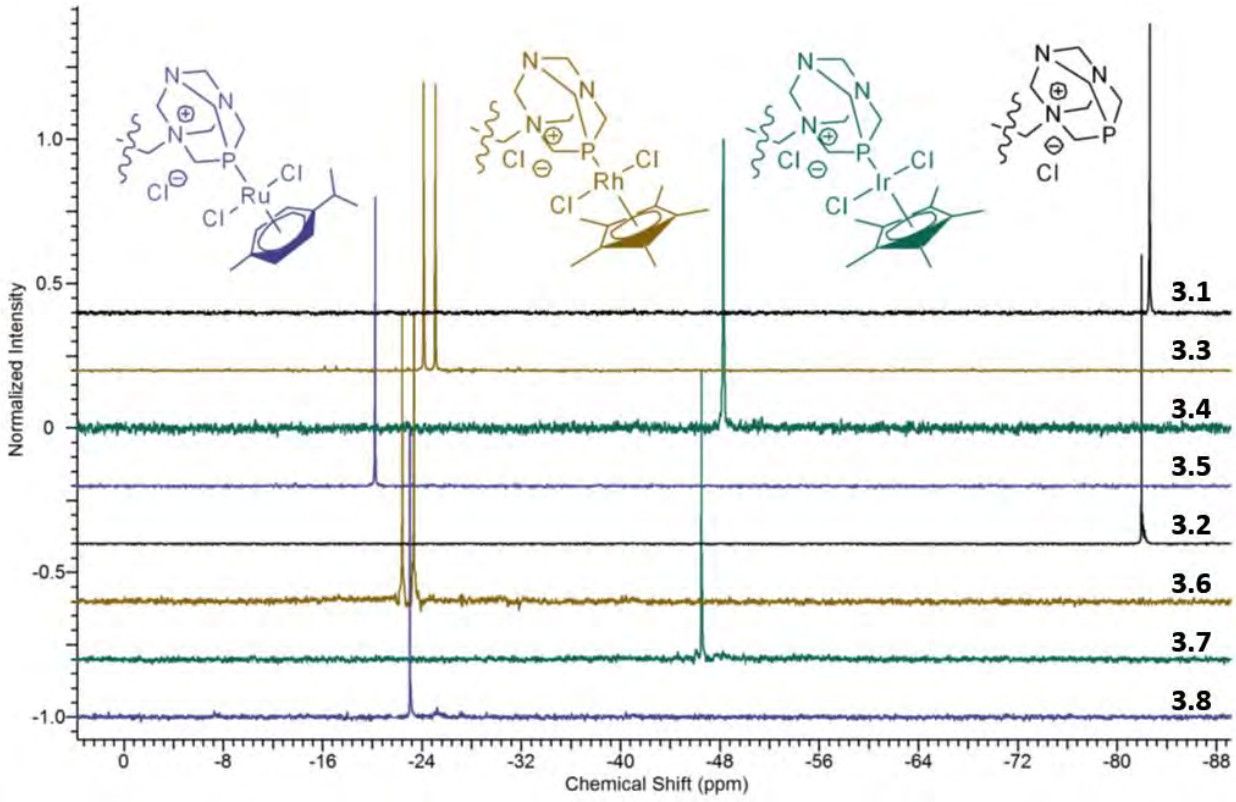

Figure 3.5 *$^{31}P\{^1H\}$ NMR spectra of* **3.1-3.8** *displaying the downfield shift of the free ligands (black), iridium(III) (teal), rhodium(III) (gold) and ruthenium(II) (purple) complexes with mono- (above) and trinuclear (below).*

For the rhodium(III) complexes a doublet was observed in the $^{31}P\{^1H\}$ NMR spectra at δ -24.63 ppm ($^1J_{Rh\text{-}P}$ = 150 Hz) for **3.3** and at δ -22.89 ppm ($^1J_{Rh\text{-}P}$ = 151 Hz) for **3.6** (Table 3.3). The doublet is attributed to the phosphorous-rhodium coupling and further corroborates the rhodium coordination to the phosphorous. The ^1J coupling constants are consistent with similar rhodium(III)-phosphanes reported.[13, 22-24] The iridium(III) complexes **3.4** and **3.7** display the most upfield singlets in the $^{31}P\{^1H\}$ NMR spectra of the alkylated PTA complexes at δ -48.77 ppm and at δ -46.52 ppm, respectively. Far upfield chemical shifts are common for iridium(III)-phosphanes.[25] This shielding effect is due to the significantly larger shielding constant of iridium(III) in comparison to that of rhodium(III) and ruthenium(II), which are comparable.[26] This explains why the resonances in the $^{31}P\{^1H\}$ NMR spectra for the rhodium(III) and ruthenium(II) complexes are clustered together in the narrow range δ -24.63

to -20.23 ppm. The ruthenium(II) complex **3.8** exhibits a signal at -23.03 ppm and this is consistent with the observed resonances for the known mono-[27] and binuclear[15] analogues.

Table 3.3 *$^{31}P\{^1H\}$ NMR resonance signals and HR-ESI-MS data for the complexes* **3.3-3.8***.*

Compound Number	**$^{31}P\{^1H\}$ NMR** [ppm]	**HR-ESI-MS** [*m/z*]
3.3[a]	-24.63 (d, $^1J_{Rh-P}$ = 150 Hz)[c]	558.0898 $[M-Cl]^+$
3.4[a]	-48.77 (s)	646.1473 $[M-Cl]^+$
3.5[a]	-20.23 (s)	554.0833 $[M-Cl]^+$
3.6[b]	-22.89 (d, $^1J_{Rh-P}$ = 151 Hz)[d]	478.0514 $[M-5Cl+2H]^{3+}$
3.7[b]	-46.52 (s)	570.1178 $[M-5Cl+2H]^{3+}$
3.8[b]	-23.03 (s)	480.0599 $[M-5Cl+2H]^{3+}$

[a]Recorded in CD_3OD; [b]Recorded in D_2O.

HR-ESI-Mass spectral analysis of complexes **3.3-3.8,** display base peaks which were assigned as fragments of the molecular ion which correspond to the formula weight of the proposed structures (Table 3.3). The mononuclear alkylated PTA complexes **3.3-3.5** exhibit *m/z* peaks which were assigned to the ion with the loss of the stabilizing chloride counter-ion $[M-Cl]^+$ and were consistent with the expected isotopic mass distribution pattern of the respective metal. The trinuclear complexes **3.6-3.8** show a *m/z* base peak which corresponds to the triple charged adduct $[M-5Cl+2H]^{3+}$.

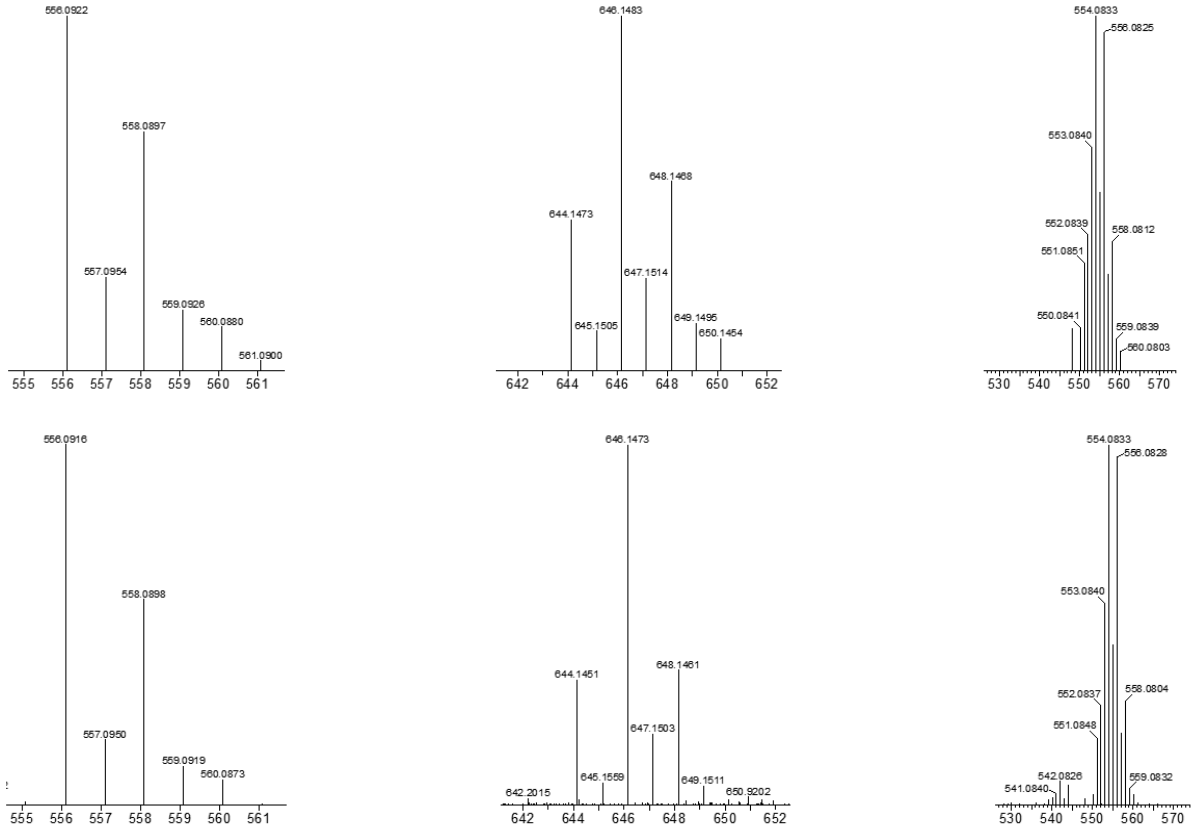

Figure 3.6 *Calculated (top) and experimental (bottom) expanded HR-ESI-MS traces for mononuclear alkylated PTA complexes* ***3.3*** *(left),* ***3.4*** *(center) and* ***3.5*** *(right).*

The alkylated PTA complexes **3.3-3.8** displayed elemental analysis percentages outside of acceptable limits, despite extensive drying, and similarly upon recalculation of the percentages with the inclusion of water gave percentages within acceptable limits. In the ^{1}H NMR spectrum a peak assigned as water was observed, which supports the inclusion of water in the sample.

3.3. *In vitro* Biological Activity

The *in vitro* cytotoxicity of the mono- and trinuclear alkylated PTA compounds **3.1-3.8** was established against WHCO1 human esophageal cancer cells. This squamous cell carcinoma of the esophagus was selected due to the significant prevalence of this form of cancer in African countries.[28]

Table 3.4 *IC_{50} values determined against WHCO1 human esophageal cancer cells for compounds **3.1-3.8**.*

Compound Number	Metal	IC_{50} (μM)
		WHCO1
3.1	-	>250
3.2	-	>250
3.3	Rh	94.1 ± 8.2
3.4	Ir	48.3 ± 8.8
3.5	Ru	105.3 ± 6.4
3.6	3 Rh	61.2 ± 10.0
3.7	3 Ir	111.5 ± 4.2
3.8	3 Ru	66.0 ± 9.6
Cisplatin	Pt	9.2 ± 0.1[29]

Ligands **3.1-3.2** were inactive against the WHCO1 cells. The dependence of the presence of a coordinated metal is seen in the increase in activity for complexes **3.3-3.8** from the ligands **3.1-3.2**. The rhodium(III) and ruthenium(II) complexes displayed a size dependent activity relationship (Figure 3.7). The trinuclear alkylated PTA complexes **3.6** and **3.8** exhibited IC_{50} values of 61.2 μM and 66.0 μM, respectively displaying enhanced activity over the mononuclear analogues **3.3** and **3.5**. This increase in cytotoxicity can be attributed to the increase in the number of metal centers.[30-32] It should be noted that the mononuclear alkylated PTA iridium(III) complex **3.4** displayed the greatest activity in the WHCO1 cell line, with an

IC_{50} value of 48.3 μM (Table 3.4) and shows greater than a two fold increase in cytotoxicity compared to its corresponding trinuclear iridium(III) analogue **3.7** (Figure 3.7).

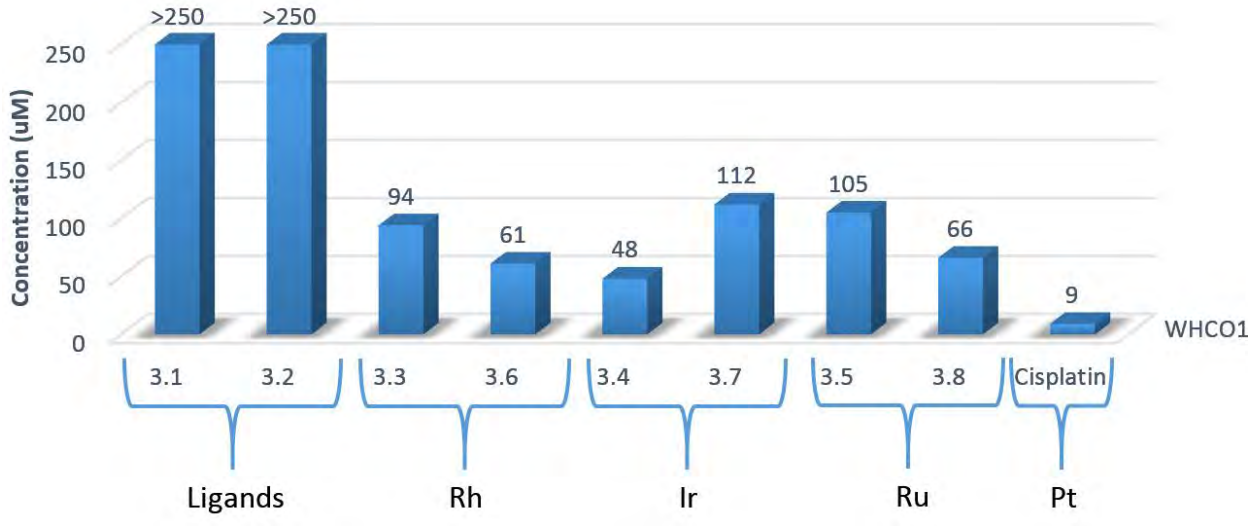

Figure 3.7 *Cytotoxicity of alkylated PTA compounds* ***3.1-3.8*** *and cisplatin against WHCO1.*

Since the cytotoxicity of **3.4** in WHCO1 superseded that of the entire series, the aqueous stability and ability of **3.4** to interact with small molecules of biological importance, was investigated and monitored by NMR spectroscopy. The aim of these studies is to provide mechanistic insight to rationalize the observed biological activities of these complexes.

3.4. Aqueous Stability

Metal complexes appear to undergo a number of different processes *in vivo,* including ligand substitution to form aqua species.[33] Aqueous stability investigation is an important part of preclinical testing of potential drug candidates. These hydrolysis studies clarify the stability of complexes in solution.

The aqueous stability of **3.4** in D_2O was investigated to assess the ability of this complex to form the activated aqua species. D_2O was chosen as a media as it represents the solvent with which this series of complexes are dissolved in to prepare the stock solutions for *in vitro* cytotoxicity studies. Using ^{1}H and $^{31}P\{^{1}H\}$ NMR spectroscopy the stability was monitored over 48 hours at the physiological temperature of 37 ^{o}C.

After 48 hours in solution the mononuclear alkylated PTA iridium(III) complex **3.4** showed no sign of aqueous instability. Both the ^{1}H and $^{31}P\{^{1}H\}$ NMR spectra remained constant over the

tested time. The lack of the appearance of any other signals, such as degradation species, in the $^{31}P\{^{1}H\}$ NMR spectra confirm the aqueous stability of **3.4** (Figure 3.8).

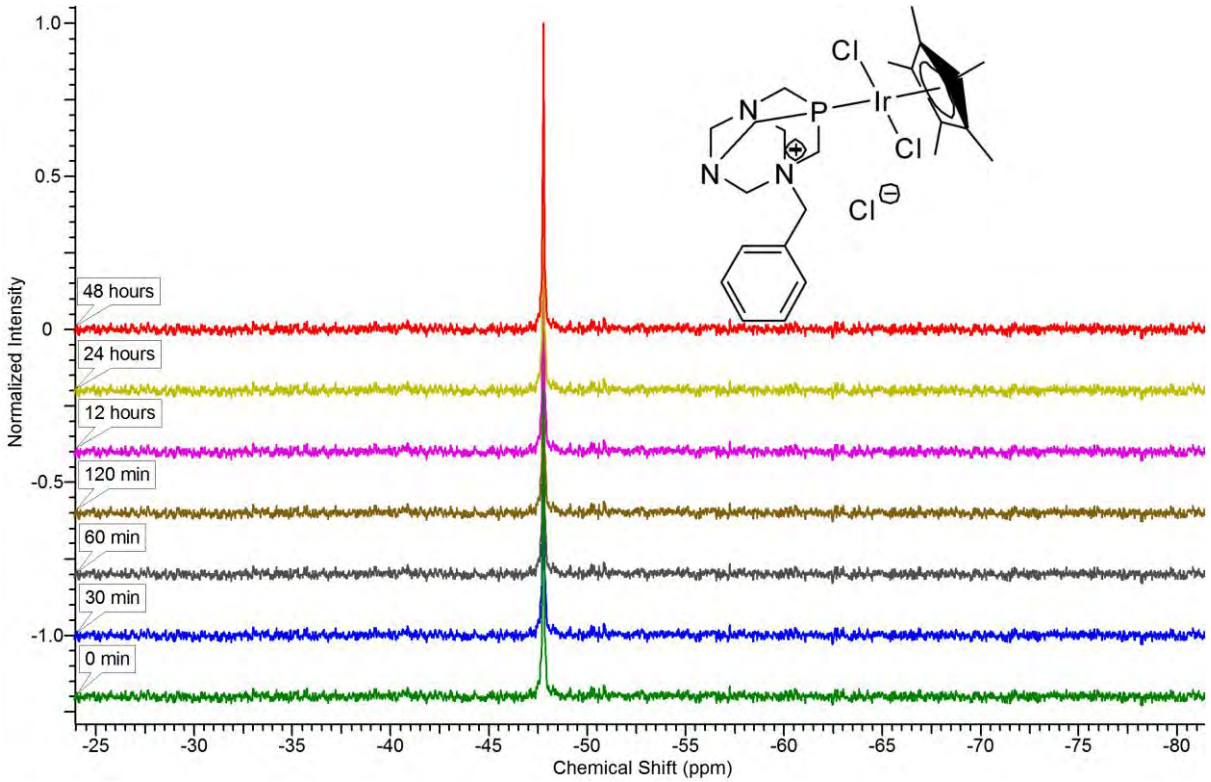

Figure 3.8 *$^{31}P\{^{1}H\}$ NMR spectra showing the aqueous stability of mononuclear **3.4** in D_2O over 48 hours.*

The stability of **3.4** in aqueous media suggests that the active aqua species is unable to form, in this iridium(III) complex. This could explain the relatively low cytotoxicity of this alkylated PTA complex, being the most active against WHCO1 cells. Thus, the cytotoxicity of these complexes is due to some other mode of action and is not because of aquation to form the active aqua species. Though **3.4** is inert in water, it has been reported that in the presence of other ligands (such as in biological media), complexes do in fact coordinate to molecules of biological importance.[34]

3.5. Interactions with Model DNA 5'-GMP

One of the most important targets for PGM anticancer complexes is regarded to be DNA. PGM complexes initially bind to the negatively charged phosphate backbone of DNA yet guanine

residues are considered to be the preferred binding target due to the softer nucleobase donor atoms.[35] Changes to the secondary structure of DNA as a result of coordination prevent further replication or transcription. However this should not be mistaken for the potential sole mode of action.

The ability of the mononuclear alkylated PTA complex **3.4** to interact with the DNA model nucleotide 5'-GMP in D_2O at 37 °C was monitored by ^1H and $^{31}P\{^1H\}$ NMR spectroscopy for 48 hours.

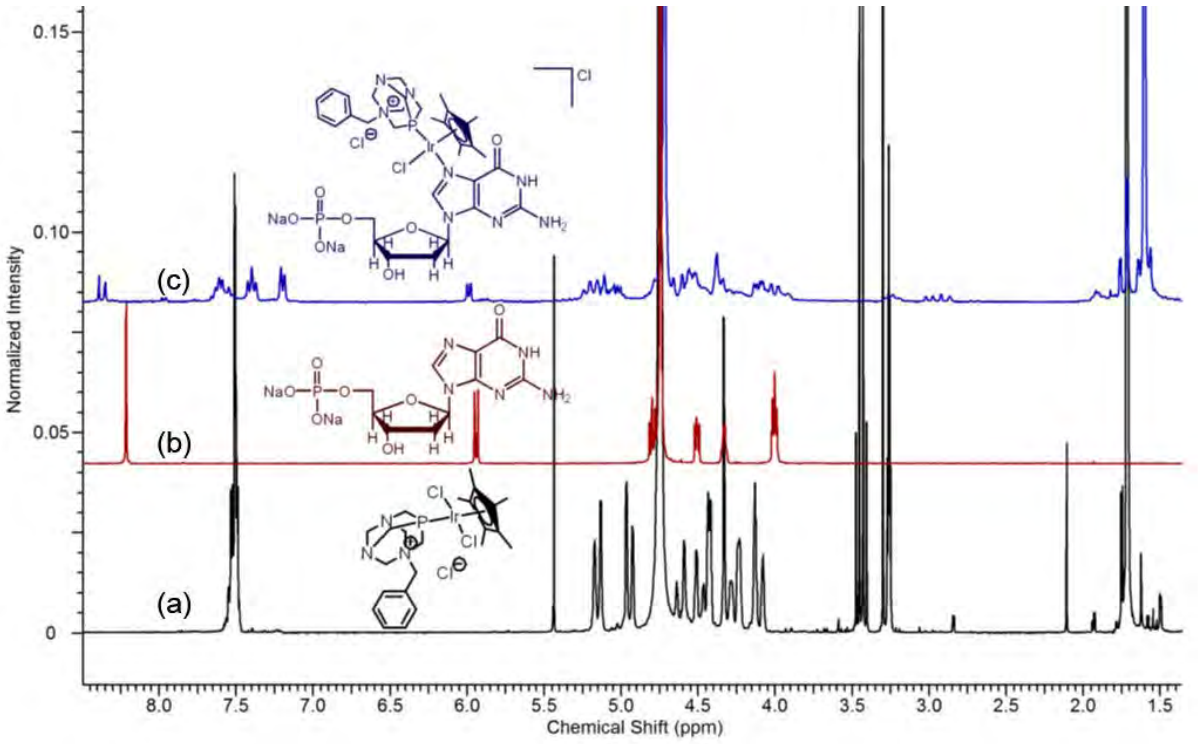

Figure 3.9 *^1H NMR spectra in D_2O of (a)* ***3.4*** *(black), (b) 5'-GMP (red) and (c) reaction mixture of* ***3.4*** *with 5'-GMP (blue).*

Equimolar amounts of 5'-GMP and **3.4** were reacted together and the DNA model, 5'-GMP, was observed to coordinate to the metal *via* the N_7 atom complex. A downfield shift is observed in the ^1H NMR spectrum of the reaction of the signal for the proton, H8, adjacent to N7 from δ 8.22 ppm (Figure 3.9b) to δ 8.40 ppm (Figure 3.9c). The equivalence of the integration of this signal to the doublet upfield at δ 6.02 ppm (^3J = 7 Hz), assigned as the proton on the carbon bonded to the guanosine base pair, confirms its identity as H8. The split nature of this signal could be attributed to coupling with the NMR spin-active phosphorous of the PTA moiety or potentially the formation of diastereoisomers. Similar shifts for iridium(III) complexes have

been observed (See Chapter 2). The multiplet observed at (Figure 3.9a) δ 7.57 ppm assigned to the H1-H3 of the phenyl ring split into the three signals at (Figure 3.9c) δ 7.25 ppm (d, ^{3}J = 8 Hz, 2H, H3), δ 7.45 ppm (t, ^{3}J = 8 Hz, 2H, H2) and δ 7.66 ppm (d, ^{3}J = 6 Hz, 1H, H1). This was confirmed by two-dimensional (2D) ^{1}H-^{1}H correlation (COSY) NMR spectroscopy as the signals at δ 7.66 ppm (H1) and δ 7.25 ppm (H3) both exhibited coupling with δ 7.45 ppm (H2).

In the ^{31}P{^{1}H} NMR spectrum of the mixture of **3.4** and 5'-GMP, a shift in the signal for **3.4** occurred from δ -48.77 ppm to δ -19.88 ppm along with the appearance of a new signal at δ -2.42 ppm. These two signals are assigned as the **3.4**-5'-GMP complexation product, with the most upfield signal being assigned to the PTA moiety and the downfield signal being assigned to the nucleotide. This data compliments the observation of the shift of the proton signal for H8 in the ^{1}H NMR spectrum and that coordination occurs though N7.[36] It has been reported for other transition metals that metals may coordinate to mononucleotides through N7 and/or *via* the phosphate moiety of the sugar backbone.[37-38]

3.6. Interactions with Histidine

Ruthenium(III) complexes (N)KP1339 and NAMI-A, which are currently undergoing clinical trials, have high affinities for proteins,[39-43] due to their nitrogen and sulfur content, and it is supposed that this may be a reason for their selectivity and ability of targeting tumor cells.[44] Transferrin, the protein responsible for supplying cells with iron used in cell growth and division, is present in plasma and other bodily fluids and easily accessible for binding metal based drugs. It has been reported that NAMI-A and KP1019, the predecessor of (N)KP1339 and imadozolium salt analogue, bind to transferrin on the histidine residue in place of iron. The amino acid, l-histidine is a good constituent of proteins and was thus chosen for this study.

The mononuclear complex **3.4** was reacted with an equimolar amount of histidine in an aqueous solution. Interactions between **3.4** and the amino acid were confirmed by shifts observed in the ^{1}H and ^{31}P{^{1}H} NMR spectra (Figure 3.10). The downfield shifts of the signals at δ 7.05 ppm and δ 7.76 ppm (Figure 3.10b) to δ 7.12 ppm and δ 7.92 ppm (Figure 3.10c) respectively indicate that coordination is most likely occurring at the tertiary nitrogen on the imidazole ring of the amino acid by displacement of the iridium-chloride to form a cationic species.

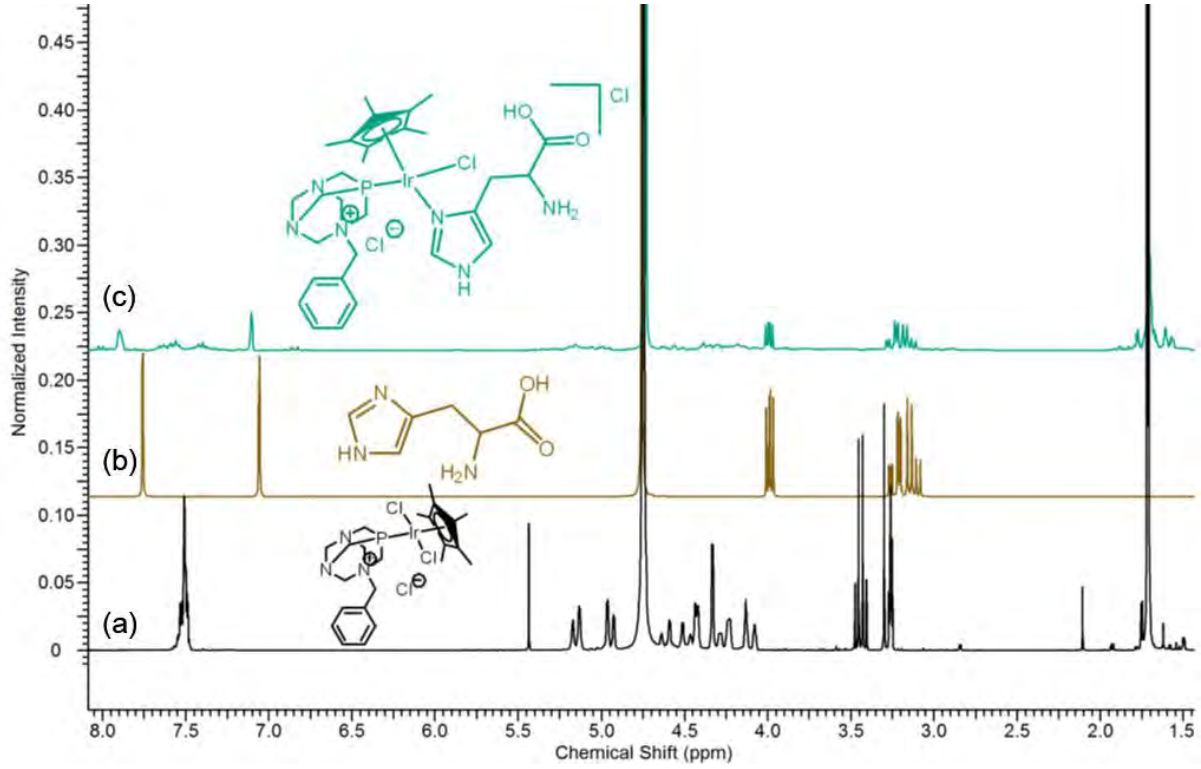

Figure 3.10 *^{1}H NMR spectra in D_2O of (a)* ***3.4*** *(black), (b) histidine (brown) and (c) reaction mixture of* ***3.4*** *with histidine (turquoise).*

In the $^{31}P\{^{1}H\}$ NMR spectrum of the mixture of **3.4** and histidine a shift in the signal for **3.4** occurred from δ -48.77 ppm to δ -51.51 ppm, confirming coordination of histidine.

3.7. DNA Binding Study

It should be clear that the simple reaction of metal ions with isolated nucleotides is not conclusively comparable to that with double-stranded DNA.[45] To further probe the ability of **3.4** to interact with the macromolecule DNA, UV-Vis absorption studies were performed with Red Salmon testes DNA, isolated from the sperm cells. This is a good source of non-mammalian DNA from the species *Oncerhynchus keta*. This non-mammalian DNA suffices for this *in vitro* DNA interaction study and is commonly used to monitor DNA interactions *via* UV-Vis spectroscopy.[46-52]

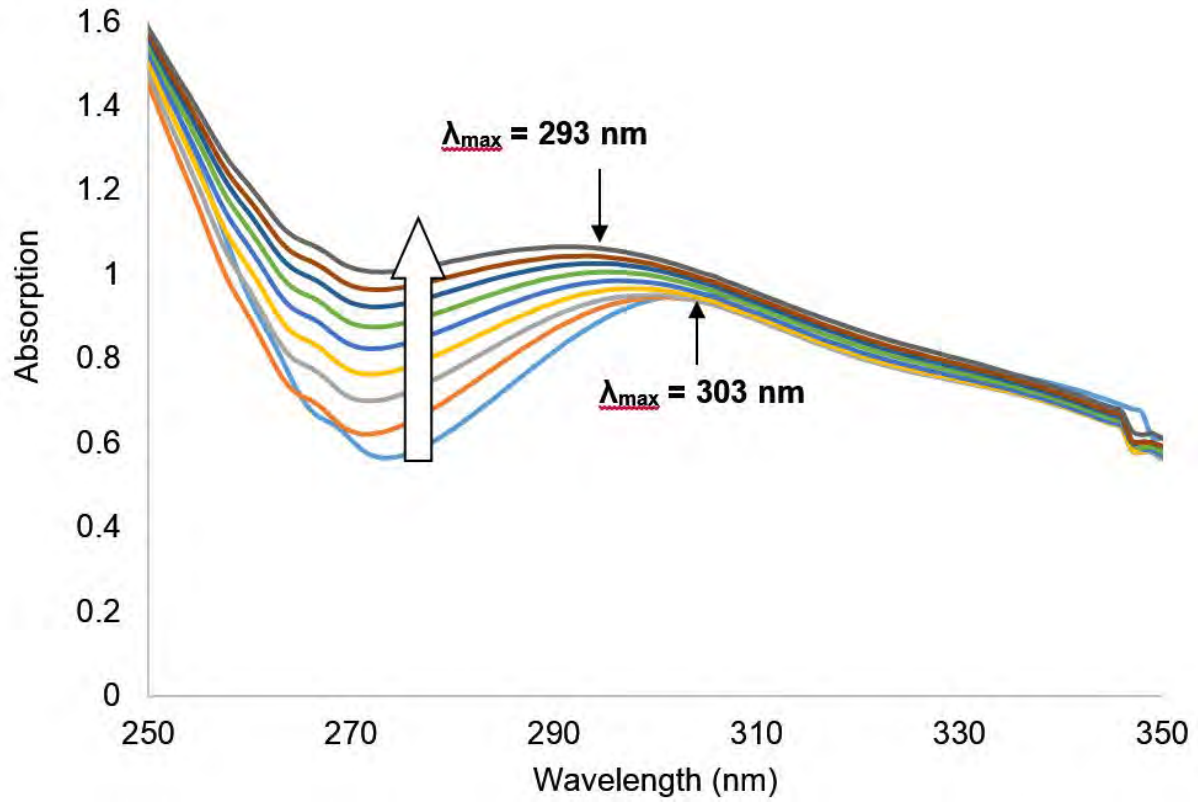

***Figure 3.11**: UV absorption spectra of 0.33 mM **3.4** in 0.2 mM HEPES buffer, pH 7.4, in H_2O in the absence (bottom blue) and then in the presence of increasing concentration of Red Salmon testes DNA.*

It is known that the hormone and neurotransmitter, Norepinephrine binds to DNA and results in a red hyperchromic shift at λ_{max}.[53] On the other hand a red hypochromic shift at λ_{max} in the UV absorption spectra is observed upon incremental addition of DNA to Schiff base containing Cu(II), Co(II) and Ni(II) complexes.[54] Shifts in intensities or bands in the UV absorption spectra are indicative of interactions between DNA and metal complexes.[55-56]

Changes in the absorbance are commonplace in the UV absorption spectra of DNA, due to the nature of its double helix. Hyperchromic shifts are associated with the electrostatic binding of complexes to the macromolecule which in turn causes partial unwinding of the double helix and exposes more DNA base pairs. Hypochromic shifts are related to complexes which exhibit the ability to intercalate with DNA.[57]

The absorbance of **3.4**, in a HEPES buffered solution at pH 7.4, at 303 nm increased (hyperchromic shift) upon incremental addition of DNA. The DNA concentration was increased to a final concentration of 12.86 nM. In addition to this hyperchromic effect a blue shift of λ_{max} was observed from 303 nm to 293 nm (Figure 3.11).

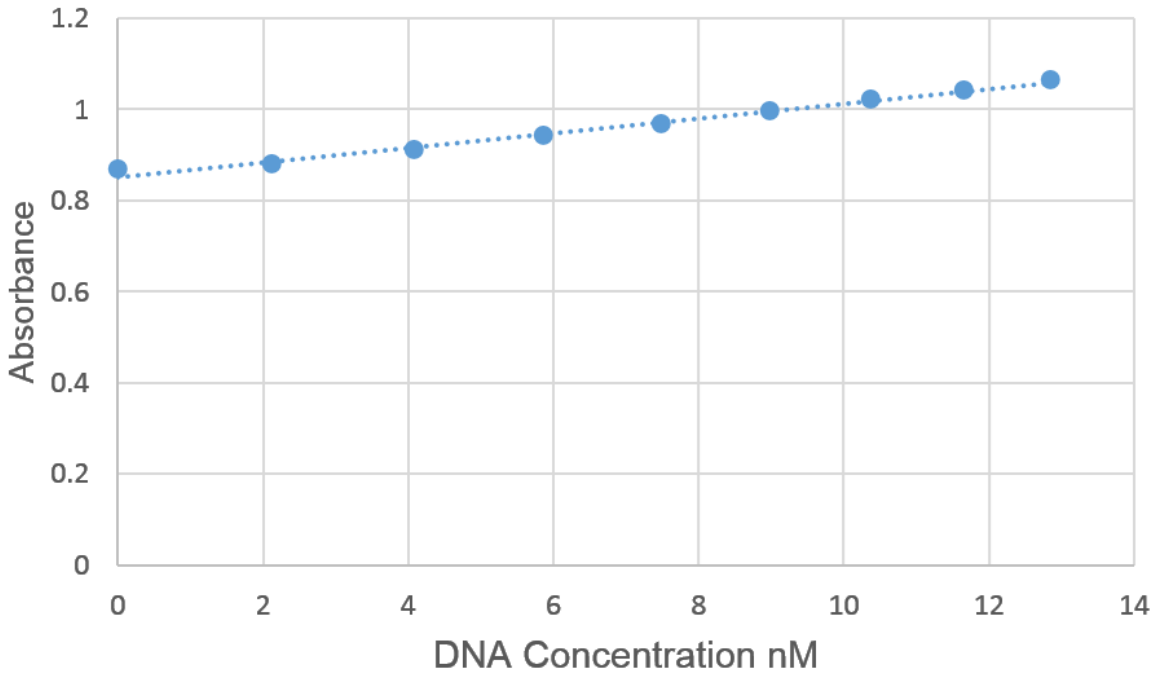

***Figure 3.12**: UV absorption spectra of 0.33 mM **3.4** in 0.2 mM HEPES buffer, pH 7.4, in H_2O at λ = 293 nm with increasing concentrations of Red Salmon testes DNA.*

It should be clarified that the hyperchromic effect, where the absorbance of the solution increased from 0.87 to 1.06 (Figure 3.12), is more than the sum of the absorbance of the DNA or metal complex components and thus it can be inferred that the binding of **3.4** to DNA results in this shift.

3.8. Overall Summary

Six new rhodium(III), iridium(III) and ruthenium(II) complexes **3.3-3.8** were synthesized from the ligands **3.1-3.2**, which were prepared from the alkylation of PTA. **3.1-3.8** were prepared in poor to excellent yields and were characterized using NMR spectroscopy and mass spectrometry. ^{1}H and $^{31}P\{^{1}H\}$ NMR spectroscopy show that the ligand coordinates to the metal-arene through the phosphorous of the alkylated PTA in a monodentate fashion.

The cationic alkylated PTA PGM complexes **3.3-3.8** exhibit low to moderate antiproliferative activity against the esophageal WHCO1 cancer cell line. The rhodium(III) and ruthenium(II) trinuclear complexes **3.6** and **3.8**, respectively, displayed greater activity than their

mononuclear analogues. It is unclear as to why the mononuclear complex **3.4** is the most active of this series. Future investigative studies can be performed to probe understanding into this anomaly. The mononuclear complex **3.4** showed aqueous stability and confirmed the ability of alkylated PTA PGM complexes to interact with 5'-GMP, by coordination *via* the N7 atom, and histidine as confirmed by NMR studies. **3.4** also displayed the ability to interact with Red Salmon testes DNA and resulted in a hyperchromic blue shift of λ_{max}.

3.9. References

[1] A.D. Phillips, L. Gonsalvi, A. Romerosa, F. Vizza and M. Peruzzini, *Coord. Chem. Rev.* **2004**, *248*, 955-993.

[2] J. Bravo, S. Bolano, L. Gonsalvi and M. Peruzzini, *Coord. Chem. Rev.* **2010**, *254*, 555-607.

[3] R. Pettinari, F. Marchetti, F. Condello, C. Pettinari, G. Lupidi, R Scopelliti, S. Mukhopadhyay, T. Riedel and P.J. Dyson, *Organometallics* **2014**, *33*, 3709-3715.

[4] A. Weiss, R.H. Berndsen, M. Dubois, C. Muller, R. Schibli, A.W. Griffioen, P.J. Dyson and P. Nowak-Sliwinska, *Chem. Sci.* **2014**, *5*, 4742-4748.

[5] C. Scolaro, T.J. Geldbach, S. Rochat, A. Dorcier, C. Gossens, A. Bergamo, M. Cocchietto, I. Tavernelli, G. Sava, U. Rothlisberger and P.J. Dyson, *Organometallics* **2006**, *25*, 756-765.

[6] S. Chatterjee, S. Kundu, A. Bhattacharyya, C.G. Hartinger and P.J. Dyson, *J. Biol. Inorg. Chem.* **2008**, *13*, 1149-1155.

[7] D.J. Daigle and A.B. Pepperman, *J. Heterocycl. Chem.* **1975**, *12*, 579-580.

[8] D.J. Daigle, A.B. Pepperman and J. Vail, *J. Heterocycl. Chem.* **1974**, *11*, 407-408.

[9] E. Garcia-Moreno, E. Cerrada, M.J. Bolsa, A. Luquin and M. Laguna, *Eur. J. Inorg. Chem.* **2013**, 2020-2030.

[10] S. Schäfer, W. Frey, A.S.K. Hashmi, V. Cmrecki, A. Luquin and M. Laguna, *Polyhedron* **2010**, *29*, 1925-1932.

[11] E. García-Moreno, S. Gascón, E. Atrián-Blasco, M.J. Rodriguez-Yoldi, E. Cerrada and M. Laguna, *Eur. J. Med. Chem.* **2014**, *79*, 164-172.

[12] F-X. Legrand, F. Hapiot a, S. Tilloy, A. Guerriero, M. Peruzzini, L. Gonsalvi and E. Monflier, *Appl. Catal. A* **2009**, *362*, 62-66.

[13] A. Dorcier, C.G. Hartinger, R. Scopelliti, R.H. Fish, B.K. Keppler and P. J. Dyson, *J. Inorg. Biochem.* **2008**, *102*, 1066-1076.

[14] Z. Almodares, S.J. Lucas, B.D. Crossley, A.M. Basri, C.M. Pask, A.J. Hebden, R.M. Phillips and P.C. McGowan, *Inorg. Chem.* **2014**, *53*, 727-736.

[15] D.J. Darensbourg, F. Joó, M. Kannisto, Á. Kathó and J.H. Reibenspies, *Organometallics* **1992**, *11*, 1990-1993.

[16] J.P. Hermes, F. Sander, T. Peterle, R. Urbani, T. Pfohl, D. Thompson and M. Mayor, *Chem. Eur. J.* **2011**, *17*, 13473-13481.

[17] D.N. Akbayeva, L. Gonsalvi, W. Oberhauser, M. Peruzzini, F. Vizza, P. Brüggeller, A. Romerosa, G. Savad and A. Bergamod, *Chem. Commun.* **2003**, 264-265.

[18] R. Pettinari, C. Pettinari, F. Marchetti, C.M. Clavel, R Scopelliti and P.J. Dyson, *Organometallics* **2013**, *32*, 309-316.

[19] A. García-Fernández, J. Díez, A. Manteca, J. Sánchez, R. García-Navas, B.G. Sierra, F. Mollinedo, M.P. Gamasaa and E. Lastra, *Dalton Trans.* **2010**, *39*, 10186-10196.

[20] A. Udvardy, C.B. Bényei, P. Juhász, F. Joó and Á. Kathó, *Polyhedron* **2013**, *60*, 1-9.

[21] P.R. Sharp, D.W. Hoard and C.L. Barnes, *J. Am. Chem. Soc* **1990**, *112*, 2024-2026.

[22] S. Bolaño, M. Plaza, J. Bravo, J. Castro, M. Peruzzini, L. Gonsalvi, G. Ciancaleoni and A. Macchioni, *Inorg. Chim. Acta* **2010**, *363*, 509-516.

[23] S. Bolaño, A. Albinati, J. Bravo, M. Caporali, L. Gonsalvi, L. Male, M. Rodríguez-Rocha, A. Rossin and M. Peruzzini, *J. Organomet. Chem.* **2008**, *693*, 2397-2406.

[24] A. Dorcier, W.H. Ang, S. Bolaño, L. Gonsalvi, L. Juillerat-Jeannerat, G. Laurenczy, M. Peruzzini, A.D. Phillips, F. Zanobini and P.J. Dyson, *Organometallics* **2006**, *25*, 4090-4096.

[25] M. Erlandsson, V.R. Landaeta, L. Gonsalvi, M. Peruzzini, A.D. Phillips, P.J. Dyson and G. Laurenczy, *Eur. J. Inorg. Chem.* **2008**, 620-627.

[26] D. Thomas, (9/2/1997), Retrieved 17/8/2015, from http://www.chembio.uoguelph.ca/educmat/atomdata/shield/shield.htm

[27] V. Cadierno, J. Francos and J. Gimeno, *Chem. Eur. J.* **2008**, *14*, 6601-6605.

[28] D. Hendricks and M.I. Parker, *Life* **2002**, *53*, 263-268.

[29] C.H. Kaschula, R. Hunter, N. Stellenboom, M.R. Caira, S. Winks, T. Ogunleye, P. Richards, J. Cotton, K. Zilbeyaz, Y. Wang, V. Siyo, E. Ngarande and M.I. Parker, *Eur. J. Med. Chem.* **2012**, *50*, 236-254.

[30] P. Govender, A.K. Renfrew, C.M. Clavel, P. J. Dyson, B. Therrien and Gregory S. Smith, *Dalton Trans.* **2011**, *40*, 1158-1167.

[31] P. Govender, L.C. Sudding, C.M. Clavel, P. J. Dyson, B. Therrien and G. S. Smith, *Dalton Trans.* **2013**, *42*, 1267-1277.

[32] R. Payne, P. Govender, B. Therrien, C.M. Clavel, P. J. Dyson and G. S. Smith, *J. Organomet. Chem.* **2013**, *729*, 20-27.

[33] C. Scolaro, C.G. Hartinger, C.S. Allardyce, B.K. Keppler and P.J. Dyson, *J. Inorg. Biochem.* **2008**, *102*, 1743-1748.

[34] W.H. Ang, E. Daldini, C. Scolaro, R. Scopelliti, L. Juillerat-Jeannerat and P.J. Dyson, *Inorg. Chem.* **2006**, *45*, 9006-9013.

[35] H. Chen, J.A. Parkinson, R.E. Morris and P.J. Sadler, *J. Am. Chem. Soc.* **2003**, *125*, 173-186.

[36] B.S. Murray, L. Menin, R. Scopelliti and P.J. Dyson, *Chem. Sci.* **2014**, *5*, 2536-2545.

[37] E. Sletten and B. Lie, *Acta Cryst.* **1976**, *B32*, 3301-3304.

[38] K. Aoki, General conclusion from solid state studies of nucleotide-metal ion complexes in *Metal Ions in Biological Systems*, A. Sigel and H. Sigel, New York, **1997**, pp. 479-501.

[39] M. Groessl, C.G. Hartinger, K. Polec-Pawlak, M. Jarosz and B.K. Keppler, *Electrophoresis* **2008**, *29*, 2224-2232.

[40] M. Groessl, E. Reisner, C.G. Hartinger, R. Eichinger, O. Semenova, A.R. Timerbaev, M.A. Jakupec, V.B. Arion and B.K. Keppler, *J. Med. Chem.* **2007**, *50*, 2185-2193.

[41] E. S. Antonarakis and A. Emadi, *Cancer Chemother. Pharmacol.* **2010**, *66*, 1-9.

[42] O. Dömötör, C. G. Hartinger, A. K. Bytzek, T. Kiss, B. K. Keppler and E. A. Enyedy, *J. Biol. Inorg. Chem.* **2013**, *18*, 9-17.

[43] S. Leijen, S. A. Burgers, P. Baas, D. Pluim, M. Tibben, E. van Werkhoven, E. Alessio, G. Sava, J. H. Beijnen and J. H. M. Schellens, *Invest. New Drugs* **2015**, *33*, 201-214.

[44] C.G. Hartinger, S. Zorbas-Seifried, M.A. Jakupec, B. Kynast, H. Zorbas and B.K. Keppler, *J. Inorg. Biochem.* **2006**, *100*, 891-904.

[45] S. Zorbas-Seifried, C.G. Hartinger, K. Meelich, M. Galanski, B.K. Keppler and H. Zorbas, *Biochemistry* **2006**, *45*, 14817-14825.

[46] M. Banik and T. Basu, *Dalton Trans.* **2014**, *43*, 3244-3259.

[47] M. Deiana, K. Matczyszyn, J. Massin, J. Olesiak-Banska, C. Andraud and M. Samoc, *PLoS One* **2015**, *10*, e0129817.

[48] N. Hadjiliadis and E. Sletten, *Metal Complex - DNA Interactions*, John Wiley & Sons, **2009**, 41.

[49] E.M.S. Castanheira, M.S.D. Carvalho, A.R.O. Rodrigues, R.C. Calhelha and M-J.R.P. Queiroz, *Nanoscale Res. Lett.* **2011**, *6*, 1-8.

[50] R. Sarkar and S.K. Pal, *Biopolymers* **2006**, *83*, 675-686.

[51] N. Shu-yan, J. Gui-fen, Z. Shu-sheng, L. Ying and Y. Fan, *Chem. Res. Chinese U.* **2005**, *21*, 149-153.

[52] Y. Lin, Y. Zhang, Y. Qiao, J. Huang and B. Xu, *J. Colloid Interface Sci* **2011**, *362*, 430-438.

[53] M. Aslanoglu and N. Oge, *Turk. J. Chem.* **2005**, *29*, 477-485.

[54] R. Gomathi, A. Ramu and A. Murugan, *Bioinorg. Chem. Appl.* **2014**, 1-12.

[55] S. Tabassum, M. Zaki, F. Arjmand and I. Ahmad, *J. Photochem. Photobiol. B* **2012**, *114*, 108-118.

[56] K. Suntharalingam, O. Mendoza, A.A. Duarte, D.J. Mann and R. Vilar, *Metallomics* **2013**, *5*, 514-523.

[57] N. Shahabadi, S. Kashanian, M. Khosravi and M. Mahdavi, *Trans. Metal. Chem.* **2010**, *35*, 699-705.

Chapter 4: Synthesis, Characterization and Antitumor Activity of New Trinuclear Sulfonated Rh(III), Ir(III) and Ru(II) Complexes

4. Introduction

Sulfonated compounds experience a high degree of water solubility and this is an attractive chemical property in the field of anticancer research. However, little research towards the application as potential antitumor agents has been explored.

Chachoyan and Sagradyan prepared sodium diphenylphosphinebenzene-*m*-sulfonate (DPM) complexes with Rh(I) and Ru(II) (Figure 4.1).[1] Toxicity and antitumor activities of these complexes were investigated in mice and rats containing tumors which were transplanted. Both the ruthenium(II) and rhodium(I) complexes were found to be nontoxic, LD_{100} = 1000 - 1250 mg/kg, and they both exhibited antitumor activity.

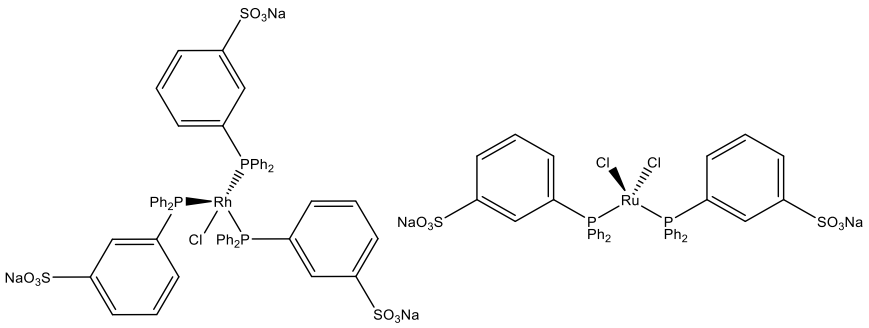

***Figure 4.1**: Water soluble sulfonated complexes $[Rh(DPM)_3Cl]$ (left) and $[Ru(DPM)_2Cl_2]$ (right).*

Wang and co-workers prepared a Ru(II) complex, $[Ru(bpy)_2(py\text{-}SO_3)]^+$, where bpy = 2,2'-bipyridine and py-SO_3 = pyridine-2-sulfonate (Figure 4.2).[2] This complex dissociates its sulfonated pyridine ligand upon irradiation from light within the visible spectrum, where λ > 470 nm. DNA was found to be photocleaved by the production of free radical species from the homolysis.

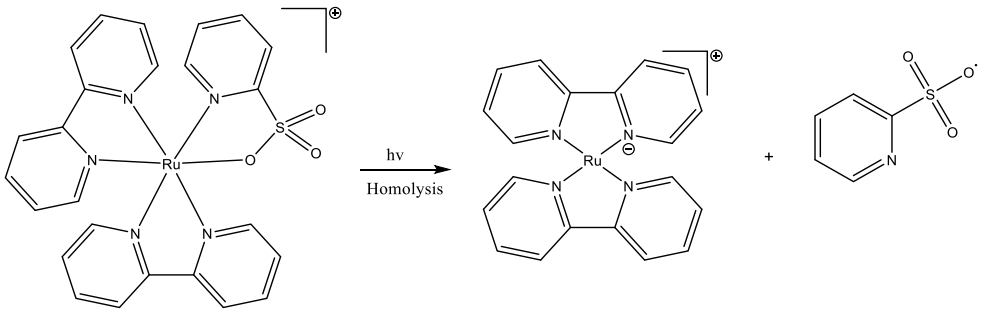

***Figure 4.2**: Homolysis of $[Ru(bpy)_2(py\text{-}SO_3)]^+$ upon irradiation, resulting in radical formation for DNA cleavage.*

Garcia and co-workers prepared a water-soluble sulfonated ruthenium-arene complex, $[Ru(C_5H_5)(DPM)(2,2'\text{-bipy})][CF_3SO_2]$ (Figure 4.3) which was found to target the endomembrane system and disrupt golgi bodies and mitochondria.[3] The cytotoxic activity against a set of human cancer cell lines was investigated (A2780, A2780*cis*R, MCF7, MDAMB231, HT29, PC3 and the non-tumorigenic V79).

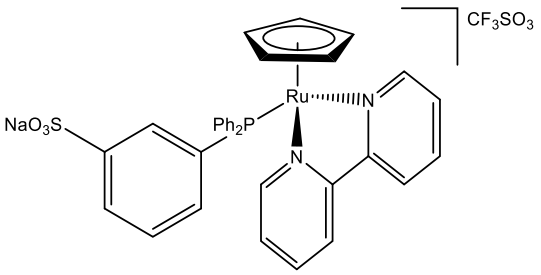

***Figure 4.3**: Sulfonated ruthenium(II) arene complex, $[Ru(C_5H_5)(DPM)(2,2'\text{-bipy})][CF_3SO_3]$.*

Bergamini and co-workers prepared the first examples of PTA zwitterionic complexes, $[PtCl_2(PTA^+C_3H_6SO_3^-)_2]$ and $[RuCl(PPh_3)Cp(PTA^+C_3H_6SO_3^-)]$ from sultones (Figure 4.4).[4] The antiproliferative activity of the complexes and the ligand were tested against the cisplatin sensitive human ovarian cell line, A2780, and the cisplatin resistant human ovarian cell line SKOV3.

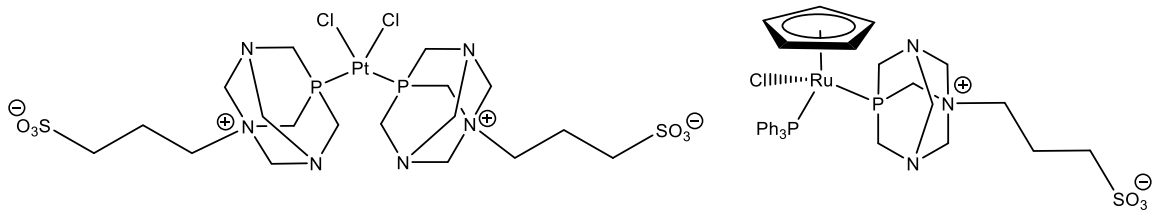

***Figure 4.4**: [PtCl$_2$(PTA$^+$C$_3$H$_6$SO$_3^-$)$_2$] (left) and [RuCl(PPh$_3$)Cp(PTA$^+$C$_3$H$_6$SO$_3^-$)] (right).*

The incorporation of the sulfonate moiety results in an increase of water solubility, which is desirable for potential anticancer complexes which generally have low water solubility. Many mononuclear sulfonated metal complexes exhibit significant antitumor actitivity, as previously highlighted. This potency may be do to the ionic nature which the sulfonate moeity provides.

To date and to the best of my knowledge, no sulfonated polynuclear metal-arene systems have been developed or reported. In this chapter, the synthesis, characterization and biological evaluation of new trinuclear sulfonated rhodium(III) and iridium(III) pentamethylcyclopentadienyl complexes are described. For comparative purposes, sulfonated mononuclear analogues were also prepared. The discussion of spectroscopic and analytical techniques used to confirm the proposed metal complex structures and the biological activity of these metal complexes is contained within this chapter.

4.1. Synthesis and Characterization of Water-Soluble Sulfonated Anionic Complexes

The mono- and trimeric ligands **4.1** and **4.4** were synthesized using known methods.[5] Ligands **4.1** and **4.4** were reacted with the precursors dichloro(pentamethylcyclopentadienyl)-rhodium(III) dimer or dichloro(pentamethylcyclopentadienyl)iridium(III) dimer to yield the corresponding mononuclear anionic complexes **4.2-4.3** (Scheme 4.1) or trinuclear anionic complexes **4.5-4.6** (Scheme 4.2).

The mono- **4.2-4.3** and trinuclear anionic complexes **4.5-4.6** were prepared by stirring the appropriate ligand and sodium acetate in ethanol followed by addition of the appropriate dimer. The resulting products **4.3-4.4** and **4.5-4.6** were isolated as hygroscopic red or yellow to brown solids, in low to moderate yields, and are soluble in water and most polar organic solvents.

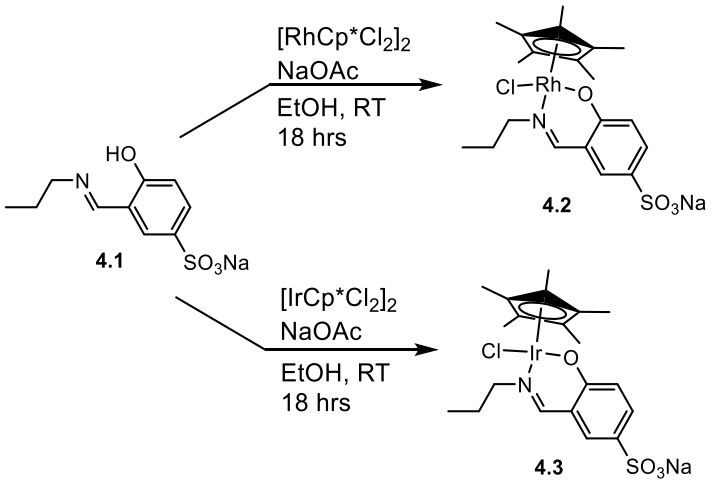

Scheme 4.1 *Synthesis of mononuclear sulfonated N,O-salicylaldiminato anionic complexes* ***4.2-4.3****.*

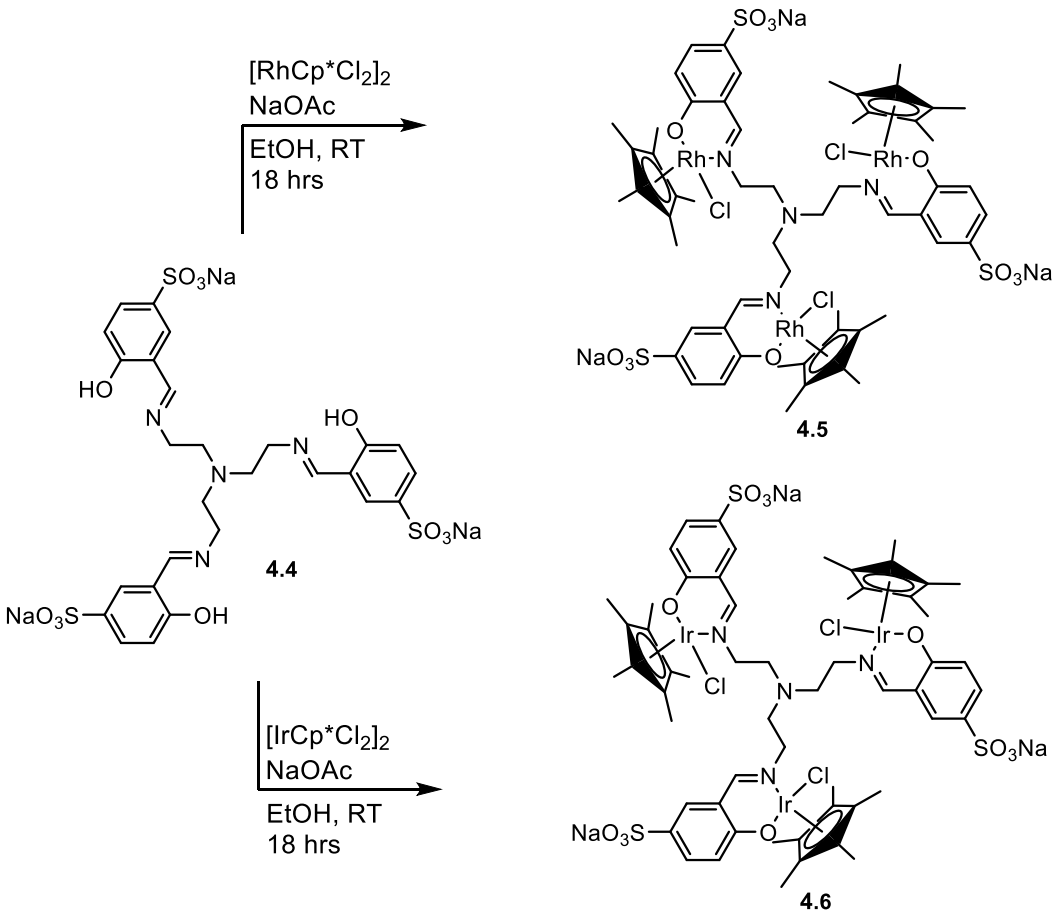

Scheme 4.2 *Synthesis of trinuclear sulfonated N,O-salicylaldiminato anionic complexes* ***4.5-4.6****.*

The mono- and trinuclear *N,O*-salicylaldiminato ruthenium(II) anionic complexes were unable to be isolated. Various solvents including methanol, ethanol, dichloromethane and acetone were used in the presence of bases such as sodium acetate and sodium hydride. However, ^{1}H NMR analysis of the brown oils or powders obtained only revealed mixtures of unreacted ligand **4.1** or **4.4** and dichloro(*p*-cymene)ruthenium(II) dimer with no coordinated product formed. No further attempts were performed to coordinate ruthenium(II) to these systems.

The new anionic complexes **4.2-4.3** and **4.5-4.6** were fully characterized using several spectroscopic and analytical techniques. Coordination to the metal-arene is bidentate in nature. Evidence of the coordination occurring *via* the imine nitrogen and phenolic oxygen to the metal-arene were obtained from the NMR and IR analyses.

The NMR spectra of complexes **4.2-4.3** and **4.5-4.6** were recorded in $(CD_3)_2SO$ and show relevant peaks for the proposed structures.

The ^{1}H NMR spectra for the mono- and trinuclear sulfonated *N,O*-salicylaldiminato anionic complexes **4.2-4.3** and **4.5-4.6** all show an upfield shift of the imine proton to ca. δ 8.04 ppm from δ 8.58 ppm for the mononuclear anionic complexes **4.2-4.3** or to ca. δ 8.14 ppm from δ 8.56 ppm for the trinuclear complexes **4.5-4.6** (Table 4.1). The absence of the downfield signal for the phenolic proton of the ligands **4.1** and **4.4** at ca. δ 13.84 ppm confirms that metal coordination occurs *via* the imine nitrogen and phenolic oxygen.

Table 4.1 *Selected spectroscopic and analytical data for N,O-salicylaldiminato* anionic *complexes* ***4.2-4.3*** *and* ***4.5-4.6****.*

Compound Number	**^{1}H NMR** (imine) [ppm][a]	**^{13}C{^{1}H} NMR** (imine) [ppm][a]	**FT-IR** Imine [cm^{-1}][b]	**HR-ESI-MS** [*m/z*][c]
4.2	8.02	163.58	1623	514.0308 [M-Na]$^{-}$
4.3	8.05	160.67	1621	604.0961 [M-Na]$^{-}$
4.5	8.17	165.10	1618	373.1396 [M-3Cl+Na]$^{4+}$
4.6	8.10	162.20	1617	583.1314 [M-3Cl]$^{3+}$

[a]Recorded in $(CD_3)_2SO$; [b]Recorded with ATR; [c]**4.2-4.3** performed in positive mode, **4.5-4.6** performed in negative mode.

The ^{13}C{^{1}H} NMR spectra of the anionic complexes **4.2-4.3** and **4.5-4.6** gave the expected number of carbon signals. For the rhodium(III) complexes **4.2** and **4.5** a downfield shift for the imine carbon to ca. δ 164.34 ppm from the reported literature value of ca. δ 162.1 ppm was

observed,[5] while conversely for the iridium(III) complexes **4.3** and **4.6** an upfield shift to ca. δ 161.44 ppm is observed.

In the ^{1}H NMR spectra for complexes **4.2-4.3** and **4.5-4.6** the methyl protons of the pentamethylcyclopentadienyl ligand are observed at ca. δ 1.44 ppm (Figure 4.5). The signals for the protons H1 and H3 of the *n*-propyl chain of the mononuclear complexes **4.2-4.3** are observed as triplets at ca. δ 3.89 ppm, H3, and ca. δ 0.87 ppm, H1. The signal for the protons H2 in the mononuclear complexes **4.2-4.3** coalesce with the signal for the methyl protons H12.

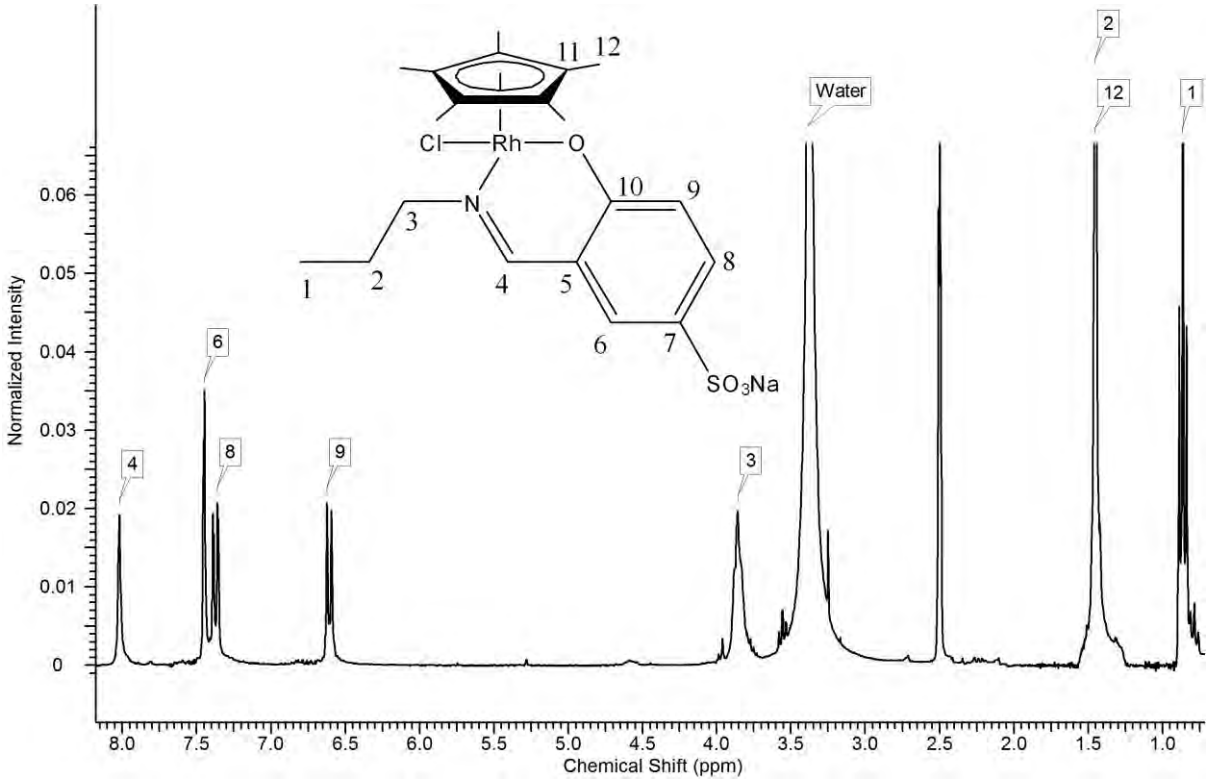

Figure 4.5 *^{1}H NMR spectrum of mononuclear N,O-salicylaldiminato anionic complex **4.2**.*

In the ^{13}C{^{1}H} NMR spectra for the complexes **4.3-4.6** the carbon resonances of the pentamethylcyclopentadienyl ring are observed at ca. δ 95.68 ppm for the rhodium(III) and ca. δ 84.43 ppm for the iridium(III) complexes. The carbon signals for the methyl substituents on the arene are observed at ca. δ 8.38 ppm for the rhodium(III) and ca. δ 8.36 ppm for the iridium(III) complexes (Figure 4.6).

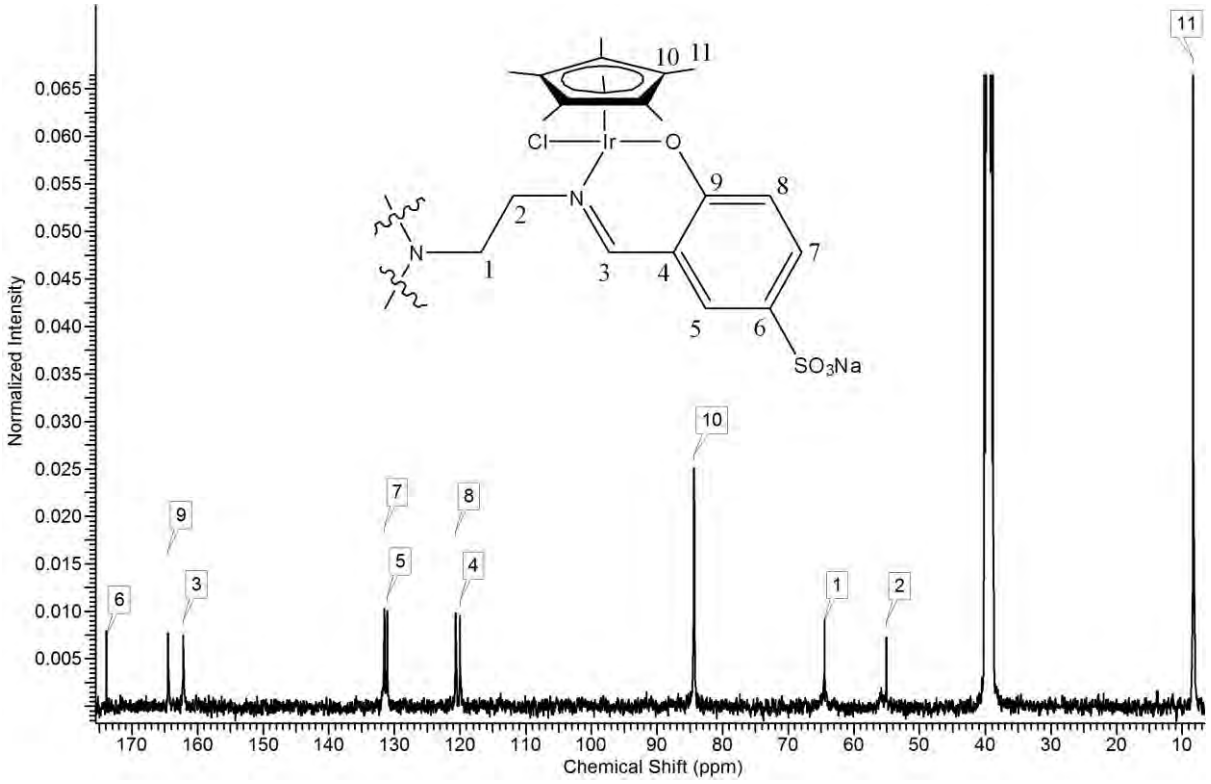

Figure 4.6 *$^{13}C\{^1H\}$ NMR spectrum of trinuclear N,O-salicylaldiminato anionic complex* ***4.6****.*

The signals in the $^{13}C\{^1H\}$ NMR spectra for the aliphatic carbons in the mononuclear anionic complexes **4.2-4.3** of the *n*-propyl chain are observed at ca. δ 67.03 ppm, C3, ca. δ 23.43 ppm, C2, and ca. δ 11.21 ppm, C1. The aliphatic carbon atoms of the trinuclear anionic complexes **4.5-4.6** display signals at ca. δ 63.33 ppm, C1, and ca. δ 55.60 ppm, C2.

The signal in the ^1H NMR spectra for the aliphatic $–CH_2$ protons H1, adjacent to the nitrogen core, in the trinuclear anionic complexes **4.5-4.6** coalesce with the signal for the methyl protons H11 of the pentamethylcyclopentadienyl, in both cases. This is observed in the two dimensional ^1H-^{13}C HSQC NMR spectrum (Figure 4.7). In the trinuclear complexes the signal for H2 of the tris-2-(5-sulfinatosalicylaldimine ethyl)amine ligand is observed as a multiplet at either δ 4.00 ppm, **4.5**, or δ 4.33 ppm, **4.6**. This multiplicity can be explained by the introduction of a chiral center at the coordinated metal-arene.

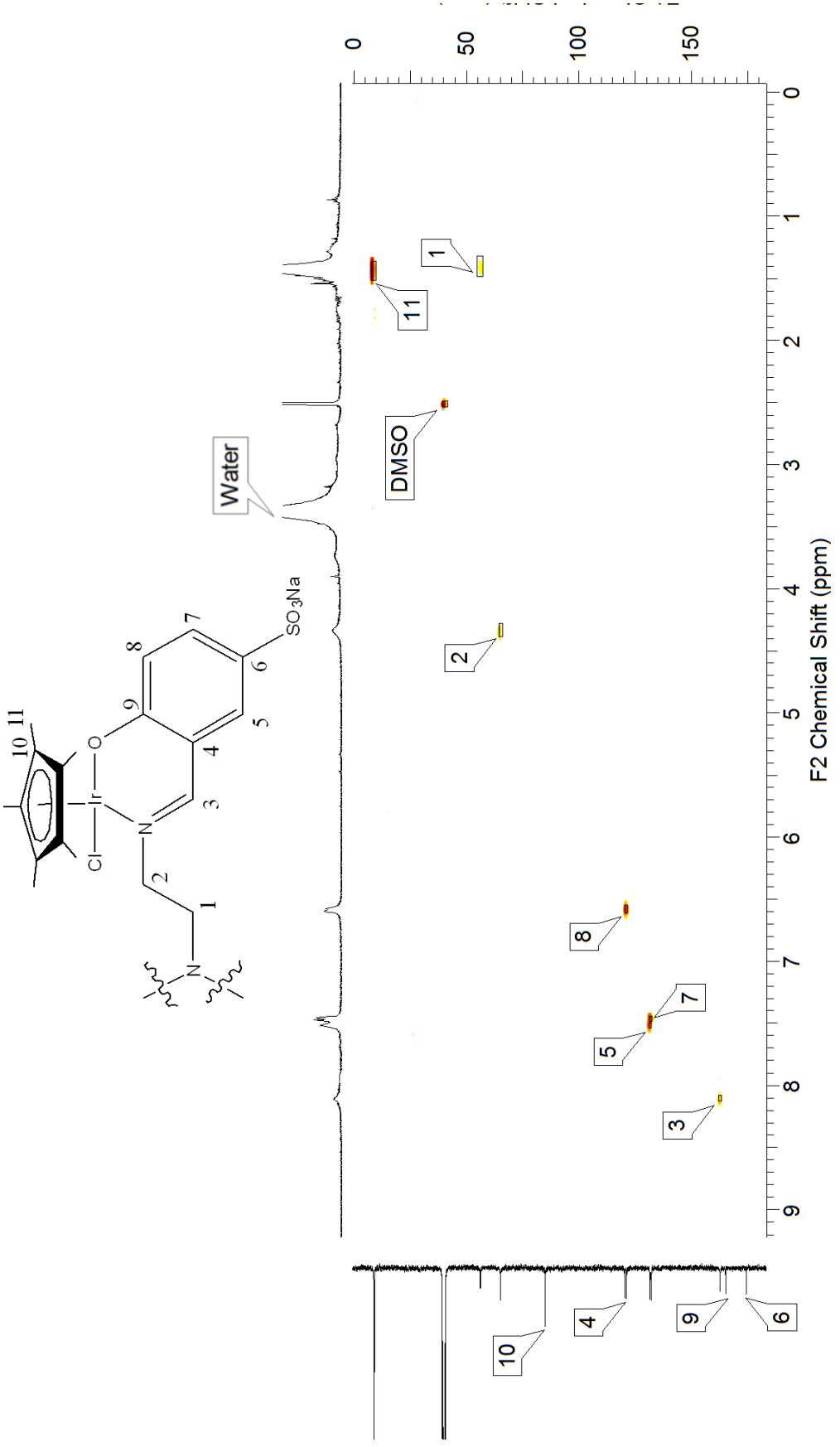

Figure 4.7 *^{1}H-^{13}C HSQC NMR spectrum of trinuclear N,O-salicylaldiminato anionic complex* ***4.6****.*

The sulfonated *N,O*-salicylaldiminato anionic complexes **4.2-4.3** and **4.5-4.6** display a shift in the $C=N_{imine}$ stretching vibration to lower wavenumbers. The mononuclear anionic complexes **4.2-4.3** display a shift from 1634 cm^{-1} to ca. 1622 cm^{-1} (Figure 4.8), while the trinuclear anionic complexes **4.5-4.6** display a shift from 1635 cm^{-1} to ca. 1618 cm^{-1}. These shifts to lower frequencies are as a result of a weaker $C=N_{imine}$ bond due to the electron-withdrawing nature of the aromatic ring and the coordinated metal center. Similar shifts in the stretching frequency for the $C=N_{imine}$ have been reported.[6]

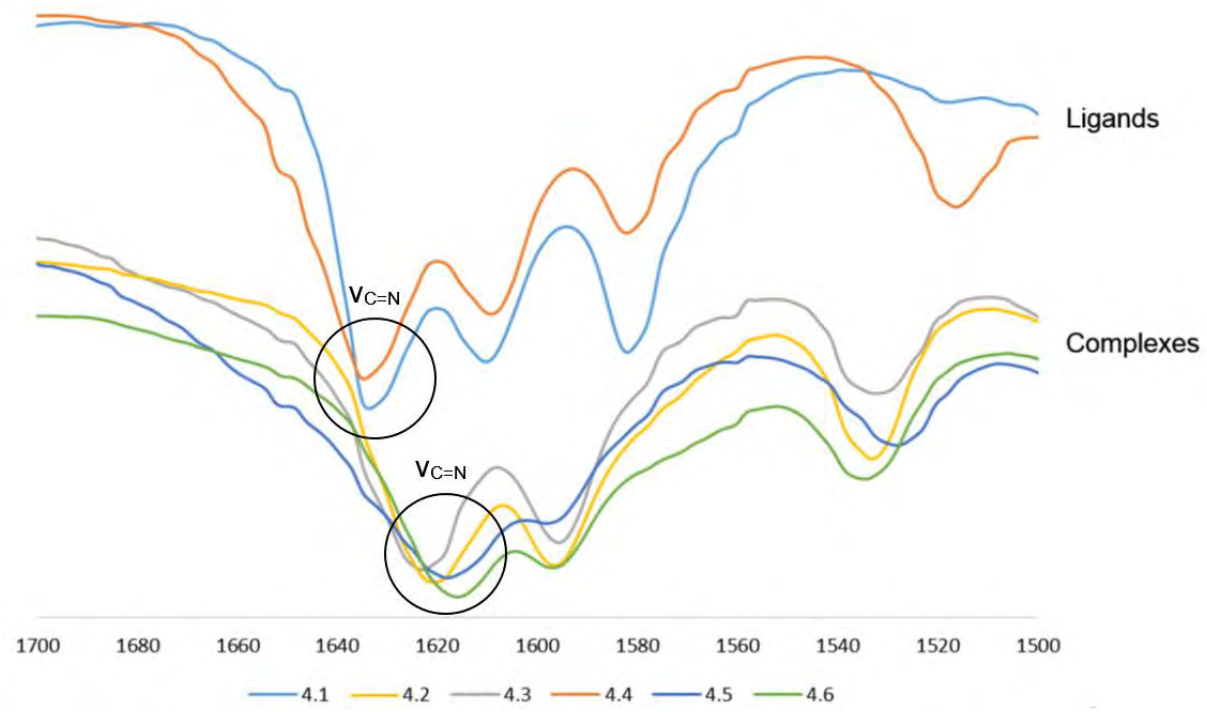

Figure 4.8 *IR spectra displaying range of 1500-1700 cm^{-1} of N,O-salicylaldiminato anionic compounds* ***4.1-4.6****.*

Mass spectral analysis confirmed the proposed structures. The mononuclear anionic complexes **4.2-4.3** display molecular-ion base peaks which correspond to the loss of the sodium ion in the negative mode, $[M\text{-}Na]^-$, and the loss of the chlorido ligand in the positive mode, $[M\text{-}Cl]^+$. The trinuclear iridium(III) anionic complex **4.6** displays a base peak which corresponds to the loss of three chlorido ligands in the positive mode, $[M\text{-}3Cl]^{3+}$, while the trinuclear rhodium(III) complex **4.5** displays a peak which is assigned as a sodium adduct, $[M\text{-}3Cl+Na]^{4+}$.

Elemental analysis results of the rhodium(III) and iridium(III) anionic complexes displayed percentages outside of acceptable limits due to the hygroscopic nature of the complexes

4.2-4.3 and **4.5-4.6**. Recalculation of the percentages with the inclusion of water gave percentages within acceptable limits.

4.2. Synthesis and Characterization of Sulfonated Complexes

Ligands **4.1** and **4.4** were reacted with the precursors, dichloro(pentamethylcyclopentadienyl) rhodium(III) dimer or dichloro(pentamethylcyclopentadienyl)iridium(III) dimer followed by an *N*-pyridyl donor ligand to displace the metal-chloro ligand. The *N*-pyridyl donor ligands used were: pyridine, 4-methylpyridine, 4-phenylpyridine, 4-ferrocenylpyridine. The resulting mononuclear complexes **4.7-4.14** (Scheme 4.3) or trinuclear complexes **4.15-4.22** (Scheme 4.4) were isolated as tetraphenylborate salts.

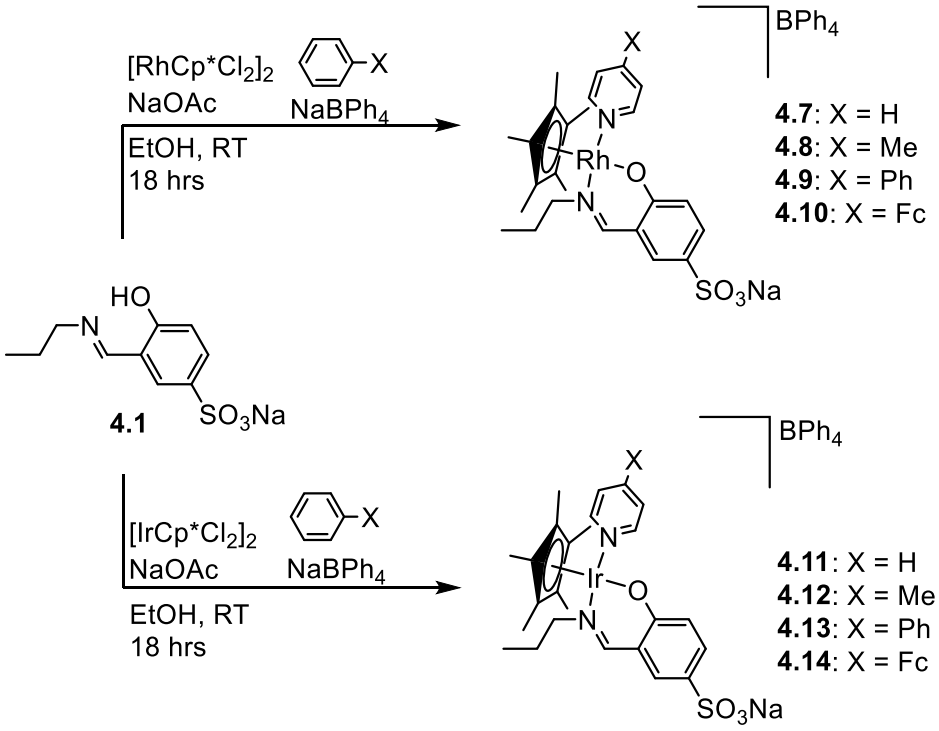

Scheme 4.3 *Synthesis of trinuclear sulfonated N,O-salicylaldiminato complexes **4.7-4.14**.*

The mono- **4.7-4.14** and trinuclear complexes **4.15-4.22** were prepared by stirring the appropriate ligand and sodium acetate in ethanol followed by addition of the appropriate dimer and *N*-donor ligand. The resulting products **4.7-4.14** were precipitated from the reaction using *iso*-propanol and were isolated as hygroscopic red to yellow or brown solids, in low to good yields, and are soluble in most polar organic solvents. The sulfonated complexes **4.7-4.22**

suffered a decrease in water solubility due to the presence of the tetraphenylborate salt counterion and these complexes were only partially water soluble.

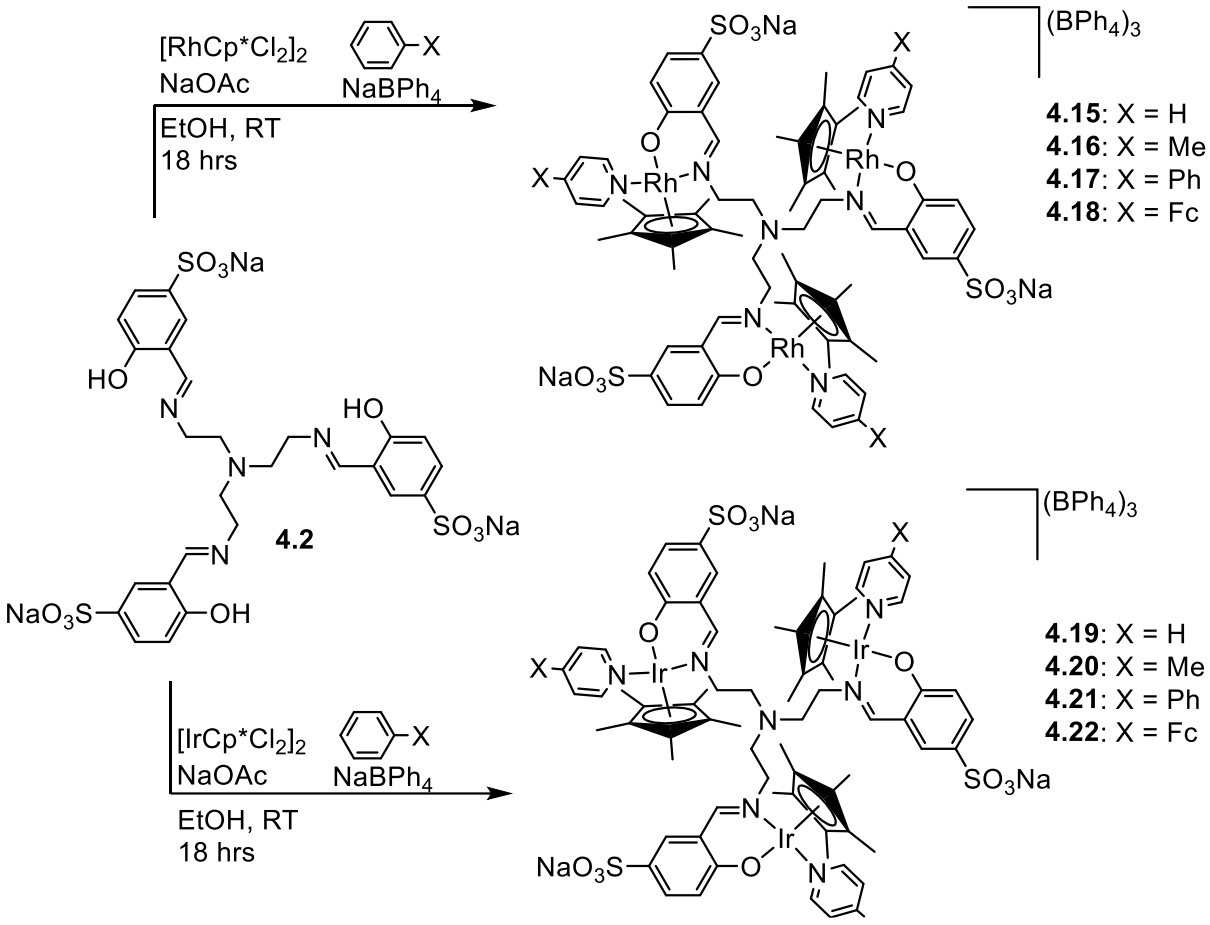

Scheme 4.4 *Synthesis of trinuclear sulfonated N,O-salicylaldiminato complexes* ***4.15-4.22****.*

The complexes **4.7-4.22** are new compounds and were fully characterized with spectroscopic and analytical techniques. NMR and FT-IR analyses confirm the bidentate nature of the coordination of the imine nitrogen and phenolic oxygen with pyridine-ligand derivatives coordinated to the metal-arene.

The NMR spectra of complexes **4.7-4.22** were recorded in deuterated dimethylsulfoxide, $(CD_3)_2SO$, and show relevant peaks for the proposed structures.

All the mono- and trinuclear sulfonated *N,O*-salicylaldiminato complexes **4.7-4.22** in the ^1H NMR spectra exhibit an upfield shift of the signal for the imine proton relative to the free ligand. The rhodium(III) complexes **4.7-4.10** and **4.15-4.18** exhibit the greatest shift of the signal for

the imine upon coordination to the metal-Cp* for this signal from δ 8.58 ppm to ca. δ 8.24 ppm. The signal for the rhodium(III) complexes is further upfield in comparison to the iridium(III) complexes **4.11-4.14** and **4.19-4.22** which shifted to ca. δ 8.41 ppm from δ 8.56 ppm. The range of the imine signals, δ 8.16 – 8.65 ppm, for the *N,O*-salicylaldiminato complexes **4.7-4.22** with the *N*-donor ligand are further downfield than the range of the imine signals of the *N,O*-salicylaldiminato complexes **4.3-4.6**, δ 8.02 – 8.17 ppm. This deshielding effect can be attributed to the presence of the *N*-pyridyl ligand which displaces the metal-chloro ligand and results in a positive metal center and exposes the methyl protons of the pentamethylcyclopentadienyl ligand to a greater magnetic field and thus resonate downfield.

The $^{13}C\{^{1}H\}$ NMR spectra of the complexes **4.7-4.22** gave the expected number of carbon signals. All sulfonated *N,O*-salicylaldiminato complexes **4.7-4.22** exhibited a downfield shift in the signal for the imine carbon upon coordination to the metal-Cp*. For the mononuclear rhodium(III) complexes **4.7-4.11** a shift for the signal of the imine carbon to ca. δ 165.93 ppm, and for the trinuclear rhodium(III) complexes **4.15-4.18** a shift for the signal of the imine carbon to ca. δ 163.00 ppm from the reported literature value of ca. δ 162.1 ppm was observed.[5] For the mono- and trinuclear iridium(III) complexes **4.11-4.14** and **4.19-4.22** a shift to ca. δ 163.48 ppm is observed.

In the ^{1}H NMR spectra of complexes **4.7-4.22** the methyl protons of the pentamethylcyclopentadienyl ligand are observed at ca. δ 1.54 ppm, which is downfield of the signals of the methyl protons of the pentamethylcyclopentadienyl ligand of complexes **4.3-4.6**.

In the $^{13}C\{^{1}H\}$ NMR spectra of complexes **4.7-4.22** the carbons of the pentamethylcyclopentadienyl ring are observed at ca. δ 95.11 ppm for the rhodium(III) and ca. δ 91.95 ppm for the iridium(III) complexes. The carbon signals for the methyl substituents on the arene are observed at ca. δ 8.11 ppm for the rhodium(III) (Figure 4.3) and ca. δ 7.94 ppm for the iridium(III) complexes. These trends for similar signals were previously observed in Chapter 2 and 3.

For complexes **4.7-4.22**, the signals in the ^{1}H NMR spectra for the protons and the carbon atoms in the $^{13}C\{^{1}H\}$ NMR spectra of the *n*-propyl chain and tris-2-(5-sulfinatosalicylaldimine ethyl)amine scaffold display comparable chemical shifts as for those previously mentioned for the anionic complexes **4.2-4.3** and **4.5-4.6**.

Additional evidence to attest to the successful coordination of the *N*-donor ligand and displacement of the chlorido ligand was confirmed by NMR spectroscopy. The presence of a downfield diagnostic doublet signal in the ^{1}H NMR spectra for the protons adjacent to the nitrogen of the pyridyl ligand confirms the coordination of the *N*-donor ligand (Figure 4.9). This doublet for H13 in the mononuclear complexes **4.7-4.14** and H12 in the trinuclear complexes

4.15-4.22 is observed in the range δ 8.41 – 8.89 ppm. In the $^{13}C\{^{1}H\}$ NMR spectra the signals for C13 in the mononuclear complexes **4.7-4.14** and C12 in the trinuclear complexes **4.15-4.22** is observed in the range δ 149.46 – 153.71 ppm.

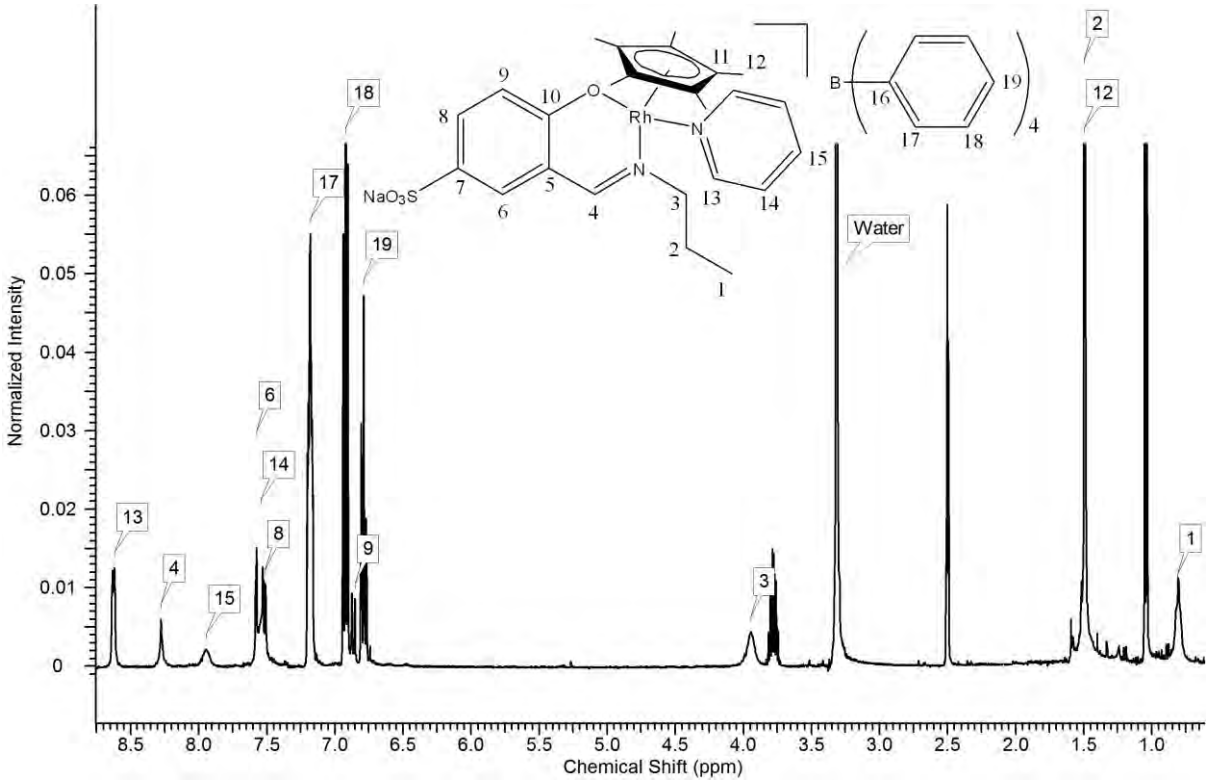

Figure 4.9 *^{1}H NMR spectrum of N,O-salicylaldiminato rhodium(III) pyridyl complex **4.7**.*

In the sulfonated *N,O*-salicylaldiminato complexes **4.8, 4.12, 4.16** and **4.20**, where 4-methylpyridine has displaced the chlorido ligand, a diagnostic signal is present upfield for the methyl group *para-* to the nitrogen of the pyridine ring. In the ^{1}H NMR spectra this methyl group exhibits a singlet in the range δ 2.34 – 2.78 ppm. As shown in the representative example of complex **4.8**, 2D ^{1}H-^{13}C HSQC NMR was used to assign all the signals in the ^{1}H and $^{13}C\{^{1}H\}$ NMR spectra (Figure 4.10). The signal for the methyl protons assigned as the singlet at δ 2.38 ppm displays coupling into a carbon resonance which lies in the aliphatic range at δ 20.40 ppm, confirming the presence of the 4-methylpyridyl ligand.

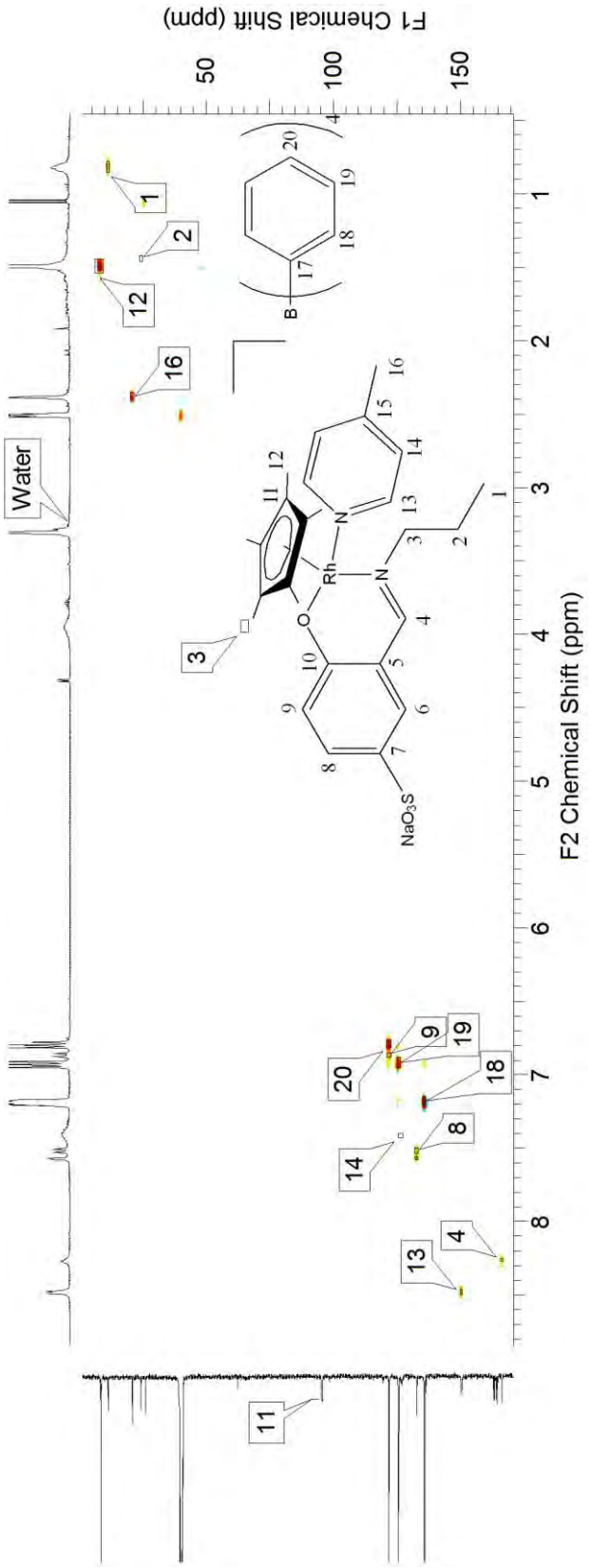

Figure 4.10 *^{1}H-^{13}C HSQC NMR spectrum of mononuclear N,O-salicylaldiminato complex* ***4.8****.*

Where 4-phenylpyridine was used to displace the metal-chloro ligand in the sulfonated *N,O*-salicylaldiminato complexes **4.9, 4.13, 4.17** and **4.21** the aromatic region of the ^{1}H NMR spectra displayed many signals due to the large number and variety of aromatic protons. 2D ^{1}H-^{1}H COSY NMR spectroscopy proved to be particularly useful in assigning the aromatic signals in the ^{1}H NMR spectra. A representative example of complex **4.9** displays assigned signals in the ^{1}H-^{1}H COSY NMR spectrum (Figure 4.11).

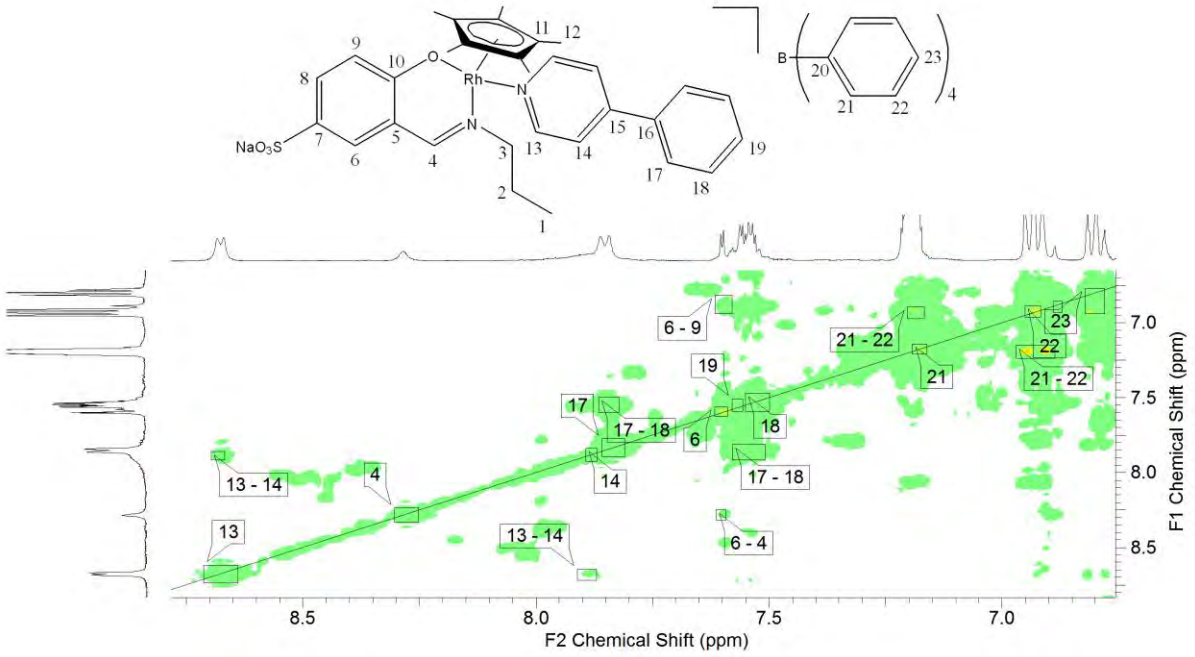

Figure 4.11 *Aromatic region of ^{1}H-^{1}H COSY NMR spectrum of trinuclear N,O-salicylaldiminato complex* ***4.9****.*

In the 4-ferrocenylpyridine containing sulfonated *N,O*-salicylaldiminato complexes **4.10, 4.14, 4.18** and **4.22** many of the ^{1}H and ^{13}C{^{1}H} NMR spectra displayed similarities to those of the complexes containing the 4-methylpyridine ligand. In the ^{1}H NMR two singlets of equal intensity in the range δ 4.57 – 5.12 ppm were assigned as the protons of the substituted Cp ring. Further upfield a large singlet was observed at ca. δ 4.07 ppm which was assigned as the unsubstituted Cp ring. The representative example of complex **4.10** displays assigned signals in the ^{1}H NMR spectrum (Figure 4.12). In the ^{13}C{^{1}H} NMR spectra the tertiary carbon atom of the Cp ring was assigned as ca. δ 77.69 ppm, the aromatic carbons of the substituted Cp ring were assigned as ca. δ 71.75 ppm and ca. δ 70.15 ppm and the aromatic carbons of the unsubstituted ring as ca. δ 67.50 ppm.

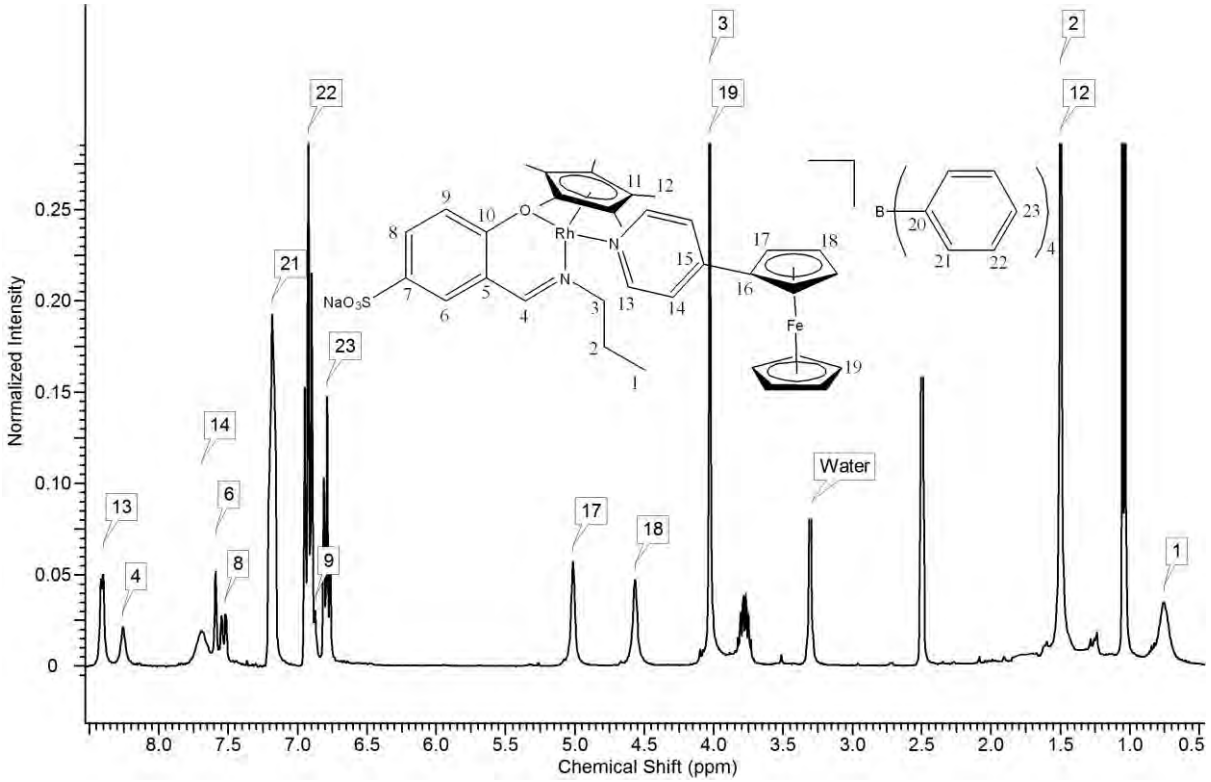

Figure 4.12 *^{1}H NMR spectrum of mononuclear N,O-salicylaldiminato complex* ***4.10****.*

Similarly, like complexes **4.2-4.3** and **4.5-4.6**, the sulfonated *N,O*-salicylaldiminato complexes **4.7-4.22** display a shift in the C=N_{imine} stretching vibration to lower wavenumbers. The *N*-pyridine containing complexes **4.7, 4.11, 4.15** and **4.19** display a shift from ca. 1635 cm^{-1} to ca. 1619 cm^{-1}, while the *N*-methylpyridine containing complexes **4.8, 4.12, 4.16** and **4.20** display a shift to ca. 1618 cm^{-1}, the *N*-phenylpyridine containing complexes **4.9, 4.13, 4.17** and **4.21** display a shift to ca. 1611 cm^{-1} and the *N*-ferrocenylpyridine containing complexes **4.10, 4.14, 4.18** and **4.22** display a shift to ca. 1609 cm^{-1}. These shifts to lower frequencies by varying the *N*-pyridyl donor ligand are due to a weakening of the C=N_{imine} bond due to the electron withdrawing nature of the *N*-donor ligand (Figure 4.13), with the *N*-ferrocenylpyridine ligand being the most electron withdrawing.

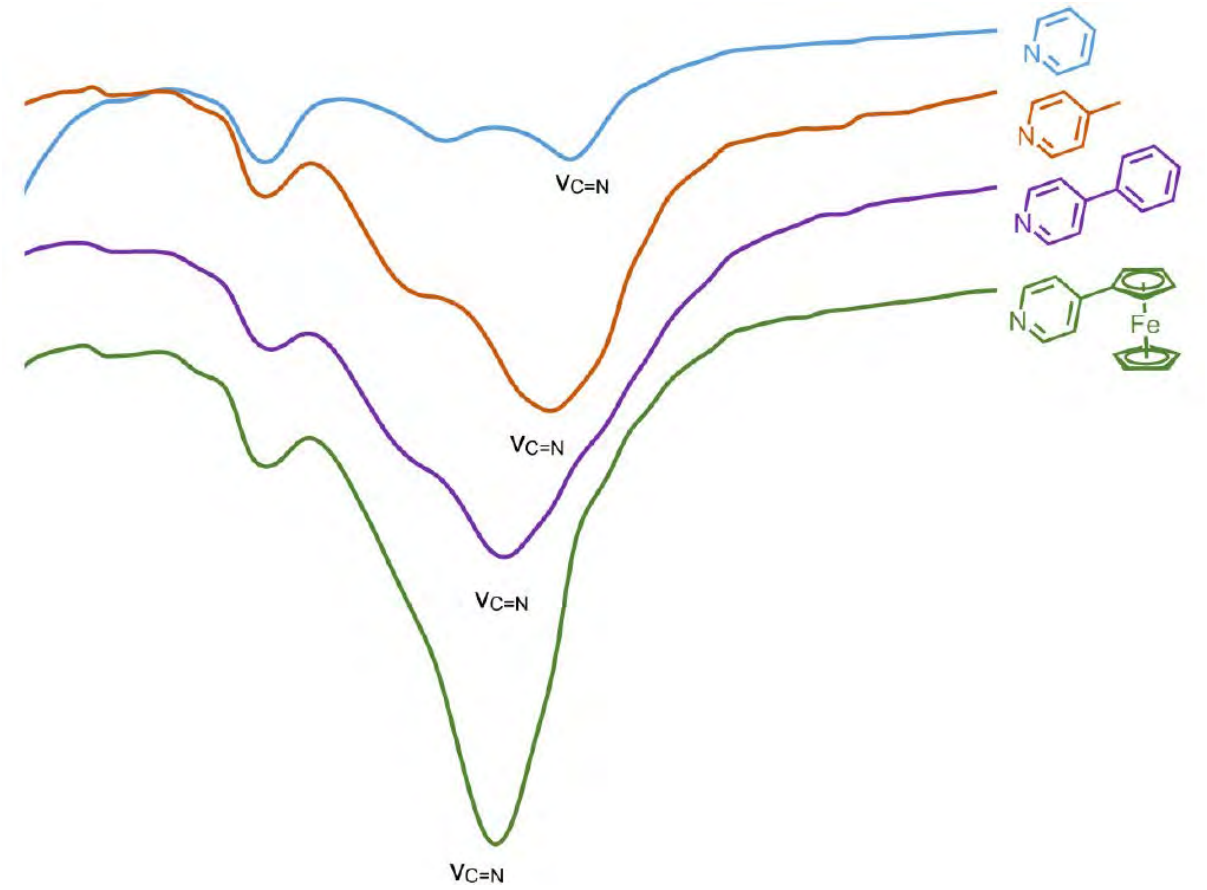

Figure 4.13 *IR spectra over range 1550-1675 cm^{-1} of N,O-salicylaldiminato complexes* ***4.15-4.18****.*

Mass spectral analysis confirmed the proposed structures. The mononuclear complexes **4.7-4.14** display a base peak in the positive mode which corresponds to the proton adduct which has undergone loss of the tetraphenylborate counterion, the sodium and the *N*-donor ligand. The rhodium(III) complexes **4.7-4.10** display the proton adduct at ca. 480 and at ca. 570 for the iridium(III) complexes **4.11-4.14**. The trinuclear rhodium(III) complexes **4.15-4.18** display a base peak which corresponds to the sodium adduct with an overall charge of +4, and which has undergone a loss of the tetraphenylborate counterions and the *N*-donor ligands. The trinuclear iridium(III) complexes **4.19-4.22** display a base peak which corresponds to the acetonitrile and potassium adduct with an overall charge of +5, and which has undergone a loss of the tetraphenylborate counterions, the sodium ions and the *N*-donor ligand. The rhodium(III) complexes **4.15-4.18** display the proton adduct at ca. 373, while this is found at ca. 405 for the iridium(III) complexes **4.19-4.22**.

Elemental analysis results of the rhodium(III) and iridium(III) complexes displayed percentages outside of acceptable limits, even after extensive drying, due to the hygroscopic

nature of the complexes **4.7-4.22**. Recalculation of the percentages with the inclusion of water gave percentages within acceptable limits.

4.3. *In vitro* Biological Activity

The *in vitro* cytotoxicity of the monomeric and mononuclear (Table 4.2) and trimeric and trinuclear (Table 4.3) sulfonated salicylaldimine compounds **4.1-4.22** was established against WHCO1 human esophageal cancer cells.

*Monomeric and Mononuclear Compounds **4.1-4.3** and **4.7-4.14***

The monomeric ligand **4.1** and the mononuclear anionic complexes **4.2-4.3** displayed inactivity against WHCO1 cells. The rhodium(III) complex **4.2** displayed an IC_{50} value of 169.1 μM, while the iridium(III) analogue **4.3** exhibited an IC_{50} value in excess of 300 μM.

However, the displacement of the metal chloro-ligand by varying *N*-donors, such as pyridine, 4-methylpyridine, 4-phenylpyridine or 4-ferrocenylpyridine, results in a cationic rhodium(III) or iridium(III) metal center and the activity of these complexes increased several-fold. The complexes **4.5-4.8** and **4.9-4.12** exhibited superior activity to the anionic chlorido complexes **4.2-4.3**.

This increase in activity due to the presence of an *N*-donor such as pyridine has been previously reported by Sadler and co-workers.[7] It was reported that an iridium(III) complex containing an *N*-donor ligand displayed a different method of action to that of cisplatin compared to the chloro-analogue. This activity was attributed to the iridium(III) complex containing an *N*-donor ligand having a greater ability to accumulate within the cancer cells. In addition to this, the iridium(III) complex containing an *N*-donor ligand generated higher levels of reactive oxygen species. The presence of the strongly bound pyridine-ligand results in a decreased rate of formation of the aqua species, when compared to that of the chloro-analogue. The increase in activity of the pyridine-analogue is contrasted by the loss of activity when the metal chloro-ligand of a Ru(II) complex is substituted with pyridine.[8]

In another reported study of iridium(III) complexes containing *N*-donor ligands by Sadler and co-workers it was observed that *N*-donor ligands with greater electron-donating abilities resulted in higher activities against tested cell lines.[9] The electron-donating ligand was thought to strengthen the M-pyridyl bond and resulted in fewer side reactions with molecules the complex might encounter on the way to the target site. No significant hydrolysis to form an

aqua species was observed, yet these iridium(III) complexes displayed potent activity against A2780, A549 (lung cancer) and MCF-7 (breast cancer).

Table 4.2 *IC_{50} values determined against WHCO1 human esophageal cancer cells for sulfonated N,O-salicylaldiminato compounds **4.1-4.3**, **4.7-4.14** and cisplatin.*

Compound Number	Metal	Ligand	IC_{50} ± SD (μM)
			WHCO1
4.1	-	-	>300
4.2	Rh	Cl	169.10 ± 13.22
4.3	Ir	Cl	>300
4.7	Rh	*N*[a]	37.27 ± 4.50
4.8	Rh	*N*-Me[b]	36.29 ± 5.47
4.9	Rh	*N*-Ph[c]	24.90 ± 10.70
4.10	Rh	*N*-Fc[d]	31.86 ± 10.01
4.11	Ir	*N*[a]	58.02 ± 19.31
4.12	Ir	*N*-Me[b]	59.55 ± 23.72
4.13	Ir	*N*-Ph[c]	49.48 ± 19.01
4.14	Ir	*N*-Fc[d]	>270
Cisplatin	Pt	-	9.2 ± 0.1[10]

[a]*N* = Pyridine; [b]*N*-Me = 4-methylpyridine; [c]*N*-Ph = 4-phenylpyridine; [d]*N*-Fc = 4-ferrocenylpyridine.

The mononuclear rhodium(III) complexes **4.7-4.10**, containing *N*-donor type ligands display similar activities with IC_{50} values in the range 24.90 - 37.27 μM. These rhodium(III) complexes are more active than the iridium(III) analogues, **4.11-4.13**, which displayed activities in the range 49.48 – 59.55 μM. The iridium(III) complex **4.14** containing the 4-ferrocenylpyridine ligand was inactive against the WHCO1 esophageal cancer cells with an IC_{50} value of >270 μM. The lack of activity of **4.14** was investigated by probing its stability in DMSO solution in the following section. The mononuclear complexes **4.2-4.3** and **4.7-4.14** were less active

against the WHCO1 esophageal cancer cells than cisplatin which has an IC_{50} value of 9.20 μM.[10]

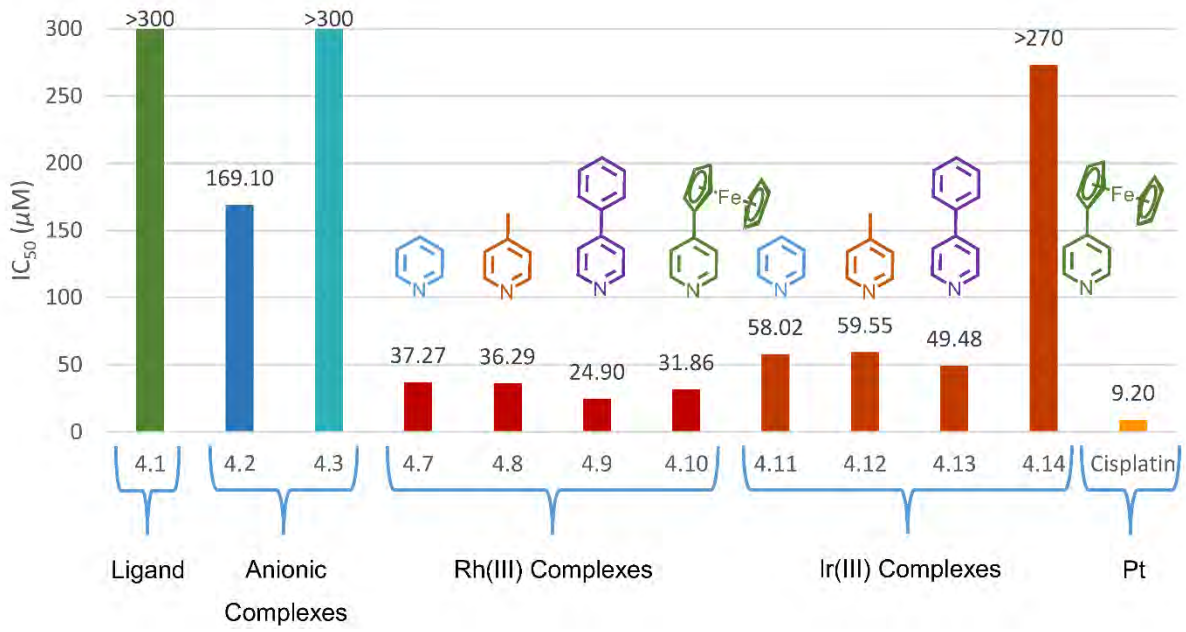

Figure 4.14 *Cytotoxicity of sulfonated N,O-salicylaldiminato compounds* ***4.1-4.3, 4.7-4.14*** *and cisplatin against WHCO1.*

Trimeric and Trinuclear Compounds ***4.4-4.6*** *and* ***4.15-4.22***

The trimeric sulfonated salicylaldimine ligand **4.4**, like the monomeric ligand **4.1**, was also inactive against the WHCO1 esophageal cancer cells with an IC_{50} value in excess of 300 μM. However, upon coordination of the metal an increase in activity is once again observed. The trinuclear anionic complexes **4.5-4.6** display an increased activity in comparison to the free ligand **4.4**.The trinuclear rhodium(III) anionic complex **4.5**, with an IC_{50} of 43.87 μM, is more active than the iridium(III) analogue, with an IC_{50} value of 200.80 μM. This trend of the anionic rhodium(III) complex being more active than the anionic iridium(III) complex was also observed in the mononuclear series of **4.2-4.3**.

It is of interest that it is observed that the activity is once again significantly increased by the displacement of the metal chlorido-ligand by various *N*-donors (Figure 4.14). This effect is observed in all of the complexes **4.15-4.22**, with the exception of complex **4.17**, where a slight loss of activity is apparent.

Table 4.3 *IC_{50} values determined against WHCO1 human esophageal cancer cells for sulfonated N,O-salicylaldiminato compounds **4.4-4.6**, **4.15-4.22** and cisplatin.*

Compound Number	Metal	Ligand	IC_{50} ± SD (μM)
			WHCO1
4.4	-	-	>300
4.5	3 Rh	Cl	43.87 ± 31.86
4.6	3 Ir	Cl	200.80 ± 9.85
4.15	3 Rh	*N*[a]	30.61 ± 18.62
4.16	3 Rh	*N*-Me[b]	33.21 ± 16.28
4.17	3 Rh	*N*-Ph[c]	54.96 ± 40.38
4.18	3 Rh	*N*-Fc[d]	0.56 ± 0.49
4.19	3 Ir	*N*[a]	12.96 ± 8.99
4.20	3 Ir	*N*-Me[b]	6.22 ± 4.49
4.21	3 Ir	*N*-Ph[c]	9.57 ± 4.57
4.22	3 Ir	*N*-Fc[d]	49.46 ± 16.67
Cisplatin	Pt	-	9.2 ± 0.1[10]

[a]*N* = Pyridine; [b]*N*-Me = 4-methylpyridine; [c]*N*-Ph = 4-phenylpyridine; [d]*N*-Fc = 4-ferrocenylpyridine.

The series of trinuclear iridium(III) complexes **4.19-4.21** have IC_{50} values in the range 6.22 – 12.96 μM and have superior activity over the trinuclear rhodium(III) analogues **4.15-4.17** with IC_{50} values in the range 30.61 – 54.96 μM (Figure 4.15). It has been previously reported that iridium(III)-Cp* complexes with *N*-donor ligands have potent antitumor activities.[11] As observed in both the mono- and trinuclear series the rhodium(III) complexes **4.10** and **4.18** both have increased activity in comparison to the iridium(III) analogues **4.14** and **4.22**, against the WHCO1 cancer cells.

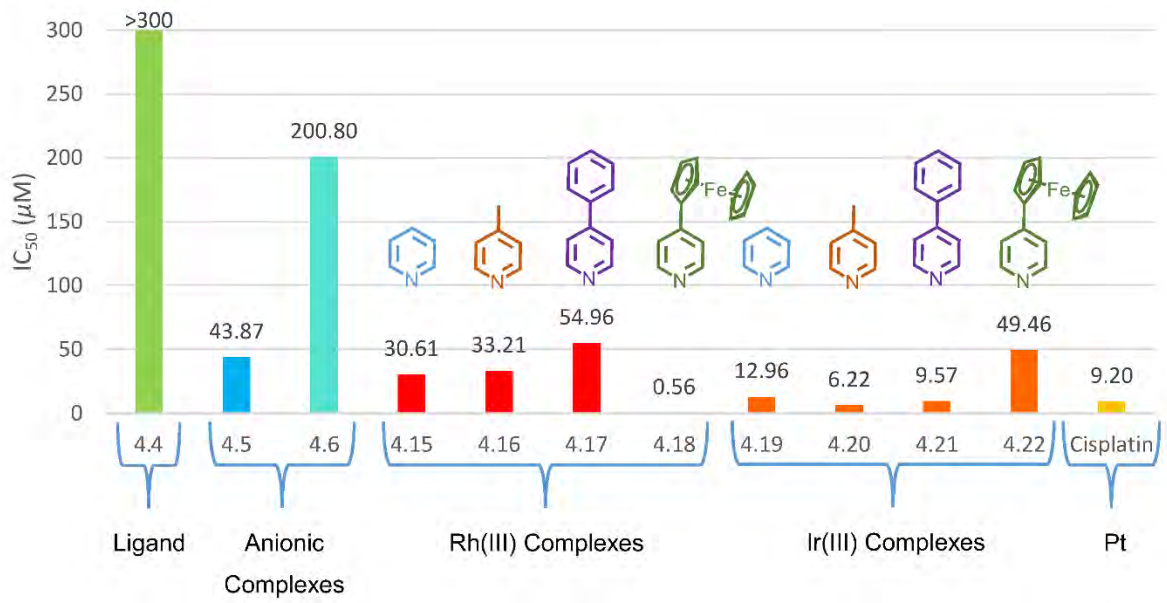

Figure 4.15 *Cytotoxicity of sulfonated N,O-salicylaldiminato compounds* ***4.4-4.6, 4.15-4.22*** *and cisplatin against WHCO1.*

The trinuclear iridium(III) complexes **4.19-4.21** are similar in activity to that of cisplatin against the WHCO1 cancer cells. The most active complex was the trinuclear rhodium(III) complex **4.18**, containing the 4-ferrocenylpyridine ligand, with an IC_{50} value of 0.56 μM. Interestingly a dinuclear ruthenium(II) complex with a *N*-ferrocenoyl pyridine ligand prepared by Süss-Fink and co-workers displayed remarkable antitumor activity and this potency was attributed to the complex's redox ability.[12-13]

4.4. Aqueous and DMSO Stability

Due to the interesting trends and activity of these complexes the aqueous stability was investigated. The aim of these studies is to provide mechanistic insight to rationalize the observed biological activities of these complexes. The stability, and ability to form activated aqua species[14-15], of a select few complexes was monitored using ^{1}H NMR spectroscopy over time at a physiological temperature of 37 ^{o}C.

The mononuclear rhodium(III) complex **4.10** and mononuclear iridium(III) complex **4.14** contain 4-ferrocenylpyridine and are bimetallic in nature. The rhodium(III) analogue **4.10** displays a remarkable difference in activity against WHCO1 cells to that of the inactive iridium(III) analogue **4.14**. This can be explained by the decrease in stability of **4.14** in DMSO,

as investigated by ^{1}H NMR spectroscopy, in comparison to **4.10**. However, in contrast to this, both **4.10** and **4.14** exhibited stability in a 50:50 mixture of CD_3OD and H_2O for 48 hours.

The biologically inactive iridium(III) 4-ferrocenylpyridine complex **4.14** slowly allows dissociation of the 4-ferrocenylpyridine ligand in DMSO and displays full substitution of the metal chloro-ligand with DMSO within 48 hours, as observed by ^{1}H NMR spectroscopy. The dissociation product renders the complex inactive against WHCO1, as observed by the high IC_{50} value. Similarly, the metal-chloro analogues **4.2-4.3** both undergo displacement of the metal chloro-ligand over 48 hours by DMSO, as observed by ^{1}H NMR spectroscopy (Figure 4.16). This was confirmed by the addition of DMSO to a solution of **4.2** or **4.3** in CD_3OD. In complex **4.14** the lability of the 4-ferrocenylpyridine ligand in DMSO and that of the metal-chloro ligand in complexes **4.2-4.3** could explain their similar lack of biological activities against WHCO1 cells.

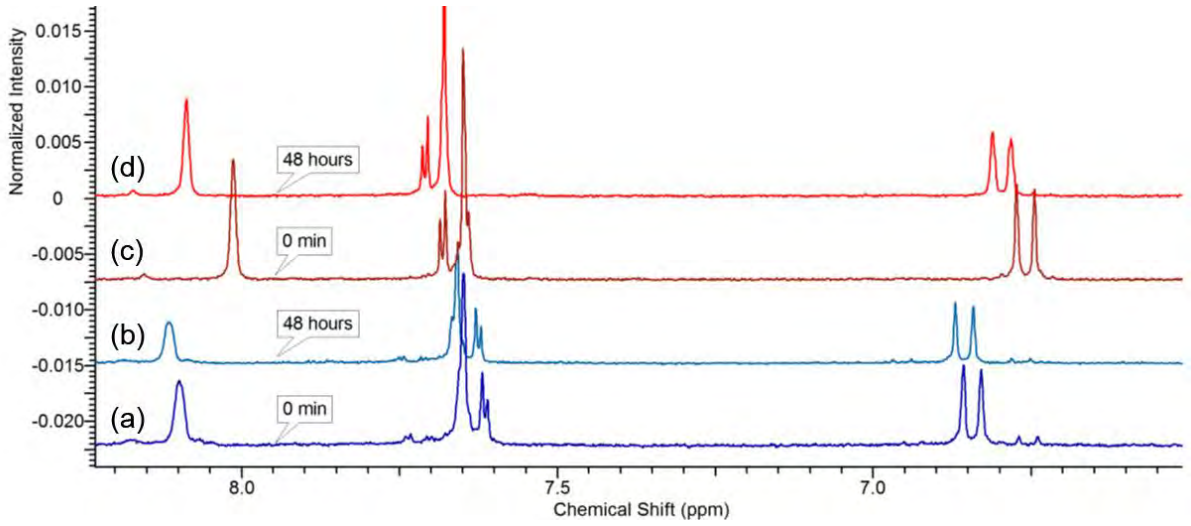

Figure 4.16 *Expanded ^{1}H NMR spectra of mononuclear (a) rhodium(III) complex **4.2** and (c) iridium(III) complex **4.3**. Shifts due to DMSO coordination in CD_3OD are shown for (b) rhodium(III) and (c) iridium(III) complexes.*

The rhodium(III) 4-ferrocenylpyridine complex **4.10** and the other *N*-donor-containing mono- and trinuclear complexes **4.7-4.9** and **4.11-4.22** all proved to be stable in DMSO for prolonged periods of time, up to 3 weeks. This stability towards DMSO might explain the similar biological activities of these complexes against WHCO1 cells. This is in contrast to the iridium(III) 4-ferrocenylpyridine complex **4.14** possibly due to the ability of the 4-ferrocenylpyridine ligand to strongly coordinate to the rhodium(III) metal center in complex **4.10**. It is of interest to note that the trinuclear iridium(III) complex **4.22** containing 4-ferrocenylpyridine did not undergo

dissociation of the 4-ferrocenylpyridine ligand this could explain the increased antitumor activity of the trinuclear complex compared to the mononuclear analogue **4.10**. This increase in stability of the trinuclear complex **4.22** compared to **4.10** may be due to the nature of the trimeric ligand used.

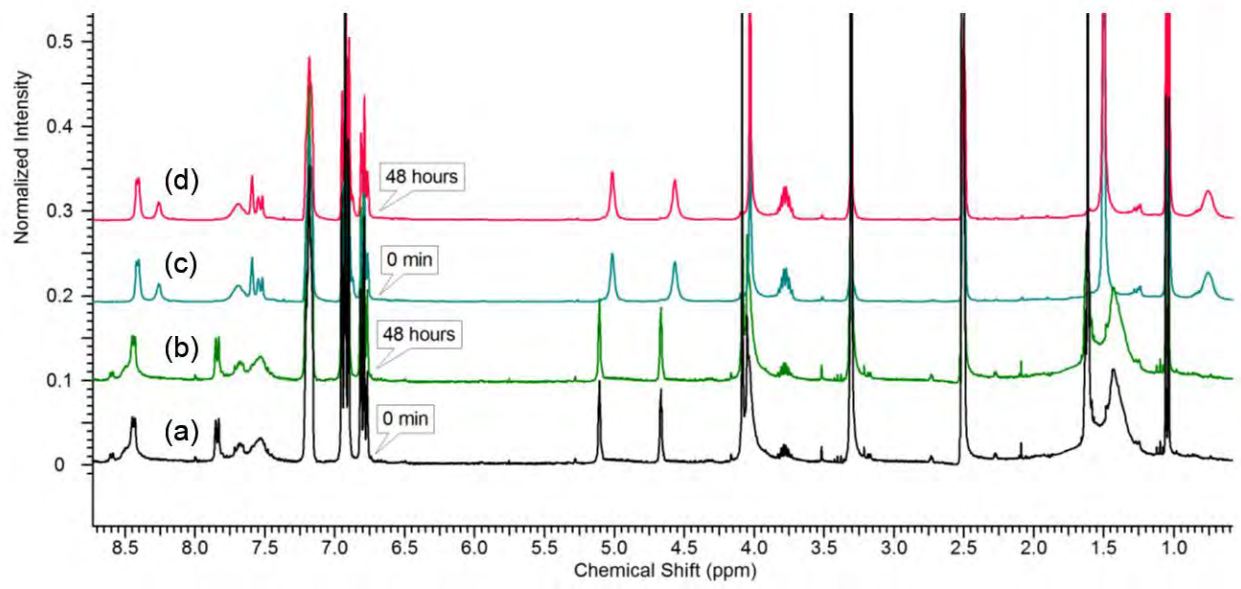

Figure 4.17 *^{1}H NMR spectra of trinuclear (a) rhodium(III) complex **4.18** and (c) mononuclear rhodium(III) complex **4.10** over 48 hours.*

As the activity of the trinuclear rhodium(III) complex **4.18** against the WHCO1 cancer cells was the highest within this series, investigations into the stability in solution and in the presence of 50:50 DMSO and H_2O were carried out by ^{1}H NMR spectroscopy. After 48 hours in solution **4.18** showed no signs of degradation or formation of the aqua species, as the ^{1}H spectra remained unchanged over the tested time. Though **4.18** exhibits stability in DMSO, it has been reported that complexes may coordinate to other molecules.[16]

4.5. Interactions with Model DNA 5'-GMP

Due to the ability of many PGM anticancer complexes[17-18], and those tested in Chapters 2 and 3 in this study, which interact with DNA base-pairs,[19-21] the ability of **4.18** to interact with 5'-GMP was monitored using ^{1}H NMR spectroscopy in a 50:50 mixture of $(CD_3)_2SO$ and water at 37 ^{o}C for 48 hours. The trinuclear complex **4.18** was selected for this study as it was the most active against WHCO1 cancer cells.

The trinuclear sulfonated rhodium(III) complex **4.18** was reacted with 3 equivalents of the DNA base-pair, 5'-GMP. The base pair was observed to coordinate to the rhodium(III) metal *via* the N7 atom complex. In the ^{1}H NMR spectrum of the reaction mixture, a downfield shift from δ 8.22 ppm (Figure 4.18a) to δ 8.49 ppm (Figure 4.18c) is observed for the proton H8 of the guanosine base pair which confirms that displacement of the *N*-ferrocenylpyridine ligand occurs over the 48 hours.

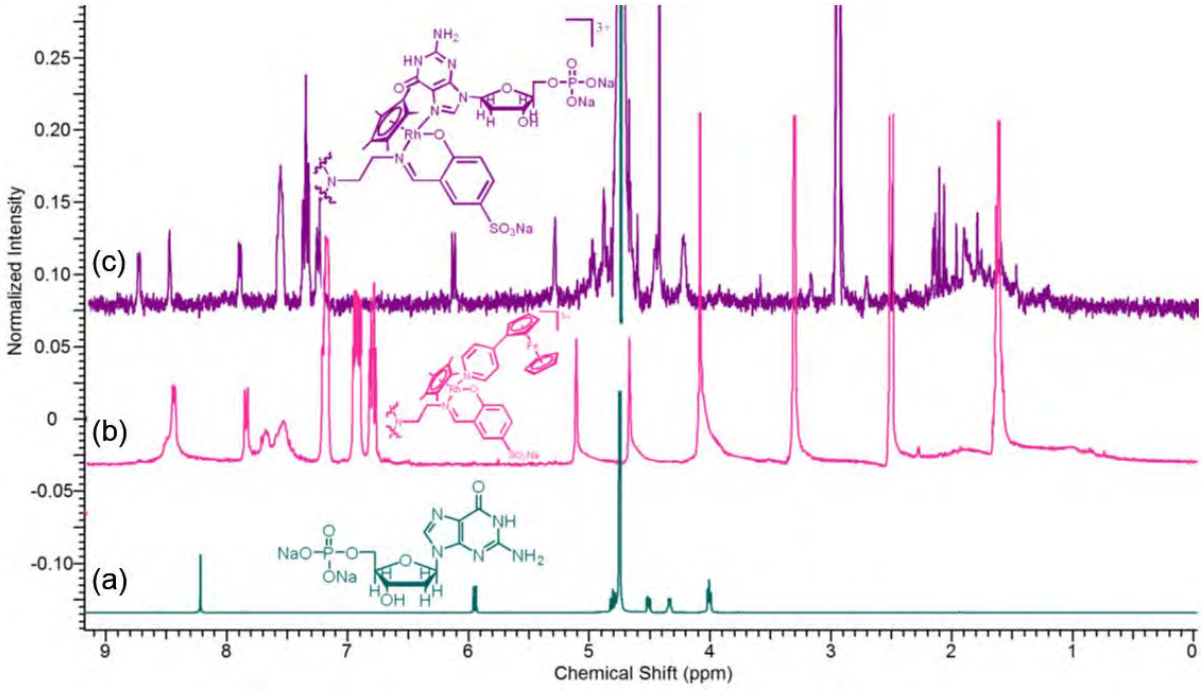

Figure 4.18 *^{1}H NMR spectra of (a) 5'-GMP (cyan), (b)* ***4.18*** *(pink) and (c) reaction mixture of* ***4.18*** *with 5'-GMP (purple).*

Observation of these shifts of signals in the ^{1}H NMR spectrum have been previously reported and similar shifts have been observed for the interactions between other metal complexes and mononucleotides *via* the N7.[22]

4.6. Overall Summary

Four new anionic sulfonated rhodium(III) and iridium(III) complexes **4.2-4.3** and **4.5-4.6** were prepared from the ligands **4.1** and **4.4**, which were prepared via Schiff base condensation. Sixteen new rhodium(III) and iridium(III) complexes **4.7-4.22** were synthesized from ligands **4.1** and **4.4** and a variety of *N*-donor ligands were used to displace the metal-chloro ligand. These mononuclear and trinuclear complexes were isolated as tetraphenylborate salts.

Compounds **4.1-4.22** were isolated in poor to excellent yields and were characterized using a mixture of spectroscopic and analytical techniques. ^{1}H NMR spectroscopy indicated that coordination of the ligand to the metal-arene takes place *via* the imine nitrogen and the phenolic oxygen in a bidentate manner.

The ligands **4.1** and **4.4** are inactive as antitumor agents against the esophageal WHCO1 cancer cell line. Upon coordination of the metal-arene to yield the anionic rhodium(III) and iridium(III) complexes **4.2-4.3** and **4.5-4.6** some antitumor activity is observed. The complexes **4.7-4.22**, containing *N*-donor ligands, exhibit significant activity against the WHCO1 cell line. An activity to size-dependent relationship was observed, in that the trinuclear complexes **4.5-4.6** and **4.15-4.22** exhibited greater activity than the mononuclear complexes **4.2-4.3** and **4.7-4.14**. The trinuclear complexes **4.15-4.22** containing *N*-donor ligands display the greatest activity, while the most active complex in this series of sulfonated compounds is the sulfonated trinuclear rhodium(III) complex **4.18** containing *N*-ferrocenylpyridine. It is currently unclear as to why these trends exist. Future investigative studies will be performed to probe the method of action which may shed light on the observed activities. In the mononuclear series **4.2-4.3** and **4.7-4.14** and the trinuclear anionic complexes **4.5-4.6** the rhodium(III) complexes all displayed superior antitumor activities over the iridium(III) analogues. However, the iridium(III) complexes **4.19-4.22** exhibited greater activities than the trinuclear rhodium(III) complexes **4.15-4.17**. Despite the inertness of the complex towards water and DMSO, **4.18** displays the ability to interact with 5'-GMP, *via* the N7 atom.

4.7. References

[1] A.A. Chachoyan and L.I. Sagradyan, *Biol. Zhurnal Armenii* **1987**, *40*, 399-400.

[2] Y. Zheng, Q. Zhou, W. Lei, Y. Hou, K. Li, Y. Chen, B. Zhanga and X. Wang, *Chem. Commun.* **2015**, *51*, 428-430.

[3] T.S. Morais, F.C. Santos, T.F. Jorge, L. Côrte-Real, P.J.A. Madeira, F. Marques, M.P. Robalo, A. Matos, I. Santos and M.H. Garcia, *J. Inorg. Biochem.* **2014**, *130*, 1-14.

[4] P. Bergamini, L. Marvelli, A. Marchi, V. Bertolasi, M. Fogagnolo, P. Formaglio and F. Sforza, *Inorg. Chim. Acta* **2013**, *398*, 11-18.

[5] E.B. Hager, B.C.E. Makhubela and G.S. Smith, *Dalton Trans.* **2012**, *41*, 13927-13935.

[6] B.C.E. Makhubela, M. Meyer and G.S. Smith, *J. Organomet. Chem.* **2014**, 229-241.

[7] Z. Liu, I. Romero-Canelon, B. Qamar, J.M. Hearn, A. Habtemariam, N.P.E. Barry, A.M. Pizarro, G.J. Clarkson and P.J. Sadler, *Angew. Chem. Int. Ed.* **2014**, *53*, 3941-3946.

[8] F. Wang, A. Habtemariam, E.P.L. van der Geer, R. Ferández, M. Melchart, R.J. Deeth, R. Aird, S. Guichard, F.P.A. Fabbiani, P. Lozano-Casal, I.D.H. Oswald, D.I. Jodrell, S. Parsons and P.J. Sadler, *Proc. Natl. Acad. Sci. USA* **2005**, *102*, 18269-18274.

[9] Z. Liu, I. Romero-Canelon, A. Habtemariam, G. J. Clarkson and P. J. Sadler, *Organometallics* **2014**, *33*, 5324-5333.

[10] C.H. Kaschula, R. Hunter, N. Stellenboom, M.R. Caira, S. Winks, T. Ogunleye, P. Richards, J. Cotton, K. Zilbeyaz, Y. Wang, V. Siyo, E. Ngarande and M.I. Parker, *Eur. J. Med. Chem.* **2012**, *50*, 236-254.

[11] A.J. Millett, A.Habtemariam, I.Romero-Canelon, G.J. Clarkson and P.J. Sadler, *Organometallics* **2015**, 2683-2694.

[12] M. Auzias, B. Therrien, G. Süss-Fink, P. Štěpnička, W.H. Ang and P. J. Dyson, *Inorg. Chem.* **2008**, *47*, 578-583.

[13] C. Mu, S. W. Chang, K. E. Prosser, A. W. Y. Leung, S. Santacruz, T. Jang, J. R. Thompson, D. T. T. Yapp, J. J. Warren, M. B. Bally, T. V. Beischlag and C. J. Walsby, *Inorg. Chem.* **2016**, *55*, 177-190.

[14] C. Gossens, A. Dorcier, P.J. Dyson and U. Rothlisberger, *Organometallics* **2007**, *26*, 3969-3975.

[15] C. Scolaro, C.G. Hartinger, C.S. Allardyce, B.K. Keppler and P.J. Dyson, *J. Inorg. Biochem.* **2008**, *102*, 1743-1748.

[16] W.H. Ang, E. Daldini, C. Scolaro, R. Scopelliti, L. Juillerat-Jeannerat and P.J. Dyson, *Inorg. Chem.* **2006**, *45*, 9006-9013.

[17] A.E. Egger, C.G. Hartinger, A.K. Renfrew and P.J. Dyson, *J. Biol. Inorg. Chem.* **2010**, *15*, 919-927.

[18] M. Groessl, Y.O. Tsybin, C.G. Hartinger, B.K. Keppler and P.J. Dyson, *J. Biol. Inorg. Chem.* **2010**, *15*, 677-688.

[19] H. Chen, J.A. Parkinson, R.E. Morris and P.J. Sadler, *J. Am. Chem. Soc.* **2003**, *125*, 173-186.

[20] A. Dorcier, P. J. Dyson, C. Gossens, U. Rothlisberger, R. Scopelliti and I. Tavernelli, *Organometallics* **2005**, *24*, 2114-2123.

[21] A. Dorcier, C.G. Hartinger, R. Scopelliti, R.H. Fish, B.K. Keppler and P. J. Dyson, *J. Inorg. Biochem.* **2008**, *102*, 1066-1076.

[22] B.S. Murray, L. Menin, R. Scopelliti and P.J. Dyson, *Chem. Sci.* **2014**, *5*, 2536-2545.

Chapter 5: Experimental

5. General Remarks

All solvents used were analytical grade and dried over molecular sieves. All reactions were carried out in air unless otherwise stated. All samples were dried under vacuum.

1,2,3,4,5-Pentamethylcyclopentadiene, 1,3,5-tris(bromomethyl)benzene, 1,3,5-triaza-7-phosphaadamantane, α-phellandrene, 2-pyridine carboxaldehyde, 4-aminophenylmethanol, 4-methylpyridine, 4-phenylpyridine, benzaldehyde, benzyl chloride, HEPES buffer, histidine, nucleotide guanosine 5′-monophosphate, pyridine, Red Salmon testes DNA, salicylaldehyde, sodium acetate, sodium hexafluorouphosphate, sodium tetraphenylborate, triethylamine and trimesyl acid chloride were all purchased from Sigma-Aldrich and used as received. Ruthenium trichloride trihydrate, rhodium trichloride trihydrate and iridium chloride trihydrate were purchased from Heraeus SA. $[Ru(\eta^6\text{-}p\text{-}Pr^iC_6H_4Me)Cl_2]_2$,[1] $[Rh(\eta^5\text{-}C_5Me_5)Cl_2]_2$[2] or $[Ir(\eta^5\text{-}C_5Me_5)Cl_2]_2$[2] were prepared using known literature reported procedures. Deuterated solvents were purchased from Sigma-Aldrich.

5.1. Instrumentation

^1H, $^{13}C\{^1H\}$, $^{31}P\{^1H\}$, $[^1H\text{-}^{13}C]$ NMR spectra were recorded at ambient temperature on a Bruker Ultrashield 400 Plus spectrometer (^1H:400.22 MHz; $^{13}C\{^1H\}$: 100.65 MHz; $^{31}P\{^1H\}$: 162.00 MHz) and chemical shifts were referenced to tetramethylsilane (TMS) as an internal standard for ^1H, and $^{13}C\{^1H\}$ NMR spectra and H_3PO_4 as an external standard for $^{31}P\{^1H\}$ NMR spectra.

EI-MS was carried out on a JEOL GCMateII mass spectrometer. ESI-MS and HR-ESI-MS were carried out on a Waters API Quattro Micro Triple Quadrupole electrospray ionization mass spectrometer in the positive or negative mode.

FT-IR spectra were recorded as KBr pellets or as pure solids by ATR using a Perkin-Elmer Spectrum 100 FT-IR spectrometer.

EA were conducted with a Thermo Flash 1112 Series CHNS-O Analyser.

Melting points were determined using a Büchi Melting Point Apparatus B-540.

UV-Vis absorption studies were performed using a Cary UV-Vis spectrophotometer using a 1 cm path length quartz cuvette to carry out the measurements.

The solubility of compounds were evaluated by dissolving accurately known masses into measured volumes of water.

5.2. Synthesis of *N,C*-Benzaldimine, *N,N*-Pyridylimine and *N,O*-Salicylaldimine Ligands

5.2.1. Preparation Monomeric Ligands (2.1-2.3)

5.2.1.1.Preparation of 2.1 and 2.3

4-(Benzylideneamino)benzyl alcohol, **2.1**,[3] and 4-(salicylideneamino)benzyl alcohol, **2.3**,[4] were synthesized using known literature reported procedures.

5.2.1.2. 4-(Pyridylideneamino)benzyl alcohol (2.2)

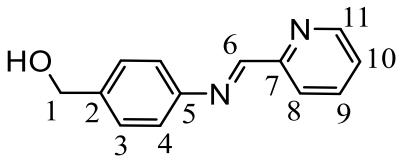

4-Aminophenylmethanol (523 mg, 4.24 mmol), dissolved in EtOH (15 ml), was reacted with 2-pyridinecarboxaldehyde (0.500 g, 4.67 mmol) and the reaction mixture was stirred overnight at room temperature. The solvent was removed by rotary evaporation and yielded the crude product, which was dissolved in a minimal amount of dichloromethane and the ligand **2.2** was precipitated using hexane. The ligand was dried under vacuum for 12 hours.

Pale brown solid, **yield**: 771 mg, 86%. **MP.**: 57.7-70.9°C. **^{1}H NMR** ($CDCl_3$): δ(ppm) = 8.72 (d, 1H, H_{11}, ^3J = 4 Hz), 8.59 (s, 1H, H_6), 8.21 (d, 1H, H_8, ^3J= 8Hz), 7.82 (t, 1H, H_9, 8 Hz), 7.42 (d, 2H, H_3, ^3J = 8 Hz), 7.38 (m, 1H, H_{10}), 7.28 (d, 2H, H_4, ^3J = 12 Hz), 4.73 (d, 2H, H_1, ^3J = 4 Hz), 2.07 (b, 1H, -OH). **^{13}C{^{1}H} NMR** ($CDCl_3$): δ(ppm) = 160.42 (C_6), 154.77 (C_7), 150.42 (C_5), 149.59 (C_{11}), 139.72 (C_2), 136.55 (C_9), 127.85 (C_3), 124.98 (C_{10}), 121.76 (C_8), 121.21 (C_4), 64.83 (C_1). **FT-IR** (KBr): 3253 (bs) ν(O-H), 1630 (s) ν(C=N_{imine}), 1583 (m) ν(C=$N_{pyridyl}$), 1504 (s) ν(aromatic C=C), 1021 (s) ν(C-O). **EI-MS**: *m/z* 212.07 $[M]^+$. **Elemental Analysis** (Calculated for $C_{13}H_{12}N_2O$): C, 73.57; H, 5.70; N, 13.20; Found: C, 71.87; H, 5.52; N, 13.84.

5.2.2. Preparation of Trimeric Ligands (2.4-2.6)

General Procedure

To a stirring solution of **2.1** (360 mg, 1.70 mmol for **2.4**) or **2.2** (400 mg, 1.89 mmol for **2.5**) or **2.3** (400 mg, 1.76 mmol for **2.6**) in DCM (20 ml), triethylamine (230 mg, 2.27 mmol for **2.4**; 765 mg, 7.56 mmol for **2.5** and 712 mg, 7.04 mmol for **2.6**) and trimesyl chloride (150 mg, 0.568 mmol for **2.4**; 161 mg, 0.608 mmol for **2.5** and 150 mg, 0.568 mmol for **2.6**) were added. The solution was stirred at room temperature overnight. The solvent was removed under reduced pressure and 2-butanone was added to the solid product. After filtration, the solvent was removed from the filtrate using rotary evaporation and the solid product was purified by dissolution in minimal DCM and precipitation with hexane.

5.2.2.1.Tris(4-(2-benzylimine)benzyl)benzene-1,3,5-tricarboxylate ligand (2.4)

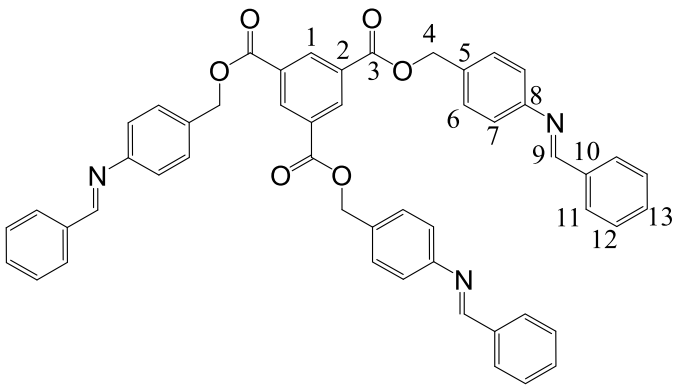

Yellow solid, **yield**: 307 mg, 69%. **MP.**: 148ºC (decomposed). **^{1}H NMR** ($CDCl_3$): *δ*(ppm) = 8.92 (s, 3H, H_1), 8.45 (s, 3H, H_9), 7.88 (d, 6H, H_{11}, ^3J = 4 Hz**),** 7.47 (m, 15H, H_6 H_{12} H_{13}), 7.22 (d, 6H, H_7, ^3J = 6 Hz), 5.41 (s, 6H, H_4). **^{13}C{^{1}H} NMR** ($CDCl_3$): *δ*(ppm) = 164.79 (C_3), 160.60 (C_9), 157.69 (C_5), 136.27 (C_8), 133.10 (C_{10}), 128.71 (C_{11}), 128.86 (C_{12} C_{13}), 134.74 (C_1), 131.38 (C_6), 130.25 (C_2), 67.07 (C_4). **FT-IR** (KBr): 1724 (s) *ν*(C=O), 1628 (m) *ν*(C=N_{imine}), 1577 (s) *ν*(aromatic C=C), 1231 (s) *ν*(C-C(O)-O). **ESI-MS**: *m/z* 266.15 $[M+3H]^{3+}$. **Elemental Analysis** (Calculated for $C_{51}H_{39}N_3O_6$): C, 77.55; H, 4.98; N, 5.32; Found: C, 77.68; H, 4.78; N, 5.51.

5.2.2.2.Tris(4-(2-pyridylimine)benzyl)benzene-1,3,5-tricarboxylate ligand (2.5)

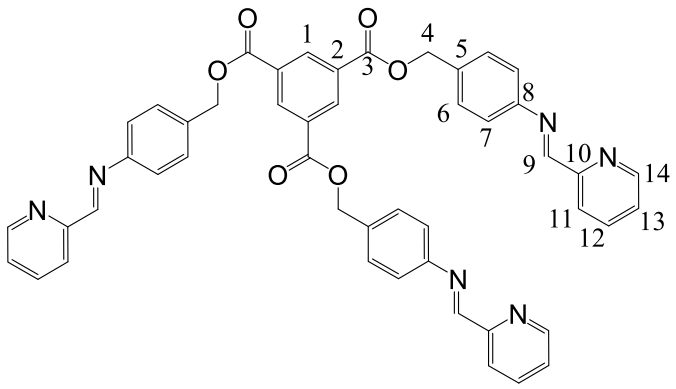

Pale brown solid, **yield**: 443 mg, 92%. **MP.**: 151ºC (decomposed). **^{1}H NMR** ($CDCl_3$): *δ*(ppm) = 8.95 (s, 3H, H_1), 8.75 (d, 3H, H_{14}, ^{3}J = 4 Hz), 8.65 (s, 3H, H_9), 7.92 (d, 3H, H_{11}, ^{3}J = 4 Hz), 7.85 (t, 3H, H_{12}, ^{3}J = 4 Hz), 7.55 (m, 6H, H_6), 7.41 (t, 3H, H_{13}, ^{3}J = 4 Hz), 7.31 (m, 6H, H_7), 5.45 (s, 6H, H_4). **^{13}C{^{1}H} NMR** ($CDCl_3$): *δ*(ppm) = 165.25 (C_3), 160.49 (C_9), 149.65 (C_{14}), 148.21 (C_{10}), 146.43 (C_8), 137.06 (C_{11}), 136.76 (C_{12}), 134.72 (C_5), 134.12 (C_1), 130.43 (C_2), 129.53 (C_6), 125.25 (C_{13}), 67.00 (C_4). **FT-IR** (KBr): 1719 (s) *ν*(C=O), 1597 (m) *ν*(C=N_{imine}), 1521 (s) *ν*(aromatic C=C), 1234 (s) *ν*(C-C(O)-O). **ESI-MS**: *m/z* 265.28 $[M+3H]^{3+}$. **Elemental Analysis** (Calculated for $C_{48}H_{36}N_6O_6$): C, 72.72; H, 4.58; N, 10.60; Found: C, 72.45; H, 4.70; N, 10.08.

5.2.2.3.Tris(4-(2-salicylaldimine)benzyl)benzene-1,3,5-tricarboxylate ligand (2.6)

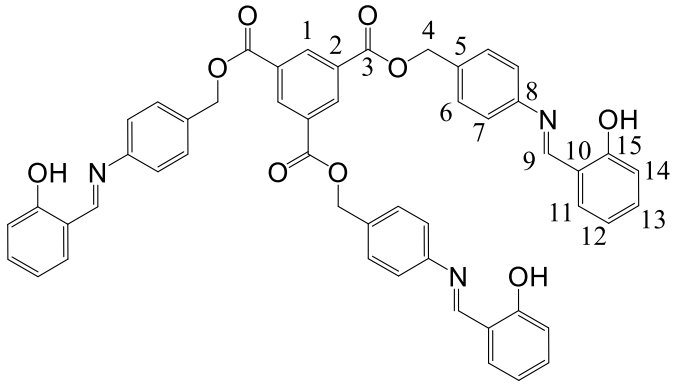

Yellow solid, **yield**: 473 mg, 99%. **MP.**: 115.5-119.8ºC. **^{1}H NMR** ($CDCl_3$): *δ*(ppm) = 13.01 (bs, 3H, -OH), 8.85 (s, 3H, H_1), 8.55 (s, 3H, H_9), 7.46 (d, 6H, ^{3}J = 8 Hz), 7.32 (d, 6H, H_{11}, ^{3}J = 8 Hz), 7.23 (d, 3H, ^{3}J = 8 Hz), 6.95 (d, 3H, ^{3}J = 8 Hz), 6.87 (t, 3H, ^{3}J = 8 Hz), 5.37 (s, 6H, H_4). **^{13}C{^{1}H} NMR** ($CDCl_3$): *δ*(ppm) = 164.58 (C_3), 163.10 (C_9), 161.28 (C_{15}), 155.53 (C_5), 148.97 (C_8), 136.82 (C_2), 134.80, 133.29 (C_{13}), 132.33 (C_{11}), 129.62 (C_6), 121.40 (C_7), 119.73 (C_{10}), 119.05 (C_{12}), 117.33 (C_{14}), 66.94 (C_4). **FT-IR** (KBr): 1728 (s) *ν*(C=O), 1622 (s) *ν*(C=N), 1602 (s) *ν*(aromatic C=C), 1573 (s) *ν*(aromatic C=C), 1280 (s) *ν*(C-O), 1232 (s) *ν*(C-C(O)-O). **ESI-**

MS: *m/z* 280.10 $[M+3H]^{3+}$. **Elemental Analysis** (Calculated for $C_{51}H_{39}N_3O_9$): C, 73.11; H, 4.69; N, 5.02; Found: C, 73.45; H, 4.80; N, 4.40.

5.3. Synthesis of Mononuclear Complexes

5.3.1. Synthesis of Mononuclear *N,C*-Benzaldiminato Complexes (2.7-2.8)

General Procedure

The ligand **2.1** (50.0 mg, 0.237 mmol for **2.7** and 53.0 mg, 0.251 mmol for **2.8**) was dissolved in MeOH (20 ml) and NaOAc added (20.4 mg, 0.285 mmol for **2.7** and 21.6 mg, 0.264 mmol for **2.8**). $[Rh(\eta^5\text{-}C_5Me_5)Cl_2]_2$ (73.0 mg, 0.118 mmol for **2.7**) or $[Ir(\eta^5\text{-}C_5Me_5)Cl_2]_2$ (100 mg, 0.126 mmol for **2.8**) was added to the solution which was stirred for 2 hours, after which the MeOH was removed by rotary evaporation yielding a solid residue. The residue was dissolved in acetone, filtered by gravity and the solvent of the filtrate was removed under reduced pressure. The solid products **2.7-2.8** were purified by dissolution in a minimal amount of DCM and precipitated using Et_2O.

5.3.1.1. 4-(Benzylaldimine)phenylmethanol rhodium(III) complex (2.7)

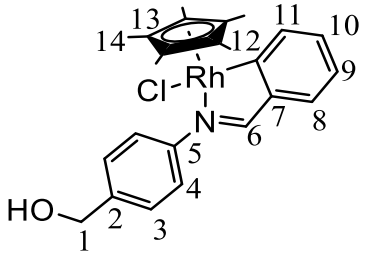

Red solid, **yield**: 25.0 mg, 22%. **MP.**: 189ºC (decomposed). **^{1}H NMR** ($CDCl_3$): δ(ppm) 8.17 (s, 1H, H_6), 7.85 (d, 1H, H_8, ^3J = 7 Hz), 7.62 (d, 2H, H_3, ^3J = 7 Hz), 7.53 (d, 1H, H_{11}), 7.42 (d, 2H, H_4, ^3J = 6 Hz), 7.26 (t, 1H, H_{10}, ^3J = 8 Hz), 7.06 (t, 1H, H_9, ^3J = 7 Hz), 4.75 (s, 2H, H_1), 1.43 (s, 15H, H_{14}). **^{13}C{^{1}H} NMR** ($CDCl_3$): δ(ppm) = 185.39 (C_{12}), 172.29 (C_6), 150.31 (C_7), 146.31 (C_5), 140.21 (C_2), 136.37 (C_8), 131.42 (C_{10}), 129.38 (C_{11}), 127.56 (C_3), 122.71 (C_9), 122.20 (C_4), 96.24 (C_{13}), 64.61 (C_1), 8.93 (C_{14}). **FT-IR (KBr)**: 3380 (bs) ν(O-H), 2910 (m) ν(C-H_{Cp^*}), 1588 (s) ν(C=N), 1542 (s) ν(aromatic C=C), 1432 (s) δ(C-H), 1376 δ(-CH_{3Cp^*}), 1154 (s) ν(C-O), 1050 (s) ν(C-O). **ESI-MS**: *m/z* 448.11 $[M\text{-}Cl]^+$. **Elemental Analysis** (Calculated for $C_{24}H_{27}ClNORh$): C, 59.58; H, 5.62; N, 2.89; Found: C, 59.59; H, 5.53; N, 2.98.

5.3.1.2. 4-(Benzylaldimine)phenylmethanol iridium(III) complex (2.8)

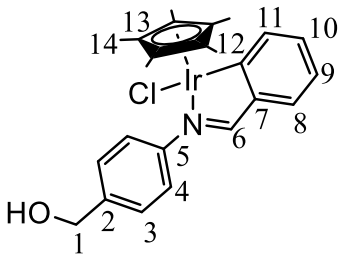

Orange solid, **yield**: 94.0 mg, 65%. **MP.**: 184ºC (decomposed). **^{1}H NMR** ($CDCl_3$): *δ*(ppm) 8.30 (s, 1H, H_6), 7.85 (d, 1H, H_8, ^3J = 8 Hz), 7.57 (d, 2H, H_4, ^3J = 12 Hz), 7.38 (d, 2H, H_3, ^3J = 8 Hz), 7.62 (d, 1H, H_{11}, ^3J = 8 Hz), 7.20 (t, 1H, H_9, ^3J = 8 Hz), 7.03 (t, 1H, H_{10}, ^3J = 8 Hz), 4.75 (s, 2H, H_1), 1.48 (s, 15H, H_{14}). **^{13}C{^{1}H} NMR** ($CDCl_3$): *δ*(ppm) = 175.46 (C_6), 170.59 (C_{12}), 151.21 (C_5), 146.93 (C_5), 140.03 (C_2), 135.13 (C_8), 132.48 (C_9), 129.59 (C_{10}), 127.46 (C_3), 122.65 (C_4), 122.01 (C_{11}), 89.21 (C_{13}), 64.75 (C_1), 8.76 (C_{14}). **FT-IR** (KBr): 3392 (bs) *ν*(O-H), 2909 (m) *ν*(C-H_{Cp^*}), 1583 (s) *ν*(C=N), 1536 (s) *ν*(aromatic C=C), 1499 (s) *δ*(C-H), 1377 *δ*(-CH_{3Cp^*}), 1153 (s) *ν*(C-O), 1052 (s) *ν*(C-O). **ESI-MS**: *m/z* 538.17 $[M\text{-}Cl]^+$. **Elemental Analysis** (Calculated for $C_{24}H_{27}ClNOIr$): C, 50.29; H, 4.75; N, 2.44; Found: C, 50.43; H, 4.83; N, 2.39.

5.3.2. Synthesis of Mononuclear *N,N*-Pyridylimine Complexes (2.9-2.11)

General Procedure

The ligand **2.2** (83.0 mg, 0.495 mmol for **2.9**; 53.0 mg, 0.251 mmol for **2.10** and 69.0 mg, 0.327 mmol for **2.11**) was dissolved in MeOH (20 ml) and reacted with $[Rh(\eta^5\text{-}C_5Me_5)Cl_2]_2$ (146 mg, 0.237 mmol for **2.9**) or $[Ir(\eta^5\text{-}C_5Me_5)Cl_2]_2$ (100 mg, 0.126 mmol for **2.10**) or $[Ru(\eta^6\text{-}p\text{-}Pr^iC_6H_4Me)Cl_2]_2$ (100 mg, 163 mmol for **2.11**) and stirred for 30 minutes, after which the solvent was reduced by rotary evaporation. $NaPF_6$ (83.0 mg, 0.495 mmol for **2.9**; 44.0 mg, 0.264 mmol for **2.10** and 58.0 mg, 0.343 mmol for **2.11**) was added to the concentrated solution, inducing the precipitation of the cationic complexes (**2.9-2.11**) which were filtered and collected using a Hirsch funnel. The solids were washed with diethyl ether prior to drying under reduced pressure.

5.3.2.1. 4-(Pyridylaldimine)phenylmethanol rhodium(III) complex (2.9)

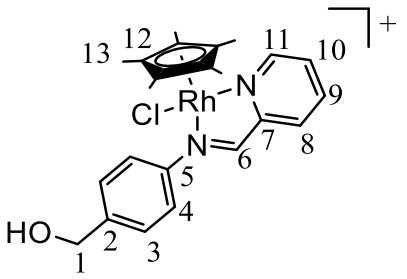

Yellow solid, **yield**: 238 mg, 99%. **MP.**: 224ºC (decomposed). **^{1}H NMR** ($(CD_3)_2CO$): δ(ppm) = 9.19 (d, 1H, H_{11}, ^{3}J = 8 Hz), 8.95 (s, 1H, H_6), 8.43 (t, 1H, H_9, ^{3}J = 8 Hz), 8.41 (d, 1H, H_8, ^{3}J = 4 Hz), 8.05 (t, 1H, H_{10}, ^{3}J = 8 Hz), 7.82 (d, 2H, H_4, ^{3}J = 8 Hz), 7.66 (d, 2H, H_3, ^{3}J = 8 Hz), 4.80 (d, 2H, H_1, ^{3}J = 8 Hz), 4.43 (t, 1H, -OH, ^{3}J = 8 Hz), 1.60 (s, 15H, C_{13}). **^{13}C{^{1}H} NMR** ($(CD_3)_2CO$): δ(ppm) = 166.62 (C_6), 154.27 (C_7), 152.78 (C_{11}), 147.63 (C_5), 144.55 (C_2), 140.45 (C_9), 129.90 (C_8), 129.80 (C_{10}), 127.37 (C_3), 122.41 (C_4), 97.61 (C_{12}), 63.07 (C_1), 7.96 (C_{13}). **^{31}P{^{1}H} NMR** ($(CD_3)_2CO$): δ(ppm) = -144.25 (sep, P-F). **FT-IR** (KBr): 3387 (bs) ν(O-H), 2918 (m) ν(C-H_{Cp^*}), 1598 (s) ν(C=N_{imine}), 1568 (s) ν(aromatic C=C), 1420 (s) δ(C-H), 1383 δ(-CH_{3Cp^*}), 1038 (s) ν(C-O). **ESI-MS**: *m/z* 485.09 $[M\text{-}PF_6]^+$. **Elemental Analysis** (Calculated for $C_{23}H_{27}ClF_6N_2OPRh$): C, 43.79; H, 4.31; N, 4.44; Found: C, 43.73; H, 4.00; N, 4.60.

5.3.2.2. 4-(Pyridylaldimine)phenylmethanol iridium(III) complex (2.10)

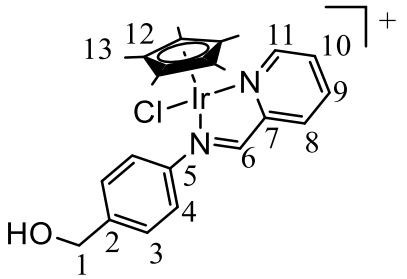

Bright orange solid, **yield**: 149 mg, 82%. **MP.**: 215ºC (decomposed). **^{1}H NMR** ($(CD_3)_2CO$): δ(ppm) = 9.35 (s, 1H, H_6), 9.19 (d, 1H, H_{11}, ^{3}J = 8 Hz), 8.52 (d, 1H, H_8, ^{3}J = 8 Hz), 8.39 (t, 1H, H_9, ^{3}J = 8 Hz), 8.02 (t, 1H, H_{10}, ^{3}J = 8 Hz), 7.76 (d, 2H, H_4, ^{3}J = 8 Hz), 7.64 (d, 2H, H_3, ^{3}J = 8 Hz), 4.79 (d, 2H, H_1, ^{3}J = 8 Hz), 4.46 (t, 1H, -OH, ^{3}J = 8 Hz), 1.57 (s, 15H, C_{13}). **^{13}C{^{1}H} NMR** ($(CD_3)_2CO$): δ(ppm) = 168.09 (C_6), 155.90 (C_7), 152.34 (C_{11}), 148.00 (C_5), 144.86 (C_2), 140.61 (C_9), 130.43 (C_{10}), 129.89 (C_8), 127.30 (C_3), 122.53 (C_4), 90.35 (C_{12}), 62.99 (C_1), 7.66 (C_{13}). **^{31}P{^{1}H} NMR** ($(CD_3)_2CO$): δ(ppm) = -144.24 (sep, P-F). **FT-IR** (KBr): 3411 (bs) ν(O-H), 2918 (m) ν(C-H_{Cp^*}), 1622 (s) ν(C=N_{imine}), 1561 (s) ν(aromatic C=C), 1417 (s) δ(C-H), 1387 δ(-

CH_{3Cp^*}), 1035 (s) *v*(C-O). **ESI-MS**: *m/z* 575.14 $[M\text{-}PF_6]^+$. **Elemental Analysis** (Calculated for $C_{23}H_{27}ClF_6IrN_2OP$): C, 38.36; H, 3.78; N, 3.89; Found: C, 38.07; H, 3.33; N, 3.05.

5.3.2.3. 4-(Pyridylaldimine)phenylmethanol ruthenium(II) complex (2.11)

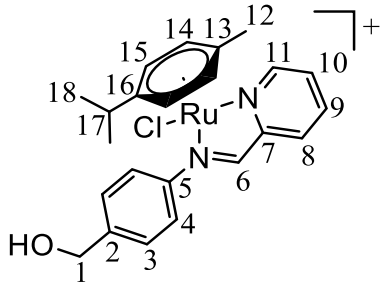

Yellow solid, **yield**: 162 mg, 79%. **MP.**: 201ºC (decomposed). **^{1}H NMR** ($(CD_3)_2CO$): *δ*(ppm) = 9.63 (d, 1H, H_{11}, ^3J = 8 Hz), 8.91 (s, 1H, H_6), 8.39-8.33 (m, 2H, H_9 H_{10}), 7.90 (d, 1H, H_8, ^3J = 8 Hz), 7.87 (d, 2H, H_3, ^3J = 8 Hz), 7.62 (d, 2H, H_4, ^3J = 8 Hz), 6.11 (d, 1H, H_{14A}, ^3J = 8 Hz), 5.77 (d, 1H, H_{14B}, ^3J = 8 Hz), 5.73 (d, 1H, H_{15A}, ^3J = 8 Hz), 5.62 (d, 1H, H_{15B}, ^3J = 8 Hz), 4.79 (s, 2H, H_1), 2.77-2.68 (m, 1H, H_{17}), 2.30 (s, 3H, H_{12}), 1.13 (d, 6H, H_{18}, ^3J = 4 Hz). **^{13}C{^{1}H} NMR** ($(CD_3)_2CO$): *δ*(ppm) = 167.65 (C_6), 156.96 (C_{11}), 156.09 (C_7), 152.06 (C_5), 145.83 (C_2), 140.94 (C_9), 130.96 (C_{10}), 129.93 (C_8), 128.33 (C_3), 123.42 (C_4), 107.52 (C_{16}), 105.15 (C_{13}), 86.42 (C_{14A}), 86.75 (C_{14B}), 87.37 (C_{15A}), 87.80 (C_{15B}), 63.98 (C_1), 32.04 (C_{17}), 22.46 (C_{18A}), 22.29 (C_{18B}), 19.00 (C_{12}). **^{31}P{^{1}H} NMR** ($(CD_3)_2CO$): *δ*(ppm) = -144.21 (sep, P-F). **FT-IR** (KBr): 3435 (bs) *v*(O-H), 2918 (m) *v*(C-$H_{p\text{-}Cy}$), 1628 (s) *v*(C=N_{imine}), 1602 (s) *v*(aromatic C=C), 1420 (s) *δ*(C-H), 1389 *δ*(-$CH_{3p\text{-}Cy}$), 1032 (s) *v*(C-O). **ESI-MS**: *m/z* 483.08 $[M\text{-}PF_6]^+$. **Elemental Analysis** (Calculated for $C_{23}H_{26}ClF_6N_2OPRu$): C, 43.99; H, 4.17; N, 4.46; Found: C, 43.66; H, 3.88; N, 4.63.

5.3.3. Synthesis of Mononuclear *N,O*-Salicylaldiminato Complexes (2.12-2.14)

General Procedure

The ligand **2.3** (74.0 mg, 0.326 mmol for **2.12**; 57.0 mg, 0.251 mmol for **2.13** and 50.0 mg, 0.220 mmol for **2.14**) was dissolved in MeOH (20 ml) and NaOAc added (28.0 mg, 0.342 mmol for **2.12**; 22.0 mg, 0.264 mmol for **2.13** and 19.0 mg, 0.285 mmol for **2.14**). $[Rh(\eta^5\text{-}C_5Me_5)Cl_2]_2$ (68.0 mg, 0.110 mmol for **2.12**) or $[Ir(\eta^5\text{-}C_5Me_5)Cl_2]_2$ (100 mg, 0.126 mmol for **2.13**) or $[Ru(\eta^6\text{-}p\text{-}Pr^iC_6H_4Me)Cl_2]_2$ (100 mg, 163 mmol for **2.14**) was added to the solution which was stirred for 2 hours, after which the MeOH was removed by rotary evaporation yielding a solid residue.

The residue was dissolved in acetone, filtered by gravity and the solvent of the filtrate was removed under reduced pressure. The solid products **2.12-2.14** were purified by dissolution in a minimal amount of DCM and precipitated using Et_2O.

5.3.3.1. 4-(Salicylaldimine)phenylmethanol rhodium(III) complex (2.12)

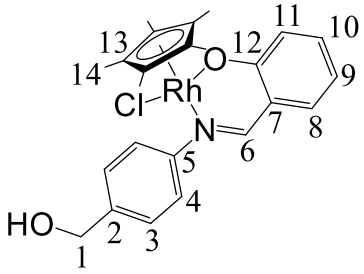

Red solid, **yield**: 87.0 mg, 79%. **MP.**: 185ºC (decomposed). **^{1}H NMR** ($CDCl_3$): *δ*(ppm) 7.90 (s, 1H, H_6), 7.61 (d, 2H, H_4, ^3J = 8 Hz), 7.44 (d, 2H, H_3, ^3J = 8 Hz), 7.20-7.15 (m, 2H, H_8 H_{10}), 6.74 (d, 1H, H_{11}, ^3J = 8 Hz), 6.37 (t, 1H, H_9, ^3J = 4Hz), 4.61 (s, 2H, H_1), 1.34 (s, 15H, C_{14}). **^{13}C{^{1}H} NMR** ($CDCl_3$): *δ*(ppm) = 166.34 (C_{12}), 164.39 (C_6), 153.83 (C_5), 139.89 (C_2), 135.32 (C_8), 135.20 (C_{10}), 127.08 (C_3), 124.86 (C_4), 124.09 (C_{11}), 114.07 (C_9), 93.67 (C_{13}), 64.53 (C_1), 8.43 (C_{14}). **FT-IR** (KBr): 3280 (bs) *ν*(O-H), 2961 (m) *ν*(C-H_{Cp^*}), 1617 (s) *ν*(C=N), 1598 (s) *ν*(aromatic C=C), 1446 (s) *δ*(C-H), 1318 *δ*(-CH_{3Cp^*}), 1153 (s) *ν*(C-O), 1018 (s) *ν*(C-O). **ESI-MS**: *m/z* 464.11 $[M\text{-}Cl]^+$. **Elemental Analysis** (Calculated for $C_{24}H_{27}ClNO_2Rh$): C, 57.67; H, 5.44; N, 2.80; Found: C, 57.29; H, 5.43; N, 2.38.

5.3.3.2. 4-(Salicylaldimine)phenylmethanol iridium(III) complex (2.13)

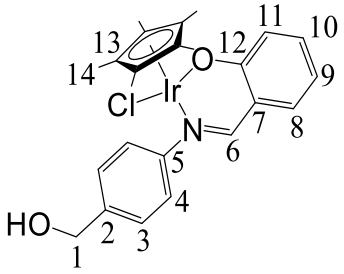

Yellow solid, **yield**: 127 mg, 86%. **MP.**: 182ºC (decomposed). **^{1}H NMR** ($CDCl_3$): *δ*(ppm) 7.99 (s, 1H, H_6), 7.67 (d, 2H, H_4, ^3J = 8 Hz), 7.37 (d, 2H, H_3, ^3J = 8 Hz), 7.33 (t, 1H, H_{10}, ^3J = 8 Hz), 7.10 (d, 1H, H_8, ^3J = 8 Hz), 6.96 (d, 1H, H_{11}, ^3J = 8 Hz), 6.44 (t, 1H, H_9, ^3J = 8 Hz), 4.74 (s, 2H, H_1), 1.31 (s, 15H, C_{14}). **^{13}C{^{1}H} NMR** ($CDCl_3$): *δ*(ppm) = 163.95 (C_{12}), 160.94 (C_6), 155.02 (C_5), 140.11 (C_2), 135.19 (C_{10}), 134.50 (C_8), 125.05 (C_3), 126.79 (C_4), 123.26 (C_9), 114.95 (C_{11}),

85.75 (C_{13}), 64.46 (C_1), 8.46 (C_{14}). **FT-IR** (KBr): 3373 (bs) *v*(O-H), 2918 (m) *v*(C-H_{Cp^*}), 1610 (s) *v*(C=N), 1591 (s) *v*(aromatic C=C), 1443 (s) *δ*(C-H), 1327 *δ*(-CH_{3Cp^*}), 1150 (s) *v*(C-O), 1030 (s) *v*(C-O). **ESI-MS**: *m/z* 554.17 $[M\text{-}Cl]^+$. **Elemental Analysis** (Calculated for $C_{24}H_{27}ClIrNO_2$): C, 48.93; H, 4.62; N, 2.38; Found: C, 48.64; H, 4.40; N, 2.38.

5.3.3.3. 4-(Salicylaldimine)phenylmethanol ruthenium(II) complex (2.14)

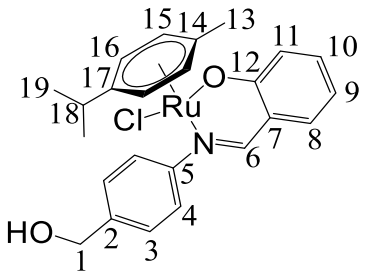

Orange solid, **yield**: 106 mg, 65%. **MP.**: 205ºC (decomposed). **^{1}H NMR** ($CDCl_3$): *δ*(ppm) 7.94 (s, 1H, H_6), 7.82 (d, 2H, H_4, ^3J = 12 Hz), 7.39 (d, 2H, H_3, ^3J = 8 Hz), 7.23 (t, 1H, H_{10}, ^3J = 12 Hz), 7.05 (d, 1H, H_8), 7.00 (d, 1H, H_{11}, ^3J = 8 Hz), 6.43 (t, 1H, H_9, ^3J = 8 Hz), 5.40 (d, 1H, H_{15A}, ^3J = 8 Hz), 5.34 (d, 1H, H_{15B}, ^3J = 4 Hz), 5.10 (d, 1H, H_{16A}, ^3J = 4 Hz), 4.73 (s, 2H, H_1), 4.30 (d, 1H, H_{16B}, ^3J = 8 Hz), 2.56-2.52 (m, 1H, H_{18}), 2.01 (s, 3H, H_{13}), 1.12 (d, 3H, H_{19A}, ^3J = 8 Hz), 1.08 (d, 3H, H_{19B}, ^3J = 8 Hz). **^{13}C{^{1}H} NMR** ($CDCl_3$): *δ*(ppm) = 165.37 (C_{12}), 164.40 (C_6), 157.41 (C_5), 141.45 (C_2), 136.16 (C_8), 135.27 (C_{10}), 127.03 (C_3), 123.72 (C_4), 122.03 (C_{11}), 113.51 (C_9), 100.62 (C_{17}), 97.99 (C_{14}), 86.64 (C_{15A}), 83.44 (C_{15B}), 83.13 (C_{16A}), 81.48 (C_{16B}), 62.94 (C_1), 30.44 (C_{18}), 22.64 (C_{19A}), 21.97 (C_{19B}), 18.50 (C_{18}). **FT-IR** (KBr): 3412 (bs) *v*(O-H), 2984 (m) *v*(C-$H_{p\text{-}Cy}$), 1612 (s) *v*(C=N), 1598 (s) *v*(aromatic C=C), 1442 (s) *δ*(C-H), 1331 *δ*(-$CH_{3p\text{-}Cy}$), 1146 (s) *v*(C-O), 1017 (s) *v*(C-O). **ESI-MS**: *m/z* 462.10 $[M\text{-}Cl]^+$. **Elemental Analysis** (Calculated for $C_{24}H_{26}ClNO_2Ru$): C, 58.00; H, 5.27; N, 2.82; Found: C, 58.37; H, 5.30; N, 2.81.

5.4. Synthesis of Trinuclear Complexes (2.15-2.22)

5.4.1. Synthesis of Trinuclear *N,C*-Benzaldiminato Complexes (2.15-2.16)

General Procedure

The ligand **2.4** (71.0 mg, 0.0890 mmol for **2.15** and 66.1 mg, 0.0837 mmol for **2.16**) was dissolved in MeOH (20 ml) and NaOAc added (23.0 mg, 0.279 mmol for **2.15** and 24.0 mg, 0.293 mmol for **2.16**). $[Rh(\eta^5\text{-}C_5Me_5)Cl_2]_2$ (83.3 mg, 0.135 mmol for **2.15**) or $[Ir(\eta^5\text{-}C_5Me_5)Cl_2]_2$ (100 mg, 0.126 mmol for **2.16**) was added to the solution which was stirred for 2 hours, after

which the MeOH was removed by rotary evaporation yielding a solid residue. The residue was dissolved in acetone, filtered by gravity and the solvent of the filtrate was removed under reduced pressure. The solid products **2.15-2.16** were purified by dissolution in minimal DCM and precipitation by Et_2O collected using a Hirsch funnel.

5.4.1.1. Tris(4-(benzylaldimine)benzyl)benzene-1,3,5-tricarboxylate rhodium(III) complex (2.15)

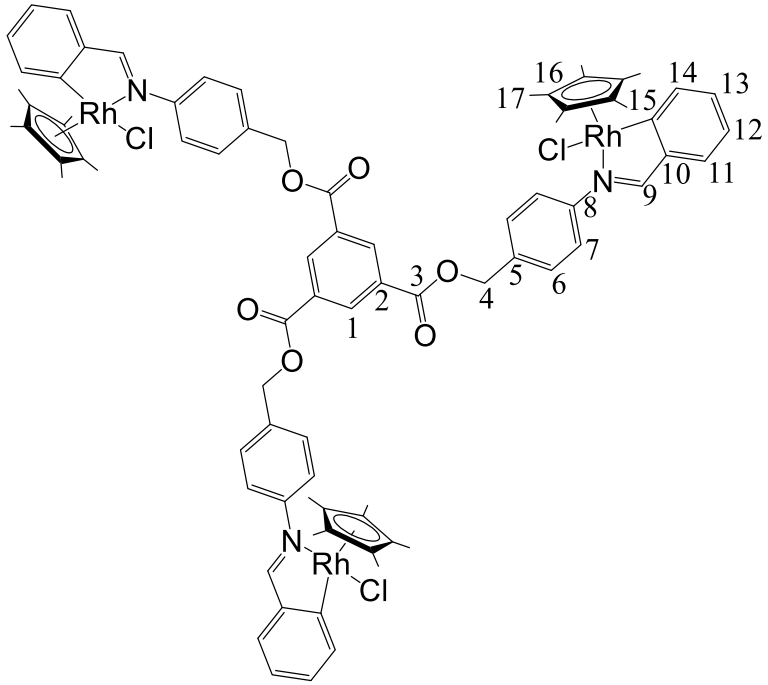

Red solid, **yield**: 34 mg, 36%. **MP.**: 216ºC (decomposed). **^{1}H NMR** (CD_3Cl_3): δ(ppm) = 8.91 (s, 3H, H_1), 8.46 (s, 3H, H_9), 7.91 (m, 3H, H_{11}), 7.49 (m, 9H, H_7 H_{12}), 7.23 (m, 9H, H_6 H_{13}), 7.00 (m, 3H, H_{14}), 5.42 (s, 6H, H_4), 1.62 (s, 45H, C_{17}). **^{13}C{^{1}H} NMR** (CD_3Cl_3): δ(ppm) = 176.61 (C_{15}), 168.85 (C_3),167.68 (C_9), 147.96 (C_8), 140.42 (C_5), 132.06 (C_1), 136.73 (C_{11}), 133.63 (C_{13}), 129.81 (C_6), 129.66 (C_{14}), 128.92 (C_2), 122.72 (C_{12}), 98.68 (C_{16}), 66.34 (C_4), 8.59 (C_{17}). **FT-IR** (KBr): 3029 (m) ν(C-H_{Cp^*}), 1724 (s) ν(C=O), 1614 (s) ν(C=N_{imine}), 1578 (s) ν(aromatic C=C), 1451 (s) δ(C-H), 1374 δ(-CH_{3Cp^*}), 1230 (s) ν(C-C(O)-O). **ESI-MS**: *m/z* 500.11 $[M\text{-}3Cl]^{3+}$. **Elemental Analysis** (Calculated for $C_{81}H_{81}Cl_3N_3O_6Rh_3$): C, 60.52; H, 5.08; N, 2.61; Found: C, 60.61; H, 5.21; N, 2.45.

5.4.1.2. Tris(4-(benzylaldimine)benzyl)benzene-1,3,5-tricarboxylate iridium(III) complex (2.16)

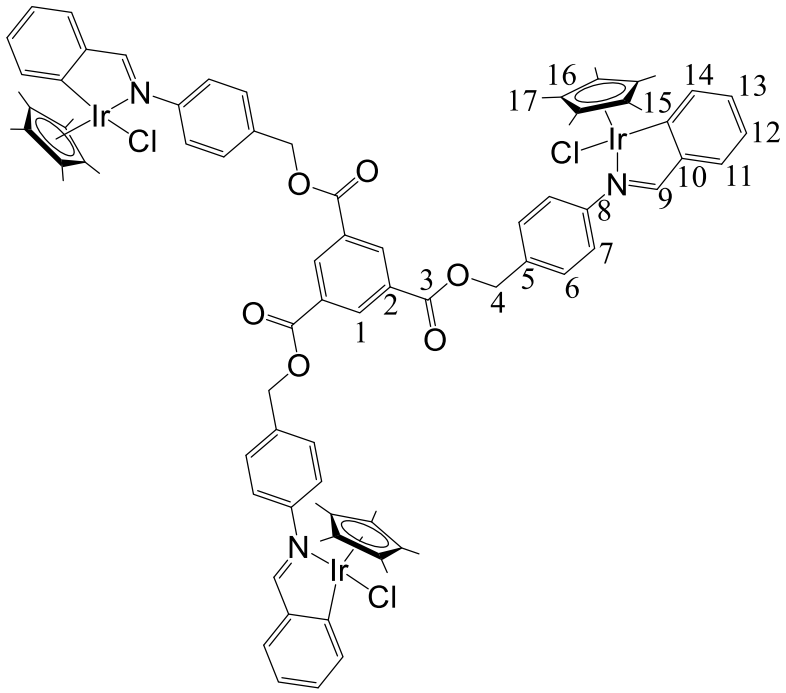

Pale brown solid, **yield**: 93 mg, 59%. **MP.**: 221ºC (decomposed). **^{1}H NMR** (CD_3Cl_3): δ(ppm) = 8.91 (s, 3H, H_1), 8.35 (s, 3H, H_9), 7.92 (d, 3H, H_{11}, J = 7 Hz), 7.66 (m, 3H, H_7), 7.58 (d, 6H H_7, J = 8 Hz), 7.40 (d, 6H, H_6, J = 5 Hz), 7.32 (m, 3H, H_{13}), 7.22 (m, 3H, H_{14}), 5.39 (s, 6H, H_4), 1.50 (s, 45H, C_{17}). **^{13}C{^{1}H} NMR** (CD_3Cl_3): δ(ppm) = 176.07 (C_{15}), 168.42 (C_9), 166.61 (C_3), 149.39 (C_8), 141.48 (C_5), 133.45 (C_1), 138.29 (C_{11}), 132.49 (C_{13}), 129.00 (C_6 C_{14}), 128.20 (C_2), 122.28 (C_{12}), 84.84 (C_{16}), 67.91 (C_4), 8.37 (C_{17}). **FT-IR** (KBr): 3091 (m) ν(C-H_{Cp^*}), 1723 (s) ν(C=O), 1613 (s) ν(C=N_{imine}), 1579 (s) ν(aromatic C=C), 1450 (s) δ(C-H), 1379 δ(-CH_{3Cp^*}), 1231 (s) ν(C-C(O)-O). **ESI-MS**: *m/z* 590.16 $[M-3Cl]^{3+}$. **Elemental Analysis** (Calculated for $C_{81}H_{81}Cl_3Ir_3N_3O_6$): C, 51.87; H, 4.35; N, 2.24; Found: C, 51.99; H, 4.28; N, 2.19.

5.4.2. Synthesis of Trinuclear *N,N*-Pyridylimine Complexes (2.17-2.19)

General Procedure

The ligand **2.5** (100 mg, 0.126 mmol for **2.17**; 66.0 mg, 0.0837 mmol for **2.18** and 86.0 mg, 0.109 mmol for **2.19**) was dissolved in DCM and EtOH (50:50, 20 ml) and either $[Rh(\eta^5\text{-}C_5Me_5)Cl_2]_2$ (121 mg, 0.196 mmol for **2.17**) or $[Ir(\eta^5\text{-}C_5Me_5)Cl_2]_2$ (100 mg, 0.126 mmol for **2.18**) or $[Ru(\eta^6\text{-}p\text{-}Pr^iC_6H_4Me)Cl_2]_2$ (100 mg, 163 mmol for **2.19**) was added to the solution, which was stirred for 2 hours, after which the solvent was reduced by rotary evaporation. $NaPF_6$ (74.0 mg, 0.441 mmol for **2.17**; 49.0 mg, 0.293 mmol for **2.18** and 64.0 mg, 0.381 mmol

for **2.19**) was added to the concentrated solution causing the precipitation of the cationic complexes (**2.17**-**2.19**) which were filtered and collected using a Hirsch funnel.

5.4.2.1. Tris(4-(pyridylimine)benzyl)benzene-1,3,5-tricarboxylate rhodium(III) complex (2.17)

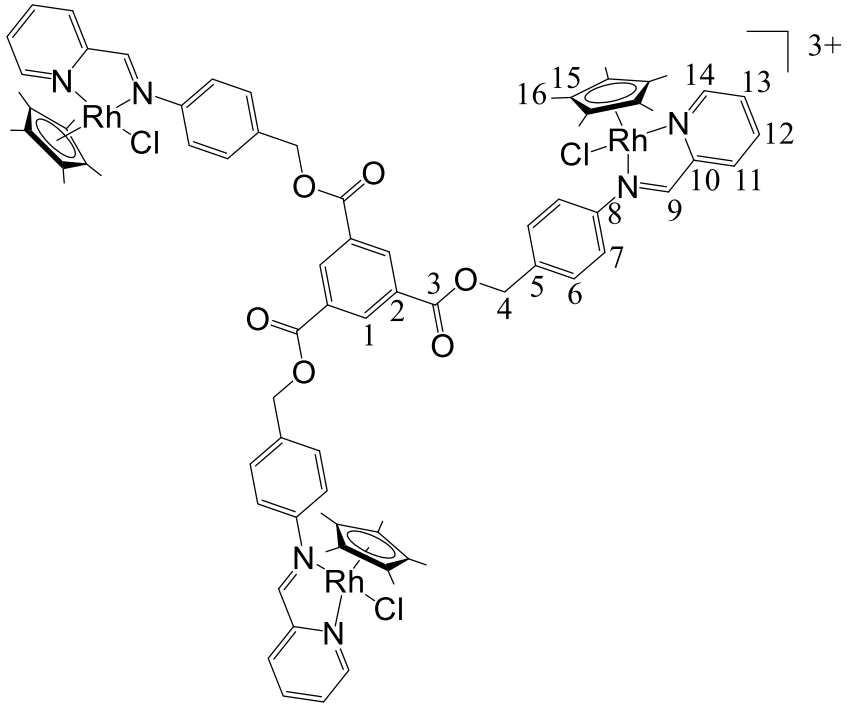

Yellow solid, **yield**: 75 mg, 29%. **MP.**: 227ºC (decomposed). **^{1}H NMR** ($(CD_3)_2CO$): *δ*(ppm) = 9.19 (d, 3H, H_{14}, ^{3}J = 4 Hz), 8.95 (s, 3H, H_9), 8.94 (s, 3H, H_1), 8.40-8.31 (m, 6H, H_{11} H_{12}), 8.03 (m, 3H, H_{13}), 7.91 (d, 6H, H_7, ^{3}J = 4 Hz), 7.84 (d, 6H, H_6, ^{3}J = 4 Hz), 5.61 (s, 6H, H_4), 1.57 (s, 45H, C_{16}).**^{13}C{^{1}H} NMR** ($(CD_3)_2CO$): *δ*(ppm) = 168.49 (C_9), 166.19 (C_3), 154.20 (C_{10}), 153.28 (C_{14}), 148.72 (C_8), 140.99 (C_{12}), 137.46 (C_5), 133.93 (C_1), 130.52 (C_{11} C_{13}), 129.73 (C_6), 128.44 (C_2), 122.88 (C_7), 97.60 (C_{15}), 66.91 (C_4), 8.76 (C_{16}). **^{31}P{^{1}H} NMR** ($(CD_3)_2CO$): *δ*(ppm) = -144.26 (sep, P-F). **FT-IR** (KBr): 3090 (m) *ν*(C-H_{Cp^*}), 1728 (s) *ν*(C=O), 1617 (s) *ν*(C=N_{imine}), 1596 (s) *ν*(aromatic C=C), 1452 (s) *δ*(C-H), 1377 *δ*(-CH_{3Cp^*}), 1238 (s) *ν*(C-C(O)-O). **ESI-MS**: *m/z* 537.75 $[M\text{-}3PF_6]^{3+}$. **Elemental Analysis** (Calculated for $C_{78}H_{81}Cl_3F_{18}N_6O_6P_3Rh_3$): C, 45.73; H, 3.99; N, 4.10; Found: C, 45.75; H, 4.08; N, 4.49.

5.4.2.2. Tris(4-(pyridylimine)benzyl) benzene-1,3,5-tricarboxylate iridium(III) complex (2.18)

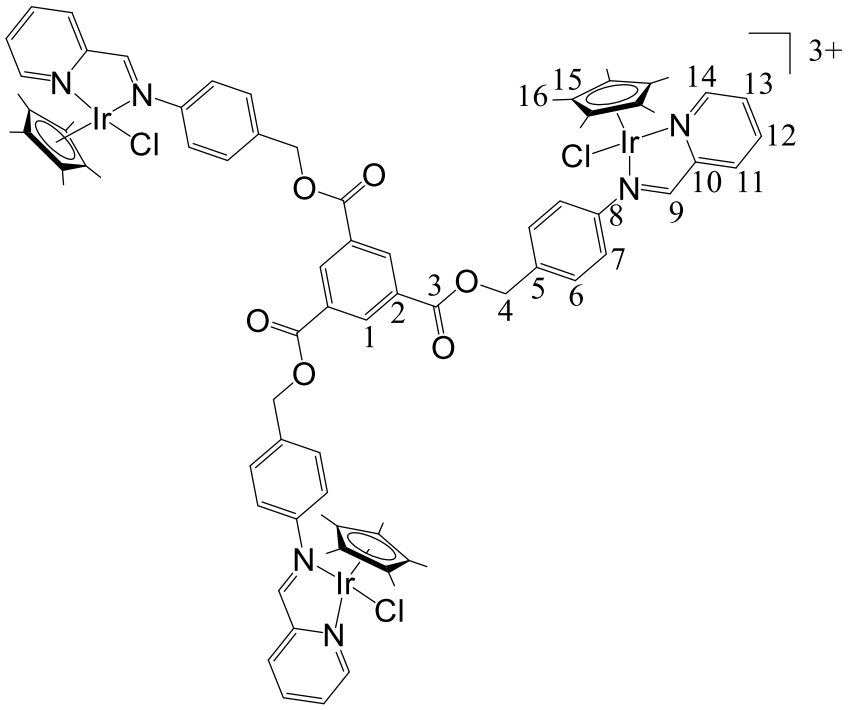

Brown solid, **yield**: 68 mg, 70%. **MP.**: 221ºC (decomposed). **^{1}H NMR** ($(CD_3)_2CO$): δ(ppm) = 9.19 (d, 3H, H_{14}, ^{3}J = 4 Hz), 8.94 (s, 3H, H_1), 8.40-8.31 (m, 6H, H_{11} H_{12}), 8.03 (m, 3H, H_{13}), 7.91 (d, 6H, H_7, ^{3}J = 4 Hz), 7.84 (d, 6H, H_6, ^{3}J = 4 Hz), 5.61 (s, 6H, H_4), 1.57 (s, 45H, C_{16}). **^{13}C{^{1}H} NMR** ($(CD_3)_2CO$): δ(ppm) = 168.49 (C_9), 166.19 (C_3), 154.20 (C_{10}), 153.28 (C_{14}), 148.72 (C_8), 140.99 (C_{12}), 137.46 (C_5), 133.93 (C_1), 130.52 (C_{11} C_{13}), 129.73 (C_6), 128.44 (C_2), 123.29 (C_7), 97.60 (C_{15}), 66.91 (C_4), 8.76 (C_{16}). **^{31}P{^{1}H} NMR** ($(CD_3)_2CO$): δ(ppm) = -144.26 (sep, P-F). **FT-IR** (KBr): 3090 (m) ν(C-H_{Cp^*}), 1728 (s) ν(C=O), 1617 (s) ν(C=N_{imine}), 1596 (s) ν(aromatic C=C), 1452 (s) δ(C-H), 1377 δ(-CH_{3Cp^*}), 1238 (s) ν(C-C(O)-O). **ESI-MS**: *m/z* 627.14 $[M-3PF_6]^{3+}$. **Elemental Analysis** (Calculated for $C_{78}H_{81}F_{18}Ir_3N_6O_6P_3$): C, 40.44; H, 3.52; N, 3.63; Found: C, 40.88; H, 3.68; N, 3.40.

5.4.2.3. Tris(4-(pyridylimine)benzyl) benzene-1,3,5-tricarboxylate ruthenium(II) complex (2.19)

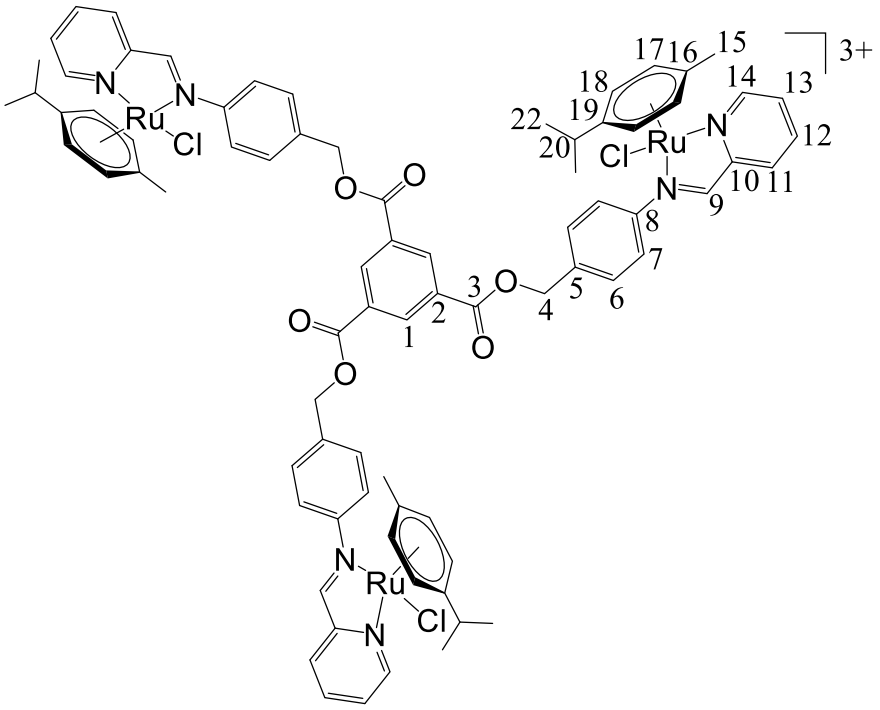

Yellow solid, **yield**: 86 mg, 77%. **MP.**: 194ºC (decomposed). **^{1}H NMR** ($(CD_3)_2CO$): *δ*(ppm) = 9.66 (d, 3H, H_{14}, ^{3}J = 4 Hz), 8.99 (s, 3H, H_1), 8.97 (s, 3H, H_9), 8.38-8.36 (m, 6H, H_{12} H_{13}), 8.01 (d, 6H, H_6, ^{3}J = 8 Hz), 7.93 (m, 3H, H_{11}), 7.84 (d, 6H, H_7, ^{3}J = 8 Hz), 6.14-6.11 (m, 3H, H_{17A}), 5.82-5.77 (m, 6H, H_{17B} H_{18A}), 5.66 (s, 9H, H_{18B} H_4), 2.82 (m, 3H, H_{20}), 2.30 (s, 9H, H_{22}), 1.13 (s, 18H, H_{15}). **^{13}C{^{1}H} NMR** ($(CD_3)_2CO$): *δ*(ppm) = 167.44 (C_9), 163.56 (C_3), 154.56 (C_{10}), 156.00 (C_{14}), 149.48 (C_8), 139.98 (C_{12}), 138.09 (C_5), 134.42 (C_1), 130.19 (C_{13}), 129.96 (C_2), 129.27 (C_6), 129.10 (C_{11}), 122.91 (C_7), 102.80 (C_{19}), 98.68 (C_{16}), 86.90 (C_{17A}), 86.19 (C_{17B}), 85.73 (C_{18A}), 85.46 (C_{18B}), 66.29 (C_4), 31.04 (C_{20}), 21.46 (C_{22A}), 21.28 (C_{22B}), 17.99 (C_{15}). **^{31}P{^{1}H} NMR** ($(CD_3)_2CO$): *δ*(ppm) = -144.20 (sep, P-F). **FT-IR** (KBr): 2970 (m) *ν*(C-$H_{p\text{-}Cy}$), 1729 (s) *ν*(C=O), 1611 (m) *ν*(C=N_{imine}), 1508 (s) *ν*(aromatic C=C), 1445 (s) *δ*(C-H), 1383 *δ*(-$CH_{3p\text{-}Cy}$), 1236 (s) *ν*(C-C(O)-O). **ESI-MS**: *m/z* 536.17 $[M\text{-}3PF_6]^{3+}$. **Elemental Analysis** (Calculated for $C_{78}H_{78}Cl_3F_{18}N_6O_6P_3Ru_3$): C, 45.93; H, 3.85; N, 4.12; Found: C, 46.17; H, 3.66; N, 3.63.

5.4.3. Synthesis of Trinuclear *N,O*-Salicylaldiminato Complexes (2.20-2.22)

General Procedure

The ligand **2.6** (90.0 mg, 0.108 mmol for **2.20**; 70.1 mg, 0.0837 mmol for **2.21** and 91.0 mg, 0.109 mmol for **2.22**) was dissolved in MeOH (20 ml) and NaOAc added (27.0 mg, 0.329 mmol for **2.20**; 24.0 mg, 0.239 mmol for **2.21** and 31.0 mg, 0.381 mmol for **2.22**). $[Rh(\eta^5\text{-}C_5Me_5)Cl_2]_2$ (100 mg, 0.162 mmol for **2.20**) or $[Ir(\eta^5\text{-}C_5Me_5)Cl_2]_2$ (100 mg, 0.126 mmol for **2.21**) or $[Ru(\eta^6\text{-}p\text{-}Pr^iC_6H_4Me)Cl_2]_2$ (100 mg, 163 mmol for **2.22**) was added to the solution which was stirred for 2 hours, after which the MeOH was removed by rotary evaporation yielding a solid residue. The residue was dissolved in acetone, filtered by gravity and the solvent of the filtrate was removed under reduced pressure. The solid products **2.20-2.22** were purified by dissolution in minimal DCM and precipitation by Et_2O.

5.4.3.1. Tris(4-(salicylaldimine)benzyl) benzene-1,3,5-tricarboxylate rhodium(III) complex (2.20)

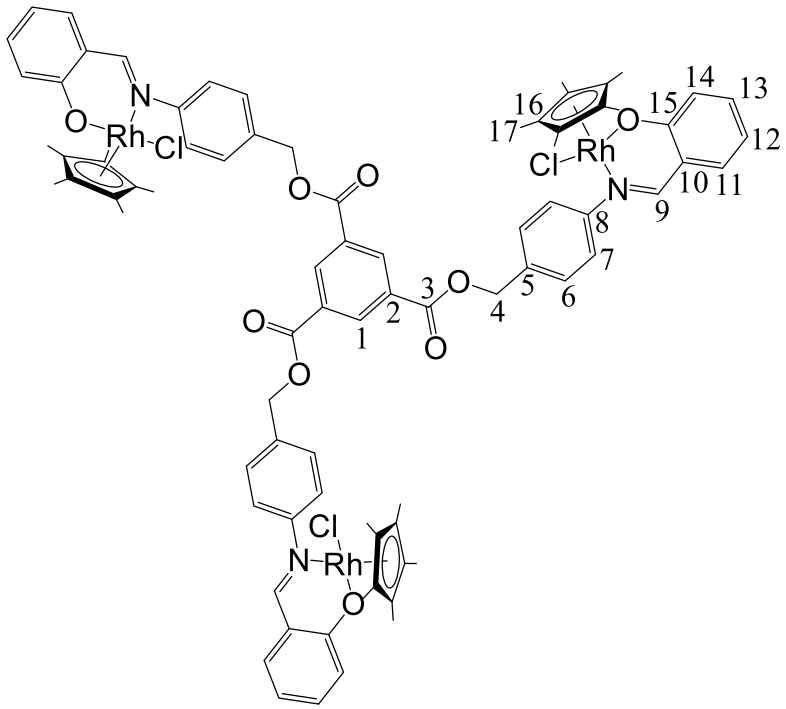

Orange solid, **yield**: 93 mg, 52%. **MP.**: 226ºC (decomposed). **^{1}H NMR** ($CDCl_3$): δ(ppm) = 8.95 (s, 3H, H_1), 7.96 (s, 3H, H_9), 7.90 (d, 6H, H_7, ^3J = 12 Hz), 7.49 (d, 6H, H_6, ^3J = 4 Hz), 7.23 (t, 3H, H_{12}, ^3J = 8 Hz), 7.04 (m, 6H, $H_{14}H_{11}$), 6.43 (t, 3H, H_{13}, ^3J = 8 Hz), 5.49 (s, 6H, H_4), 1.32 (s, 45H, C_{17}). **^{13}C{^{1}H} NMR** ($CDCl_3$): δ(ppm) = 166.49 (C_3), 164.66 (C_{15}), 164.58 (C_9), 154.64 (C_8), 135.38 (C_{11} C_{12}), 134.88 (C_1), 134.15 (C_5), 131.38 (C_2), 128.62 (C_6), 124.20 (C_{14}), 119.47 (C_{10}), 114.19 (C_{13}), 93.64 (C_{16}), 66.82 (C_4), 8.44 (C_{17}). **FT-IR** (KBr): 2961 (m) ν(C-H_{Cp^*}), 1728 (s)

v(C=O), 1612 (s) *v*(C=N), 1600 (s) *v*(aromatic C=C), 1463 (s) *δ*(C-H), 1377 *δ*(-CH_{3Cp^*}), 1231 (s) *v*(C-C(O)-O). **ESI-MS**: *m/z* 516.10 $[M\text{-}3Cl]^{3+}$. **Elemental Analysis** (Calculated for $C_{81}H_{81}Cl_3N_3O_9Rh_3$): C, 58.76; H, 4.93; N, 2.54; Found: C, 58.92; H, 4.69; N, 2.30.

5.4.3.2. Tris(4-(salicylaldimine)benzyl) benzene-1,3,5-tricarboxylate iridium(III) complex (2.21)

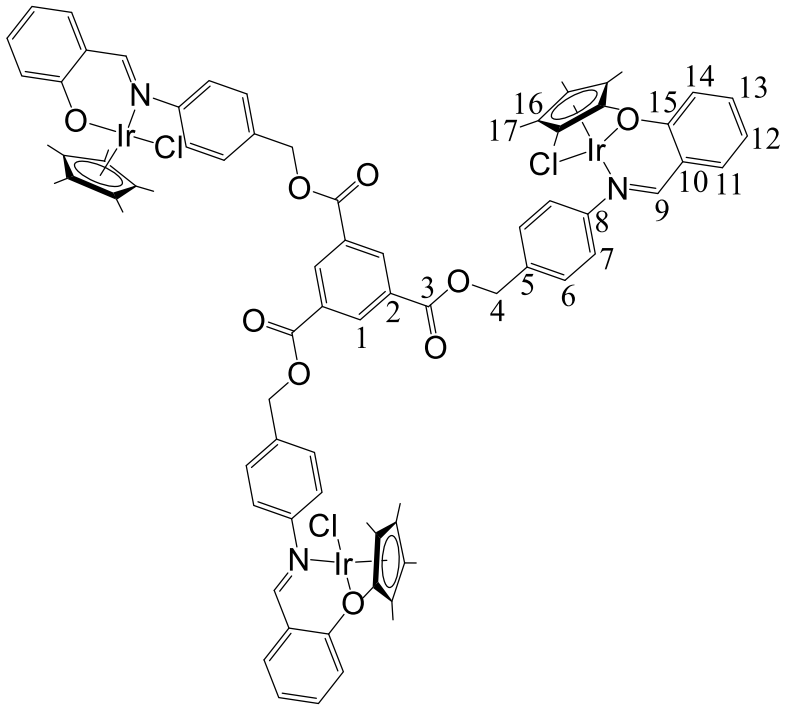

Brown solid, **yield**: 70 mg, 43%. **MP.**: 236ºC (decomposed). **^{1}H NMR** ($CDCl_3$): *δ*(ppm) = 8.93 (s, 3H, H_1), 8.01 (s, 3H, H_9), 7.75 (d, 6H, H_7, ^3J = 8 Hz), 7.48 (d, 6H, H_6, ^3J = 8 Hz), 7.35 (t, 3H, H_{13}, ^3J = 8 Hz), 7.09 (d, 3H, H_{11}, ^3J = 8 Hz), 6.97 (d, 3H, H_{14}, ^3J = 8 Hz), 6.45 (t, 3H, H_{12}, ^3J = 8 Hz), 5.47 (s, 6H, H_4), 1.32 (s, 45H, C_{17}). **^{13}C{^{1}H} NMR** ($CDCl_3$): *δ*(ppm) = 167.55 (C_3), 164.10 (C_{15}), 161.03 (C_9), 150.30 (C_8), 135.35 (C_{13}), 134.89 (C_1), 134.53 (C_{14}), 132.27 (C_5), 131.37 (C_2), 128.37 (C_6), 123.39 (C_{11}), 120.29 (C_{10}), 115.04 (C_{12}), 85.77 (C_{16}), 66.75 (C_4), 8.47 (C_{17}). **FT-IR** (KBr): 3051 (m) *v*(C-H_{Cp^*}), 1729 (s) *v*(C=O), 1613 (s) *v*(C=N), 1602 (s) *v*(aromatic C=C), 1464 (s) *δ*(C-H), 1380 *δ*(-CH_{3Cp^*}), 1228 (s) *v*(C-C(O)-O). **ESI-MS**: *m/z* 605.50 $[M\text{-}3Cl]^{3+}$. **Elemental Analysis** (Calculated for $C_{81}H_{81}Cl_3Ir_3N_3O_9$): C, 50.58; H, 4.24; N, 2.18; Found: C, 50.94; H, 3.99; N, 2.46.

5.4.3.3. Tris(4-(pyridylimine)benzyl) benzene-1,3,5-tricarboxylate ruthenium(II) complex (2.22)

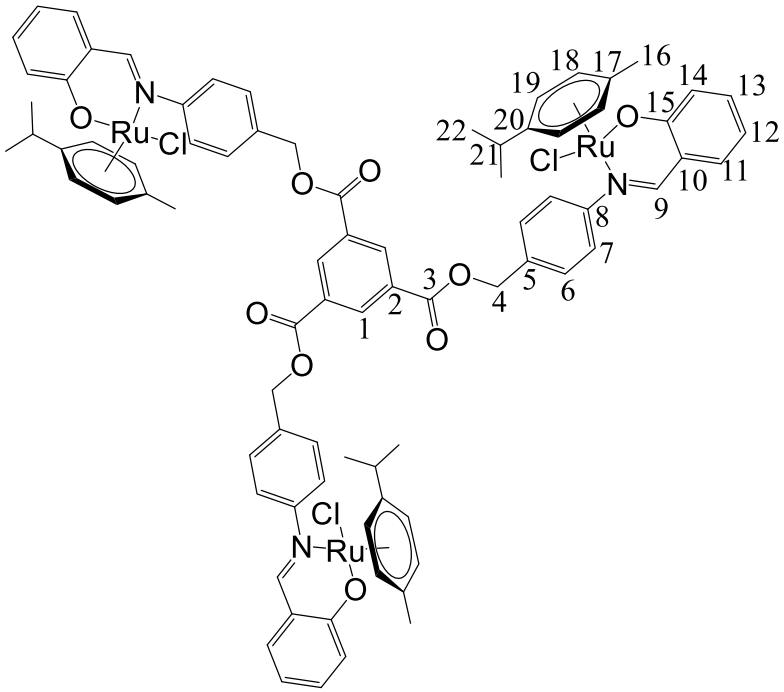

Orange solid, **yield**: 130 mg, 72%. **MP.**: 166ºC (decomposed). **^{1}H NMR** ($CDCl_3$): δ(ppm) = 8.98 (s, 3H, H_1), 7.73 (s, 3H, H_9), 7.71 (d, 6H, H_7, ^{3}J = 8 Hz), 7.54 (d, 6H, H_6, ^{3}J = 8 Hz),7.22 (t, 3H, H_{13}, ^{3}J = 4 Hz), 6.99 (d, 3H, H_{11}, ^{3}J = 8 Hz), 6.92 (t, 3H, H_{12}, ^{3}J = 8 Hz), 6.42 (d, 3H, H_{14}, ^{3}J = 4 Hz), 5.63 (d, 3H, H_{18A}, ^{3}J = 4 Hz), 5.41 (d, 3H, H_{18B}, ^{3}J = 4 Hz), 5.03 (d, 3H, H_{19A}, ^{3}J = 4 Hz), 4.28 (d, 3H, H_{19B}, ^{3}J = 8 Hz), 2.60 (m, 3H, H_{21}), 2.10 (s, 9H, H_{16}), 1.15 (d, 9H, H_{22A}, ^{3}J = 8 Hz), 1.11 (d, 9H, H_{22B}, ^{3}J = 8 Hz). **^{13}C{^{1}H} NMR** ($CDCl_3$): δ(ppm) = 165.40 (C_3), 164.74 (C_{15}),164.46 (C_9), 158.56 (C_8), 135.73 (C_{13}), 135.57 (C_{12}), 135.00 (C_1), 134.18 (C_5), 131.38 (C_2), 128.90 (C_6), 124.22 (C_7), 122.71 (C_{11}), 118.15 (C_{10}), 114.37 (C_{14}), 101.53 (C_{20}), 98.18 (C_{17}), 83.31 (C_{18A}), 80.50 (C_{18B}), 78.96 (C_{19A}), 78.08 (C_{19B}), 66.86 (C_4), 30.38 (C_{20}), 22.71 (C_{22A}), 21.70 (C_{22B}), 18.49 (C_{16}). **FT-IR** (KBr): 2966 (m) ν(C-$H_{p\text{-}Cy}$), 1728 (s) ν(C=O), 1614 (m) ν(C=N), 1602 (s) ν(aromatic C=C), 1443 (s) δ(C-H), 1383 δ(-$CH_{3p\text{-}Cy}$), 1231 (s) ν(C-C(O)-O). **ESI-MS**: *m/z* 514.10 $[M\text{-}3Cl]^{3+}$. **Elemental Analysis** (Calculated for $C_{81}H_{78}Cl_3N_3O_9Ru_3$): C, 59.07; H, 4.77; N, 2.55; Found: C, 58.89; H, 4.61; N, 2.60.

5.5. Synthesis of Alkylated PTA Ligands (3.1-3.2)

5.5.1. Preparation of Monomeric Ligand (3.1)

1-Benzyl-1,3,5-triaza-7-phosphaadamantan-1-ium chloride was prepared using known literature reported procedures.[5]

5.5.2. Synthesis of Trimeric Ligand (3.2)

5.5.2.1. 1,3,5-tris(chloromethyl)benzene

1,3,5-tris(chloromethyl)benzene was synthesized using known literature reported procedures.[6]

5.5.2.2. 1,1',1''-(benzene-1,3,5-triyltris(methylene))tris(1,3,5-triaza-7-phosphaadamantan-1-ium) chloride (3.2)

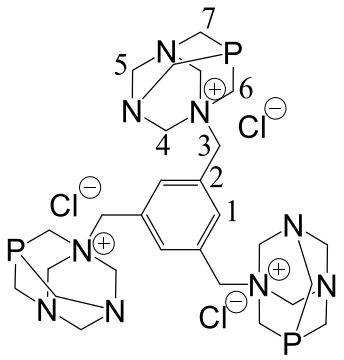

1,3,5-tris(chloromethyl)benzene (99.9 mg, 0.447 mmol) was dissolved in acetone (10 ml) and excess PTA (281 mg, 1.79 mmol) was added. The reaction was refluxed overnight. A beige solid was isolated by suction filtration and washed with THF and DCM.

Beige solid, **yield**: 302 mg, 97%. **MP.**: 180.2ºC (decomposed). **^{1}H NMR** (D_2O): δ = 7.95 (s, 3H, H_1), 5.07-5.17 (12H, H_4 N^+CH_2N), 4.78 (d, ^2J = 12 Hz, 6H, H_5 NCH_2N), 4.47 (d, ^2J = 3 Hz, 6H, H_6 N^+CH_2P), 4.38 (s, 6H, H_3), 3.93-4.08 (m, 12H, H_7 NCH_2P). **^{13}C NMR** (D_2O): δ = 139.38 (C_1), 127.67 (C_1), 79.18 (C_4 N^+CH_2N), 69.46 (C_5 NCH_2N), 65.23 (C_3), 52.93 (d, $J_{P\text{-}C}$ = 24 Hz, C_6 N^+CH_2P), 45.61 (d, $J_{P\text{-}C}$ = 14 Hz, C_7 NCH_2P). **^{31}P NMR** (D_2O): δ = -82.07. **HR-ESI-MS(+)**: 196.0998 $[M\text{-}3Cl]^{3+}$. **Elemental Analysis** (Calculated for $C_{27}H_{45}Cl_3N_9P_3.3H_2O$): C, 43.30; H, 6.86; N, 16.83; Found: C, 43.03; H, 6.83; N, 16.88. **S_{20}°$_C$** = 44 mg/ml H_2O.

5.5.3. Synthesis of Mononuclear Alkylated PTA Complexes (3.3-3.5)

General Procedure

3.1 (50.0 mg, 0.176 mmol for **3.3** and **3.4**) was dissolved in EtOH (10 ml). $[Rh(\eta^5\text{-}C_5Me_5)Cl_2]_2$ (54.4 mg, 0.0881 mmol for **3.3**) or $[Ir(\eta^5\text{-}C_5Me_5)Cl_2]_2$ (70.2 mg, 0.0881 mmol for **3.4**) was then added and stirred for 3 hours, filtered by gravity and then the filtrate removed under reduced pressure. Precipitation from $MeOH/Et_2O$ yielded the solid products **3.3-3.4**.

5.5.4. Mononuclear alkylated PTA rhodium(III) complex (3.3)

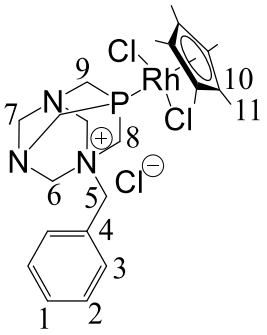

Red solid. **Yield**: 90 mg, 57%. **MP.**: 167.4-169.8ºC. **^{1}H NMR** (D_2O): δ = 7.52-7.59 (m, 5H, H_1-H_4), 4.98-5.18 (4H, H_6 N^+CH_2N), 4.70 (d, ^2J = 13 Hz, 1H, H_7 NCH_2N), 4.47 (d, ^2J = 4 Hz, 2H, H_8 N^+CH_2P), 4.38 (d, ^2J = 6 Hz, 1H, H_7 NCH_2N), 4.34 (d, ^2J = 2 Hz, 2H, H_5), 4.16-4.51 (4H, H_9 NCH_2P), 1.72 (d, $J_{Rh\text{-}H}$ = 4 Hz, 15H, H_{11}). **^{13}C{^{1}H} NMR** (D_2O): δ = 132.88 (C_3), 131.33 (C_1), 129.60 (C_2), 124.20 (C_4), 101.95 (C_{10}), 79.28 (C_6 N^+CH_2N), 69.38 (C_7 NCH_2N), 66.47 (C_5), 51.48 (d, $J_{P\text{-}C}$ = 13 Hz, C_8 N^+CH_2P), 46.08 (d, $J_{P\text{-}C}$ = 14 Hz, C_9 NCH_2P), 9.00 (C_{11}). **^{31}P{^{1}H} NMR** (D_2O): δ = -24.63 ($J_{Rh\text{-}P}$ = 150 Hz). **HR-ESI-MS(+)**: *m/z* = 558.0898 $[M\text{-}Cl]^+$. **Elemental Analysis** (Calculated for $C_{23}H_{34}Cl_3N_3PRh.3H_2O$): C, 42.71; H, 6.23; N, 6.50; Found: C, 42.32; H, 6.29; N, 6.32. **S_{20^oC}** = 21 mg/ml H_2O.

5.5.5. Mononuclear alkylated PTA iridium(III) complex (3.4)

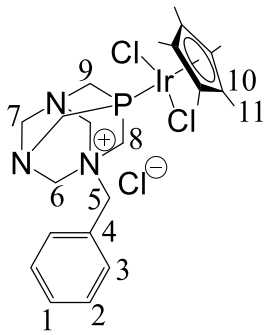

Yellow solid. **Yield**: 105 mg, 55%. **MP.**: 178.2-180.4°C. **^{1}H NMR** (D_2O): δ = 7.54-7.60 (m, 5H, H_1-H_4), 4.98-5.22 (4H, H_6 N^+CH_2N), 4.51-4.69 (2H, H_7 NCH_2N), 4.48 (d, ^2J = 5 Hz, 2H, H_8 N^+CH_2P), 4.38 (d, ^2J = 2 Hz, 2H, H_5), 4.13-4.34 (4H, H_9 NCH_2P), 1.77 (d, $J_{H\text{-}P}$ = 4 Hz, 15H, H_{11}) . **^{13}C{^{1}H} NMR** (D_2O): δ = 134.21 (C_3), 132.30 (C_1), 130.77 (C_2), 126.38 (C_4), 95.65 (C_{10}), 81.19 (C_6 N^+CH_2N), 71.06 (C_7 NCH_2N), 66.90 (C_5), 51.85 (d, $J_{P\text{-}C}$ = 22 Hz, C_8 N^+CH_2P), 46.82 (d, $J_{P\text{-}C}$ = 22 Hz, C_9 NCH_2P), 9.50 (C_{11}). **^{31}P{^{1}H} NMR** (D_2O): δ = -48.77. **HR-ESI-MS(+)**: 646.1473 $[M\text{-}Cl]^+$. **Elemental Analysis** (Calculated for $C_{23}H_{34}Cl_3IrN_3P.3H_2O$): C, 37.53; H, 5.48; N, 5.71; Found: C, 37.21; H, 5.49; N, 5.46. **$S_{20}°_C$** = 16 mg/ml H_2O.

5.5.6. Mononuclear alkylated PTA ruthenium(II) complex (3.5)

The mononuclear alkylated PTA ruthenium(II) complex was synthesized using known literature reported procedures.[7]

5.6. Synthesis of Trinuclear Complexes (3.6-3.8)

General Procedure

3.2 (50.0 mg, 0.0719 mmol for **3.6-3.8**) was dissolved in a mixture of MeOH (5 ml) and DCM (5 ml). $[Rh(\eta^5\text{-}C_5Me_5)Cl_2]_2$ (66.7 mg, 0.108 mmol for **3.6**) or $[Ir(\eta^5\text{-}C_5Me_5)Cl_2]_2$ (86.0 mg, 0.108 mmol for **3.7**) or $[Ru(\eta^6\text{-}p\text{-}Pr^iC_6H_4Me)Cl_2]_2$ (66.0 mg, 0.108 mmol for **3.8**) was then added and stirred for 3 hours, filtered by gravity and then the filtrate removed under reduced pressure. Precipitation from $MeOH/Et_2O$ yielded the solid products **3.6-3.8**.

5.6.1. Trinuclear alkylated PTA rhodium(III) complex (3.6)

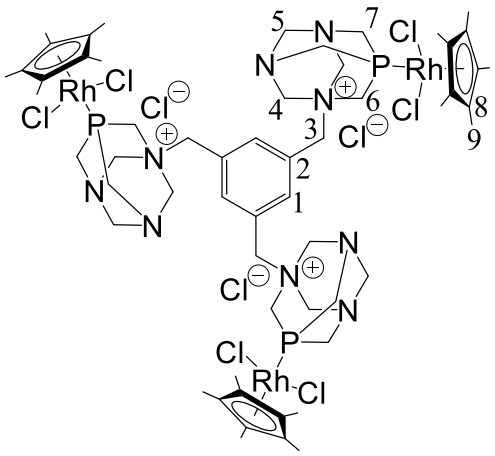

Red solid. **Yield**: 85 mg, 46%. **MP.**: 212.18ºC (decomposed). **^{1}H NMR** (D_2O): δ = 7.87 (s, 3H, H_1), 5.06-5.26 (12H, H_4 N^+CH_2N), 4.96 (d, J_{H-P} = 12 Hz, 6H, H_5 NCH_2N), 4.53 (d, J_{H-P} = 9 Hz, 6H, H_6 N^+CH_2P), 4.43 (s, 6H, H_3), 4.18-4.31 (12H, H_7 NCH_2P), 1.71 (s, 45H, H_9). **^{13}C{^{1}H} NMR** (D_2O): δ = 143.72 (C_1), 126.53 (C_2), 102.02 (C_8), 80.62 (C_4 N^+CH_2N), 69.27 (C_5 NCH_2N), 65.02 (C_3), 49.45 (d, J_{P-C} = 24 Hz, C_6 N^+CH_2P), 45.82 (d, J_{P-C} = 16 Hz, C_7 NCH_2P), 9.06 (d, J = 10 Hz, C_9). **^{31}P{^{1}H} NMR** (D_2O): δ = -22.89 (J_{Rh-P} = 151 Hz). **HR-ESI-MS(+)**: 478.0514 $[M-5Cl+2H]^{3+}$. **Elemental Analysis** (Calculated for $C_{57}H_{90}Cl_9N_9P_3Rh_3.8H_2O$): C, 38.76; H, 6.05; N, 7.14; Found: C, 38.73; H, 5.67; N, 6.78. **$S_{20ºC}$** = 12 mg/ml H_2O.

5.6.2. Trinuclear alkylated PTA iridium(III) complex (3.7)

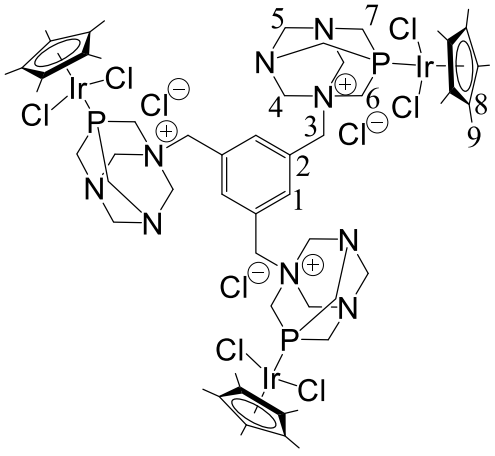

Yellow solid. **Yield**: 110 mg, 50%. **MP.**: 231.5ºC (decomposed). **^{1}H NMR** (D_2O): δ = 7.91 (s, 3H, H_1), 5.07-5.28 (12H, H_4 N^+CH_2N), 4.64 (6H, H_5 NCH_2N), 4.52 (d, J_{H-P} = 17 Hz, 6H, H_6 N^+CH_2P), 4.32 (s, 6H, H_3), 4.15-4.32 (d, J_{H-P} = 11 Hz, 12H, H_7 NCH_2P), 1.74 (s, 45H, H_9). **^{13}C{^{1}H} NMR** (D_2O): δ = 143.72 (C_1), 126.53 (C_2), 95.32 (C_8), 80.70 (C_4 N^+CH_2N), 69.48 (C_5

NCH_2N), 65.03 (C_3), 49.31 (d, J_{P-C} = 24 Hz, C_6 N^+CH_2P), 45.12 (d, J_{P-C} = 10 Hz, C_7 NCH_2P), 8.73 (C_9). **$^{31}P\{^1H\}$ NMR** (D_2O): δ = -46.52. **HR-ESI-MS(+)**: 570.1178 $[M-5Cl+2H]^{3+}$. **Elemental Analysis** (Calculated for $C_{57}H_{90}Cl_9N_9P_3Ir_3.7H_2O$): C, 33.96; H, 5.20; N, 6.25; Found: C, 33.89; H, 5.17; N, 6.15. **$S_{20°C}$** = 3 mg/ml H_2O.

5.6.3. Trinuclear alkylated PTA ruthenium(II) complex (3.8)

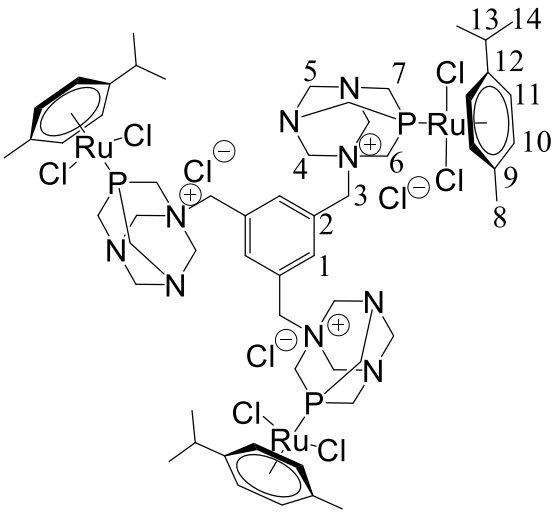

Orange solid. **Yield**: 65 mg, 36%. **MP.**: 204.4ºC (decomposed). **^1H NMR** (D_2O): δ = 7.80 (s, 3H, H_1), 5.86-5.92 (m, 12H, H_{10} H_{11}), 5.02-5.24 (12H, H_4 N^+CH_2N), 4.63 (6H, H_5 NCH_2N), 4.54 (d, J_{H-P} = 11 Hz, 6H, H_6 N^+CH_2P), 4.29-4.93 (m, 18H, H_3 H_7 NCH_2P), 2.61 (m, 3H, H_{13}), 2.04 (s, 9H, H_8), 1.20 (d, ^3J = 7 Hz, H_{14}). **$^{13}C\{^1H\}$ NMR** (D_2O): δ = 139.82 (C_1), 127.67 (C_1), 108.32 (C_{12}), 99.23 (C_9), 89.04 (C_{10}), 86.57 (C_{11}), 80.57 (C_4 N^+CH_2N), 69.11 (C_5 NCH_2N), 64.48 (C_3), 55.64 (d, J_{P-C} = 15 Hz, C_6 N^+CH_2P), 48.01 (d, J_{P-C} = 17 Hz, C_7 NCH_2P), 30.78 (C_{13}), 21.33 (C_{14}), 17.93 (C_8). **$^{31}P\{^1H\}$ NMR** (D_2O): δ = -82.07. **HR-ESI-MS(+)**: 480.0599 $[M-5Cl+2H]^{3+}$. **Elemental Analysis** (Calculated for $C_{57}H_{87}Cl_9N_9P_3Ru_3.7H_2O$): C, 39.35; H, 5.85; N, 7.25; Found: C, 39.22; H, 6.06; N, 7.45. **$S_{20°C}$** = 8 mg/ml H_2O.

5.7. Preparation of Monomeric and Trimeric Sulfonated Ligands (4.1 and 4.4)

5.7.1. 5-Sulfonato propylsalicylaldimine (4.1)

The monomeric ligand 5-sulfonato propylsalicylaldimine was synthesized using known literature reported procedures.[8]

5.7.2. Tris-2-(5-sulfinatosalicylaldimine ethyl)amine (4.4)

The trimeric ligand tris-2-(5-sulfinatosalicylaldimine ethyl)amine was synthesized using known literature reported procedures.[8]

5.8. Preparation of Anionic Sulfonated Complexes (4.2-4.3 and 4.5-4.6)

5.8.1. Anionic Mononuclear Complexes (4.2-4.3)

General Procedure

4.1 (44.7 mg, 0.169 mmol for **4.2**; 60.0 mg, 0.226 mmol for **4.3**) was dissolved in EtOH (10 ml). 1.1 molar equivalents of NaOAc (15.2 mg, 0.185 mmol for **4.2**; 20.4 mg, 0.249 mmol for **4.3**) was added and stirred for 30 minutes. $[Rh(\eta^5\text{-}C_5Me_5)Cl_2]_2$ (67.1 mg, 0.0843 mmol for **4.2**) or $[Ir(\eta^5\text{-}C_5Me_5)Cl_2]_2$ (76.9 mg, 0.124 mmol for **4.3**) was then dissolved into the solution which was stirred overnight. The solution was then filtered by gravity and then the solvent of the filtrate removed using rotary evaporation. The solid residue was dissolved in DCM and filtered by gravity, after which the DCM was reduced and precipitation from $MeOH/Et_2O$ yielded the solid products **4.2-4.3**.

5.8.1.1. Mononuclear sulfonated rhodate(III) complex (4.2)

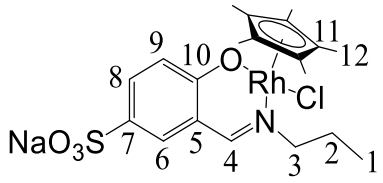

Red solid. **Yield**: 72.0 mg, 59%. **MP.**: 247.1°C (decomposed). **^{1}H NMR** ($(CD_3)_2SO$): δ = 8.02 (s, 1H, H_4), 7.45 (d, 1H, *J* = 2 Hz, H_6), 7.38 (dd, 1H, *J* = 2 Hz, *J* = 9 Hz, H_9), 6.61 (d, 1H, *J* = 9 Hz, H_8), 3.86 (t, 1H, *J* = 6 Hz, H_3), 1.45 (m, 17H, H_2 H_{12}), 0.86 (t, 3H, *J* = 7 Hz, H_1). **^{13}C{^{1}H} NMR** ($(CD_3)_2SO$): δ = 166.01 (C_7), 165.68 (C_{10}), 163.58 (C_4), 131.96 (C_9), 131.55 (C_6), 121.48 (C_8), 115.94 (C_5), 92.60 (C_{11}), 65.63 (C_3), 23.45 (C_2), 11.26 (C_1), 8.22 (C_{11}). **FT-IR** (ATR): 1623 ν(C=N_{imine}). **HR-ESI-MS(+)**: 502.0545 $[M\text{-}Cl]^+$, 480.0714 $[M\text{-}Cl\text{-}Na+H]^+$; **HR-ESI-MS(-)**: 514.0308 $[M\text{-}Na]^-$, 478.0526 $[M\text{-}Cl\text{-}Na\text{-}H]^-$. **Elemental Analysis** (Calculated for $C_{20}H_{26}ClNNaO_4RhS.1H_2O$): C, 43.22; H, 5.08; N, 2.52; S, 5.77; Found: C, 43.49; H, 5.26; N, 2.61; S, 5.58.

5.8.1.2. Mononuclear sulfonated iridate(III) complex (4.3)

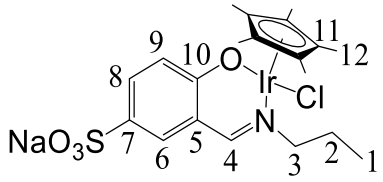

Yellow/brown solid. **Yield**: 71.2 mg, 67%. **MP.**: 210.9°C (decomposed). **^{1}H NMR** ($(CD_3)_2SO$): δ = 8.05 (s, 1H, H_4), 7.48 (d, 1H, *J* = 4 Hz, H_6), 7.42 (d, 1H, *J* = 2 Hz, H_9), 6.57 (d, 1H, *J* = 8 Hz, H_8), 3.92 (t, 1H, *J* = 7 Hz, H_3), 1.47 (m, 17H, H_2 H_{12}), 0.88 (t, 3H, *J* = 7 Hz, H_1). **^{13}C{^{1}H} NMR** ($(CD_3)_2SO$): δ = 174.73 (C_7), 164.12 (C_{10}), 160.67 (C_4), 131.50 (C_9), 131.29 (C_6), 120.43 (C_8), 114.07 (C_5), 84.45 (C_{11}), 68.42 (C_3), 23.40 (C_2), 11.16 (C_1), 8.36 (C_{11}). **FT-IR** (ATR): 1621 *v*(C=N_{imine}). **HR-ESI-MS(+)**: 593.1130 $[M\text{-}Cl]^+$, 570.1277 $[M\text{-}Cl\text{-}Na+H]^+$; **HR-ESI-MS**(-): 604.0961 $[M\text{-}Na]^-$, 568.1196 $[M\text{-}Cl\text{-}Na\text{-}H]^-$. Elemental Analysis (Calculated for $C_{20}H_{26}ClIrNNaO_4S.4H_2O$): C, 34.36; H, 4.90; N, 2.00; S, 4.59; Found: C, 34.16; H, 4.93; N, 2.13; S, 4.80.

5.8.2. Trinuclear Anionic Complexes (4.5-4.6)

General Procedure

4.4 (60.0 mg, 0.0768 mmol for **4.5**; 39.2 mg, 0.0502 mmol for **4.6**) was dissolved in EtOH (10 ml). Excess NaOAc (20.8 mg, 0.0.254 mmol for **4.5**; 12.8 mg, 0.156 mmol for **4.6**) was added and stirred for 30 minutes. $[Rh(\eta^5\text{-}C_5Me_5)Cl_2]_2$ (78.4 mg, 0.127 mmol for **4.5**) or $[Ir(\eta^5\text{-}C_5Me_5)Cl_2]_2$ (60.0 mg, 0.0753 mmol for **4.6**) was then dissolved into the solution which was stirred overnight. The solution was then filtered by gravity and then the solvent of the filtrate removed using rotary evaporation. The solid residue was dissolved in DCM and filtered by gravity, after which the DCM was reduced and precipitation from MeOH/Et_2O yielded the solid products **4.5-4.6**.

5.8.2.1. Trinuclear sulfonated rhodate(III) complex (4.5)

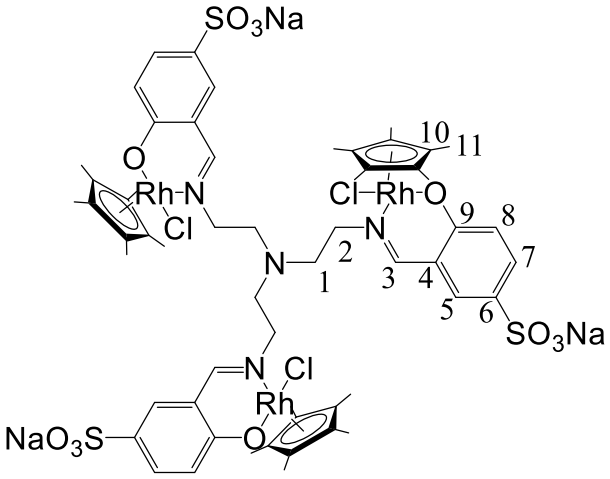

Red solid. **Yield**: 40.0 mg, 33%. **MP.**: 281.0°C (decomposed). **^{1}H NMR** ($(CD_3)_2SO$): δ = 8.17 (s, 3H, H_3), 7.44 (m, 6H, H_5 H_8), 6.66 (d, J_3 = 9 Hz, 3H, H_6), 4.00 (m, 6H, H_1), 1.43 (s, 51H, H_2 H_{11}. **^{13}C{^{1}H} NMR** ($(CD_3)_2SO$): δ = 171.90 (C_6), 165.10 (C_3), 132.03 (C_7), 131.77 (C_5), 121.75 (C_8), 119.21 (C_4), 98.75 (C_{10}), 62.11 (C_1), 55.52 (C_2), 8.53 (C_{11}). **FT-IR** (ATR): 1618 ν(C=N_{imine}). **HR-ESI-MS(+)**: 505.2332 $[M-3Na+6H]^{3+}$, 373.1396 $[M-3Cl+Na]^{4+}$. **Elemental Analysis** (Calculated for $C_{57}H_{69}Cl_3N_4Na_3O_{12}Rh_3S_3.4H_2O$): C, 41.38; H, 4.69; N, 3.39; S, 5.81; Found: C, 41.45; H, 4.73; N, 3.21; S, 5.69.

5.8.2.2. Trinuclear sulfonated iridate(III) complex (4.6)

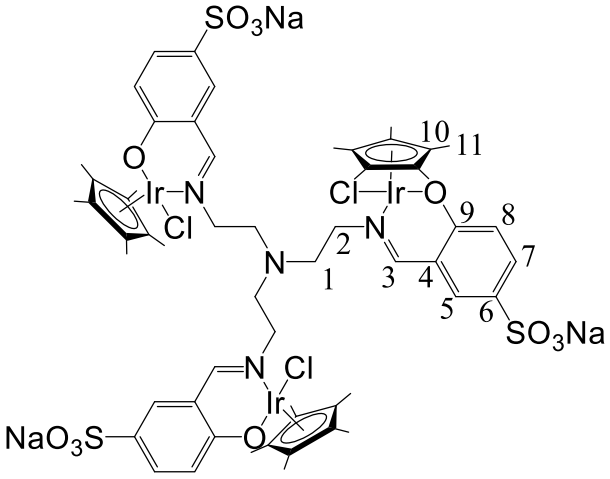

Yellow/brown solid. **Yield**: 55.0 mg, 59%. **MP.**: 212.7°C (decomposed). **^{1}H NMR** ($(CD_3)_2SO$): δ = 8.10 (s, 3H, H_3), 7.47 (m, 6H, H_5 H_8), 6.58 (d, J_3 = 9 Hz, 3H, H_6), 4.33 (m, 6H, H_1), 1.42 (s, 51H, H_2 H_{11}). **^{13}C{^{1}H} NMR** ($(CD_3)_2SO$): δ = 173.92 (C_6), 164.49 (C_9), 162.20 (C_3), 131.60 (C_7), 131.21 (C_5), 120.67 (C_8), 119.99 (C_4), 162.20 (C_3), 84.41 (C_{10}), 64.54 (C_1), 55.67 (C_2), 8.35

(C_{11}). **FT-IR** (ATR): 1617 ν(C=N_{imine}). **HR-ESI-MS(+)**: 583.1314 $[M\text{-}3Cl]^{3+}$, 441.0615 $[M\text{-}3Cl+Na]^{4}$. **Elemental Analysis** (Calculated for $C_{57}H_{69}Cl_3Ir_3N_4Na_3O_{12}S_3.3H_2O$): C, 35.95; H, 3.97; N, 2.94; S, 5.05; Found: C, 36.06; H, 4.08; N, 2.87; S, 4.95.

5.9. Preparation of Sulfonated Complexes (4.7-4.22)

5.9.1. Mononuclear Sulfonated Complexes (4.7-4.14)

General Procedure

4.1 (36.7 mg, 0.138 mmol for **4.7-4.10**; 40.0 mg, 0.151 mmol for **4.11-4.14**) was dissolved in EtOH (10 ml). 3.3 molar equivalents of NaOAc (12.5 mg, 0.152 mmol for **4.7-4.10**; 13.6 mg, 0.166 mmol for **4.11-4.14**) was added and stirred for 30 minutes. $[Rh(\eta^5\text{-}C_5Me_5)Cl_2]_2$ (47.0 mg, 0.0760 mmol for **4.7-4.10**;) or $[Ir(\eta^5\text{-}C_5Me_5)Cl_2]_2$ (66.1 mg, 0.0.829 mmol for **4.11-4.14**) was then dissolved into the solution which was stirred overnight. Pyridine (12.0 mg, 0.152 mmol for **4.7**; 13.1 mg, 0.166 mmol for **4.11**), or 4-methylpyridine (14.2 mg, 0.152 mmol for **4.8**; 15.4 mg, 0.166 mmol for **4.12**), or 4-phenylpyridine (23.6 mg, 0.152 mmol for **4.9**; 25.7 mg, 0.166 mmol for **4.13**) or 4-ferrocenylpyridine (40.0 mg, 0.152 mmol for **4.10**; 43.6 mg, 0.166 mmol for **4.14**) was then added and stirred for 2 hours. $NaBPh_4$ (52.0 mg, 0.152 mmol for **4.7-4.10**; 56.8 mg, 0.166 mmol for **4.11-4.14**) was then added. The solution was then filtered by gravity and then the solvent of the filtrate removed using rotary evaporation. The solid residue was dissolved in DCM and filtered by gravity, after which *i*PrOH was added and the solvent was reduced and precipitation occurred to yield the solid products **4.7-4.10** and **4.11-4.14** which were dried under vacuum.

5.9.1.1. Mononuclear sulfonated rhodium(III) pyridyl complex (4.7)

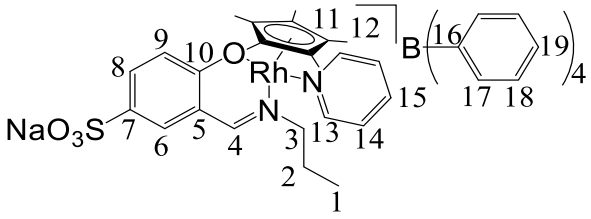

Red solid. **Yield**: 55.1 mg, 44%. **MP.**: 151.4°C (decomposed). **^{1}H NMR** ($(CD_3)_2SO$): δ = 8.63 (d, 2H, *J* = 5 Hz, H_{13}), 8.28 (s, 1H, H_4), 7.95 (m, 1H, H_{15}), 7.58 (d, 1H, *J* = 2 Hz, H_6), 7.52 (dd, 1H, *J* = 9 Hz, *J* = 2 Hz, H_9), 7.50 (m, 2H, H_{14}), 7.18 (m, 8H, H_{17}), 6.92 (t, 8H, *J* = 8 Hz, H_{18}), 6.86 (d, 1H, *J* = 9 Hz, H_8), 6.79 (t, 4H, *J* = 7 Hz, H_{19}), 3.95 (m, 2H, H_3), 1.49 (m, 17H, H_2 H_{12}),

0.81 (t, 3H, *J* = 7 Hz, H_1). **$^{13}C\{^1H\}$ NMR** ($(CD_3)_2SO$): δ = 165.94 (C_4), 164.06 (C_{16A}), 163.57 (C_{16B}), 163.08 ($C_{16C\ 4}$), 162.59 (C_{16D}), 150.36 (C_{13}), 137.70 (C_{15}), 135.49 (C_{17}), 132.51 (C_9), 132.44 (C_6), 125.22 (C_{14}), 125.20 (C_{18}), 121.66 (C_8), 121.44 (C_{19}), 115.18 (C_5), 95.08 (C_{11}), 61.97 (C_3), 23.72 (C_2), 10.83 (C_1), 7.98 (C_{12}). **FT-IR** (ATR): 1621 *v*(C=N_{imine}). **HR-ESI-MS(+)**: 480.0728 [M-BPh_4-NC_5H_5-Na+H]$^+$; **HR-ESI-MS(-)**: 478.0545 [M-BPh_4-NC_5H_5-Na-H]$^-$. **Elemental Analysis** (Calculated for $C_{49}H_{51}BN_2NaO_4RhS.2½H2O$): C, 62.23; H, 5.97; N, 2.96; S, 3.39; Found: C, 62.13; H, 6.01; N, 2.82; S, 3.32.

5.9.1.2. Mononuclear sulfonated rhodium(III) 4-methylpyridyl complex (4.8)

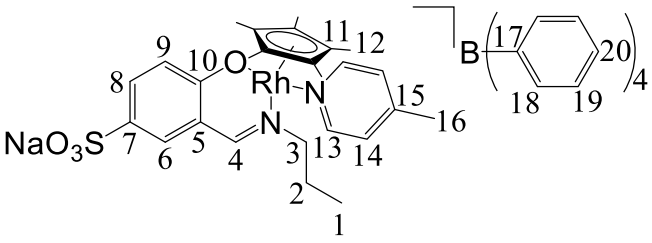

Red solid. **Yield**: 78.2 mg, 62%. **MP.**: 165.1°C (decomposed). **^1H NMR** ($(CD_3)_2SO$): δ = 8.47 (d, 2H, *J* = 6 Hz, H_{13}), 8.27 (s, 1H, H_4), 7.56 (s, 1H, H_6), 7.51 (dd, 1H, *J* = 9 Hz, *J* = 2 Hz, H_9), 7.40 (m, 2H, H_{14}), 7.21 (m, 8H, H_{18}), 6.93 (t, 8H, *J* = 7 Hz, H_{19}), 6.86 (d, 1H, *J* = 9 Hz, H_8), 6.80 (t, 4H, *J* = 7 Hz, H_{20}), 3.94 (m, 2H, H_3), 2.38 (s, 3H, H_{16}), 1.49 (m, 17H, H_2 H_{12}), 0.83 (t, 3H, *J* = 7 Hz, H_1). **$^{13}C\{^1H\}$ NMR** ($(CD_3)_2SO$): δ = 165.89 (C_4), 164.05 (C_{17A}), 163.56 (C_{17B}), 163.06 (C_{17C}), 162.57 (C_{17D}), 149.46 (C_{13}), 135.47 (C_{18}), 132.47 (C_9), 132.39 (C_6), 126.45 (C_{14}), 125.18 (C_{19}), 121.63 (C_8), 121.42 (C_{20}), 94.97 (C_{11}), 61.95 (C_3), 23.75 (C_2), 20.40 (C_{16}), 10.83 (C_1), 7.98 (C_{12}). **FT-IR** (ATR): 1619 *v*(C=N_{imine}). **HR-ESI-MS(+)**: 480.0709 [M-BPh_4-$NC_5H_4CH_3$-Na+H]$^+$; **HR-ESI-MS(-)**: 478.0551 [M-BPh_4-$NC_5H_4CH_3$-Na-H]$^-$. **Elemental Analysis** (Calculated for $C_{50}H_{53}BN_2NaO_4RhS.2½H_2O$): C, 62.57; H, 6.09; N, 2.92; S, 3.34; Found: C, 62.54; H, 6.23; N, 2.96; S, 3.26.

5.9.1.3. Mononuclear sulfonated rhodium(III) 4-phenylpyridyl complex (4.9)

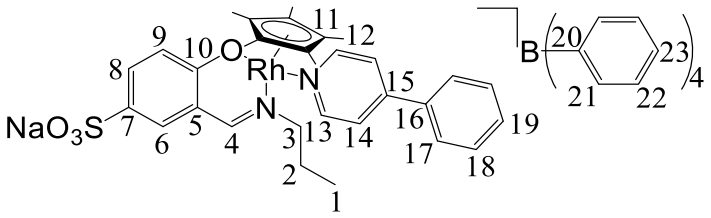

Red solid. **Yield**: 80.9 mg, 60%. **MP.**: 152.6ºC (decomposed). **^{1}H NMR** ($(CD_3)_2SO$): δ = 8.67 (d, 2H, *J* = 6 Hz, H_{13}), 8.27 (s, 1H, H_4), 7.88 (m, 2H, H_{14}), 7.84 (d, 2H, H_{17}), 7.54 (m, 4H, H_{19} H_{18} H_9), 7.10 (m, 8H, H_{21}), 6.92 (t, 8H, *J* = 8 Hz, H_{22}), 6.89 (d, 1H, *J* = 9 Hz, H_8), 6.79 (t, 4H, *J* = 7 Hz, H_{23}), 3.96 (m, 2H, H_3), 1.51 (m, 17H, H_2 H_{12}), 0.81 (t, 3H, *J* = 7 Hz, H_1). **^{13}C{^{1}H} NMR** ($(CD_3)_2SO$): δ = 165.94 (C_4), 164.06 (C_{16A}), 163.57 (C_{16B}), 163.08 ($C_{16C\ 4}$), 162.60 (C_{16D}), 150.79 (C_{13}), 135.97 (C_{19}), 135.49 (C_{21}), 132.51 (C_9), 132.45 (C_6), 129.30 (C_{18}), 126.93 (C_{17}), 125.22 (C_{22}), 121.70 (C_8 C_{14}), 121.44 (C_{23}), 115.18 (C_5), 95.09 (C_{11}), 61.97 (C_3), 23.71 (C_2), 10.81 (C_1), 8.00 (C_{12}). **FT-IR** (ATR): 1610 *ν*(C=N_{imine}). **HR-ESI-MS(+)**: 480.0717 [M-BPh_4-NC_5H_4Ph-Na+H]$^+$; **HR-ESI-MS(-)**: 478.0512 [M-BPh_4-NC_5H_4Ph-Na-H]$^-$. **Elemental Analysis** (Calculated for $C_{55}H_{55}BN_2NaO_4RhS.2H_2O$): C, 65.22; H, 5.87; N, 2.77; S, 3.17; Found: C, 65.18; H, 5.85; N, 2.70; S, 3.28.

5.9.1.4. Mononuclear sulfonated rhodium(III) 4-ferrocenylpyridyl complex (4.10)

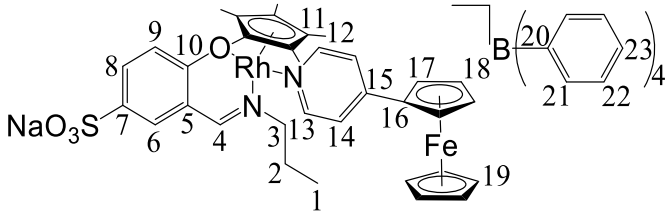

Red solid. **Yield**: 81.3 mg, 54%. **MP.**: 170.1ºC (decomposed). **^{1}H NMR** ($(CD_3)_2SO$): δ = 8.41 (d, 2H, *J* = 5 Hz, H_{13}), 8.26 (s, 1H, H_4), 7.69 (m, 2H, H_{14}), 7.59 (s, 1H, H_6), 7.54 (d, 2H, H_9), 7.18 (m, 8H, H_{21}), 6.92 (t, 8H, *J* = 7 Hz, H_{22}), 6.87 (d, 1H, *J* = 9 Hz, H_8), 6.79 (t, 4H, *J* = 7 Hz, H_{23}), 5.02 (m, 2H, H_{17}), 4.57 (m, 2H, H_{18}), 4.03 (m, 7H, H_{19} H_3), 1.50 (m, 17H, H_2 H_{12}), 0.75 (t, 3H, *J* = 7 Hz, H_1). **^{13}C{^{1}H} NMR** ($(CD_3)_2SO$): δ = 165.94 (C_4), 164.06 (C_{16A}), 163.57 (C_{16B}), 163.08 ($C_{16C\ 4}$), 162.60 (C_{16D}), 150.79 (C_{13}), 135.97 (C_{19}), 135.49 (C_{21}), 132.51 (C_9), 132.45 (C_6), 129.30 (C_{18}), 126.93 (C_{17}), 125.22 (C_{22}), 121.70 (C_8 C_{14}), 121.44 (C_{23}), 115.18 (C_5), 95.09 (C_{11}), 61.97 (C_3), 23.71 (C_2), 10.81 (C_1), 8.00 (C_{12}). **FT-IR** (ATR): 1609 *ν*(C=N_{imine}). **HR-ESI-MS(+)**: 743.1104 [M-BPh_4-Na+H]$^+$, 480.0713 [M-BPh_4-NC_5H_4Fc-Na+H]$^+$; **HR-ESI-MS(-)**:

478.0512 [M-BPh_4-NC_5H_4Fc-Na-H]$^-$. **Elemental Analysis** (Calculated for $C_{59}H_{59}BFeN_2NaO_4RhS.2½H_2O$): C, 62.72; H, 5.71; N, 2.48; S, 2.84; Found: C, 62.73; H, 5.76; N, 2.58; S, 2.71.

5.9.1.5. Mononuclear sulfonated iridium(III) pyridyl complex (4.11)

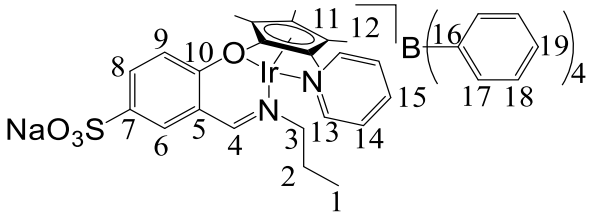

Yellow solid. **Yield**: 90.4 mg, 60%. **MP.**: 174.7°C (decomposed). **^{1}H NMR** ($(CD_3)_2SO$): δ = 8.65 (m, 2H, H_{13}), 8.34 (s, 1H, H_4), 7.95 (m, 1H, H_{15}), 7.65 (s, 1H, H_6), 7.59 (dd, 1H, *J* = 9 Hz, *J* = 2 Hz, H_9), 7.54 (m, 2H, H_{14}), 7.18 (m, 8H, H_{17}), 6.92 (t, 8H, *J* = 7 Hz, H_{18}), 6.85 (m, 1H, H_8), 6.79 (t, 4H, *J* = 7 Hz, H_{19}), 3.95 (m, 2H, H_3), 1.53 (m, 17H, H_2 H_{12}), 0.86 (m, 3H, H_1). **^{13}C{^{1}H} NMR** ($(CD_3)_2SO$): δ = 163.82 (C_{16A}), 163.66 (C_4), 163.50 (C_{16B}), 163.17 ($C_{16C\ 4}$), 162.84 (C_{16D}), 150.30 (C_{13}), 137.31 (C_{15}), 135.50 (C_{17}), 132.77 (C_9), 131.99 (C_6), 125.24 (C_{18} C_{14}), 120.94 (C_8), 121.46 (C_{19}), 115.43 (C_5), 87.18 (C_{11}), 69.71 (C_3), 23.47 (C_2), 10.75 (C_1), 8.03 (C_{12}). **FT-IR** (ATR): 1618 *ν*(C=N_{imine}). **HR-ESI-MS(+)**: 570.1290 [M-BPh_4-NC_5H_4-Na+H]$^+$, 647.2484 [M-BPh_4-Na+H]$^+$; **HR-ESI-MS(-)**: 663.3276 [M-BPh_4-Na-H]$^-$. **Elemental Analysis** (Calculated for $C_{49}H_{51}BIrN_2NaO_4S.3H_2O$): C, 56.37; H, 5.50; N, 2.68; S, 3.07; Found: C, 56.35; H, 5.70; N, 2.65; S, 3.04.

5.9.1.6. Mononuclear sulfonated iridium(III) 4-methylpyridyl complex (4.12)

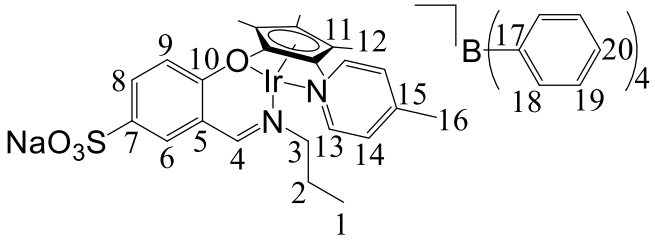

Yellow solid. **Yield**: 77.2 mg, 51%. **MP.**: 185.6°C (decomposed). **^{1}H NMR** ($(CD_3)_2SO$): δ = 8.50 (m, 2H, H_{13}), 8.30 (s, 1H, H_4), 7.61 (s, 2H, H_6), 7.59 (d, 1H, *J* = 9 Hz, H_9), 7.43 (m, 2H, H_{14}), 7.18 (m, 8H, H_{18}), 6.92 (t, 8H, *J* = 7 Hz, H_{19}), 6.85 (d, 1H, *J* = 7 Hz, H_8), 6.79 (t, 4H, *J* = 7 Hz, H_{20}), 3.94 (m, 2H, H_3), 2.38 (s, 3H, H_{16}), 1.50 (m, 17H, H_2 H_{12}), 0.84 (m, 3H, H_1). **^{13}C{^{1}H} NMR** ($(CD_3)_2SO$): δ = 163.82 (C_{17A}), 163.50 (C_{17B}), 163.44 (C_4), 163.17 (C_{17C}), 162.84 (C_{17D}), 150.06

(C_{13}), 135.50 (C_{18}), 132.68 (C_9), 131.87 (C_6), 127.44 (C_{14}), 125.23 (C_{19}), 120.81 (C_8), 121.46 (C_{20}), 115.18 (C_5), 86.75 (C_{11}), 67.02 (C_3), 23.77 (C_2), 20.43 (C_{16}), 10.73 (C_1), 8.03 (C_{12}). **FT-IR** (ATR): 1618 ν(C=N_{imine}). **HR-ESI-MS(+)**: 570.1274 [M-BPh_4-$NC_5H_5CH_3$-Na+H]$^+$; (ESI-): 568.1215 [M-BPh_4-$NC_5H_4CH_3$-Na-H]$^-$, 682.1128 [M-BPh_4-2H]$^-$. **Elemental Analysis** (Calculated for $C_{50}H_{53}BIrN_2NaO_4S.3H_2O$): C, 56.76; H, 5.62; N, 2.65; S, 3.03; Found: C, 56.77; H, 5.65; N, 2.65; S, 3.19.

5.9.1.7. Mononuclear sulfonated iridium(III) 4-phenylpyridyl complex (4.13)

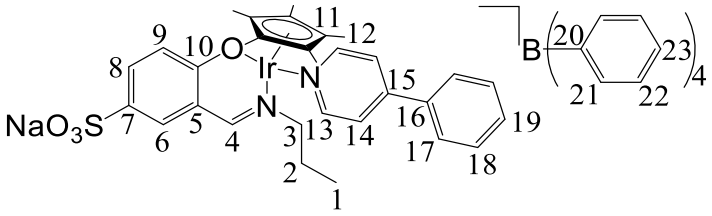

Yellow solid. **Yield**: 102.0 mg, 63%. **MP.**: 179.9ºC (decomposed). **^{1}H NMR** ($(CD_3)_2SO$): δ = 8.89 (m, 2H, H_{13}), 8.36 (s, 1H, H_4), 7.95 (m, 1H, H_{19}), 7.85 (d, 2H, J = 6 Hz, H_{17}), 7.66 (s, 1H, H_6), 7.60 (dd, J = 9 Hz, J = 2 Hz, 2H, H_{14}), 7.55 (m, 3H, H_9 H_{18}), 7.18 (m, 8H, H_{21}), 6.92 (t, 8H, J = 8 Hz, H_{22}), 6.85 (d, 1H, J = 9 Hz, H_8), 6.79 (t, 4H, J = 7 Hz, H_{23}), 3.93 (m, 2H, H_3), 1.55 (m, 17H, H_2 H_{12}), 0.86 (m, 3H, H_1). **^{13}C{^{1}H} NMR** ($(CD_3)_2SO$): δ = 164.06 (C_{16A}), 163.80 (C_4), 163.55 (C_{16B}), 163.06 (C_{16C}), 162.57 (C_{16D}), 150.55 (C_{13}), 135.46 (C_{21}), 132.79 (C_{19}), 129.25 (C_6 C_9), 127.27 (C_{18}), 126.88 (C_{17}), 125.20 (C_{22}), 121.41 (C_{23}), 120.88 (C_8 C_{14}), 114.95 (C_5), 92.79 (C_{11}), 66.60 (C_3), 23.63 (C_2), 10.73 (C_1), 8.02 (C_{12}). **FT-IR** (ATR): 1612 ν(C=N_{imine}). **HR-ESI-MS(+)**: 570.1288 [M-BPh_4-NC_5H_4Ph-Na+H]$^+$; **HR-ESI-MS(-)**: 750.1047 [M-BPh_4-2H]$^-$, 568.1277 [M-BPh_4-NC_5H_5Ph-Na-H]$^-$. **Elemental Analysis** (Calculated for $C_{55}H_{55}BIrN_2NaO_4S.3½H_2O$): C, 58.80; H, 5.53; N, 2.48; S, 2.84; Found: C, 58.69; H, 5.47; N, 2.47; S, 2.83.

5.9.1.8. Mononuclear sulfonated iridium(III) 4-ferrocenylpyridyl complex (4.14)

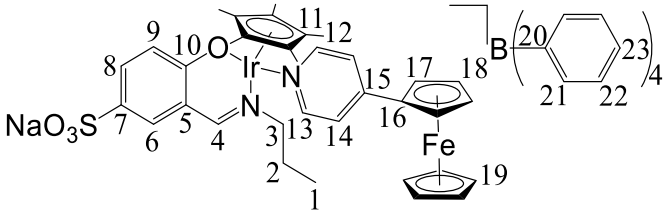

Red solid. **Yield**: 138.7 mg, 78%. **MP.**: 183.6ºC (decomposed). **^{1}H NMR** ($(CD_3)_2SO$): δ = 8.46 (d, 2H, J = 5 Hz, H_{13}), 8.28 (s, 1H, H_4), 7.73 (m, 2H, H_{14}), 7.65 (s, 1H, H_6), 7.61 (d, 2H, H_9),

7.18 (m, 8H, H_{21}), 6.92 (t, 8H, *J* = 7 Hz, H_{22}), 6.87 (d, 1H, *J* = 9 Hz, H_8), 6.79 (t, 4H, *J* = 7 Hz, H_{23}), 5.02 (m, 2H, H_{17}), 4.61 (m, 2H, H_{18}), 4.04 (m, 7H, H_{19} H_3), 1.50 (m, 17H, H_2 H_{12}), 0.73 (t, 3H, *J* = 7 Hz, H_1). **$^{13}C\{^1H\}$ NMR** ($(CD_3)_2SO$): δ = 164.02 (C_{16A}), 163.52 (C_{16B}), 163.45 (C_4), 163.03 ($C_{16C\ 4}$), 162.54 (C_{16D}), 149.77 (C_{13}), 135.44 (C_{21}), 132.55 (C_8), 131.75 (C_6), 126.57 (C_{14}), 125.15 (C_{22}), 122.55 (C_{15}), 122.45 (C_9), 121.38 (C_{23}), 116.23 (C_{15}), 92.69 (C_{11}), 78.58 (C_{16}), 71.58 (C_{17}), 70.00 (C_{19}), 67.52 (C_3), 67.15 (C_{18}), 23.66 (C_2), 10.73 (C_1), 7.99 (C_{12}). **FT-IR** (ATR): 1609 *ν*(C=N_{imine}). **HR-ESI-MS(+)**: 570.1283 [M-BPh_4-NC_5H_5Fc-Na+H]$^+$; **HR-ESI-MS(-)**: 568.1294 [M-BPh_4-NC_5H_4Fc-Na-H]$^-$, 831.6250 [M-BPh_4-Na-H]$^-$. **Elemental Analysis** (Calculated for $C_{59}H_{59}BFeIrN_2NaO_4S.4H_2O$): C, 56.87; H, 5.42; N, 2.25; S, 2.57; Found: C, 56.88; H, 5.37; N, 2.39; S, 2.73.

5.9.2. Trinuclear Sulfonated Complexes (4.15-4.22)

General Procedure

4.2 (30.0 mg, 0.0384 mmol for **4.15-4.16**; 53.6 mg, 0.0686 mmol for **4.17**; 18.0 mg, 0.0230 mmol for **4.18** and **4.22**; 20.8 mg, 0.0266 mmol for **4.19-4.21**) was dissolved in EtOH (10 ml). Excess NaOAc (10.4 mg, 0.127 mmol for **4.15-4.16**; 18.6 mg, 0.227 mmol for **4.17**; 12.5 mg, 0.152 mmol for **4.18** and **4.22**; 7.21 mg, 0.0879 mmol for **4.19-4.21**) was added and stirred for 30 minutes. $[Rh(\eta^5\text{-}C_5Me_5)Cl_2]_2$ (39.2 mg, 0.0634 mmol for **4.15-4.16**; 70.0 mg, 0.113 mmol for **4.17**; 47.0 mg, 0.0760 mmol for **4.18**) or $[Ir(\eta^5\text{-}C_5Me_5)Cl_2]_2$ (35.0 mg, 0.0439 mmol for **4.19-4.21**; 60.6 mg, 0.0760 mmol for **4.22**) was then dissolved into the solution which was stirred overnight. Pyridine (10.0 mg, 0.127 mmol for **4.15**; 6.95 mg, 0.0879 mmol for **4.19**), or 4-methylpyridine (11.8 mg, 0.127 mmol for **4.16**; 8.19 mg, 0. 0879 mmol for **4.20**), or 4-phenylpyridine (35.2 mg, 0.227 mmol for **4.17**; 13.6 mg, 0. 0879 mmol for **4.21**) or 4-ferrocenylpyridine (40.0 mg, 0.152 mmol for **4.18** and **4.22**) was then added and stirred for 2 hours. $NaBPh_4$ (43.4 mg, 0.127 mmol for **4.15-4.16**; 77.5 mg, 0.227 mmol for **4.17**; 26.0 mg, 0.152 mmol for **4.18** and **4.22**; 30.1 mg, 0.0879 mmol for **4.19-4.21**) was then added. The solution was then filtered by gravity and then the solvent of the filtrate removed using rotary evaporation. The solid residue was dissolved in DCM and filtered by gravity, after which *i*PrOH was added and the solvent was reduced and precipitation occurred to yield the solid products **4.15-4.22** which were dried under vacuum.

5.9.2.1. Trinuclear sulfonated rhodium(III) pyridyl complex (4.15)

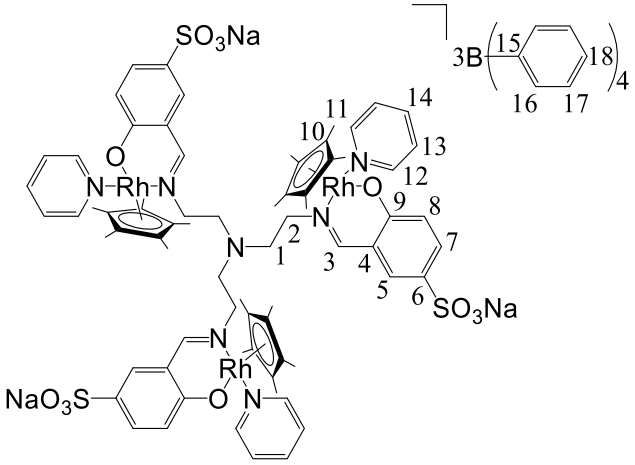

Red solid. **Yield**: 23.0 mg, 22%. **MP.**: 141.9ºC (decomposed). **^{1}H NMR** ($(CD_3)_2SO$): δ = 8.70 (m, 6H, H_{12}), 8.16 (s, 3H, H_3), 7.75 (m, 9H, H_{14} H_{13}), 7.48 (m, 6H, H_5 H_8), 7.18 (m, 24H, H_{16}), 6.92 (t, 24H, *J* = 7 Hz, H_{18}), 6.79 (m, 15H, H_{19} H_7), 4.02 (m, 6H, H_1), 1.55 (s, 51H, H_2 H_{11}). **^{13}C{^{1}H} NMR** ($(CD_3)_2SO$): δ = 164.05 (C_{15A}), 163.57 (C_{15B}), 163.32 (C_3), 163.07 (C_{15C}), 162.58 (C_{15D}), 152.79 (C_{12}), 138.98 (C_{14}), 135.48 (C_{16}), 129.27 (C_8), 128.85 (C_5), 126.61 (C_{13}), 125.21 (C_{17}), 122.82 (C_7), 121.42 (C_{18}), 115.16 (C_4), 97.91 (C_{10}), 69.73 (C_1), 61.95 (C_2), 8.73 (C_{11}). **FT-IR** (ATR): 1617 *v*($C{=}N_{imine}$), 1602 *v*($C{=}N_{pyr}$). **HR-ESI-MS(+)**: 373.1400 $[M\text{-}3BPh_4\text{-}3NC_5H_5{+}Na]^{4+}$. **Elemental Analysis** (Calculated for $C_{144}H_{144}B_3N_7Na_3O_{12}Rh_3S_3.2H_2O$): C, 63.89; H, 5.51; N, 3.62; S, 3.55; Found: C, 64.01; H, 5.71; N, 3.51; S, 3.46.

5.9.2.2. Trinuclear sulfonated rhodium(III) 4-methylpyridyl complex (4.16)

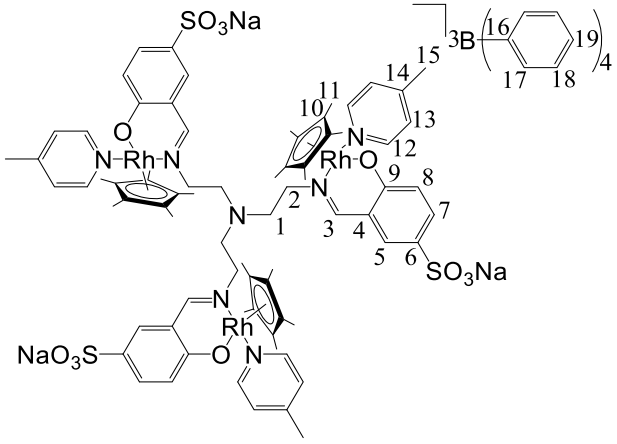

Red solid. **Yield**: 44.9 mg, 43%. **MP.**: 156.9ºC (decomposed). **^{1}H NMR** ($(CD_3)_2SO$): δ = 8.53 (d, 6H, H_{12}, *J* = 6 Hz), 8.25 (s, 3H, H_3), 7.61 (m, 6H, H_5 H_8), 7.52 (m, 6H, H_{13}), 7.18 (m, 24H, H_{17}), 6.92 (m, 27H, H_{18} H_7), 6.78 (t, 12H, H_{19}, *J* = 7 Hz), 3.98 (m, 6H, H_1), 2.73 (s, 9H, H_{15}), 1.56 (s, 51H, H_2 H_{11}). **^{13}C{^{1}H} NMR** ($(CD_3)_2SO$): δ = 164.05 (C_{16A}), 163.35 (C_{16B}), 163.05 (C_{16C}),

162.99 (C_3), 162.57 (C_{16D}), 152.06 (C_{12}), 140.61 (C_{14}), 135.46 (C_{17}), 132.61 (C_8), 132.47 (C_5), 127.42 (C_{13}), 127.17 (C_{18}), 120.65 (C_7), 121.41 (C_{19}), 114.51 (C_4), 93.85 (C_{10}), 71.57 (C_1), 61.93 (C_2), 20.54 (C_{15}), 7.98 (C_{11}). **FT-IR** (ATR): 1615 *v*(C=N_{imine}), 1600 *v*(C=N_{pyr}). **HR-ESI-MS(+)**: 373.1400 [M-3BPh_4-3$NC_5H_4CH_3$+Na]$^{4+}$. **Elemental Analysis** (Calculated for C-$_{147}H_{150}B_3N_7Na_3O_{12}Rh_3S_3.H_2O$): C, 64.65; H, 5.61; N, 3.59; S, 3.52; Found: C, 64.68; H, 5.73; N, 3.49; S, 3.48.

5.9.2.3. Trinuclear sulfonated rhodium(III) 4-phenylpyridyl complex (4.17)

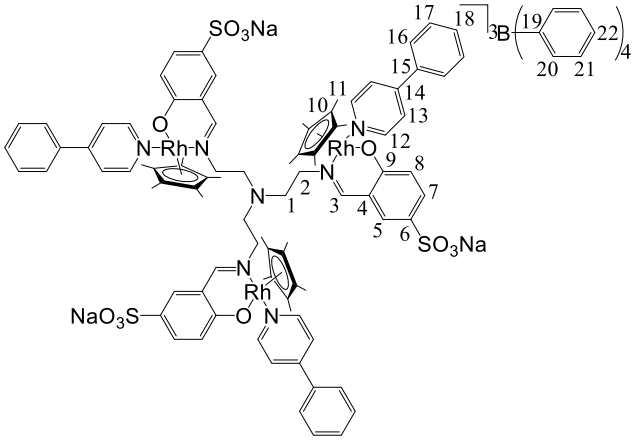

Orange solid. **Yield**: 70.0 mg, 35%. **MP.**: 201.4ºC (decomposed).). **^{1}H NMR** ($(CD_3)_2SO$): δ = 8.64 (m, 6H, H_{12}), 8.20 (s, 3H, H_3), 7.83 (m, 6H, H_{13} H_{16}), 7.54 (m, 6H, H_5 H_8), 7.54 (m, 9H, H_{17} H_{18}), 7.18 (m, 24H, H_{17}), 6.92 (m, 27H, H_{18} H_7), 6.78 (t, 12H, H_{19}, *J* = 7 Hz), 3.92 (m, 6H, H_1), 1.50 (s, 51H, H_2 H_{11}). **^{13}C{^{1}H} NMR** ($(CD_3)_2SO$): δ = 164.05 (C_{19A}), 163.55 (C_{19B}), 163.06 (C_{19C}), 163.65 (C_3), 162.57 (C_{19D}), 149.58 (C_{12}), 135.70 (C_{18}), 135.46 (C_{20}), 132.48 (C_8), 132.37 (C_5), 129.35 (C_{17}), 126.85 (C_{16}), 125.18 (C_{21}),121.42 (C_7 C_{13} C_{22}), 115.15 (C_4), 94.32 (C_{10}), 72.47 (C_1), 61.94 (C_2), 8.01 (C_{11}). **FT-IR** (ATR): 1609 *v*(C=$N_{imine + pyr}$). **HR-ESI-MS(+)**: 373.1398 [M-3BPh_4-3NC_5H_4Ph+Na]$^{4+}$. **Elemental Analysis** (Calculated for C-$_{162}H_{156}B_3N_7Na_3O_{12}Rh_3S_3.2H_2O$): C, 66.29; H, 5.49; N, 3.34; S, 3.28; Found: C, 66.35; H, 5.55; N, 3.51; S, 3.17.

5.9.2.4. Trinuclear sulfonated rhodium(III) 4-ferrocenylpyridyl complex (4.18)

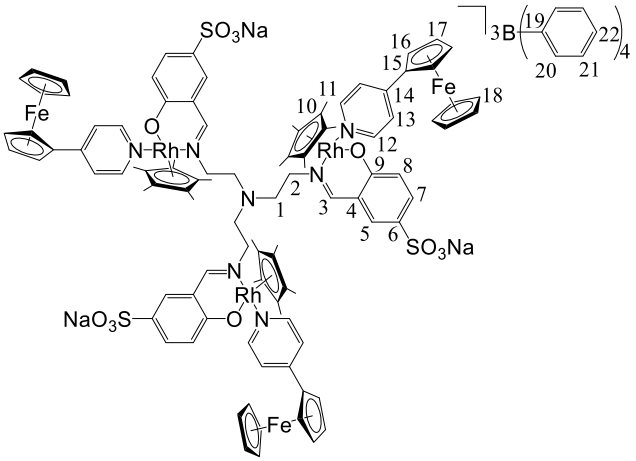

Orange solid. **Yield**: 62.1 mg, 84%. **MP.**: 173.3ºC (decomposed). **^{1}H NMR** ($(CD_3)_2SO$): δ = 8.44 (d, 6H, H_{12}, *J* = 6 Hz), 8.20 (s, 3H, H_3), 7.84 (d, 3H, H_8, *J* = 7 Hz), 7.83 (s, 3H, H_5), 7.53 (m, 6H, H_{13}), 7.18 (m, 24H, H_{20}), 6.93 (m, 27H, H_{21} H_7), 6.79 (t, 12H, H_{22}, *J* = 7 Hz), 5.11 (s, 6H, H_{16}), 4.67 (s, 6H, H_{17}), 4.09 (s, 15H, H_{18}), 4.04 (m, 6H, H_1), 1.61 (s, 51H, H_2 H_{11}). **^{13}C{^{1}H} NMR** ($(CD_3)_2SO$): δ = 163.74 (C_{19A}), 163.42 (C_{19B}), 163.09 (C_{19C}), 162.76 (C_{19D}), 162.03 (C_3), 151.67 (C_{12}), 135.40 (C_{20}), 128.87 (C_8), 128.75 (C_5), 125.09 (C_{21}), 123.28 (C_7), 122.62 (C_{14}), 122.43 (C_{13}), 121.32 (C_{22}), 115.09 (C_4), 94.60 (C_{10}), 77.46 (C_{15}), 71.70 (C_{16}), 70.17 (C_{18}), 69.99 (C_1), 67.67 (C_{17}), 61.86 (C_2), 8.18 (C_{11}). **FT-IR** (ATR): 1608 ν(C=$N_{imine + pyr}$). **HR-ESI-MS(+)**: 756.2974 $[M\text{-}_3BPh_4]^{3+}$, 373.1404 $[M\text{-}3BPh_4\text{-}3NC_5H_4Fc+Na]^{4+}$. **Elemental Analysis** (Calculated for $C_{174}H_{168}B_3Fe_3N_7Na_3O_{12}Rh_3S_3.H_2O$): C, 64.48; H, 5.29; N, 3.03; S, 2.97; Found: C, 64.58; H, 5.37; N, 3.19; S, 3.09.

5.9.2.5. Trinuclear sulfonated iridium(III) pyridyl complex (4.19)

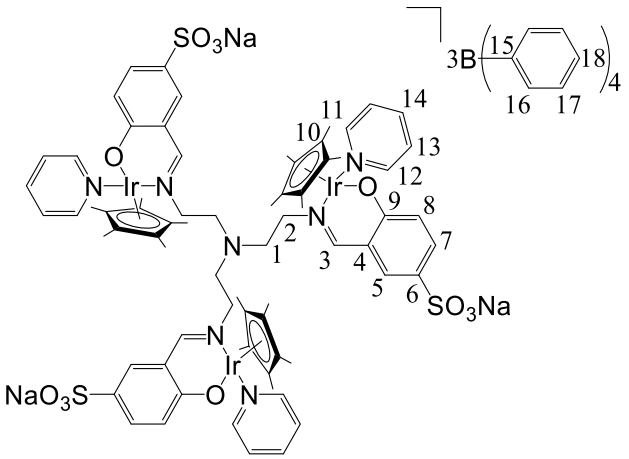

Pale brown solid. **Yield**: 63.1 mg, 81%. **MP.**: 167.8ºC (decomposed). **^{1}H NMR** ($(CD_3)_2SO$): δ = 8.78 (d, 6H, H_{12}, *J* = 5 Hz), 8.50 (s, 3H, H_3), 8.20 (t, 3H, H_{14}, *J* = 8 Hz), 7.77 (m, 6H, H_7 H_8), 7.30 (d, 6H, H_{13}, *J* = 7 Hz), 7.18 (m, 24H, H_{16}), 7.07 (d, 3H, H_8, *J* = 7 Hz), 6.92 (t, 24H, *J* = 7 Hz, H_{17}), 6.79 (t, 12H, *J* = 7 Hz, H_{19}), 4.18 (m, 6H, H_1), 1.56 (s, 51H, H_2 H_{11}). **^{13}C{^{1}H} NMR** ($(CD_3)_2SO$): δ = 171.87 (C_6), 164.05 (C_{15A}), 163.56 (C_{15B}), 163.06 (C_{15C}), 162.57 (C_{15D}), 161.33 (C_3), 153.71 (C_{12}), 139.05 (C_{14}), 135.47 (C_{16}), 129.29 (C_5), 128.89 (C_8), 125.21 (C_{17}), 125.18 (C_{13}), 122.47 (C_7), 121.42 (C_{18}), 115.15 (C_4), 93.60 (C_{10}), 64.59 (C_1), 54.31 (C_2), 8.03 (C_{11}). **FT-IR** (ATR): 1619 *v*(C=N_{imine}), 1605 *v*(C=N_{pyr}). **HR-ESI-MS(+)**: 405.1155 [M-3BPh_4-3NC_5H_5-3Na+5K+4CH_3CN]$^{5+}$, 442.0894 [M-3BPh_4-3NC_5H_5+Na]$^{4+}$. **Elemental Analysis** (Calculated for $C_{144}H_{144}B_3Ir_3N_7Na_3O_{12}S_3.3H_2O$): C, 58.14; H, 5.01; N, 3.30; S, 3.23; Found: C, 58.25; H, 5.19; N, 3.21; S, 3.41.

5.9.2.6. Trinuclear sulfonated iridium(III) 4-methylpyridyl complex (4.20)

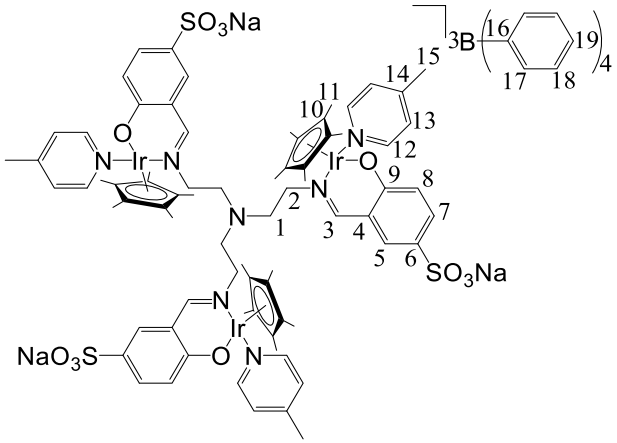

Pale brown solid. **Yield**: 60.9 mg, 77%. **MP.**: 172.7ºC (decomposed). **^{1}H NMR** ($(CD_3)_2SO$): δ = 8.60 (d, 6H, H_{12}, *J* = 7 Hz), 8.43 (s, 3H, H_3), 7.61 (m, 12H, H_{13} H_5 H_7), 7.18 (m, 24H, H_{17}),

6.92 (t, 27H, H_{18} H_8, *J* = 7 Hz), 6.78 (t, 12H, H_{19}, *J* = 7 Hz), 4.15 (m, 6H, H_1), 2.34 (s, 9H, H_{15}), 1.57 (s, 51H, H_2 H_{11}). **$^{13}C\{^1H\}$ NMR** ($(CD_3)_2SO$): δ = 175.86 (C_6), 164.04 (C_{16A}), 163.54 (C_{16B}), 163.05 (C_{16C}), 162.57 (C_{16D}), 161.31 (C_3), 153.71 (C_{12}), 140.76 (C_{14}), 135.46 (C_{17}), 129.25 (C_5), 128.89 (C_8), 125.19 (C_{17}), 127.23 (C_{13}), 121.41 (C_7 C_{19}), 115.15 (C_4), 94.26 (C_{10}), 60.26 (C_1), 53.77 (C_2), 22.79 (C_{15}), 7.81 (C_{11}). **FT-IR** (ATR): 1618 *v*($C=N_{imine + pyr}$). **HR-ESI-MS(+)**: 405.1007 $[M\text{-}3BPh_4\text{-}3NC_5H_4CH_3\text{-}3Na+5K+4CH_3CN]^{5+}$. **Elemental Analysis** (Calculated for $C_{147}H_{150}B_3Ir_3N_7Na_3O_{12}S_3 3H_2O$): C, 58.17; H, 5.18; N, 3.23; S, 3.17; Found: C, 58.23; H, 5.25; N, 3.17; S, 3.18.

5.9.2.7. Trinuclear sulfonated iridium(III) 4-phenylpyridyl complex (4.21)

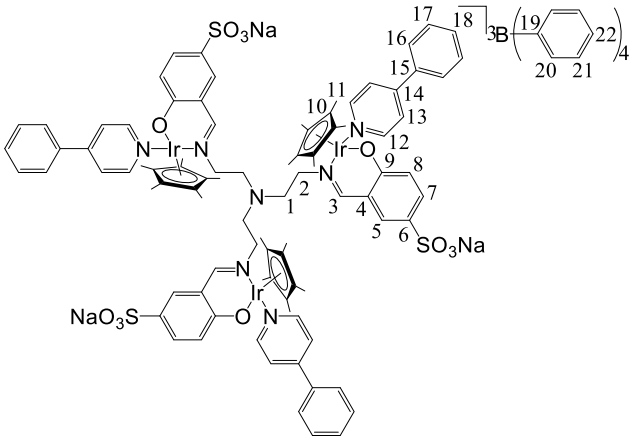

Pale brown solid. **Yield**: 60.0 mg, 71%. **MP.**: 172.4ºC (decomposed). **^1H NMR** ($(CD_3)_2SO$): δ = 8.77 (d, 6H, H_{12}, *J* = 6 Hz), 8.65 (s, 3H, H_3), 7.95 (m, 3H, H_{18}), 7.84 (d, 6H, $H_{16,}$ *J* = 5 Hz), 7.74 (m, 6H, H_7 H_5), 7.60 (m, 6H, H_{13}), 7.53 (m, 9H, H_{17} H_8), 7.18 (m, 24H, H_{20}), 6.92 (t, 24H, H_{21}, *J* = 7 Hz), 6.78 (t, 12H, H_{22}, *J* = 7 Hz), 4.12 (m, 6H, H_1), 1.60 (s, 51H, H_2 H_{11}). **$^{13}C\{^1H\}$ NMR** ($(CD_3)_2SO$): δ = 163.77 (C_{19A}), 163.44 (C_{19B}), 163.12 (C_{19C}), 162.79 (C_{19D}), 160.87 (C_3),153.60 (C_{12}), 135.42 (C_{20}), 130.93 (C_{18}),129.40 (C_8), 129.08 (C_5), 127.23 (C_{16}), 126.68 (C_{17}), 125.11 (C_{21}), 121.35 (C_{22}), 121.09 (C_7 C_{13}), 115.12 (C_4), 94.28 (C_{10}), 68.64 (C_1), 62.00 (C_2), 7.85 (C_{11}). **FT-IR** (ATR): 1611 *v*($C=N_{imine + pyr}$). **HR-ESI-MS(+)**: 405.0974 $[M\text{-}3BPh_4\text{-}3NC_5H_4Ph\text{-}3Na+5K+4CH_3CN]^{5+}$. **Elemental Analysis** (Calculated for $C_{162}H_{156}B_3Ir_3N_7Na_3O_{12}S_3.4H_2O$): C, 60.07; H, 5.10; N, 3.03; S, 2.97; Found: C, 59.98; H, 5.11; N, 3.10; S, 3.05.

5.9.2.8. Trinuclear sulfonated iridium(III) 4-ferrocenylpyridyl complex (4.22)

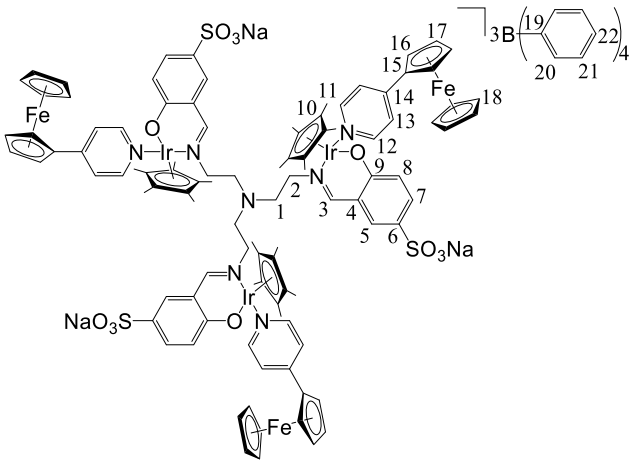

Orange solid. **Yield**: 77.0 mg, 96%. **MP.**: 172.9ºC (decomposed). **^{1}H NMR** ($(CD_3)_2SO$): δ = 8.49 (d, 6H, H_{12}, *J* = 6 Hz), 8.42 (s, 3H, H_3), 7.83 (m, 6H, H_5 H_7), 7.57 (m, 6H, H_{13}), 7.18 (m, 24H, H_{20}), 6.93 (m, 27H, H_{21} H_8), 6.79 (t, 12H, H_{22}, *J* = 7 Hz), 5.12 (s, 6H, H_{16}), 4.69 (s, 6H, H_{17}), 4.10 (m, 21H, H_{18} H_1), 1.61 (s, 51H, H_2 H_{11}). **^{13}C{^{1}H} NMR** ($(CD_3)_2SO$): δ = 163.75 (C_{19A}), 163.42 (C_{19B}), 163.09 (C_{19C}), 162.77 (C_{19D}), 161.31 (C_3), 152.30 (C_{12}), 135.41 (C_{20}), 128.76 (C_8), 128.35 (C_5), 125.11 (C_{21}), 123.49 (C_7), 122.94 (C_{14}), 123.16 (C_{13}), 121.33 (C_{22}), 115.10 (C_4), 94.12 (C_{10}), 77.04 (C_{15}), 71.96 (C_{16}), 70.28 (C_{18}), 69.57 (C_1), 67.69 (C_{17}), 61.87 (C_2), 7.79 (C_{11}). **FT-IR** (ATR): 1611 *ν*($C{=}N_{imine\ +\ pyr}$). **HR-ESI-MS(+)**: 405.0922 [M-3BPh_4-3NC_5H_4Fc-3Na+5K+4CH_3CN]$^{5+}$. **Elemental Analysis** (Calculated for $C_{174}H_{168}B_3Ir_3N_7Na_3O_{12}S_3.2H_2O$): C, 59.25; H, 4.92; N, 2.78; S, 2.73; Found: C, 59.18; H, 4.98; N, 2.88; S, 2.65.

5.10. X-ray Crystallography

Single-crystal X-ray diffraction data were collected on a Nonius Kappa-CCD diffractometer using graphite monochromated MoKα radiation (λ = 0.71073 Å). Temperature was controlled by an Oxford Cryostream cooling system (Oxford Cryostat). The strategy for the data collections was evaluated using the Bruker Nonius "Collect" program. Data were scaled and reduced using DENZO-SMN software.[9] Absorption correction was performed using SADABS.[10] The structure was solved by direct methods and refined employing full-matrix least-squares with the program SHELXL-97[11] refining on F^2. The diagrams were produced using the program PovRay[12] and graphic interface X-seed.[13]

Table 1. Crystallographic and structure refinement parameters for complexes (**2.7**-**2.9**)

Compound Number	**2.7**	**2.8**	**2.9**
Chemical formula	$C_{24}H_{27}ClNORh$	$C_{24}H_{27}ClIrNO$	$C_{23}H_{27}ClF_6N_2OPRh$
Formula weight	483.83	573.14	630.80
Crystal system	Triclinic	Triclinic	Triclinic
Space group	P-1	P-1	P-1
Crystal colour and shape	Orange block	Red block	Yellow block
Crystal size (mm)	0.17x0.13x0.04	0.10x0.08x0.07	0.16x0.09x0.04
a (Å)	8.5513(7)	10.9174(5)	8.4081(17)
b (Å)	8.6221(7)	13.4833(4)	11.002(2)
c (Å)	16.2053(12)	15.0954(7)	13.926(3)
α (°)	99.6580(10)	99.470(2)	88.55(3)
β (°)	96.9070(10)	103.502(2)	88.94(3)
γ (°)	115.1960(10)	92.553(2)	75.95(3)
V (Å^3)	1040.92(14)	2123.23(15)	1249.2(4)
Z	2	4	2
T	173(2)	173(2)	173(2)
D_c (gcm^{-3})	1.554	1.793	1.677
μ (mm^{-1})	0.963	6.428	0.919
Unique reflections	5222	9631	5702
Reflections used	4593	6877	4780
Goodness-of-fit	1.045	1.041	1.063

All non-hydrogen atoms were refined anisotropically. In **2.7** all hydrogen atoms, except H1, were placed in idealised positions and refined in riding models with U_{iso} assigned the values to be 1.2 or 1.5 times those of their parent atoms and the constraint distances of C-H ranging from 0.95 Å to 0.99 Å. The hydrogen H1 was located in the electron difference maps and refined freely. In **2.8** all hydrogen atoms, except H1A and H1B, were placed in idealised positions and refined in riding models with U_{iso} assigned the values to be 1.2 or 1.5 times U_{eq} of the atoms to which they are attached and the constraint distances of C-H ranging from 0.95 Å to 0.99 Å. The hydrogen H1A and H1B were located in the difference Fourier maps and refined with bond length constraint d(O-H) = 0.97 Å and with $U_{iso}(H) = 1.5xU_{eq}(O)$. In **2.9** all non-hydrogen atoms, except F4 and F6, were refined anisotropically. The fluorine atoms F4 and F6 were refined with isotropic displacement parameters due to their high thermal motions. In **2.10** the oxygen atom O1 was restrained with similar anisotropic displacement parameters as C1 due to high temperature factor shown by O1. In **2.11** and **2.14** the hydrogen atoms, except H1, were placed in idealised positions and refined in riding models with U_{iso} assigned

the values to be 1.2 or 1.5 times U_{eq} of the atoms to which they are attached and the constraint distances of C-H ranging from 0.95 Å to 1.00 Å. The hydrogen H1 was located in the difference Fourier maps and in **2.9** refined with bond length constraint d(O1-H1) = 0.97 Å, while in **2.10** refined with U_{iso} (H1) = U_{eq} (O1) and in **2.12** and **2.13** refined independently.

Table 2. Crystallographic and structure refinement parameters for complexes (**2.10**-**2.12**)

Compound Number	**2.10**	**2.11**	**2.12**
Chemical formula	$C_{23}H_{27}ClF_6IrN_2OP$	$C_{23}H_{26}ClF_6N_2OPRu$	$C_{24}H_{27}ClNO_2Rh$
Formula weight	720.09	627.95	499.83
Crystal system	Triclinic	Triclinic	Orthorhombic
Space group	P-1	P-1	$Pna2_1$
Crystal colour and shape	Red block	Orange plate	Red block
Crystal size (mm)	0.10x0.08x0.07	0.13x0.11x0.09	0.22x0.11x0.03
a (Å)	8.4054(2)	8.9720(3)	17.9479(13)
b (Å)	11.0226(4)	10.8592(4)	15.1006(11)
c (Å)	13.9230(4)	13.9422(4)	7.9655(6)
α (º)	88.786(2)	74.505(2)	90
β (º)	89.410(2)	82.981(2)	90
γ (º)	75.696(2)	72.044(2)	90
V (Å³)	1249.2(4)	1244.07(7)	2158.8(3)
Z	2	2	4
T	173(2)	173(2)	173(2)
D_c (gcm^{-3})	1.914	1.676	1.538
μ (mm^{-1})	5.577	0.866	0.935
Unique reflections	5683	6176	5097
Reflections used	5125	6176	4166
Goodness-of-fit	1.068	1.013	1.050

In **2.7** the structure was refined to R factor of 0.0261, the highest peak is 0.61 e $Å^{-3}$, 0.87 Å from Rh1 and the deepest hole is -0.51 e $Å^{-3}$, 0.95 Å from Rh1. In **2.8** the structure was refined to R factor of 0.0204, the highest peak is 2.48 e $Å^{-3}$, 0.93 Å from Ir1B or 2.37 e $Å^{-3}$, 1.03 Å from Ir1A and the deepest hole is -0.89 e $Å^{-3}$, 0.89 Å from Ir1B or -0.84 e $Å^{-3}$, 0.97 Å from Ir1A. In **2.9** the structure was refined to R factor of 0.0486, the highest peak is 3.15 e $Å^{-3}$, 0.63 Å from F4 and the deepest hole is -1.43 e $Å^{-3}$, 0.63 Å from F4. In **2.10** the structure was refined to R factor of 0.0204, the highest peak is 1.57 e $Å^{-3}$, 0.93 Å from N2 and the deepest hole is -0.79 e $Å^{-3}$, 0.84 Å from Ir1. In **2.11** the structure was refined to R factor of 0.0420, the highest peak is 2.45 e $Å^{-3}$, 0.88 Å from Ru1 and the deepest hole is -0.85 e $Å^{-3}$, 0.80 Å from Ru1. In

2.12 the structure was refined to R factor of 0.0386, the highest peak is 1.37 e $Å^{-3}$, 0.48 Å from H1A and the deepest hole is -0.60 e $Å^{-3}$, 0.65 Å from O1. In **2.13** the structure was refined to R factor of 0.0240, the highest peak is 0.41 e $Å^{-3}$, 0.78 Å from Ir1 and the deepest hole is -0.53 e $Å^{-3}$, 0.40 Å from Ir1. In **2.14** the structure was refined to R factor of 0.0259, the highest peak is 0.51 e $Å^{-3}$, 0.82 Å from Ru1 and the deepest hole is -0.37 e $Å^{-3}$, 0.76 Å from Ru1. CCDC Numbers for the complexes are: **2.9**: 1026858; **2.10**: 1026859; **2.11**: 1035358; **2.12**: 1026860; **2.13**: 1026861; **2.14**: 1035356.

Table 3. Crystallographic and structure refinement parameters for complexes (**2.13**-**2.14**)

Compound Number	**2.13**	**2.14**
Chemical formula	$C_{24}H_{27}ClIrNO_2$	$C_{24}H_{26}ClNO_2Ru$
Formula weight	589.12	496.98
Crystal system	Monoclinic	Monoclinic
Space group	$P2_1$	Cc
Crystal colour and shape	Orange block	Orange block
Crystal size (mm)	0.16x0.12x0.04	0.18x0.13x0.12
a (Å)	7.4741(7)	15.6588(7)
b (Å)	15.7546(13)	16.4313(8)
c (Å)	9.86.11(8)	8.8012(4)
α (º)	90	90
β (º)	112.149(2)	109
γ (º)	90	90
V (Å³)	1075.47(16)	2133.79(17)
Z	2	4
T	173(2)	173(2)
D_c (gcm^{-3})	1.819	1.547
μ (mm^{-1})	6.352	0.880
Unique reflections	5344	6270
Reflections used	4941	27056
Goodness-of-fit	1.039	1.013

5.11. NMR Experiments

5.11.1. Stability Investigation

The mononuclear complexes, **2.10** and **2.13**, and the trimeric complex **2.16** were dissolved in $(CD_3)_2SO$ and H_2O, in a 50:50 ratio, and warmed at 37 ºC, to mimic physiological conditions.

The sample was monitored by ^{1}H NMR spectroscopy for aquatic stability at varying times up to 24 hours.

The mononuclear iridium(III) complex **3.4** was dissolved in D_2O and monitored by ^{1}H and $^{31}P\{^{1}H\}$ NMR spectroscopy for aqueous stability for 48 hours.

The mononuclear sulfonated anionic complexes **4.3-4.4** were dissolved in $(CD_3)_2SO$ and monitored by ^{1}H NMR spectroscopy for stability for 48 hours, while the mononuclear sulfonated complexes **4.7-4.14** were dissolved in $(CD_3)_2SO$ and monitored by ^{1}H NMR spectroscopy daily for 3 weeks. The trinuclear sulfonated complex **4.18** was dissolved in a 50:50 mixture of $(CD_3)_2SO$ and monitored by ^{1}H NMR spectroscopy for 48 hours.

5.11.2. Interactions with 5'-GMP

The *N,N*- mononuclear complex, **2.10**, and the *N,O*- mononuclear complex, **2.13**, and an equimolar amount of 5'-GMP were dissolved in $(CD_3)_2SO$ and H_2O, in a 50:50 ratio, and warmed at 37 ^{o}C, to mimic physiological conditions. The mixture was monitored by ^{1}H NMR spectroscopy for interactions with the model DNA at varying times up to 24 hours.

The mononuclear iridium(III) complex, **3.4**, and an equimolar amount of 5'-GMP were dissolved together in D_2O and warmed to 37 ^{o}C, to mimic physiological conditions. The samples were monitored using ^{1}H and $^{31}P\{^{1}H\}$ NMR spectroscopy to monitor interactions.

The trinuclear sulfonated complex **4.18** and an equimolar amount of 5'-GMP were dissolved in $(CD_3)_2SO$ and H_2O, in a 50:50 ratio, and warmed at 37 ^{o}C. The mixture was monitored by ^{1}H NMR spectroscopy for interactions with the model DNA at varying times up to 48 hours.

5.11.3. Interactions with Histidine

The mononuclear Ir complex, **3.4**, and an equimolar amount of Histidine were dissolved together in D_2O and warmed to 37 ^{o}C, to mimic physiological conditions. The samples were monitored using ^{1}H NMR spectroscopy to monitor interactions.

5.12. UV-Vis Absorption Studies

Absorption studies of a 0.33 mM solution of **3.4** in H_2O with 0.2 mM HEPES buffer, pH 7.4 were performed in the range 350-250 nm. Solutions of Red Salmon testes DNA sodium salt were prepared fresh before each experiment using milli-Q water. 50 µL aliquots of 45 nM DNA

stock solution were added to **3.4** to make the DNA concentrations: 2.14, 4.09, 5.87, 7.50, 9.00, 10.4, 11.7 and 12.9 nM.

5.13. Biological Studies

5.13.1. Cell Culture

Human A2780 and A2780cisR ovarian cancer cells and KMST-6 cells were obtained from the European Collection of Cell Cultures (Salisbury, UK). A2780 and A2780cisR cells were grown routinely in RPMI-1640 medium, KMST-6 cells in DMEM medium, both media supplemented with 10% fetal calf serum (FCS) and antibiotics (Penicillin Streptomycin) at 37 °C and 5% CO_2. Cytotoxicity was determined using the WST-1 assay (WST-1 = (4-[3-(4-Iodophenyl)-2-(4-nitrophenyl)-2H-5-tetrazolio)-1,3-benzene disulfonate). Cells were seeded in 96-well plates as monolayers with 100 µL of cell solution (approximately 5 000 cells) per well and pre-incubated for 24 h in medium supplemented with 10% FCS. Compounds were prepared as DMSO solutions then immediately dissolved in the culture medium and serially diluted to the appropriate concentration, to give a final DMSO concentration of 0.5%. 100 µL of drug solution was added to each well and the plates were incubated for another 24 h. Subsequently, WST-1 (10 µL solution) was added to the cells and the plates were incubated for a further 3 h. The WST-1 tetrazolium salt is cleaved to a soluble formazan by a cellular mechanism, succinate-tetrazolium reductase system (EC 1.3.99.1), which occurs primarily at the cell surface. This bioreduction depends largely on the cellular production of NAD(P)H within metabolically intact and viable cells. The optical density, directly proportional to the number of surviving cells, was quantified at 450 nm, and background correction was performed at 600 nm, using a multiwell plate reader and the fraction of surviving cells was calculated from the absorbance of untreated control cells. Evaluation is based on means from three microcultures per concentration level.

The WHCO1 oesophageal cancer cell-line was derived from a biopsy of primary oesophageal squamous cell carcinoma of South African origin [14]. Cells were cultured at 37 °C under 5 % CO_2 without antibiotics in DMEM (Dulbecco's Modified Eagle Medium) containing 10 % FBS (Gibco). Cytotoxicity of compounds was evaluated using the standard MTT 3-(4,5-Dimethylthiazol-2-yl)-2,5-diphenyltetrazolium bromide (Sigma) cellular viability assay. Briefly cells were seeded at a density of 2.5 x 10^3 cells per well in 96 well plates and allowed to settle overnight. A stock solution of each compound in water (2 mM) was prepared. The compound was then added to the cells in triplicate to a concentration of 200 µM. After a 48 h incubation period, 10 µL of 5 mg/mL MTT was added and incubated with the cells for 4 h. The reaction

was then quenched by addition of 100 μL 10 % SLS in 0.01 M HCl to solubilize the formazan crystals. The plates were read at 595 nm on a Multiscan FC plate reader (Thermo Scientific), and data was analysed using Graphpad Prism 4 software, sigmoidal dose-response variable slope curve fitting.

5.14. References

[1] M. A. Bennett, T. N. Huang, T. W. Matheson and A. K. Smith, *Inorg. Synth.* **1982**, *21*, 74-78.

[2] C. White, A. Yates and P.M. Maitlis, *Inorg. Synth.* **1992**, *29*, 228-234.

[3] Ivonne A. Müller, Felix Kratz, Manfred Jung and André Warnecke, *Tetrahedron Lett.* **2010**, *51*, 4371-4374.

[4] M. Sánchez, H. Höpfl, M.E. Ochoa, N. Farfán, R. Santillan and S. Rojas-Lima, *Chem. Eur. J.* **2002**, *8*, 612-621.

[5] F-X. Legrand, F. Hapiot a, S. Tilloy, A. Guerriero, M. Peruzzini, L. Gonsalvi and E. Monflier, *Appl. Catal. A* **2009**, *362*, 62-66.

[6] J.P. Hermes, F. Sander, T. Peterle, R. Urbani, T. Pfohl, D. Thompson and M. Mayor, *Chem. Eur. J.* **2011**, *17*, 13473-13481.

[7] V. Cadierno, J. Francos and J. Gimeno, *Chem. Eur. J.* **2008**, *14*, 6601-6605.

[8] E.B. Hager, B.C.E. Makhubela and G.S. Smith, *Dalton Trans.* **2012**, *41*, 13927-13935.

[9] Z. Otwinowski and W. Minor, *Methods in Enzymology, Macromolecular Crystallography, Part A*, **1997**, 307-326.

[10] SADABS, G.M. Sheldrick, (1996)

[11] G.M. Sheldrick, *Acta Cryst.* **2008**, *A64*, 112-122.

[12] http://www.povray.org/.

[13] L.J. Barbour, *J. Supramol.Chem.* **2001**, *1*, 189-191.

[14] R.B. Veale and A.L. Thornley, *S. Afr. J. Sci.* **1989**, *85*, 375-379.

Chapter 6: Conclusions and Future Outlook

6. Conclusions

6.1 Synthesis

New mono- and trinuclear PGM complexes containing rhodium(III), iridium(III) and ruthenium(II) were synthesized and characterized using an array of spectroscopic and analytical techniques. These complexes are subdivided into three main series, based on the ligand type used.

Firstly, three Schiff base ligands were used to prepare three new trimeric ester containing ligands **2.4-2.6**. From these ligands eight mono- and eight trinuclear PGM complexes **2.7-2.22** were prepared. The characterization of these *C,N*-benzaldiminato, *N,N*-pyridylimine or *N,O*-salicylaldiminato complexes revealed that the ligands act as bidentate donors to the metal center. Single crystal X-ray diffraction was used to confirm this for the mononuclear complexes.

Secondly, A new water soluble cationic trimeric ligand **3.2** was prepared from the alkylation of PTA. The monomeric analogue **3.1** was also prepared. Both cationic ligands were metallated at the phosphorous of the alkylated PTA moiety, this was confirmed by the appropriate downfield shifts observed in the ^{31}P NMR spectra. Three mono- and three trinuclear water soluble PGM complexes **3.3-3.8**, were afforded.

Thirdly, a trimeric water soluble sulfonated ligand **4.2** was prepared *via* Schiff base condensation. The monomeric analogue was similarly prepared **4.1**. Two mono- and two trinuclear anionic PGM *N,O*-salicylaldiminato complexes **4.3-4.6** were prepared from the sulfonated ligands. A further eight mono- and eight trinuclear sulfonated complexes **4.7-4.22** were also synthesized from the same ligands. Displacement of the metal-chloro ligand was achieved with a selection of *N*-donor ligands and the complexes isolated as tetraphenylborate salts.

6.2. *In vitro* Antitumor Activity and Biological Evaluation

The ester containing trinuclear PGM complexes, mononuclear analogues and ligands were evaluated for *in vitro* antitumor activity. The monomeric ligands **2.1-2.3** were inactive, whilst

the more lipophilic trimeric ligands **2.4-2.6** displayed some slight activity. All the complexes **2.7-2.22** exhibited moderate to high activity against the human ovarian cisplatin sensitive A2780 and cisplatin resistant A2780*cis*R cancer cells. The trinuclear complexes **2.15-2.22** exhibited greater activity than the mononuclear analogues. The trinuclear cationic *N,N*-pyridylimine containing complexes **2.17-2.18** were the most active. All complexes **2.7-2.22** exhibited roughly similar activities in both the cisplatin sensitive and cisplatin resistant cell lines with the exception of one, which suggests that these complexes may have a different mode of action to that of cisplatin. The trinuclear *C,N*-benzaldiminato complexes **2.15-2.16** showed poor selectivity towards non-tumorigenic human KMST-6 skin cells, whilst the *N,N*-pyridylimine and *N,O*-salicylaldiminato complexes **2.17-2.22** were moderately selective. NMR studies performed showed that the most active complex **2.18** and mononuclear analogue **2.10** are inert in aqueous environments. The most active mononuclear *N,O*-salicylaldiminato complex **2.13** displayed the ability to interact with 5′-GMP while on the other hand the most active *N,N*-pyridylimine complex **2.10** did not, as observed by NMR studies.

The cationic alkylated PTA compounds **3.1-3.8** were evaluated for i*n vitro* antitumor activity against the human esophageal cancer cell line WHCO1. The ligands **3.1-3.2** were inactive against the tumor cells. The metal complexes **3.3-3.8** displayed activity against the esophageal cancer cells and a nuclearity dependent activity relationship was observed for the rhodium(III) and ruthenium(II) complexes. However, the most active against the esophageal cancer cells for this series was the mononuclear iridium(III) complex **3.4**. NMR studies revealed the stability of the most active complex **3.4** in an aqueous environment and the ability to interact with small molecules of biological importance, such as 5′-GMP and L-histidine. UV-Vis titrations were used to investigate the ability of **3.4** to interact with double stranded DNA.

The mono- and trinuclear water soluble anionic sulfonated complexes, ligands and mono- and trinuclear sulfonated complexes containing *N*-donor ligands were evaluated for *in vitro* antitumor activity against WHCO1 cancer cells. The water soluble ligands **4.1-4.2** displayed no activity against the esophageal cancer cells, while the anionic mono- and trinuclear metal-chloro containing complexes **4.3-4.6** exhibited poor activity. The displacement of the metal-chloro ligand by *N*-donor ligands resulted in a significant increase in activity. The sulfonated trinuclear complexes containing *N*-donor ligands **4.7-4.22** were the most active. NMR studies suggest that the anionic complexes **4.3-4.4** undergo displacement of the metal-chloro ligand by DMSO, which may explain their lack of activity. The sulfonated complexes containing *N*-donor ligands **4.7-4.22** all, with the exception of **4.14**, exhibit stability and inertness in an aqueous environment over an extended time period, as shown by NMR studies. Similarly,

NMR studies show the ability of the most active trinuclear complex **4.18** to interact with 5'-GMP.

6.3. Future Outlook

This study has displayed the great potential of PGM complexes as antitumor agents. Further exploration into different types of polymeric scaffolds or ligands may result in the fine tuning and increase in *in vitro* antitumor activity. Amide based scaffolds could be attempted to increase the water solubility[1-2] of complexes or polyether imines (PETIM) to lower the toxicity[3-4] of the ligands used.

In this study the ruthenium-arene was limited to *p*-cymene while the rhodium(III) and iridium(III) systems were only prepared with a pentamethylcyclopentadienyl ligand. Other arenes or Cp rings could be investigated to explore the influential role of this moiety on the complex's activity. These could include a cyclohexyl ring, hexamethylbenzyl ring, biphenyl ring or a glycol containing ring. These modifications allow for minor changes of the polarity[5] which may result in desired increases in activity.

The ligands prepared in this study were limited to low-valent dendrimer type scaffolds. These ligands could easily be converted in higher-valent dendrimers with minor synthetic modifications. Dendrimers have previously exhibited significant cellular permeability and retentions and these desirable properties encourage antitumor activity.[6]

NMR studies were performed in this investigation to probe the ability of the most active PGM complexes herein reported to interact with model DNA, 5′-GMP. These studies could be extended to include a wider selection of biologically important molecules to include those of amino acids, which are the fundamental building blocks of all proteins, and even small proteins or enzymes that these complexes may encounter within the blood.

Only *in vitro* antitumor activities were studied in this research. *In vivo* experiments would naturally be the next step forward for these potential drugs. A concourse of other important biological assays could be performed to better understand the biological activity of these complexes. Cellular uptake studies would allow for an understanding of each complex's ability to cross the cellular membrane. This could allow for any relationships between activity and uptake to be identified. Other DNA binding experiments such as those associated with gel electrophoresis would bring further understanding to these complexes ability to bind to DNA and these may be assayed in the presence of other molecules which would competitively bind to the DNA. Circular Dichroism studies could be performed, which would allow of qualitative identification of the type of interactions or binding of these complexes with DNA.

All of these investigations when coupled together will assist in trying to understand the potential methods of action if these complexes as antitumor agents

6.4. References

[1] R. Duncan and L. Izzo, *Adv. Drug Delivery Rev.* **2005**, *57*, 2215-2237.

[2] M. El-Sayed, M. Ginski, C. Rhodes and H. Ghandehari, *J. Controlled Release* **2002**, *252*, 355-365.

[3] S. Jain, A. Kaur, R. Puri, P. Utreja, A. Jain, M. Bhide, R. Ratnam, V. Singh, A.S. Patil, N. Jayaraman, G. Kaushik, S. Yadav and K.L. Khanduja, *Eur. J. Med. Chem.* **2010**, *45*, 4997-5005.

[4] T. R. Krishna and N. Jayaraman, *J. Org. Chem.* **2003**, *68*, 9694-9704.

[5] R.E. Aird, J. Cummings, A.A. Ritchie, M. Muir, R.E. Morris, H. Chen, P.J. Sadler and D.I. Jodrell, *Br. J. Cancer* **2002**, *86*, 1652-1657.

[6] L.C. Sudding, R. Payne, P. Govender, F. Edafe, C.M. Clavel, P.J. Dyson, B. Therrien and G.S. Smith, *J. Organomet. Chem.* **2014**, *774*, 79-85.